Order Number 9405567

Boronic acids: Inhibition of thrombin and catalysis of imine formation

Niu, Linghao, Ph.D.

City University of New York, 1993

U·M·I
300 N. Zeeb Rd.
Ann Arbor, MI 48106

BORONIC ACIDS: INHIBITION OF THROMBIN AND CATALYSIS OF IMINE FORMATION

by

LINGHAO NIU

A dissertation submitted to the Graduate Faculty in Biochemistry in partial fulfillment of the requirements for the degree of Doctor of Philosophy, The City University of New York.

1993

This manuscript has been read and accepted for the Graduate Faculty in Biochemistry in satisfaction of the dissertation requirement for the degree of Doctor of Philosophy.

June 17, 1993
Date

Chair of Examining Committee

June 17, 1993
Date

Executive Officer

Horst Schulz

Richard Pizer

Dominick Basile

William Jakinovich

Supervisory Committee

The City University of New York

ABSTRACT

BORONIC ACIDS: INHIBITION OF THROMBIN

AND CATALYSIS OF IMINE FORMATION

by

Linghao Niu

Adviser: Professor Manfred Philipp

In part I of this study, peptide boronic acids have been used as transition state analog inhibitors for thrombin, a serine protease in the blood coagulation cascade. The pH profiles of these inhibitions have been studied in comparison with those of other compounds. These include a peptide carboxamide, a peptide aldehyde, a diamidinoketone and an arsonic acid.

One of the peptide boronic acids studied here, Ac-D-Phe-Pro-boroArg, is a known slow binding inhibitor for thrombin. In an effort to investigate the origin of the slow inhibition, the inhibitory behavior of Ac-D-Phe-Pro-boroArg was compared with its analogous inhibitors. One of these, Ac-D-Phe-Pro-Arg does not contain the boronate group, the other, Z-D-Phe-Pro-boroMPG contains a neutral side chain at the P_1 position. (The boroMPG indicates methoxypropylboroglycine.)

The results demonstrate that the slow inhibition shown by Ac-D-Phe-Pro-boroArg is also shown by Ac-D-Phe-Pro-Arg. pH-dependent kinetics of the weak-to-tight binding transition are similar. In contrast, Z-D-Phe-Pro-boroMPG only displays a prompt inhibition mode. Therefore, the slow inhibition depends on the peptide sequence used. The boronate moiety of the inhibitor is not essential for the formation of the tight-binding

complex, but is required for the potent inhibitory effect.

In part II of this study, boron acids have been used as enzyme analogs. Their catalytic effects on the formation of salicylaldoxime and salicylaldehyde phenylhydrazones were studied using pH-dependent kinetics, linear free energy relationships and the solvent deuterium isotope effect. The oxime-boronate complexes were characterized by UV spectra. Their dissociation constants were determined.

The results indicate that catalytic effectiveness is improved by electron-withdrawing substituents on the boron acids. The Michaelis-Menten kinetics exhibited by diphenylborinic acid in salicylaldoxime formation allow the determination of K_m and k_{cat}. Based on these data, the possible catalytic mechanisms were proposed. Boron acids are perhaps the smallest enzyme-like catalysts found to date.

ACKNOWLEDGEMENTS

I am indebted to Dr. Manfred Philipp, my thesis adviser, for his advice and support. His patient guidance and encouragement during the entire course of this study will be remembered.

Thanks are due to Drs. Horst Schulz, Richard Pizer, Dominick Basile and William Jakinovich for serving on my thesis committee and for their helpful suggestions.

I also thank Professor R. L. Baumgarten, Chairman of the Chemistry Department of Lehman College, for his support and help for the final outcome of this study. Thanks are extended to the technical staff at the Chemistry Department of Lehman College for their kind assistance.

LIST OF ABBREVIATIONS

Ac = acetyl

Ac-D-Phe-Pro-boroArg = Ac-D-Phenylalanyl-L-Prolyl-L-boroArginine

AMC = aminomethylcoumarin

t-Boc = tertiary-butyloxycarbonyl

BSA = bovine serum albumin

Bz = benzoyl

I = ionic strength

inf. = infinity

leupeptin = Ac-Leu-Leu-Arginine

Lim = pH-independent limiting value

NAPAP = N^{α}-(2-naphthalenesulfonylglycyl)-4-amidino-D,L-phenylalaninepiperidide

opt. = optimum

*p*NA = *para*-nitroaniline

Z = benzyloxycarbonyl

Z-D-Phe-Pro-boroMPG = 1-(Z-D-Phenylalanyl-Prolineamido)-1-dihydroxyborono-4-methoxybutane

TABLE OF CONTENTS

Page

Page

Page

LIST OF TABLES

Part I

LIST OF TABLES

Part II

Page

LIST OF FIGURES

Part I

Page

Page

Page

Page

LIST OF FIGURES

Part II

Page

Page

Page

LIST OF APPENDIXES

Page

PART I

pH DEPENDENCIES FOR SUBSTRATES AND TRANSITION STATE ANALOG INHIBITORS OF THROMBIN

INTRODUCTION

Thrombin is a trypsin-like serine protease which plays central bioregulatory roles in hemostasis[1-4]. The primary physiological function of thrombin is to cleave fibrinogen into clottable fibrin. The proteolysis occurs at particular Arg-Gly bonds of the Aα and Bß chains of fibrinogen[5-6]. The interactions between these two molecules have been extensively studied[7].

Besides its main action on fibrinogen, thrombin regulates the activation of fibrinoligase (factor XIII), a transamidase which cross-links fibrin chains to form an insoluble network. Thrombin also promotes blood clotting reaction by activating factors V and VIII, potentiating its own formation from prothrombin in the manner of a positive feedback mechanism. In addition, thrombin interacts with various cells and induces platelet aggregation[8].

The X-ray crystal structure of human α-thrombin has been well defined[9-11]. The enzyme is a spherical molecule with two polypeptide chains of 36 (A-chain) and 259 (B-chain) amino acid residues. The thrombin A-chain, mainly organized in a multiple-turn conformation is connected via disulfide bridge Cys1-Cys122 with the B-chain along the molecular surface opposite to the active site.

The thrombin B-chain exhibits the characteristic polypeptide fold of trypsin-like protease. It comprises two interacting 6-stranded barrel like domains covered by turn structures and four helical regions. The catalytic residues and the substrate binding site in thrombin are integrated into a deep narrow canyon. Three amino acids, serine-195, histidine-57 and aspartate-102, which constitute the so called "charge relay system" for

catalysis are arranged similarly to those in chymotrypsin and in trypsin.

The specific pocket (primary or P_1 substrate binding site, nomenclature in ref. 14) which accommodates the guanidino alkyl side chain of arginine of the substrate extends into the interior of the active site cleft. At the base of the pocket, Asp-189 forms an ion pair with the positively charged guanidino group of arginine.

The secondary substrate binding sites include those portions on both sides of the primary binding pocket which interact with the leaving group of the substrate on one hand and the amino acid residues preceding the scissile bond (P_2 and P_3 positions) on the other hand. The substrate is positioned in such a way that the cleavable bond can be attacked by the catalytic center. Both rims of the active site cleft are primarily lined by hydrophobic residues whereas the bottom is mainly coated with polar groups.

Under physiological conditions, the activity of thrombin is balanced by the principal endogenous inhibitor, anti-thrombin III[12-13]. However, in cases of thrombotic disorder, the quick supplementation with antithrombotic drugs offers an important means of therapy. At present, heparin and coumarin drugs used as anticoagulants all have certain pharmacological disadvantages[15-16].

The most potent naturally occurring thrombin inhibitor is hirudin, a polypeptide isolated from the European medicinal leech[17-21]. However, due to its limited natural source, hirudin is not available in adequate amounts for therapeutic uses.

The development of synthetic thrombin inhibitors has become a primary approach in the search for new highly specific antithrombotic agents[22]. During the past few decades, extensive research demonstrated that transition state analogs are prominent inhibitors for hydrolytic enzymes[23-27].

The idea of transition state inhibitor originally arose from Linus Pauling's assertion that the active site of an enzyme has a conformation that is complementary to the transition state conformation of the substrate[28]. Thus, a stable analog of the transition state should exhibit enhanced binding affinity for its target enzyme. By forming a stable non-productive complex, a transition state analog would function as a potent inhibitor with desired specificity.

In the course of the enzymatic catalysis, serine proteases attack the carbonyl carbon of the scissile peptide bond by a serine hydroxyl group to generate high energy tetrahedral intermediates. Decomposition of these high energy species leads to hydrolysis products and free enzyme[29-30]. The tetrahedral intermediates formed in the substrate hydrolysis are closely related to the transition state. By mimicking crucial features of this structure, transition state analog inhibitors could be designed. Using this strategy, a variety of different synthetic antithrombotic agents have been developed[31].

Affinity studies suggest that thrombin is highly selective for an argininal residue at the P_1 position and the amino acid sequence in the flanking peptide (P_2, P_3 site) is also specially important for binding[32-34]. One of the highly specific hydrophobic peptides for thrombin is D-Phe-Pro-Arg[35]. From this sequence, the peptide aldehyde H-D-Phe-Pro-ArgH[36] and the chloromethyl ketone H-D-Phe-Pro-ArgCH_2Cl[37] were synthesized as effective thrombin inhibitors. The crystallographic study demonstrated that H-D-Phe-Pro-ArgCH_2Cl forms a tetrahedral hemiketal with the active site serine[9].

Inhibition of serine proteases by peptide aldehydes originated from Umezawa's discovery that this type of inhibitor is produced by streptomyces[38]. The first described examples are leupeptins which display inhibitory effects on plasmin, trypsin and other

proteases with a tryptic specificity. It was found that hemiacetal is formed at the active site[39].

Transforming C-terminal carboxylic group to an enzymatically non-cleavable amide also yielded a large number of selective thrombin inhibitors[40]. The molecular structures of these compounds are based upon the N^{α}-substituted cyclic amides of amidinophenylalanine. An important representative of this type of inhibitor is N^{α}-(2-naphthalenesulfonylglycyl)-4-amidino-D,L-phenylalaninepiperidide (abbreviated as NAPAP, structure in Fig.1), a strong reversible synthetic thrombin inhibitor (Ki = 6 nM[41]). The high antithrombin activity of this compound is obviously due to its affinity for the substrate binding sites of thrombin. The cationic benzamidine moiety resembles the protonated side chain of arginine of the substrate whereas the N^{α}-substituent and the carbonyl substituents of the inhibitor interact with secondary binding sites at both sides of the specificity pocket[42]. The X-ray crystallographic determinations of the NAPAP-trypsin complex and the NAPAP-human thrombin complex have been reported[43,76].

Another important class of transition state analog inhibitors of serine proteases is the boronic acids. Compared to other transition state inhibitors, boronic acids are prominent therapeutic agents because of their observed lack of toxicity. The enzyme-inhibitory properties of aliphatic and aromatic boronic acids on chymotrypsin and subtilisin were first reported in 1971[44-46]. Ten years later, the boronic acid analog of N-Acetyl-L-phenylalanine became available. This compound was synthesized by Matteson *et al.* and shown to be several orders of magnitude more effective than the aromatic boronic acids in the inhibition of chymotrypsin[27].

Following these initial studies, the potential of boronic acids as serine protease

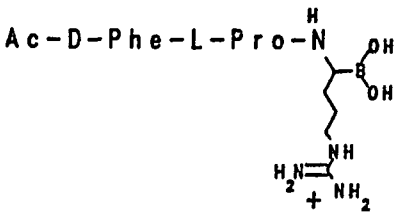

Ac-D-Phe-Pro-boroArg

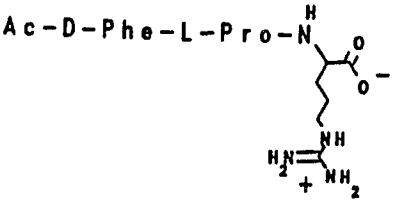

Ac-D-Phe-Pro-Arg

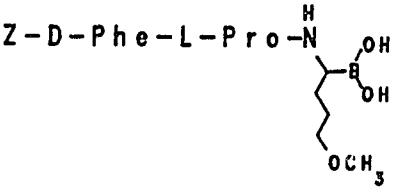

Z-D-Phe-Pro-boroMPG

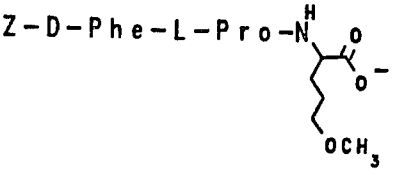

N(Z-D-Phe-Pro)-2-amino-
5-methoxypentanoic acid

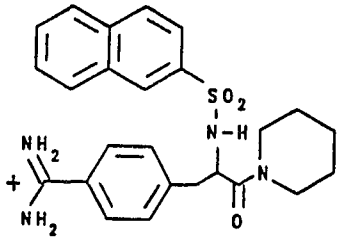

N$^{\alpha}$-(2-naphthalenesulfonylglycyl)-
4-amidino-D,L-phenylalaninepiperidide
(NAPAP)

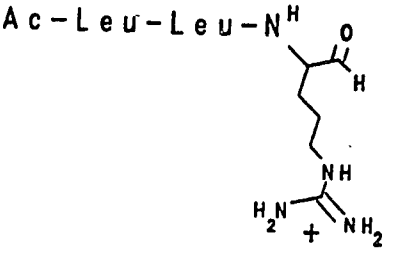

Leupeptin

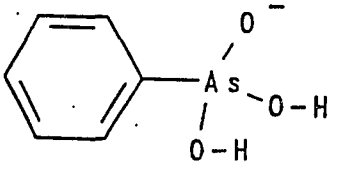

Phenylarsonic acid

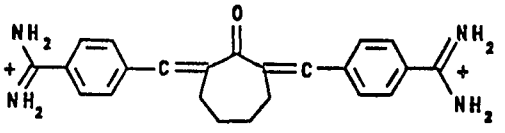

2,7-bis-(4-amidinobenzylidene)-
cycloheptan-1-one

Fig.1 Molecular structures of thrombin inhibitors used in Part I

inhibitors was further unfolded by Kettner and Shenvi, who synthesized the α-aminoboronic acid-containing analogs of sequence specific peptides and showed that these compounds are potent inhibitors for elastase, chymotrypsin and cathepsin G[47].

The inhibition mechanism of serine protease by the boronic acids has been extensively investigated. Based on the results of kinetic[45,48,50], magnetic resonance[51-54] and X-ray crystallographic research[30,55-57], the current model suggests that the trigonal boronic acids once bound, are esterified to the active site serine hydroxyl. This esterification involves proton transfer from the active site serine to the active site imidazole. The binding is facilitated by the cationic imidazolium ion and by hydrogen bonding between the proton-donating groups in the oxyanion hole and a boronic acid hydroxyl group.

In the crystal structure of a complex formed between subtilisin and the benzeneboronic acid, the boronic acid exists as a transition state-like tetrahedral anionic adduct with the active site serine residue. One -OH of boron occupies the oxyanion binding pocket and the other -OH is in the expected position of the leaving NH- group for normal peptide hydrolysis[56]. This mode of interaction has been also observed in the X-ray crystallographic analysis of a more specific enzyme-inhibitor complex formed between α-lytic protease and its strong peptide-based boronic acid inhibitor, N-*tert*-butyloxycarbonyl-Ala-Pro-boroVal[30].

In addition, the boron atom also can exist in a coordinate covalent complex with the active site imidazole[53,57-58]. NMR evidence indicates that weak, nonspecific inhibitors are bound to the active site histidine, while the stronger sequence specific peptide boronic acids are bound to the active site serine[53].

Kettner *et al.* first noticed that specific peptide boronic acids display slow-binding

inhibition on elastases[47]. They also observed this phenomena in the inhibition of human thrombin by its sequence specific peptide boronic acid, Ac-D-Phe-Pro-boroArg (where boroArg represents the boronic acid analogue of arginine at the C-terminal[66]). Up until the present time, the slow inhibition effect remains unexplained.

In the present project, one effort made was the investigation on the origin of the slow inhibition behavior of peptide boronic acids. This was done by determining the pH dependent inhibitory effect of Ac-D-Phe-Pro-boroArg on bovine thrombin in comparison with its corresponding peptide carboxylate, Ac-D-Phe-Pro-Arg. The solvent deuterium isotope effect on this slow inhibition system was also determined.

Another structurally related thrombin sequence specific peptide boronic acid studied here is 1-(Z-D-Phenylalanyl-Prolineamido)-1-dihydroxyborono-4-methoxybutane (abbreviated as Z-D-Phe-Pro-boroMPG, structure in Fig.1). Unlike Ac-D-Phe-Pro-boroArg which contains a positively charged side chain in the P_1 position, this inhibitor has a P_1 aminoboronic acid with a neutral side chain. The inhibitory activities of this boronic acid and its control peptide carboxylate, N-(Z-D-Phe-Pro-)-2-amino-5-methoxypentanoic acid, on bovine thrombin were also determined.

In order to compare the behavior of the peptide boronic acids to other inhibitors that do not contain the boronic acid group, the pH-dependent inhibition kinetics were also performed on other compounds. These include a peptide aldehyde (leupeptin, Ac-Leu-Leu-ArgH), a peptide carboxamide (NAPAP), a diamidinoketone (2,7-bis-(4-amidinobenzylidene)-cycloheptan-1-one) and an arsonic acid. Their structures are presented in Fig.1. The pK values seen in these inhibition profiles were compared with those observed in the thrombin substrate kinetics which show the pKs of the free enzyme.

The results of these experiments are expected to promise a better understanding of the mechanism of thrombin inhibition and catalysis.

EXPERIMENTAL

Materials

0.1 M ionic strength buffers used in the enzyme assays were prepared from reagent grade chemicals and deionized water according to the *Biochemists' Handbook*[59]. They were acetate for pH 4.6 to 5.4, phosphate for pH 6.0 to 7.8, diethylbarbiturate for pH 8.6, and bicarbonate for pH 9.0 to 10.6. Aside from the small amount arising from the enzyme stock solution, the buffers were free of chloride ion.

Deuterium oxide was purchased from Cambridge Isotope Laboratories. I = 0.1 M buffers used for the enzyme assays in deuterium oxide were made essentially same as those in water using deuterium oxide as solvent.

Bovine plasma thrombin was purchased from Sigma (1000 NIH units per vial) as a lyophilized powder. After reconstitution with 1 ml water, the thrombin stock solution had a pH of 6.5 with 0.15 M NaCl and 0.05 M sodium citrate.

Plasmin from porcine blood was purchased from Sigma. Its stock solution (20.5 NIH units/ml) was made in pH 7.4 0.1 M phosphate buffer.

Porcine pancreas kallikrein was purchased from Sigma. Its stock solution (111 NIH units/ml) was made in pH 7.4 0.1 M phosphate buffer.

Human kidney urokinase was purchased from Sigma. The vial contained 27 NIH units/ml in aqueous solution with 20 mg NaCl/ml.

Bovine factor Xa was purchased from American Diagnostica. The vial contained 0.097 ml solution of pH 7.5 with 75 μg protein, (0.769 mg/ml) in 20 mM Tris-HCl and 0.1 M NaCl. Each vial was equivalent to 1800nKat.

The fluorogenic thrombin substrate, N-t-Boc-Valyl-Prolyl-Arginine-7AMC-HCl, was purchased from Sigma. A stock solution of 3.9 mM was made in N,N-dimethyl formamide.

The chromogenic thrombin substrate, D-Phe-Pipecolyl-Arg-*p*NA (S-2238), without mannitol solubilizer, was a gift from Kabi Vitrum. A stock solution of 3.36 mM was made in methanol.

The plasmin substrate, D-Val-Leu-Lys-*p*NA dihydrochloride, was purchased from Sigma. A stock solution of 17.56 mM was made in N,N-dimethyl formamide.

The kallikrein substrate, N-Benzoyl-Pro-Phe-Arg-*p*NA hydrochloride, was purchased from Sigma. A stock solution of 16.99 mM was made in N,N-dimethyl formamide.

The substrate used for urokinase and factor Xa, N-Benzoyl-Ile-Glu-Gly-Arg-*p*NA acetate salt, was purchased from Sigma. A stock solution of 12.58 mM was made in N,N-dimethyl formamide.

Ac-D-Phenylalanyl-L-Prolyl-L-boroArginine benzenesulfonic acid salt (made as the pinanediol ester of the boronic acid, abbreviated as Ac-D-Phe-Pro-boroArg), was synthesized at Sandoz. A stock solution of 6.64 mM was made in methanol.

1-(Z-D-Phenylalanyl-Prolineamido)-1-dihydroxyborono-4-methoxybutane (made as the pinanediol ester of the boronic acid, abbreviated as Z-D-Phe-Pro-boroMPG) was synthesized at Sandoz. A stock solution of 7.88 mM was made in methanol.

N-(Z-D-Phe-Pro)-2-amino-5-methoxypentanoic acid, was synthesized at Sandoz. A stock solution of 20.3 mM was made in methanol.

Ac-D-Phenylalanyl-Prolyl-Arginine trifluoroacetate salt was synthesized at Sandoz. A stock solution of 8.35 mM was made in deionized water.

N^{α}-(2-naphthalenesulfonylglycyl)-4-amidino-D,L-phenylalaninepiperidide (abbreviated NAPAP), was purchased from Sigma. A stock solution of 1 mM was made in deionized water.

The peptide aldehyde, leupeptin (Ac-Leu-Leu-ArgH), was purchased from Sigma. A stock solution of 19.14 mM was made in methanol.

Phenylarsonic acid was purchased from Pfaltz & Bauer. A stock solution of 0.743 M was made in methanol.

2,7-bis-(4-amidinobenzylidene)-cycloheptan-1-one dihydrochloride salt was purchased from American Diagnostica. A stock solution of 2 mM was made in deionized water.

(1S,2S,3R,5S)-(+)-Pinanediol was purchased from Aldrich. A stock solution of 1 M was made in methanol.

7-Amino-4-methyl-coumarin was purchased from Sigma. A stock solution of 39 mM was made in N,N-dimethyl formamide.

Bovine serum albumin (abbreviated BSA) was purchased from Sigma. A stock solution of 3 mg/ml was made in deionized water.

Methods

Thrombin concentrations were determined by titration with *p*-nitrophenyl *p*'-guanidinobenzoate[60]. All enzymatic reactions were conducted in 0.1 M ionic strength

buffers containing 10 μg/ml bovine serum albumin (BSA) at 26°C.

When the fluorogenic thrombin substrate was used, reaction progress curves were observed on the SLM SPF-500C spectrofluorometer equipped with a temperature control system. The emission wavelength was 440 nm, the excitation wavelength was 350 nm. Kinetic assays using *p*-nitroanilide substrates were performed on the Vmax kinetic microplate reader at 405 nm.

pH of the assay mixtures was measured on a Radiometer PHM62 immediately after completion of each reaction.

Lotus-123 and Sigma plot were used for linear regression and non-linear data analysis respectively. Generation of pH profiles was performed on a Lotus-123 spreadsheet which was described in ref.69.

pH-dependent substrate kinetics. The pseudo-first-order hydrolysis rate of the fluorogenic thrombin substrate N-t-Boc-Valyl-Prolyl-Arginine-7-AMC (0.39 μM) was determined in various pH buffers. The values of k_{cat}/K_m were calculated by dividing the pseudo-first-order rate constant with enzyme concentration. K_m values of this substrate were determined from Lineweaver-Burk plots.

In order to observe the pH effect on the fluorescence intensity, the N-t-Boc-Valyl-Prolyl-Arginine-7-AMC hydrolysis leaving group, 7-amino-4-methyl-coumarin, was subjected to spectrofluorometric titration. This was done by determining the fluorescence intensity of 0.39 μM 7-Amino-4-methyl-coumarin in various pH buffers at the emission wavelength of 440 nm with the excitation at 350 nm.

Initial rates for the hydrolysis of the chromogenic thrombin substrate

D-Phe-Pipecolyl-Arg-*p*NA were measured over the concentration range of 18 μM to 175 μM at pH 5.0 to 8.6, 13 μM to 54 μM at pH 9.0 to 10.6. Lineweaver-Burk plots were constructed for the determination of K_m and k_{cat}.

Non-slow-binding inhibition kinetics. pH-dependent inhibitions of bovine thrombin by Z-D-Phe-Pro-boroMPG, N-(Z-D-Phe-Pro)-2-amino-5-methoxypentanoic acid, NAPAP, leupeptin, phenylarsonate and 2,7-bis-(4-amidinobenzylidene)-cycloheptan-1-one were studied using the fluorogenic substrate N-t-Boc-Valyl-Prolyl-Arginine-7-AMC. Their K_i values were measured by comparing the pseudo-first-order hydrolysis rates of the substrate for inhibited and uninhibited reactions. The substrate concentration (0.39 μM) was kept well below K_m in the assay mixtures. The type of inhibition for each inhibitor was determined by Lineweaver-Burk plot with the substrate concentration ranging from around 0.5 K_m to 3 K_m.

NAPAP was subjected to spectrophotometric titration at 247 nm using the method described in ref.71.

Inhibitions of other serine proteases related to the blood clotting system by Ac-D-Phe-Pro-boroArg and Z-D-Phe-Pro-boroMPG were determined in 0.1 M phosphate buffer of pH 7.4 containing 10 μg/ml BSA. The reactions were started by adding enzyme to mixtures of substrate and inhibitor. From Lineweaver-Burk plots, K_i values were calculated.

Bovine factor Xa and human kidney urokinase were assayed with the substrate N-Benzoyl-Ile-Glu-Gly-Arg-*p*NA ranging from 25 μM to 0.13 mM and from 0.45 mM to 2.3 mM, respectively.

Porcine pancreas kallikrein was assayed with the substrate N-Benzoyl-Pro-Phe-

Arg-*p*NA ranging from 34 μM to 0.34 mM and porcine serum plasmin was assayed with the substrate D-Val-Leu-Lys-*p*NA ranging from 70 μM to 0.42 mM.

Slow inhibition kinetics. The slow-binding thrombin inhibitor Ac-D-Phe-Pro-boroArg was studied using the substrate D-Phe-Pipecolyl-Arg-*p*NA. Assays were initiated by adding the enzyme to the mixtures of substrate and inhibitor. The reactions were allowed to proceed for 4 hrs. The substrate concentration ranges were 18 μM to 175 μM at pH 5.0 to 8.6, 13 μM to 54 μM at pH 9.0 to 10.6. The inhibitor levels were 13.3 nM at pH 6.4 to 10.0, 26.6 nM at pH 6.0, pH 10.6 and 53.2 nM at pH 5.0 to 5.4. The thrombin concentration was kept at least 5 fold below the inhibitor level in the assay mixtures.

Reaction progress curves observed for the slow-binding inhibition were analyzed by fitting equation 1[61] on a Sigma Plot spreadsheet.

$$P = P_0 + (v_i - v_f)/k' + v_f t + (v_i - v_f)e^{-k't}/k' \quad (1)$$

P is the concentration of product at time t, P_0 is the initial concentration of product, k' is the apparent first-order-rate constant for the transition from the initial velocity (v_i) to the final (steady state) velocity (v_f).

According to the slow-binding inhibition model described by Williams and Morrison[62], the following equations were used for the calculation of kinetic constants.

$$E + I \underset{k_2}{\overset{k_1}{\rightleftharpoons}} EI \underset{k_4}{\overset{k_3}{\rightleftharpoons}} EI^* \quad (2)$$

Where EI and EI* are the loose and tight enzyme-inhibitor complexes, respectively.

$$K_i(\text{initial}) = k_2/k_1 \qquad (3)$$

$$K_i(\text{initial})/K_i(\text{final}) = k_3/k_4 + 1 \qquad (4)$$

$$k' = k_4 + k_3[(I/K_i(\text{initial}))/((I/K_i(\text{initial}))+1+S/K_m)] \qquad (5)$$

K_i(initial) and K_i(final) are the dissociation constants for the EI and EI* complexes. I and S are the concentrations of inhibitor and substrate. K_m is Michaelis constant.

By fitting the absorbance versus time data to equation 1, values of v_i, v_f and k' were measured directly from the reaction progress curves at each pH. Using these curve fitting results, K_i(initial) and K_i(final) were determined from the slopes of Lineweaver-Burk plots of v_i and v_f respectively. pH profiles for the initial (fast) and final (slow) inhibitions were then generated using a Lotus-123 spreadsheet. k_3 and k_4 were calculated from equation 4 and 5 using the theoretical values of K_i(initial), K_i(final) and K_m of substrate S-2238 read directly from their pH profiles. Enzyme reactivation was observed at pH 7.08 by preincubating 3.0 nM thrombin with 26.6 nM Ac-D-Phe-Pro-boroArg for 10 min and then diluting 2 fold into the assay mixture containing 0.175 mM S-2238. The effect of pinanediol on the enzyme reactivation was examined in the same way except that the incubation mixture was diluted into the assay solution containing 0.175 mM S-2238 and 20 mM pinanediol.

The slow-binding thrombin inhibitor Ac-D-Phe-Pro-Arg was studied using the fluorogenic substrate, N-t-Boc-Valyl-Prolyl-Arginine-7AMC. The reactions were initiated by adding enzyme into the mixtures of substrate and inhibitor. The substrate concentration was 0.39 μM, the inhibitor levels were around 30 μM for pH 6.4 to 9.4, 0.3 mM for pH 5.0 to 6.0 and pH 10. The enzyme levels were around 0.5 nM for pH 7.4 to 9.7, 1.5 nM for pH 6.4 to 7.0 and 10.0, 10 nM for pH 6.0, 30 nM for pH 5.0 to 5.4.

The reaction progress was followed at each pH for 30 min and then the fluorescence infinity value of the reaction was obtained by adding extra enzyme into the same reaction cuvette. The slow inhibition reaction progress curves were analyzed using the same model as for Ac-D-Phe-Pro-boroArg. At each pH, k' was measured from the fluorescence versus time data by fitting equation 1. k_3 and k_4 were then calculated in the same way as in the case of Ac-D-Phe-Pro-boroArg. The values of initial and final K_i were determined by comparing the slopes of the initial and final (steady state) linear regions of the pseudo-first-order plot of the slow inhibition reaction progress curve with the pseudo-first-order slope of the control run in the absence of the inhibitor.

Solvent deuterium isotope effect of the slow-binding inhibition of thrombin by Ac-D-Phe-Pro-Arg was studied using I = 0.1 M deuterium oxide buffers. The kinetic assays were performed essentially the same as those done in water. In order to minimize the shift of the observed pK values in the pH profile, pH of the deuterium oxide reaction mixtures was reported as the value read directly on the pH meter without correction for the deviation near 0.4 caused by D_2O[63-64].

Determination of dissociation constants for the complexation between Ac-D-Phe-Pro-boroArg and pinanediol. The dissociation constants were measured at pH 6.45, 7.5, 9.18, and 9.64. The slow inhibition reactions were started by adding enzyme into the buffer solutions containing the substrate D-Phe-Pipecolyl-Arg-*p*NA, inhibitor Ac-D-Phe-Pro-boroArg and pinanediol. The slow inhibition effect was observed for 1 hr at various levels of pinanediol ranging from 0 to 20 mM. All the assay mixtures contained 13.3 nM inhibitor with the enzyme concentration at least 5 fold lower than the inhibitor level. The substrate concentration was about 50 μM. In the pseudo-first-order plots of the reaction progress curves, the final slopes of the linear regions of the steady state in the absence of pinanediol were compared with those in its presence. The dissociation constants were determined from the slopes of the linear plots of final slope/[pinanediol] versus final slope.

RESULTS AND DISCUSSION

pH-Dependent Substrate Kinetics

Hydrolysis of N-t-Boc-Valyl-Prolyl-Arginine-7-AMC. As shown in Fig.2, the pH profile of k_{cat}/K_m for the bovine thrombin catalyzed hydrolysis of the fluorogenic substrate N-t-Boc-Valyl-Prolyl-Arginine-7-AMC is governed by two pKs, one at 7.40 and one at 9.60. The optimal hydrolysis occurs at pH 8.50. The profile seen here is very close to that for trypsin and chymotrypsin[65].

In an effort to investigate the effect of substrate binding on the hydrolysis, K_m for N-t-Boc-Valyl-Prolyl-Arginine-7-AMC was determined at each pH. The pH dependence for $\log(1/K_m)$ in Fig.3 shows no discrete transition between pH 5 and pH 10 and a low sensitivity to pH (slope = 0.169).

In order to examine the influence of ionization of 7-amino-4-methyl-coumarin (the leaving group in the substrate hydrolysis) on the observed pH profile of K_m, spectrofluorometric titration was performed in the pH range 4.6 to 11. The titration curve is presented in Fig.4. Since there was no ionization pK observed for the coumarin in the pH range used for the kinetic measurement, it was not necessary to correct the observed fluorescence intensity for pH effect.

The nearly flat pH profile of K_m indicates that the bell-shaped curve of k_{cat}/K_m seen in Fig.2 reflects the pH dependence of k_{cat}. The pK_1 near 7 which is common to serine proteases may arise from the ionization of active site histidine while the pK_2 near 10 is presumably related to the anionic nature of thrombin active site above pH 7. Although the pK_2 is similar to that seen for other mammalian serine proteases, this pK

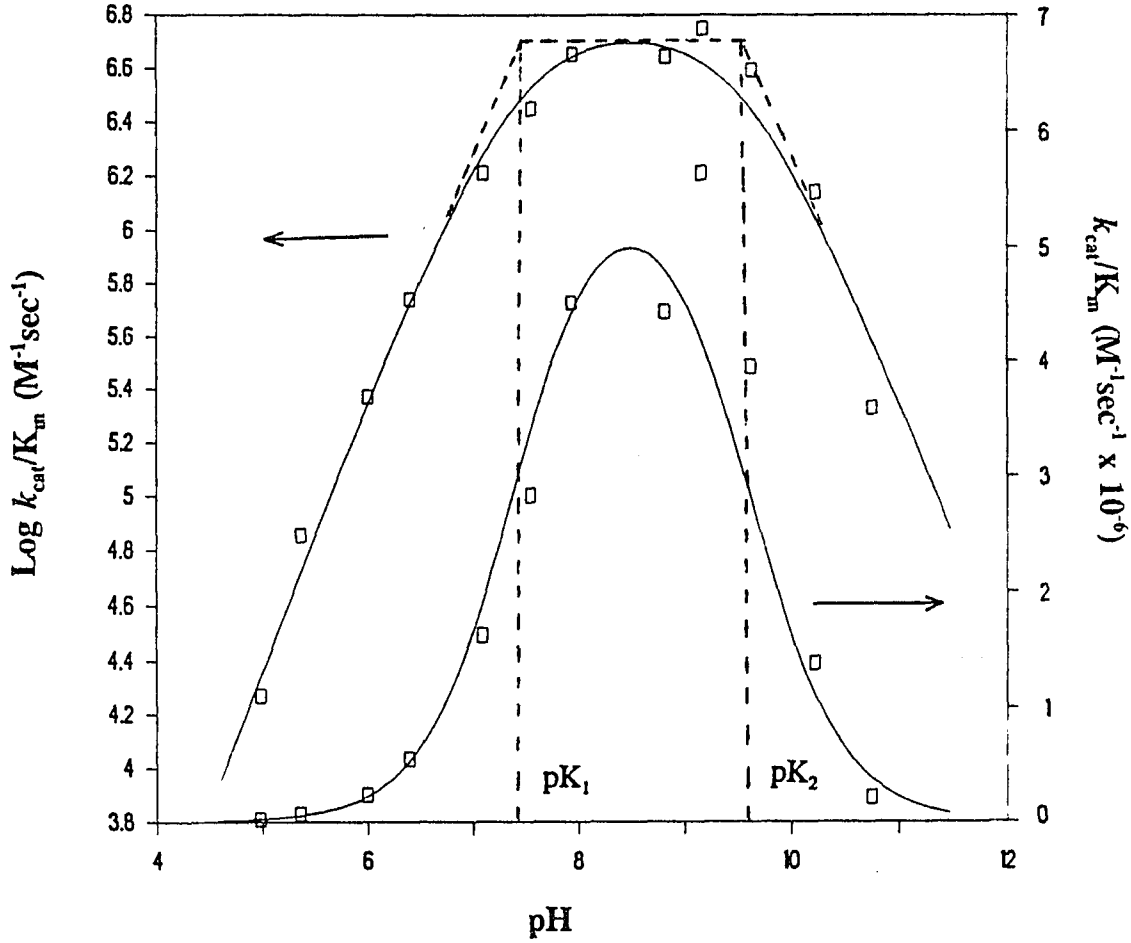

Fig.2 pH profile of k_{cat}/K_m for the bovine thrombin-catalyzed hydrolysis of N-t-Boc-Valyl-Prolyl-Arginine-7-AMC.
The theoretical curve is drawn using $pK_1 = 7.40(\pm 0.05)$, $pK_2 = 9.60(\pm 0.15)$, optimum pH = $8.50(\pm 0.10)$ and $k_{cat}/K_m(Lim) = 5.76x10^6(\pm 6.11x10^5)$ $M^{-1}sec^{-1}$.
Reaction conditions are given in the text.
(Data of Table I Appendix A)

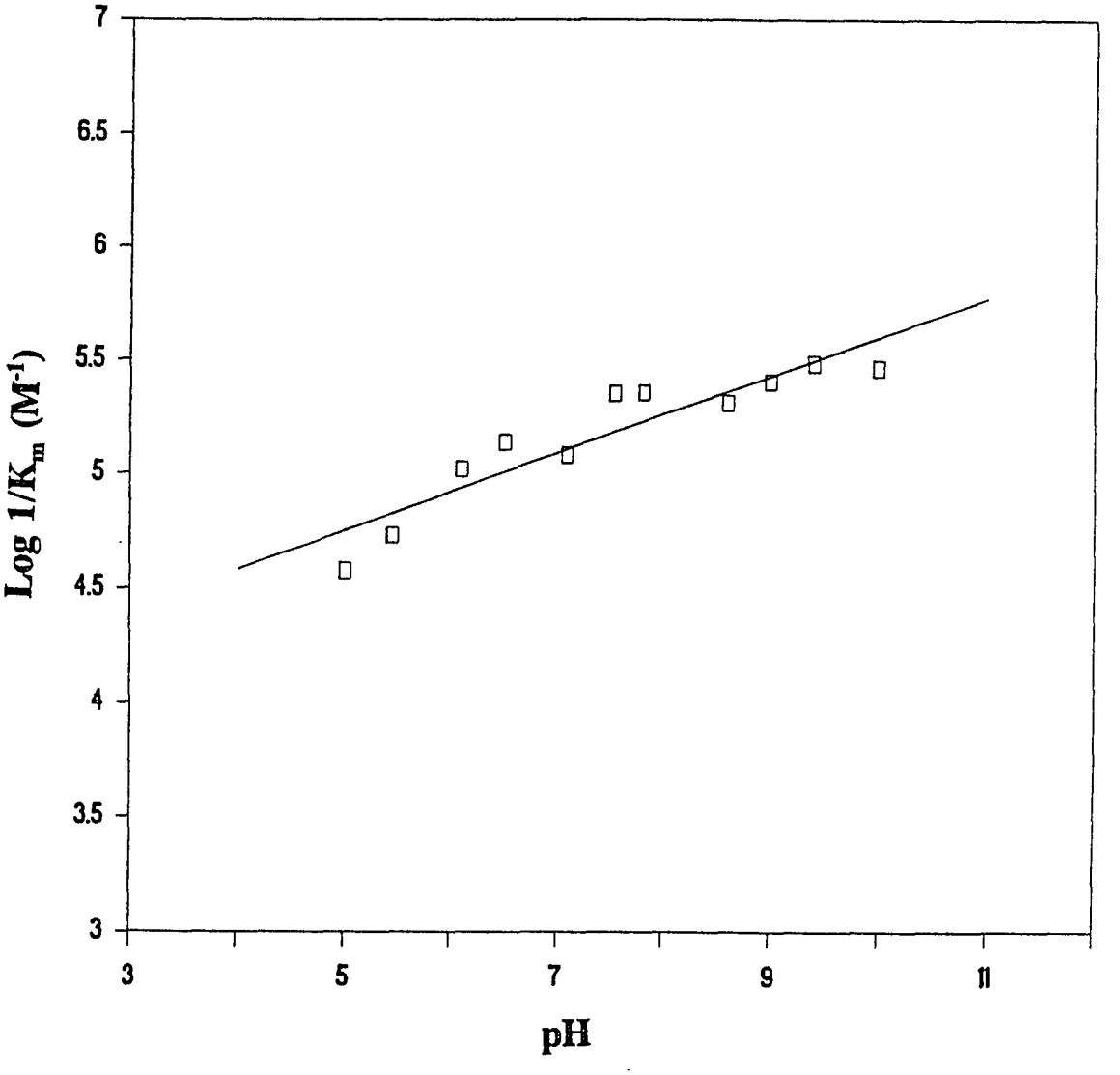

Fig.3 pH profile of K_m for the bovine thrombin-catalyzed hydrolysis of N-t-Boc-Valyl-Prolyl-Arginine-7-AMC.
The theoretical curve is drawn using slope = $0.169 \pm (0.0231)$.
Reaction conditions are given in the text.
(Data of Table II Appendix A)

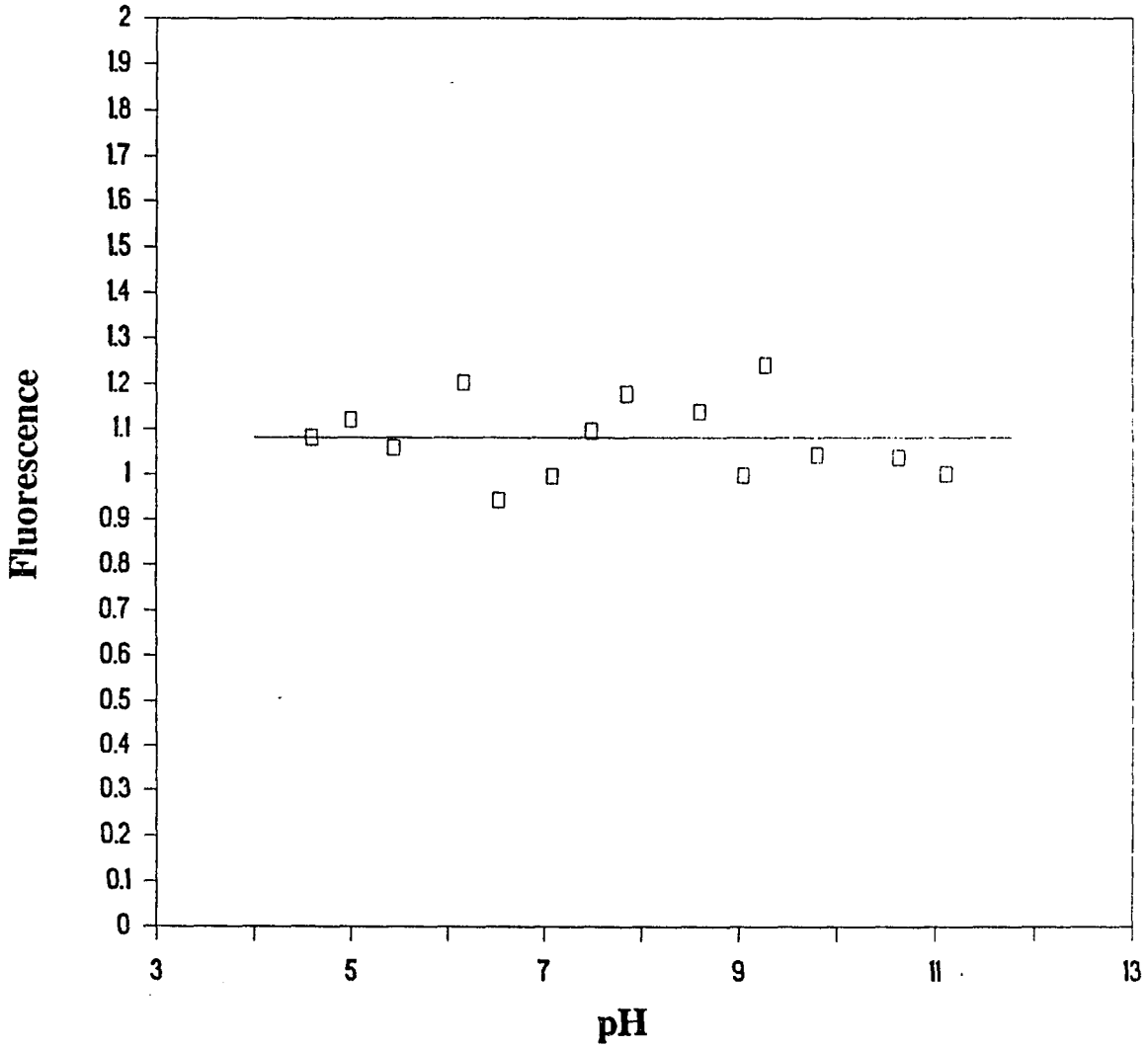

Fig.4 Spectrofluorometric titration of 3.9×10^{-7} M 7-amino-4-methyl-coumarin. The theoretical curve is drawn using slope = 0, the average fluorescence intensity = $1.081 \pm (0.0805)$. Reaction conditions are given in the text. (Data of Table III Appendix A)

is not an essential feature of serine protease since some, like subtilisin, lack it[67].

The pH dependencies for the hydrolysis of N-t-Boc-Valyl-Prolyl-Arginine-7-AMC clearly indicate that there is a free proton exchange between the thrombin-substrate complex and the assay medium.

Hydrolysis of D-Phe-Pipecolyl-Arg-*p*NA. Fig.5 and Fig.6 show the pH profiles of K_m and k_{cat} for D-Phe-Pipecolyl-Arg-*p*NA. Unlike the 7-AMC substrate, in this case, the pH profile of K_m shows a typical bell-shaped curve whereas the k_{cat} is less pH dependent. The two pKs of the enzyme control the binding of the *p*-nitroanilide substrate. The relatively pH-independent k_{cat} suggests that the substrate once bound, prevents proton transfer between the enzyme active site and the reaction environment.

The normal bell-shaped pH profile of k_{cat}/K_m for the hydrolysis of D-Phe-Pipecolyl-Arg-*p*NA seen in Fig.7 therefore mainly depends on the substrate binding. These data are close to those for human α-thrombin[68].

pH-Dependent Inhibition of Bovine Thrombin by Ac-D-Phe-Pro-boroArg

Inhibition kinetics. The initial rate data in Fig.8 indicate that Ac-D-Phe-Pro-boroArg is a competitive inhibitor for bovine thrombin. Its inhibition time course (Fig.9) clearly shows two different binding modes, one that is weaker and prompt, and one that is much stronger but forms more slowly. The pH dependent-kinetics for both the fast and slow inhibition were determined in this study.

Fig.10 shows the pH profile for the initial K_i of Ac-D-Phe-Pro-boroArg. The optimum pH for the rapid inhibition is 8.33 with the limiting K_i of 3.33 nM. The fast-

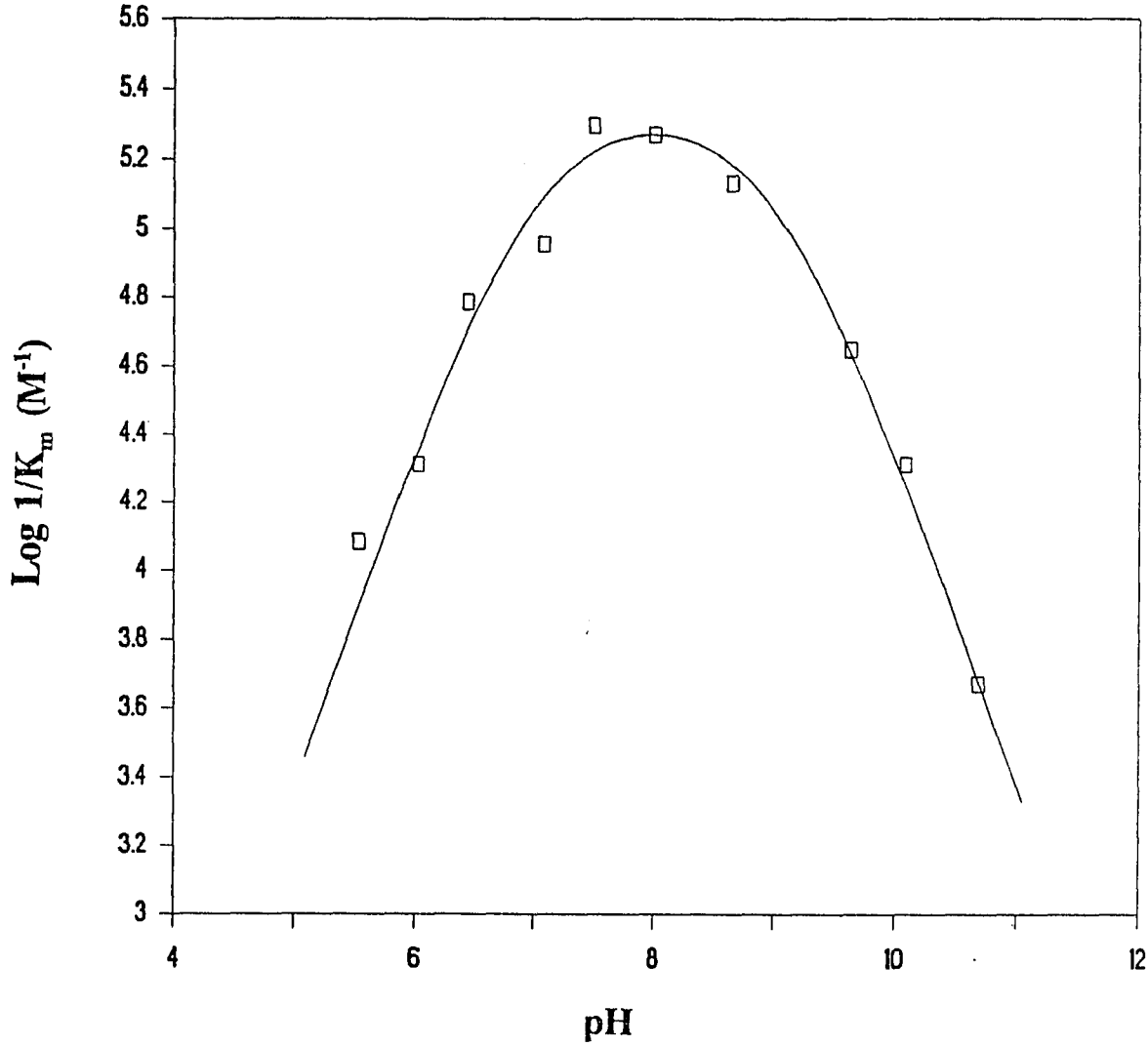

Fig.5 pH profile of K_m for the bovine thrombin-catalyzed hydrolysis of D-Phe-Pipecolyl-Arg-*p*NA. The theoretical curve is drawn using $pK_1 = 6.97(\pm 0.05)$, $pK_2 = 9.03(\pm 0.05)$, optimum pH $= 8.00 \pm (0.05)$ and $K_m(\text{Lim}) = 4.51 \times 10^{-6}(\pm 3.67 \times 10^{-7})$ M. Reaction conditions are given in the text.(Data of Table IV Appendix A)

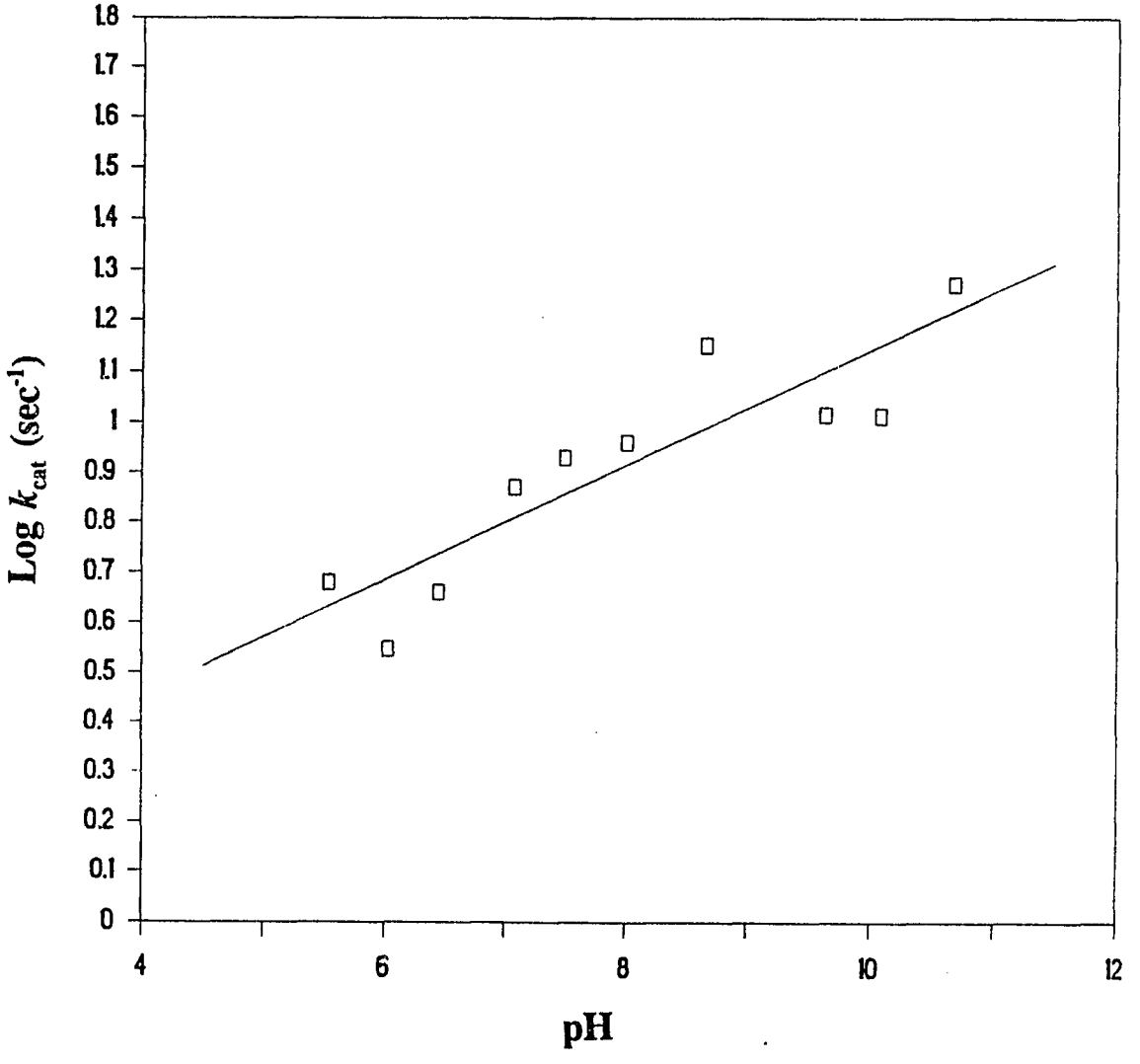

Fig.6 pH profile of k_{cat} for the bovine thrombin-catalyzed hydrolysis of D-Phe-Pipecolyl-Arg-*p*NA. The theoretical curve is drawn using slope = 0.114($\pm$0.021). Reaction conditions are given in the text. (Data of Table V Appendix A)

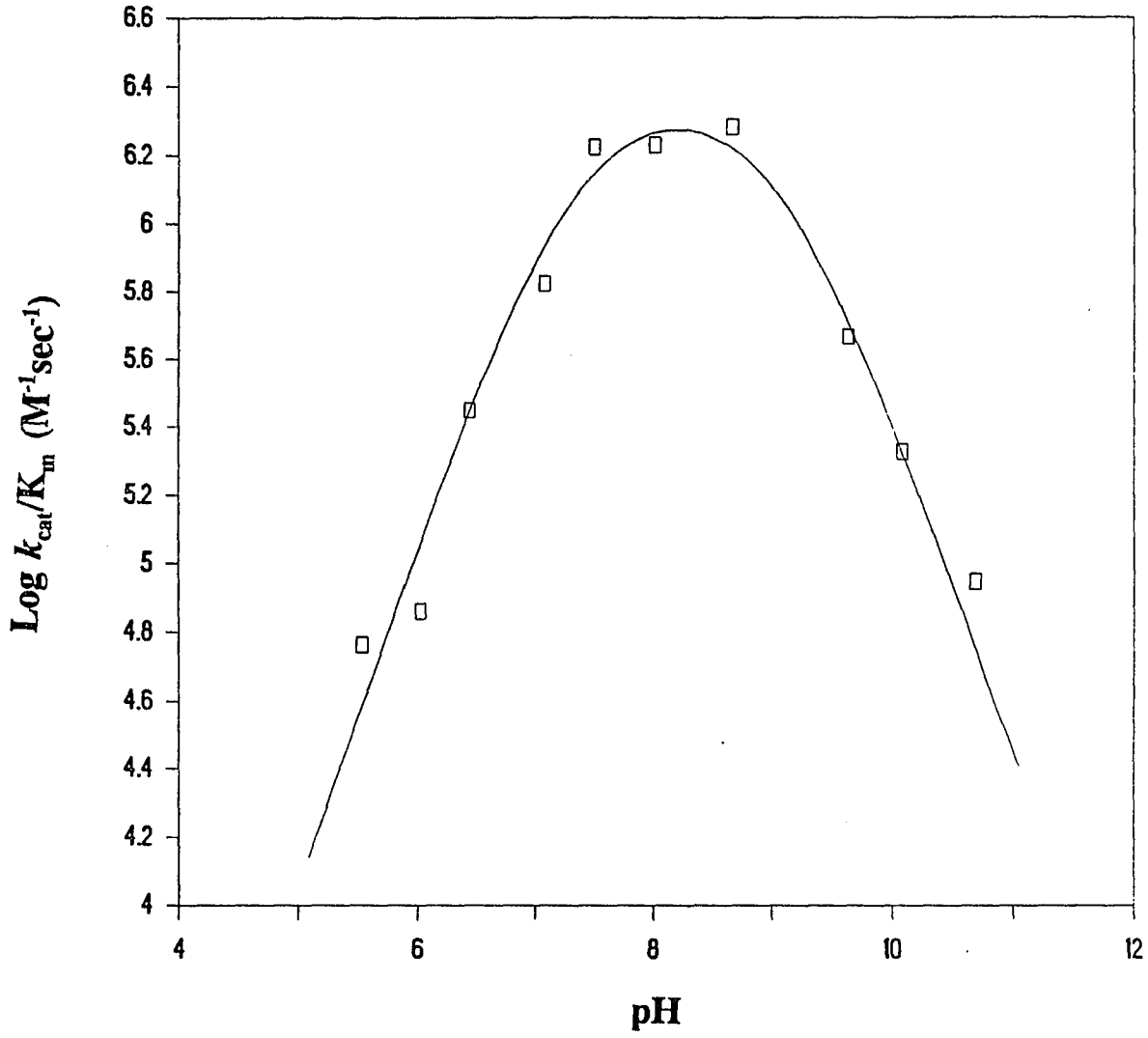

Fig.7 pH profile of k_{cat}/K_m for the bovine thrombin-catalyzed hydrolysis of D-Phe-Pipecolyl-Arg-*p*NA. The theoretical curve is drawn using $pK_1 = 7.33(\pm 0.10)$, $pK_2 = 9.07(\pm 0.10)$, optimum pH $= 8.20(\pm 0.10)$ and $k_{cat}/K_m(Lim) = 2.39x10^6(\pm 3.15x10^5)$ $M^{-1}sec^{-1}$. Reaction conditions are given in the text. (Data of Table VI Appendix A)

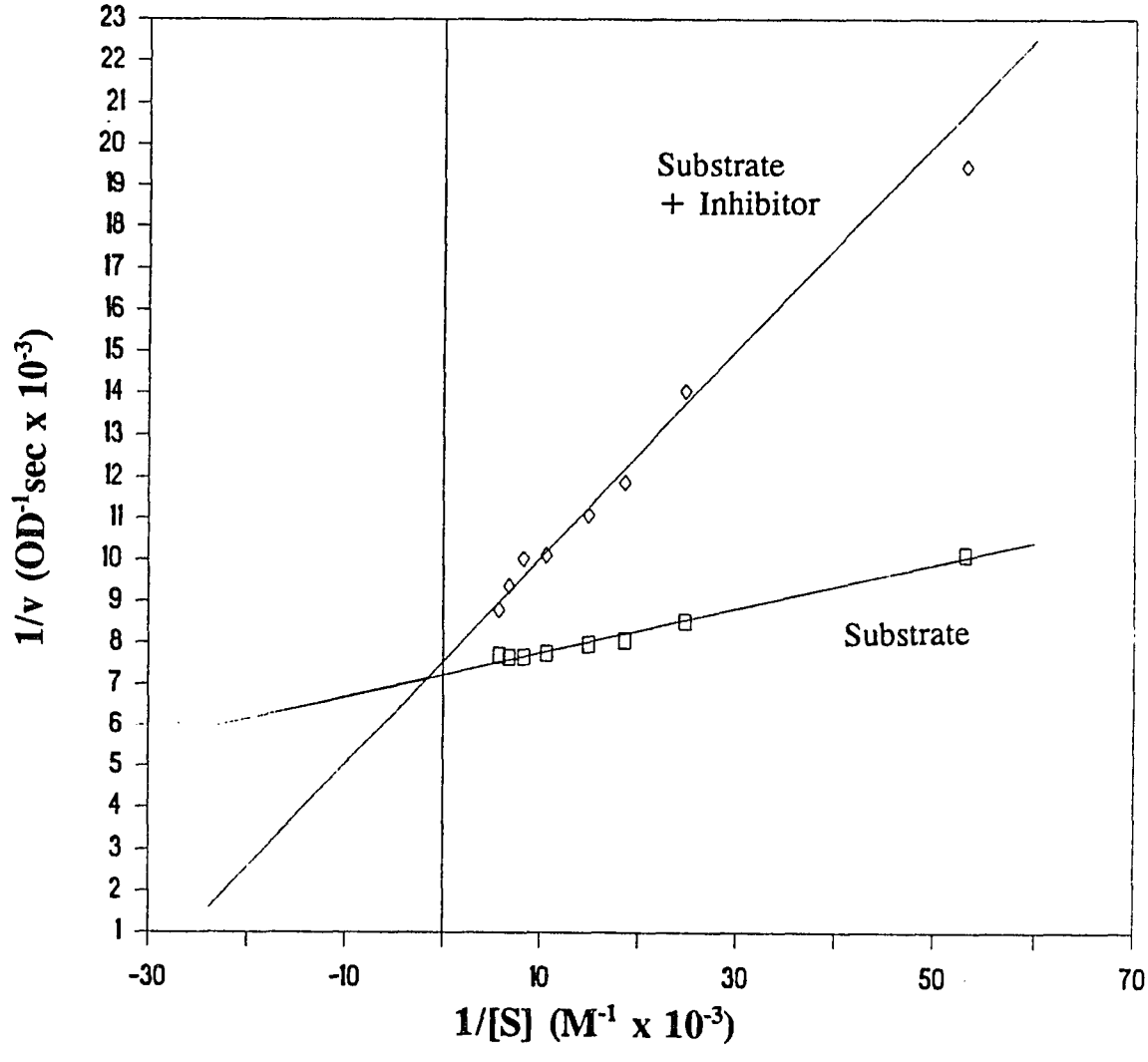

Fig.8 Initial inhibition of bovine thrombin by Ac-D-Phe-Pro-boroArg at pH 8.66. [inhibitor] = 1.33×10^{-8} M, the substrate was D-Phe-Pipecolyl-Arg-*p*NA. K_i = 4.20($\pm$0.504) nM, K_m = 7.38($\pm$0.485) μM. Reaction conditions are given in the text.
(Data of Table VII Appendix A)

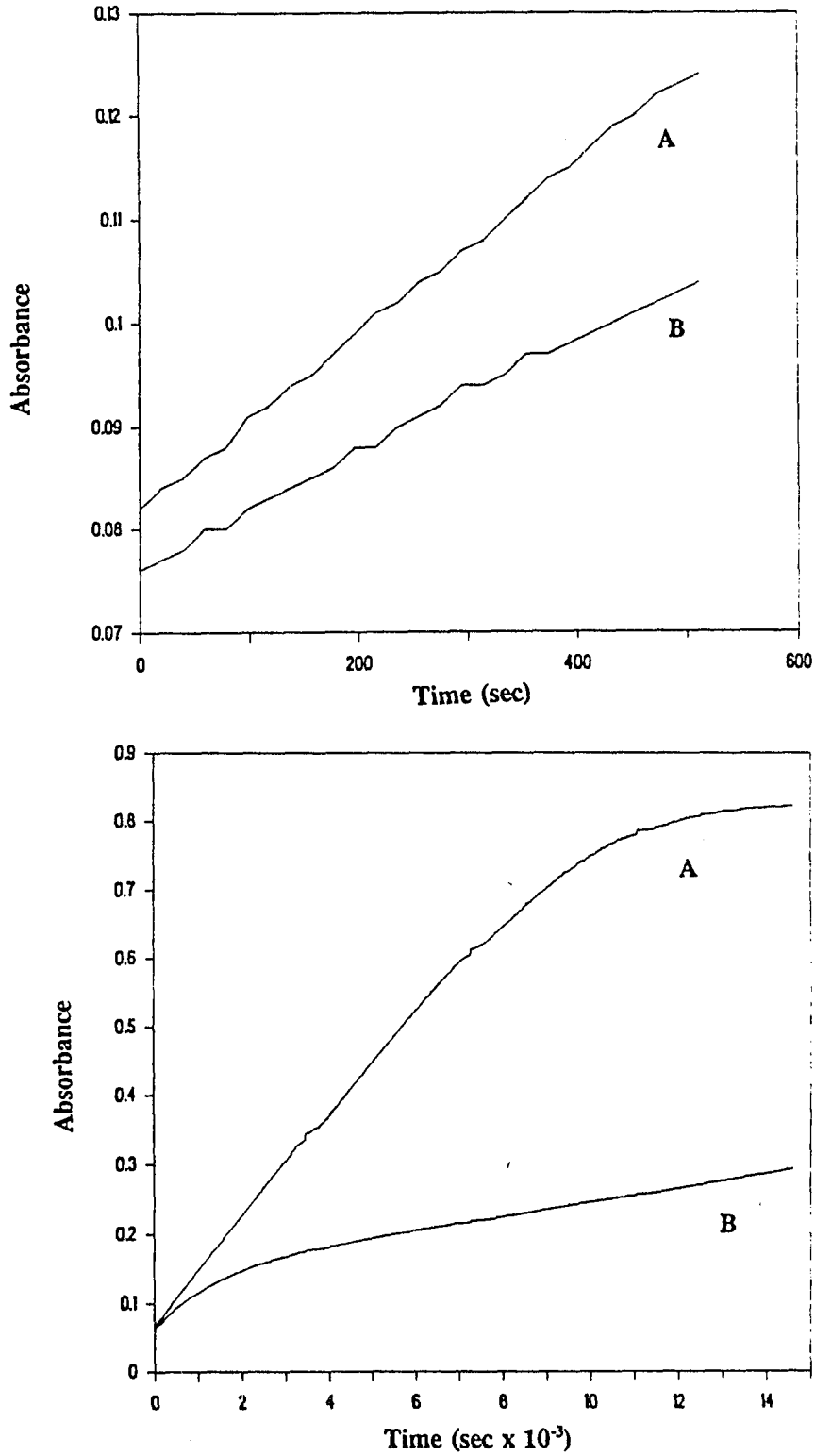

Fig.9 Slow-binding inhibition of bovine thrombin by Ac-D-Phe-Pro-boroArg at pH 7.5. Curve A is the bovine thrombin-catalyzed hydrolysis of 147.8 μM D-Phe-Pipecolyl-Arg-*p*NA. Curve B is the bovine thrombin-catalyzed hydrolysis of 147.8 μM D-Phe-Pipecolyl-Arg-*p*NA in the presence of 13.3 nM Ac-D-Phe-Pro-boroArg. Reaction conditions are given in the text.

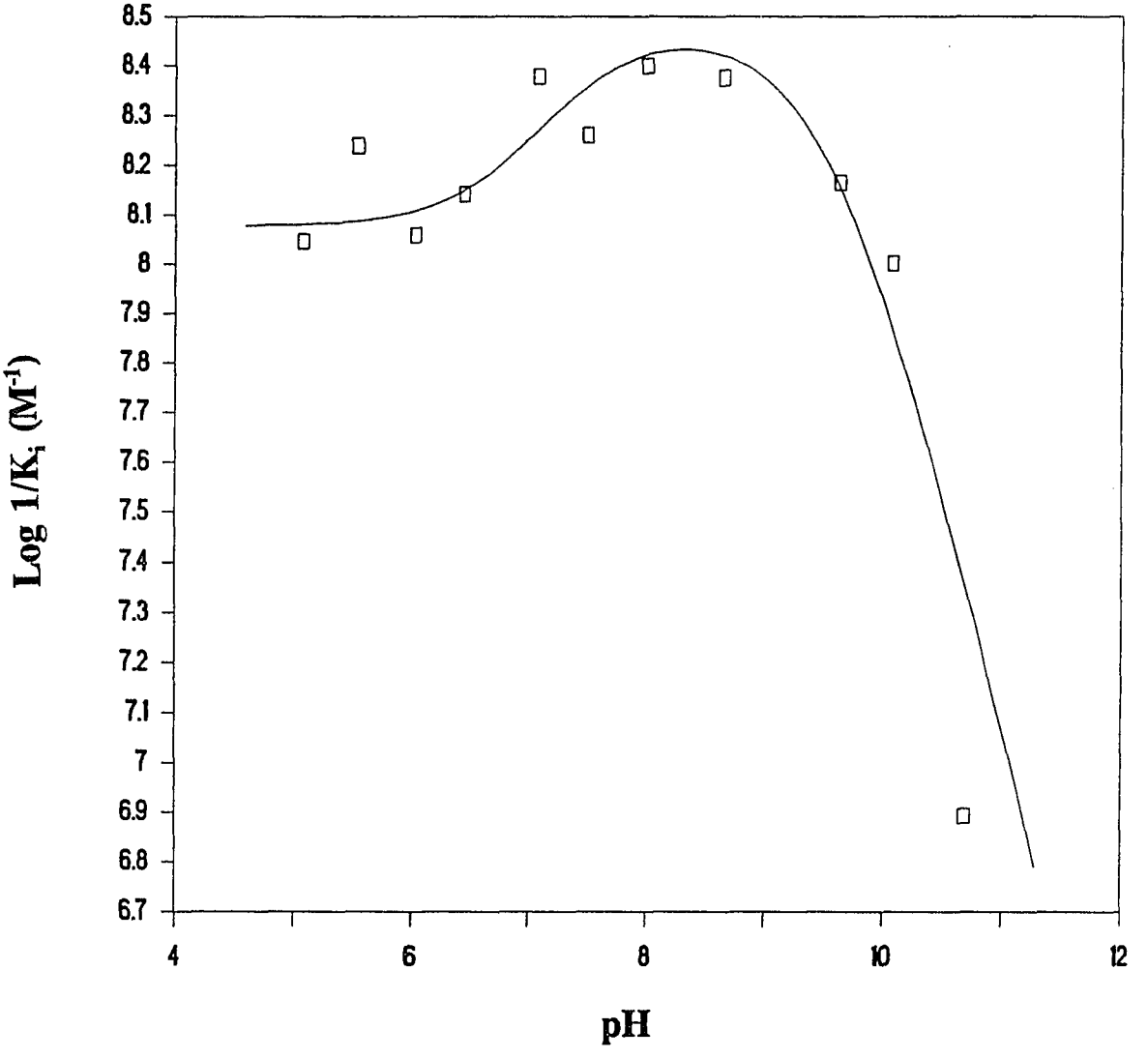

Fig.10 pH profile for the initial inhibition of bovine thrombin by Ac-D-Phe-Pro-boroArg. The theoretical curve is drawn using $pK_1 = 7.30(\pm 0.15)$, $pK_2 = 9.60(\pm 0.15)$, $pK_3 = 6.90(\pm 0.20)$, optimum pH = $8.33(\pm 0.15)$ and $K_i(Lim) = 3.33(\pm 0.667)$ nM. Reaction conditions are given in the text.
(Data of Table VIII Appendix A)

binding mode is governed by three pKs. pK_1 of 7.30 and pK_2 of 9.60 are essentially the same as that seen in the substrate kinetics. They reflect the enzyme ionizations. The pK_3 of 6.90 is believed due to the ionization of the loose thrombin-inhibitor complex. The presence of this pK suggests that the loose binding complex exchanges proton with the assay buffer.

In its slow-binding mode, Ac-D-Phe-Pro-boroArg shows a bell-shaped pH profile (Fig.11) reflecting the two pKs observed for thrombin ionizations. The optimal slow inhibition occurs at pH 8.25. Its limiting K_i is 43.7 pM.

The pH dependencies for the transition between the fast and slow inhibition modes are shown in Fig.12 and Fig.13. k_3 and k_4 are the first-order-rate constants for the conversion from the loose EI to tight EI^* and from the tight complex to loose complex respectively.

The experimental results show that the pH dependence of k_3 is bell-shaped while k_4 is independent of pH. The two pKs of the enzyme (one near 7, one near 10) control the transition from loose binding mode to tight binding mode suggesting the involvement of proton transfer in the loose binding complex. This result is consistent with the ionization of the enzyme-inhibitor complex observed in the pH profile of the initial K_i.

The flat pH profile of k_4 indicates that the proton exchange is abolished in the tight binding complex. This also agrees with the typical bell-shaped curve seen in the pH dependence of the final K_i.

Complexation between pinanediol and Ac-D-Phe-Pro-boroArg. Fig.14 shows the reactivation of bovine thrombin from the tight enzyme-inhibitor complex. Pinanediol clearly facilitates the reactivation progress. Its effect on the slow-binding inhibition

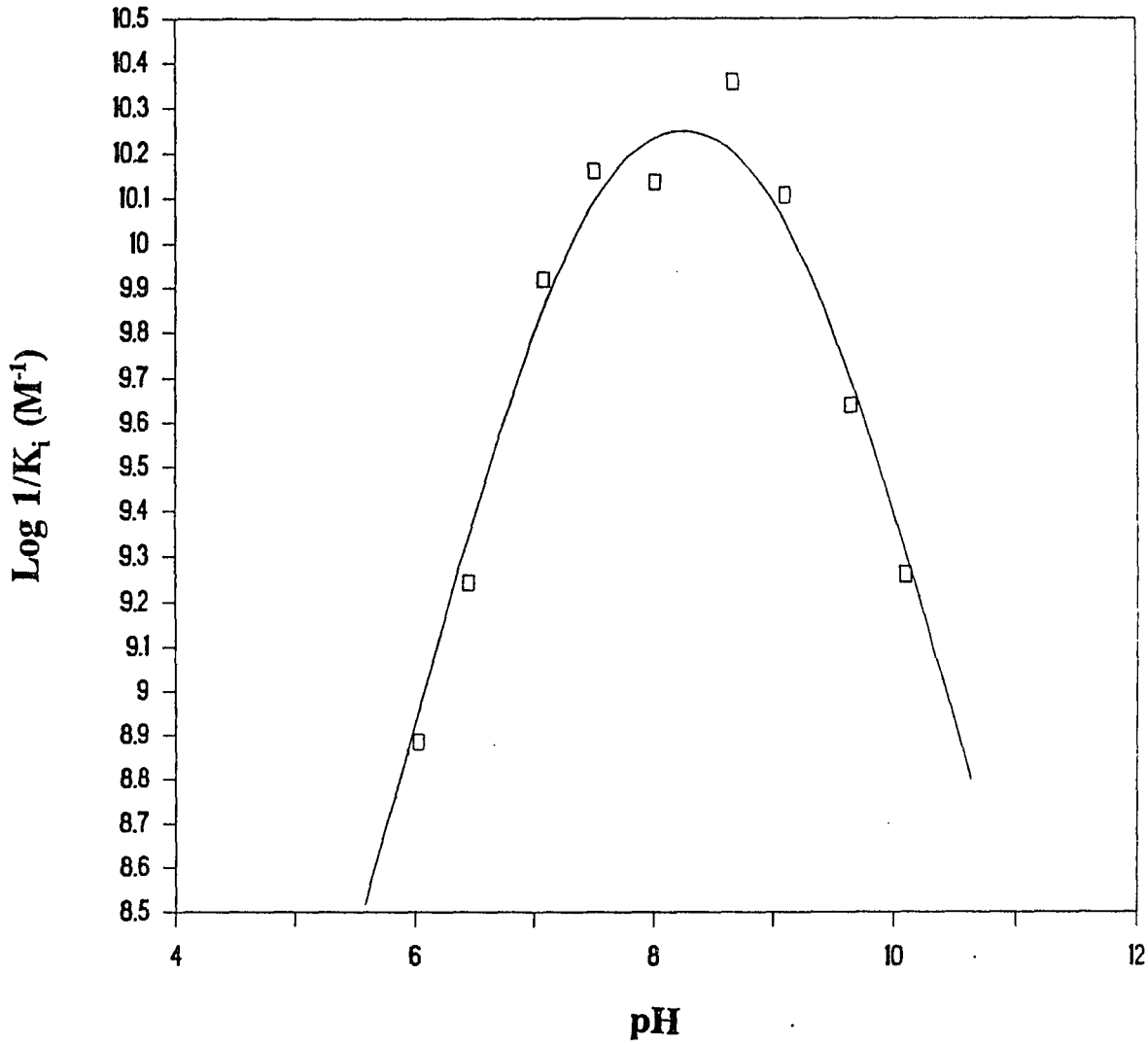

Fig.11 pH profile for the final inhibition of bovine thrombin by Ac-D-Phe-Pro-boroArg. The theoretical curve is drawn using $pK_1 = 7.42(\pm 0.10)$, $pK_2 = 9.08(\pm 0.05)$, optimum pH $= 8.25(\pm 0.07)$ and $K_i(Lim) = 43.7(\pm 8.56)$ pM.
Reaction conditions are given in the text.
(Data of Table IX Appendix A)

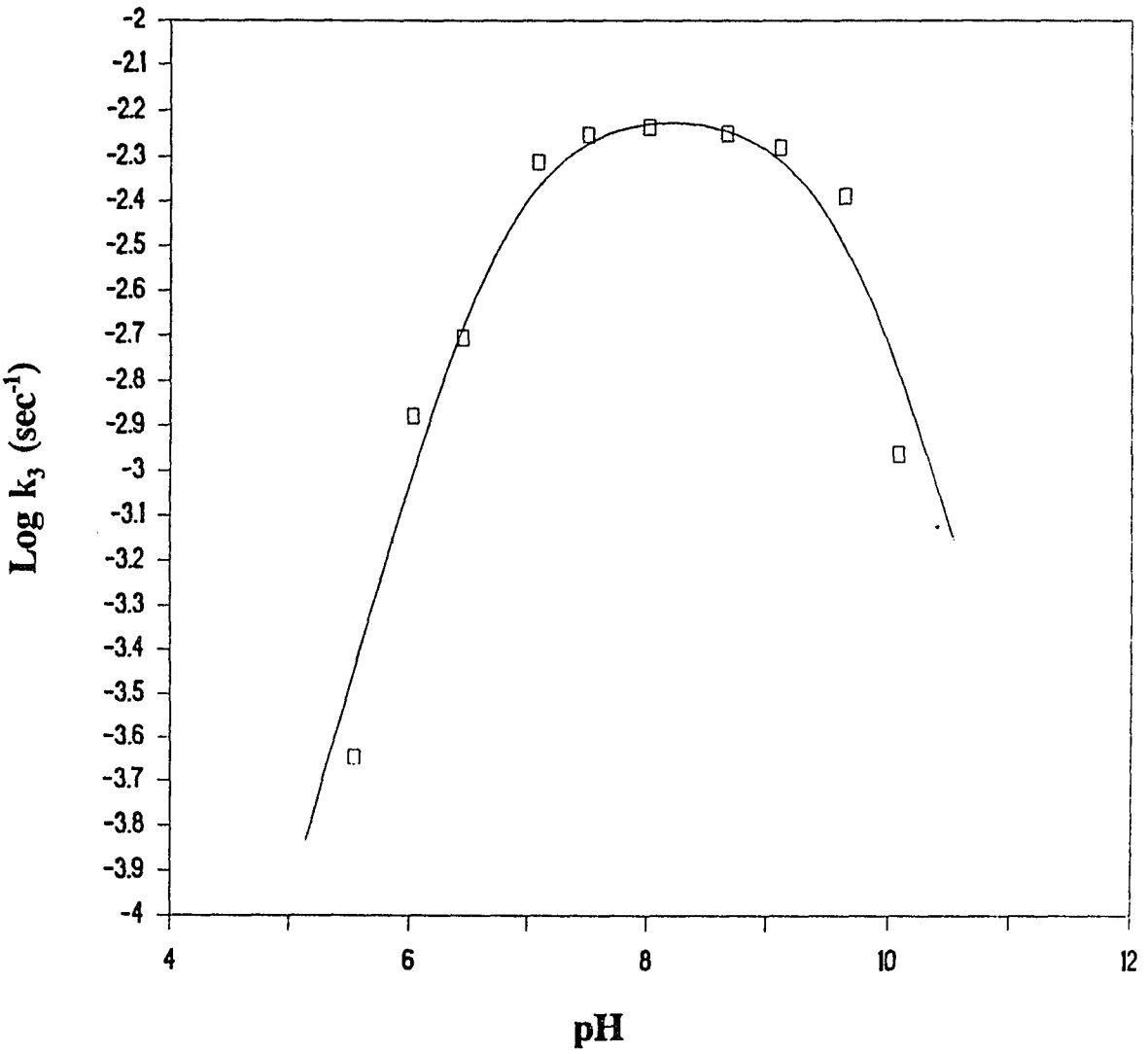

Fig.12 pH profile for the transition from initial inhibition to final inhibition of bovine thrombin by Ac-D-Phe-Pro-boroArg. k_3 is the first-order rate constant for the transition from the loose enzyme-inhibitor complex to the tight complex. The theoretical curve is drawn using
$pK_1 = 6.77(\pm 0.10)$, $pK_2 = 9.63(\pm 0.20)$, optimum pH $= 8.20(\pm 0.15)$ and $k_3(Lim) = 6.38 \times 10^{-3}(\pm 2.31 \times 10^{-4})$ sec^{-1}.
Reaction conditions are given in the text.
(Data of Table X Appendix A)

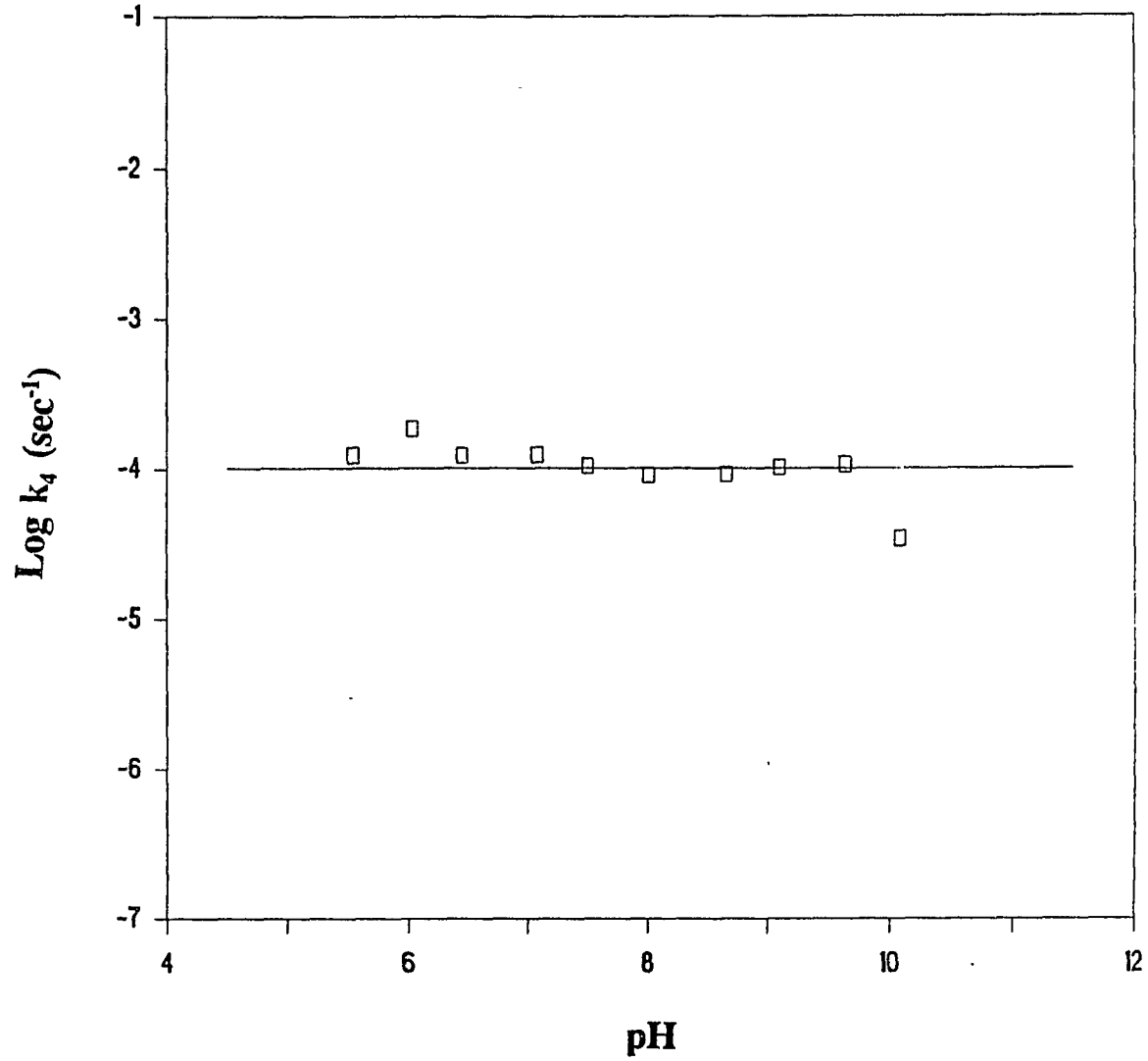

Fig.13 pH profile for the transition from final inhibition to initial inhibition of bovine thrombin by Ac-D-Phe-Pro-boroArg. k_4 is the first-order rate constant for the transition from the tight enzyme-inhibitor complex to the loose complex. The theoretical curve is drawn using
slope = 0 and average $k_4 = 1.09 \times 10^{-4} (\pm 3.88 \times 10^{-5})$ sec^{-1}.
Reaction conditions are given in the text.
(Data of Table XI Appendix A)

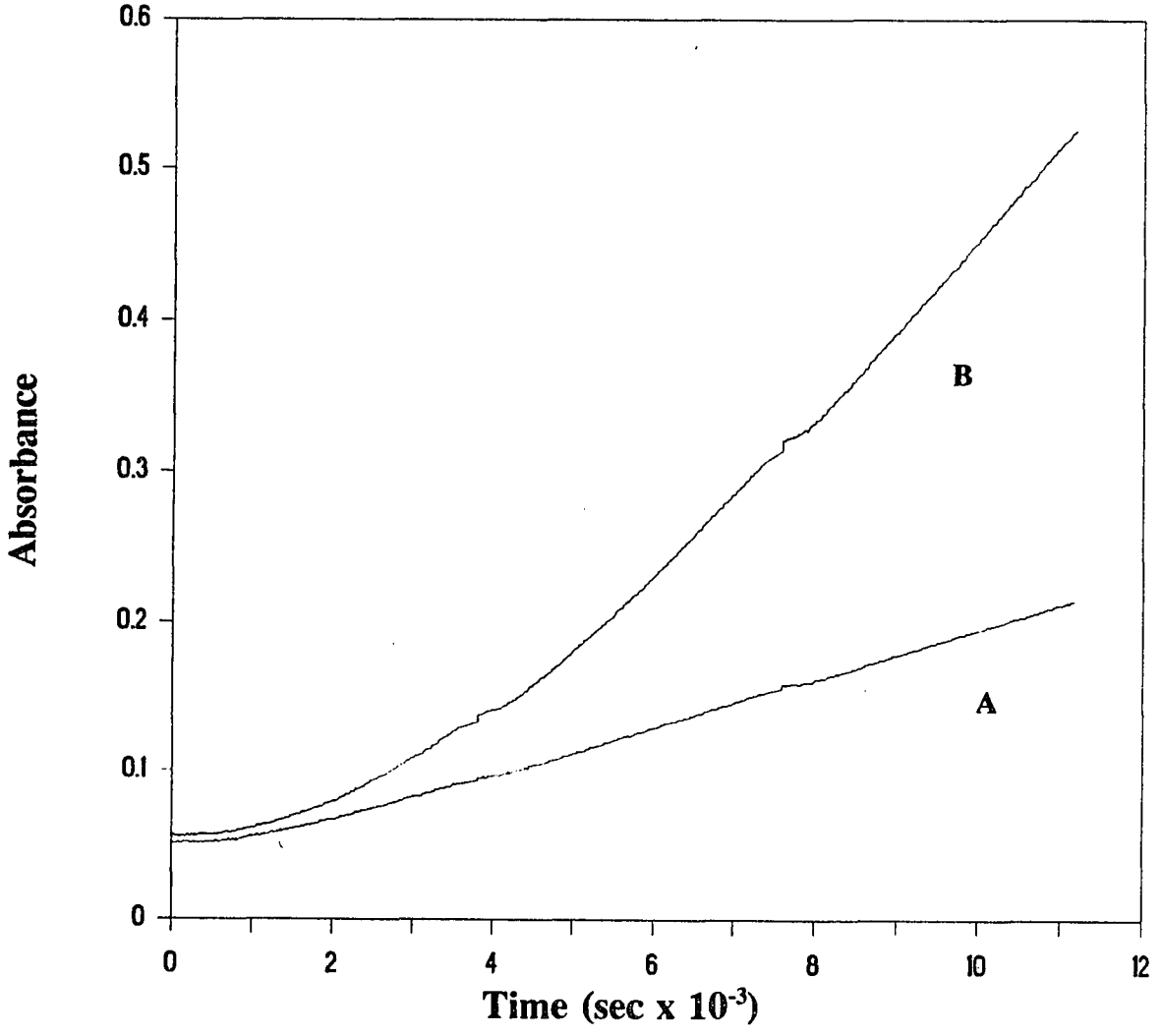

Fig.14 Reactivation of bovine thrombin at pH 7.08.
Curve A is the bovine thrombin catalyzed-hydrolysis of 174.7 μM D-Phe-Pipecolyl-Arg-*p*NA in the presence of 13.3 nM Ac-D-Phe-Pro-boroArg. Curve B is the bovine thrombin catalyzed-hydrolysis of 174.7 μM D-Phe-Pipecolyl-Arg-*p*NA in the presence of 13.3 nM Ac-D-Phe-Pro-boroArg and 20 mM pinanediol. Reaction conditions are given in the text.

shown in Fig.15 suggests that pinanediol prevents the slow inhibition by association with the inhibitor Ac-D-Phe-Pro-boroArg forming the boron-diol complex.

In order to determine the binding constants (K_{diss}) of pinanediol for Ac-D-Phe-Pro-boroArg, the slopes of the steady state of the slow inhibition were calculated from the pseudo-first-order plots. These values are plotted as a function of pinanediol concentration in Fig.16. The hyperbolic relationship is further linearized in Fig.17 for the K_{diss} determination.

Using this method, the complexation between pinanediol and this peptide boronic acid was studied at several pH (Appendix B). It is clear that the binding constants are in the millimole range (Table I). These data confirm that although the boronic acid peptide was synthesized as a pinanediol ester (see material section), it readily dissociated into free boroarginine peptide under the kinetic assay conditions.

pH-Dependent Inhibition of Bovine Thrombin by Ac-D-Phe-Pro-Arg

Inhibition kinetics. In an effort to isolate the effect of boronic acid moiety of Ac-D-Phe-Pro-boroArg, the inhibitory behavior of its control peptide carboxylic acid Ac-D-Phe-Pro-Arg on bovine thrombin was also studied.

Fig.18 shows that Ac-D-Phe-Pro-Arg also exhibits fast and slow inhibition modes indicating that the slow inhibition originates from the peptide sequence. It does not depend on the boronic acid group.

The pH profile for the initial K_i of Ac-D-Phe-Pro-Arg (Fig.19) shows three pKs. pK_1 of 7.10 reflects the ionization of enzyme. pK_2 of 8.00 is consistent with the one observed in the pH dependence of Z-D-Phe-Pro-Arg[69]. This suggests that the peptide

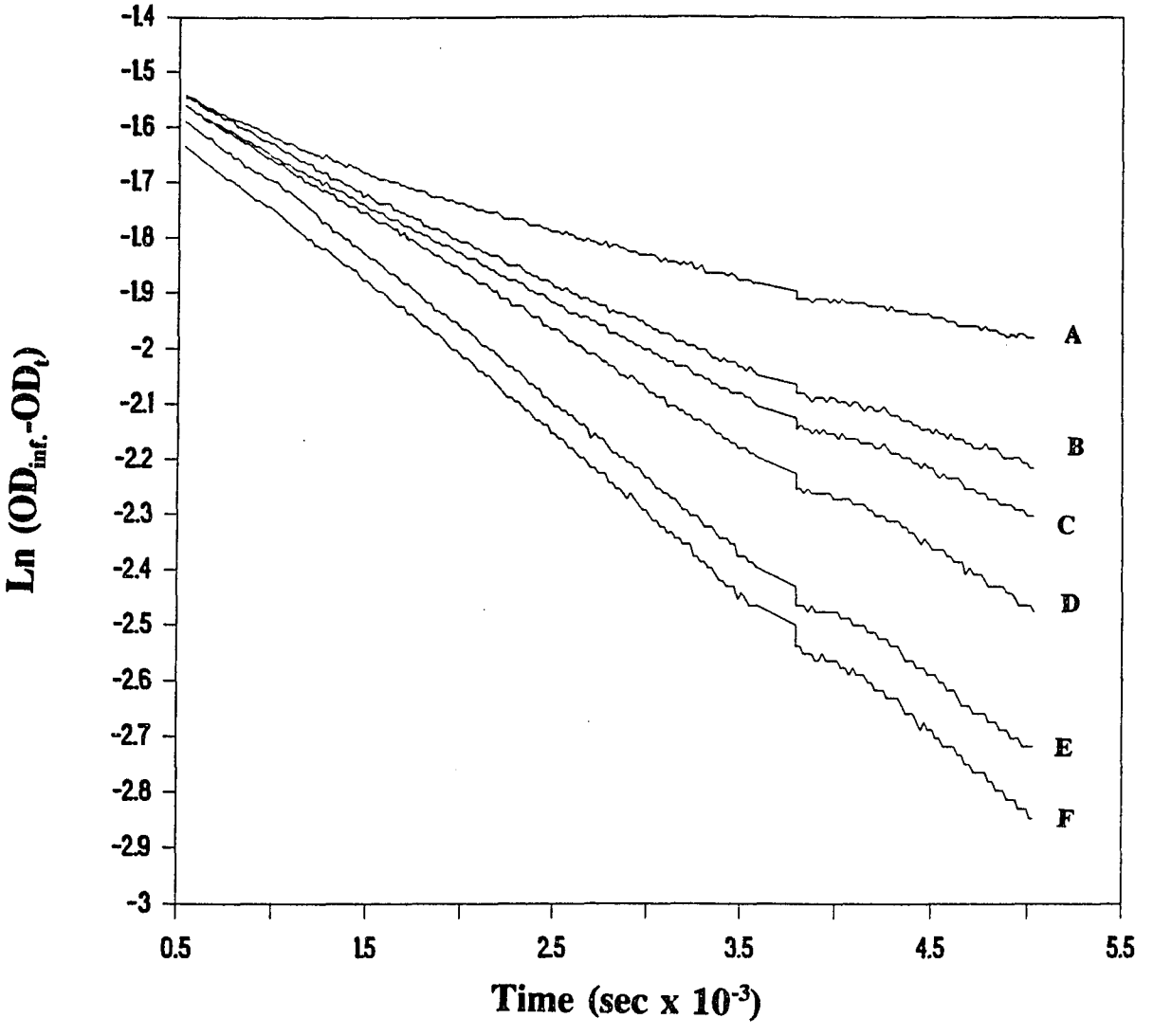

Fig.15 Effect of pinanediol on the slow-binding inhibition of bovine thrombin by Ac-D-Phe-Pro-boroArg at pH 6.45. The substrate was D-Phe-Pipecolyl-Arg-*p*NA.
Curve A is the assay run with 47 μM substrate, 13.3 nM inhibitor. Curve B is the assay run with 47 μM substrate, 13.3 nM inhibitor and 0.313 mM pinanediol. Curve C is the assay run with 47 μM substrate, 13.3 nM inhibitor and 0.625 mM pinanediol. Curve D is the assay run with 47 μM substrate, 13.3 nM inhibitor and 2.50 mM pinanediol. Curve E is the assay run with 47 μM substrate, 13.3 nM inhibitor and 20.0 mM pinanediol. Curve F is the assay run with 47 μM substrate in the absence of inhibitor and pinanediol.
Reaction conditions are given in the text.

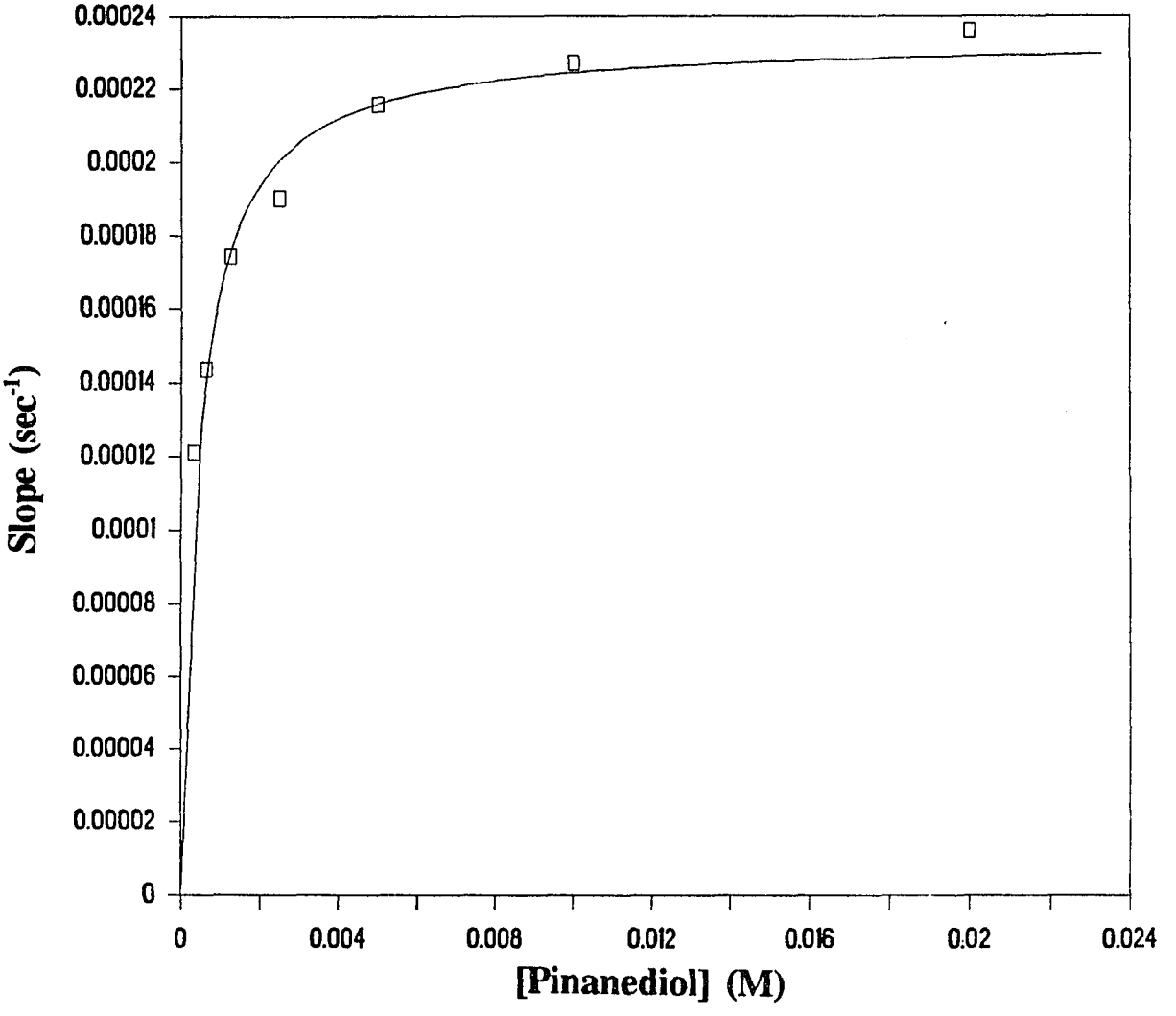

Fig.16 Complexation between pinanediol and Ac-D-Phe-Pro-boroArg at pH 6.45. The enzyme assay was run with 47 μM substrate, D-Phe-Pipecolyl-Arg-*p*NA, 13.3 nM inhibitor.
Reaction conditions are given in the text.
(Data of Table XII Appendix A)

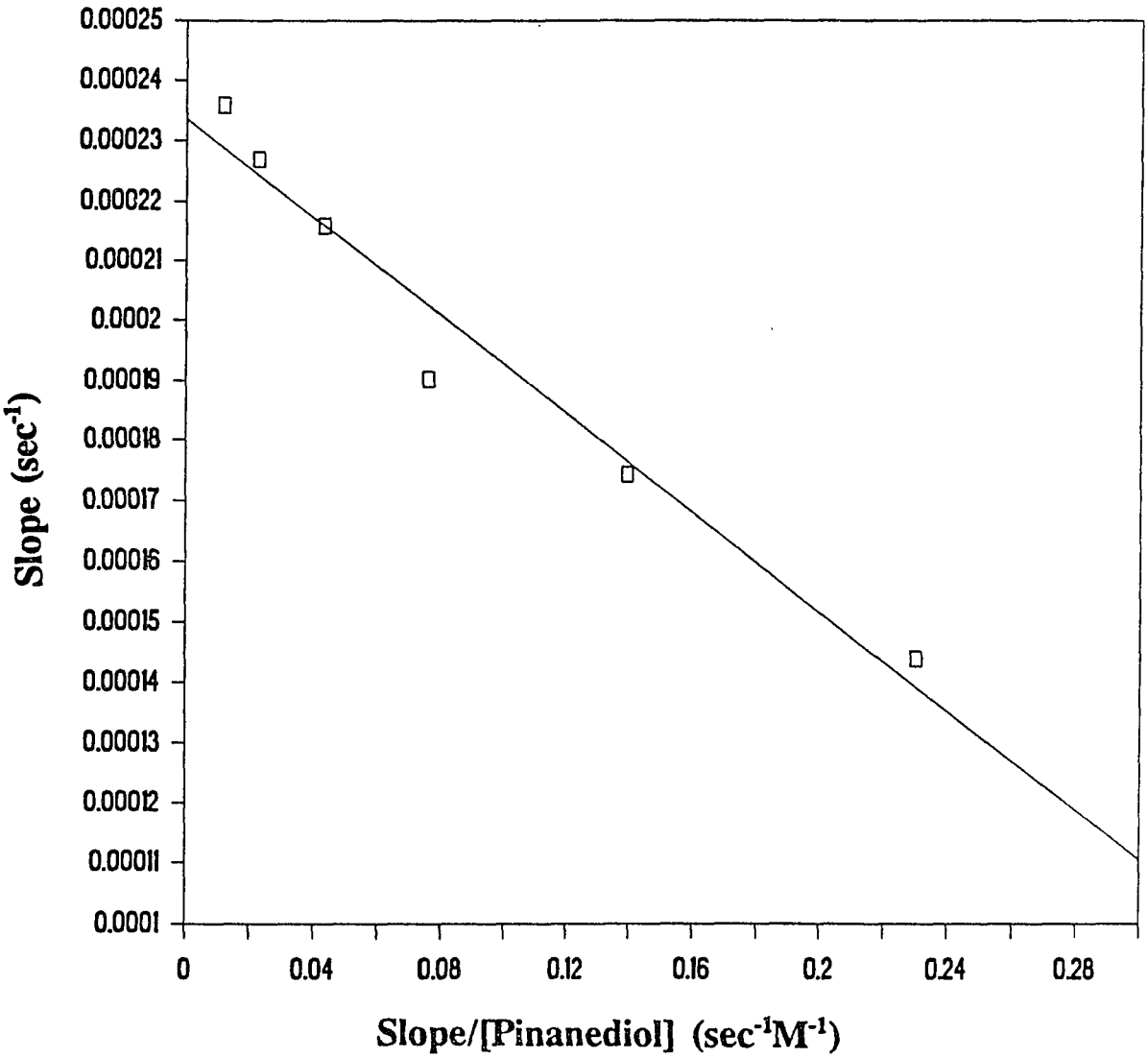

Fig.17 Complexation between pinanediol and Ac-D-Phe-Pro-boroArg at pH 6.45. The enzyme assay was run with 47 μM substrate, D-Phe-Pipecolyl-Arg-*p*NA, 13.3 nM inhibitor. K_{diss} = 0.4105($\pm$0.0408) mM. Reaction conditions are given in the text.
(Data of Table XII Appendix A)

See Appendix B for other similar plots in this system at different pH values.

Table I Dissociation Constants for the Complexation between Ac-D-Phe-Pro-boroArg and Pinanediol [a]

pH	K_{diss} (M)
6.45	4.105×10^{-4} ($\pm 4.08 \times 10^{-5}$)
7.50	1.233×10^{-3} ($\pm 9.54 \times 10^{-5}$)
9.18	1.550×10^{-3} ($\pm 3.90 \times 10^{-4}$)
9.64	1.830×10^{-3} ($\pm 2.41 \times 10^{-4}$)

[a] Reaction conditions are given in the text.

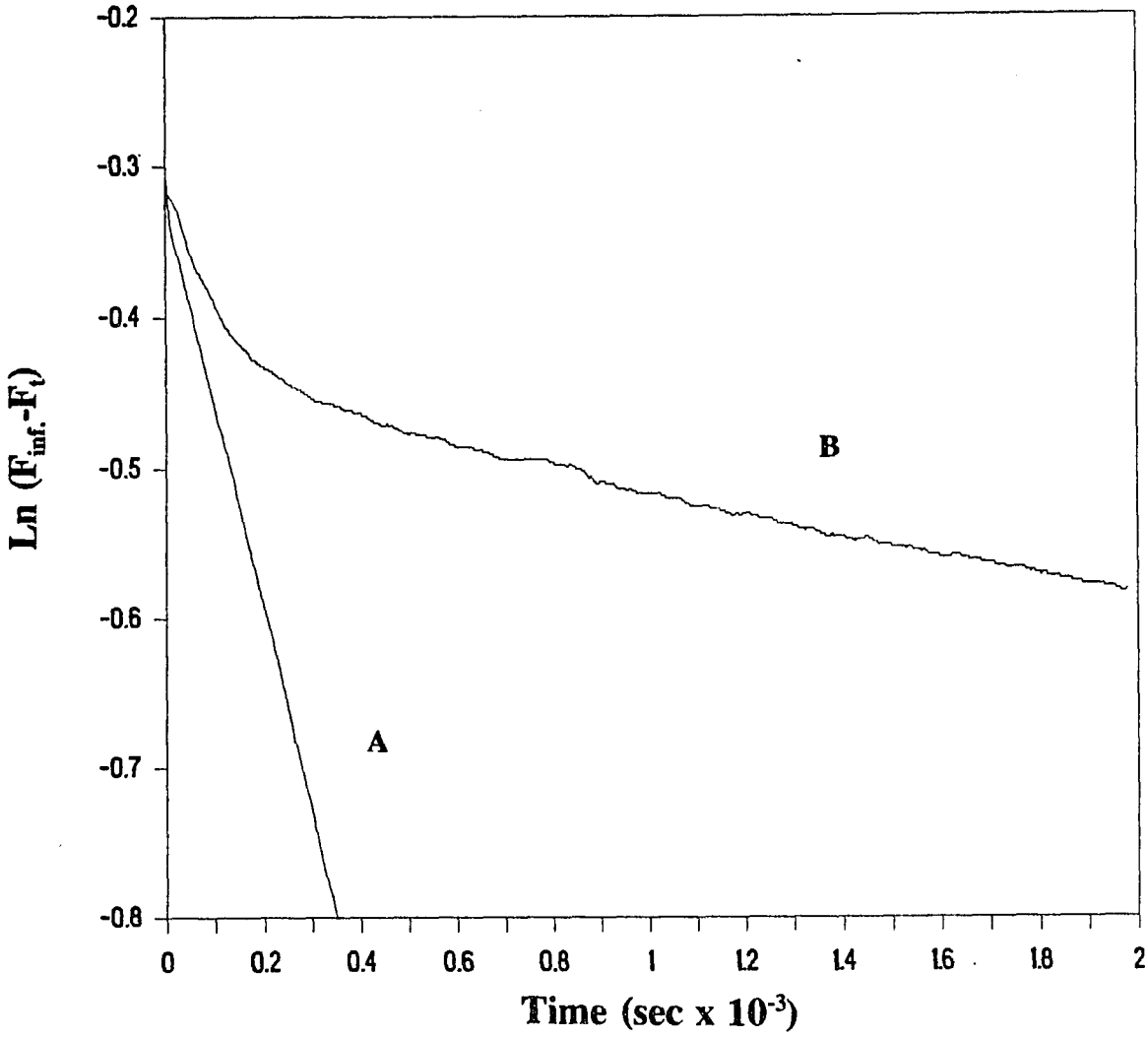

Fig.18 Slow-binding inhibition of bovine thrombin by Ac-D-Phe-Pro-Arg at pH 7.8. Curve A is the bovine thrombin-catalyzed hydrolysis of 0.3896 μM N-t-Boc-Valyl-Prolyl-Arginine-7-AMC.
Curve B is the bovine thrombin-catalyzed hydrolysis of 0.3896 μM N-t-Boc-Valyl-Prolyl-Arginine-7-AMC in the presence of 33.4 μM Ac-D-Phe-Pro-Arg. Reaction conditions are given in the text.

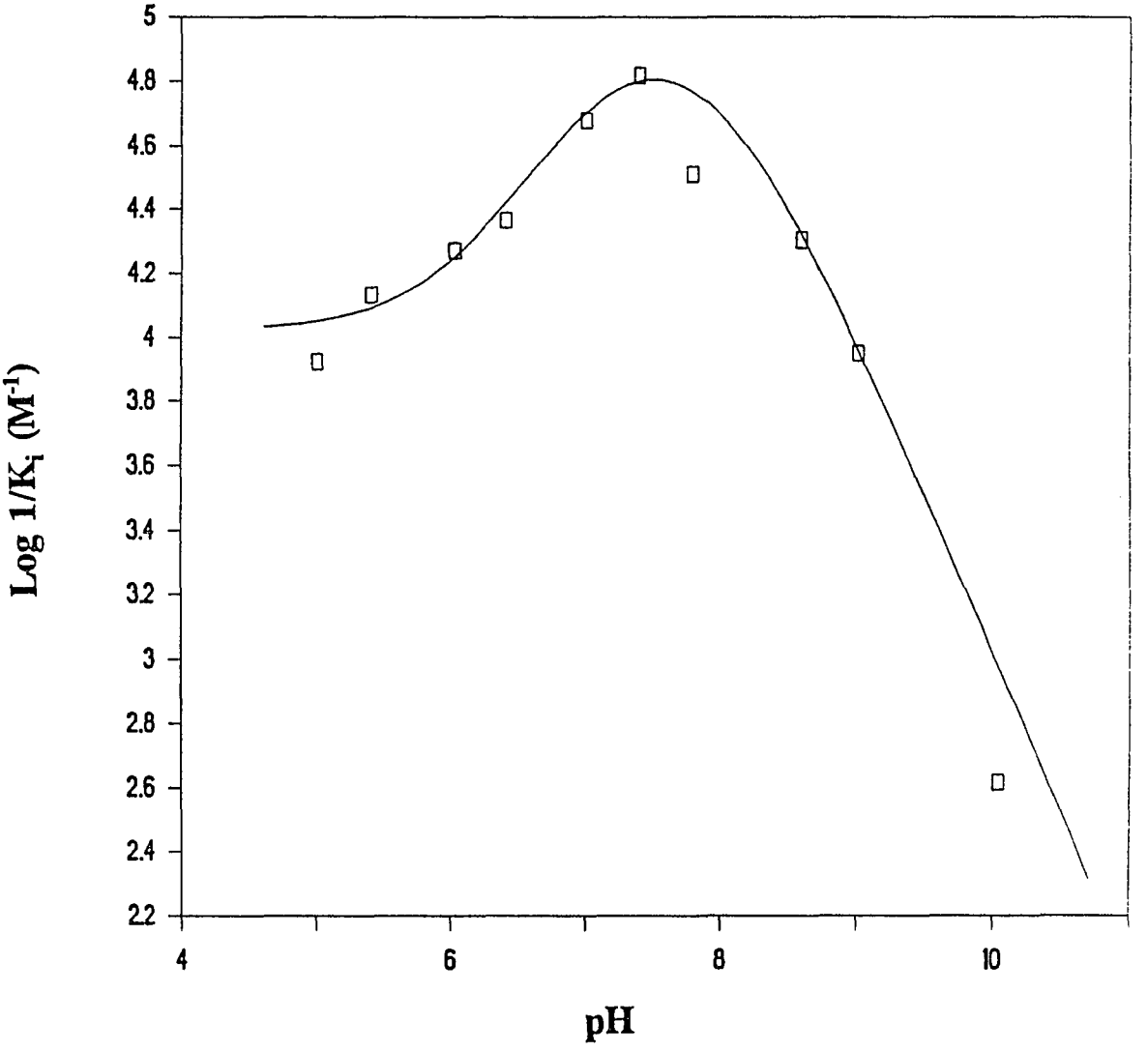

Fig.19 pH profile for the initial inhibition of bovine thrombin by Ac-D-Phe-Pro-Arg. The theoretical curve is drawn using $pK_1 = 7.10(\pm 0.10)$, $pK_2 = 8.00(\pm 0.15)$, $pK_3 = 6.10(\pm 0.15)$, optimum pH $= 7.51(\pm 0.12)$ and $K_i(Lim) = 9.52(\pm 1.05)$ μM. Reaction conditions are given in the (Data of Table XIII Appendix A)

binds in a configuration that places the arginine carboxylate anion away from the active site serine. Wrong-way binding is one possibility. The pK_3 of 6.10 seen here relates to the ionization of the loose binding complex. This behavior is similar to that observed in the fast inhibition of the boronic acid peptide Ac-D-Phe-Pro-boroArg.

Fig.20 shows the pH dependence of the final K_i of Ac-D-Phe-Pro-Arg. In this curve, the pK near 8 seen in the fast inhibition profile exhibits as pK_1 while the enzyme's pK near 7 is shown as pK_2.

The fast inhibition of Ac-D-Phe-Pro-Arg has an optimal pH at 7.51 with the limiting K_i of 9.52 μM. For its slow inhibition, the optimal K_i of 1.32 μM is observed at pH 7.70. These K_i values are much higher than those observed in the boroarginine peptide inhibition suggesting that the presence of boronate group is important for the potent inhibitory effect of the boronic acid peptide.

The pH effects on the transition between the fast and slow binding modes for Ac-D-Phe-Pro-Arg are shown in Fig.21 and Fig.22. It is clear that the pH dependencies for the binding mode conversion seen here are very similar to those observed in the case of the peptide boronic acid Ac-D-Phe-Pro-boroArg. While the conversion from the loose enzyme-inhibitor complex to the tight binding complex depends on pH, its reverse transition process is pH-independent. The values of k_3(Lim)/k_4(Average), the equilibrium constants for the binding mode transition, are 58.5($\pm$35.6) and 27.7($\pm$12.7) for Ac-D-Phe-Pro-boroArg and Ac-D-Phe-Pro-Arg respectively. This suggests that the slow inhibition effects of the peptide boronic acid and its carboxylate analog share a common mechanism. The boronic acid group is not essential for the formation of the tight-binding complexes.

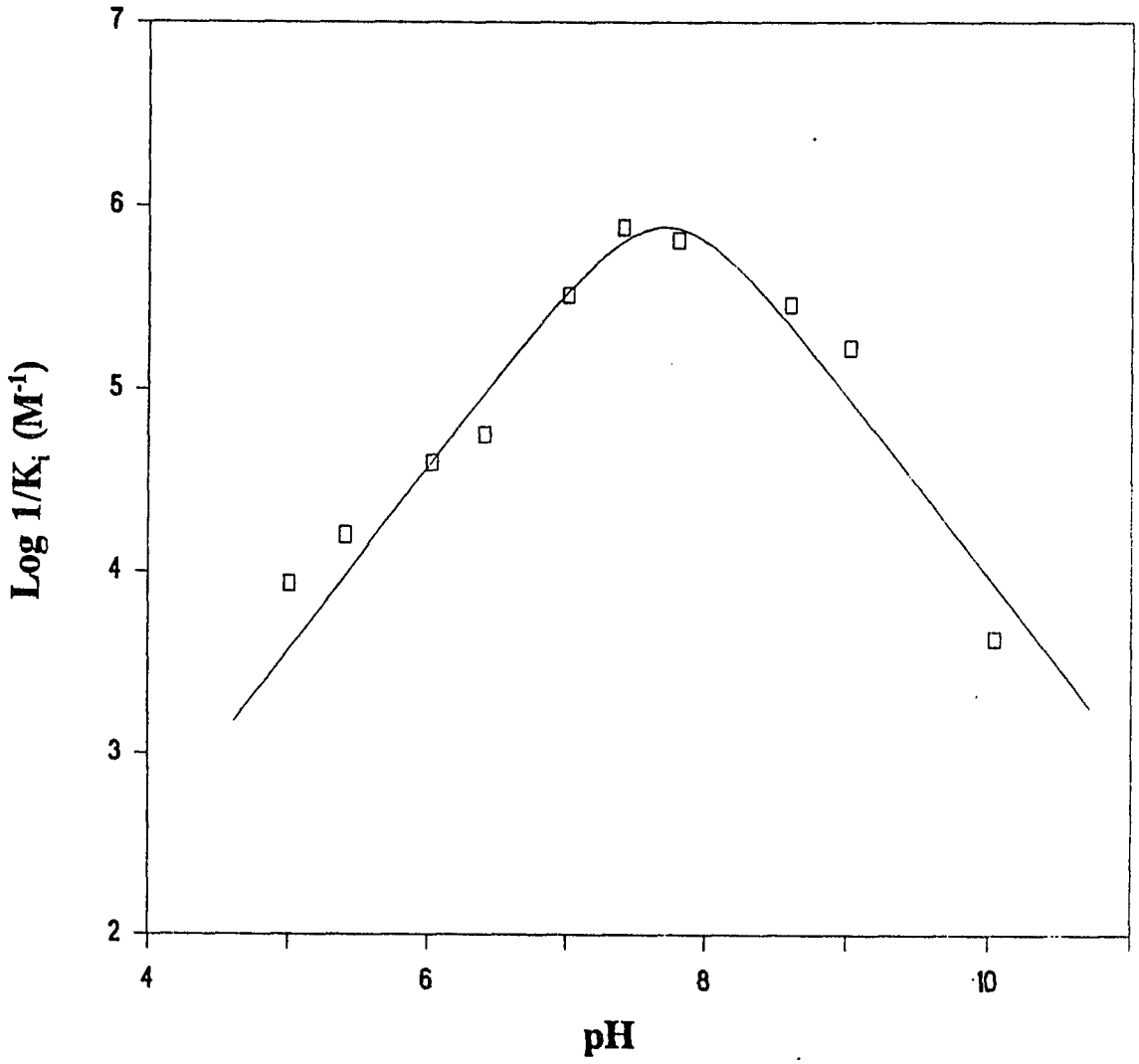

Fig.20 pH profile for the final inhibition of bovine thrombin by Ac-D-Phe-Pro-Arg. The theoretical curve is drawn using $pK_1 = 8.05(\pm 0.15)$, $pK_2 = 7.35(\pm 0.15)$, optimum pH $= 7.70(\pm 0.15)$ and K_i(optimum) $= 1.32(\pm 0.229)$ μM.
Reaction conditions are given in the text.
(Data of Table XIV Appendix A)

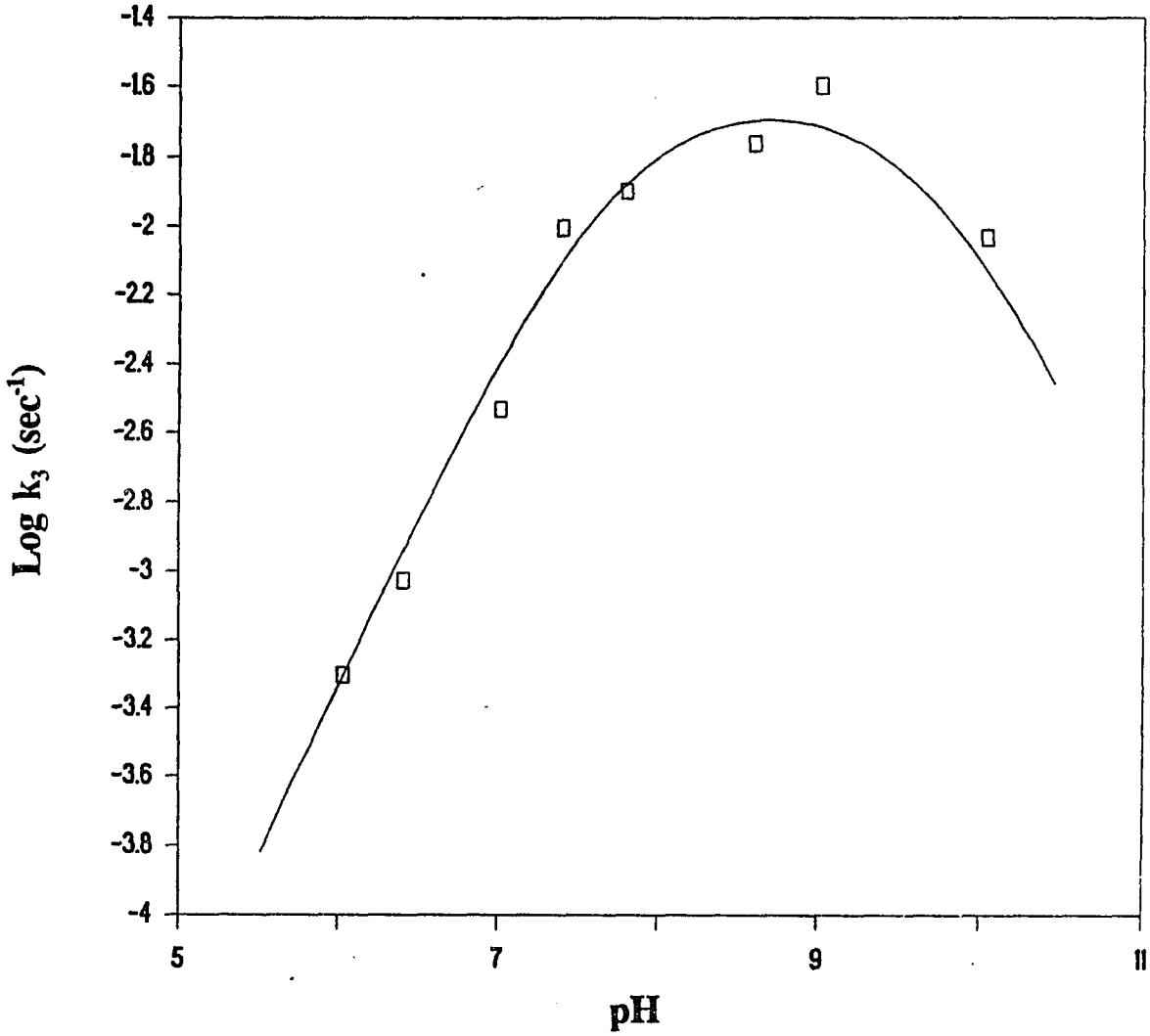

Fig.21 pH profile for the transition from initial inhibition to final inhibition of bovine thrombin by Ac-D-Phe-Pro-Arg. k_3 is the first-order rate constant for the transition from the loose enzyme-inhibitor complex to the tight complex. The theoretical curve is drawn using $pK_1 = 7.72(\pm 0.10)$, $pK_2 = 9.69(\pm 0.15)$, optimum pH $= 8.70(\pm 0.12)$ and $k_3(\text{Lim}) = 2.44\text{x}10^{-2}(\pm 2.88\text{x}10^{-3})$ sec^{-1}.
Reaction conditions are given in the text.
(Data of Table XV Appendix A)

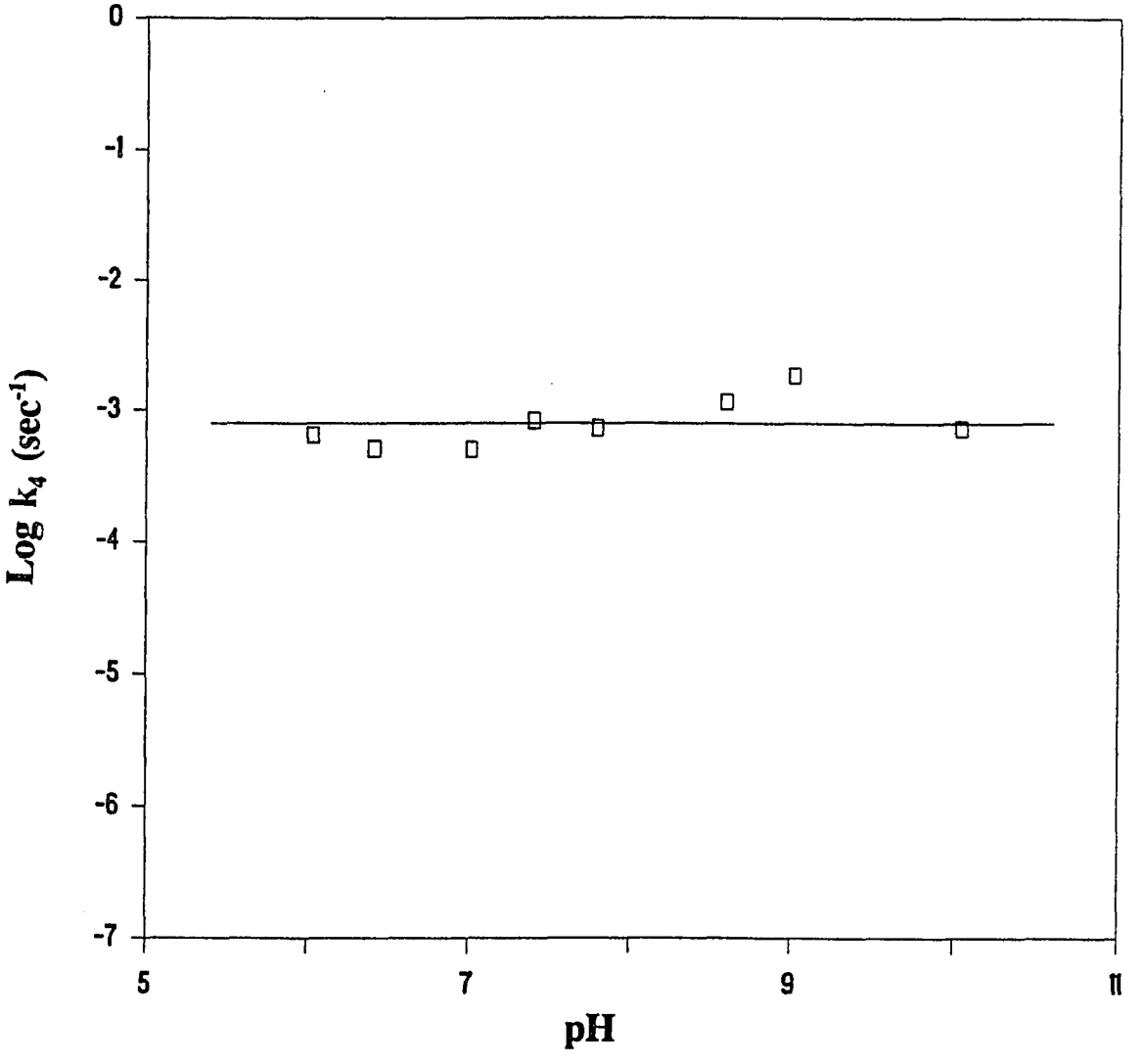

Fig.22 pH profile for the transition from final inhibition to initial inhibition of bovine thrombin by Ac-D-Phe-Pro-Arg. k_4 is the first-order rate constant for the transition from the tight enzyme-inhibitor complex to the loose complex. The theoretical curve is drawn using slope = 0 and average $k_4 = 8.802 \times 10^{-4} (\pm 2.05 \times 10^{-4})$ sec^{-1}.
Reaction conditions are given in the text.
(Data of Table XVI Appendix A)

Solvent deuterium isotope effect. This experiment was done in order to study the proton transfer for this slow inhibition system. The pH profiles of the kinetic constants determined in deuterium oxide are presented in Fig.23, Fig.24, Fig.25 and Fig.26. These results are in good agreement with those obtained in water.

As seen in Table II, the values of K_i(initial), K_i(final) and k_4 measured in H_2O and D_2O are close, but a significant isotope effect is reflected in k_3. The value of k_{3H}/k_{3D} is 2.88($\pm$0.756). It clearly indicates the proton transfer in the fast to slow inhibition transition. The data also further support the pH dependent k_3 and the ionization of the enzyme-inhibitor complex reflected in the pH profile of the loose binding inhibition.

pH-Dependent Inhibition of Bovine Thrombin by Z-D-Phe-Pro-boroMPG and N-(Z-D-Phe-Pro)-2-amino-5-methoxypentanoic acid

Inhibition kinetics for Z-D-Phe-Pro-boroMPG. Z-D-Phe-Pro-boroMPG is a peptide boronic acid containing a neutral side chain at P_1 position. It is a competitive thrombin inhibitor (Fig.27) that only exhibits a rapid binding mode.

The pH profile of K_i for Z-D-Phe-Pro-boroMPG is shown in Fig.28. The best binding of the inhibitor is at pH 8.25 with the limiting K_i of 5.0 nM. The binding is controlled by the pK of enzyme near 7 on one hand and a double proton ionization pK_2 of 9.4 on the other hand. One origin of the double ionization is presumably related to the thrombin's pK_2 near 10 which is seen in the substrate hydrolysis. The other origin of the pK_2 perhaps is related to the ionization of boronic acid.

Inhibition kinetics for N-(Z-D-Phe-Pro)-2-amino-5-methoxypentanoic acid. As a control for the peptide boroMPG, the peptide carboxylic acid, N-(Z-D-Phe-Pro)-2-

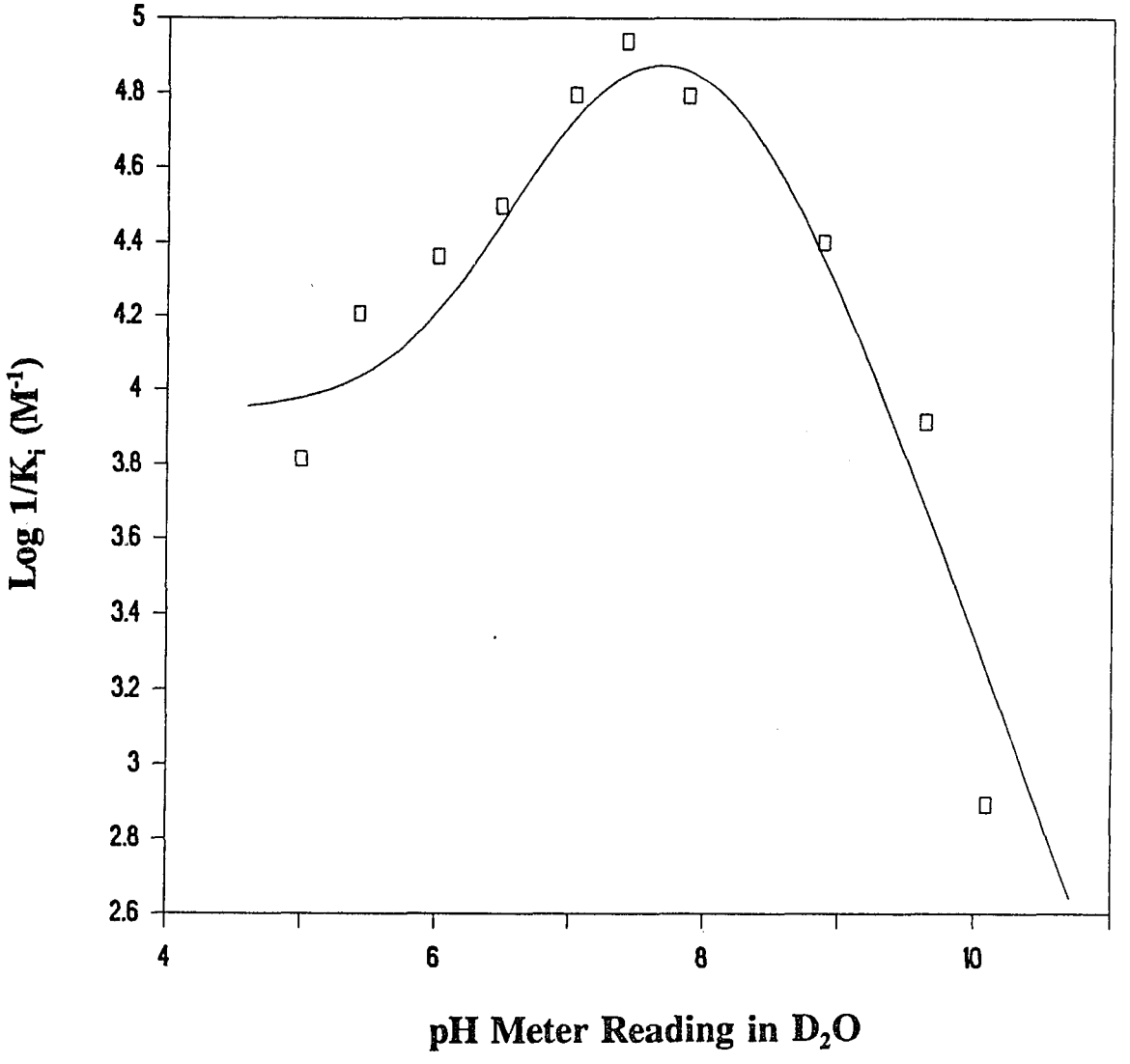

Fig.23 pH profile for the initial inhibition of bovine thrombin by Ac-D-Phe-Pro-Arg in deuterium oxide buffer. The theoretical curve is drawn using $pK_1 = 7.10(\pm 0.15)$, $pK_2 = 8.30(\pm 0.15)$, $pK_3 = 6.00(\pm 0.15)$, optimum pH = $7.70(\pm 0.15)$ and $K_i(Lim) = 9.09(\pm 1.95)$ μM. Reaction conditions are given in the text.
(Data of Table XVII Appendix A)

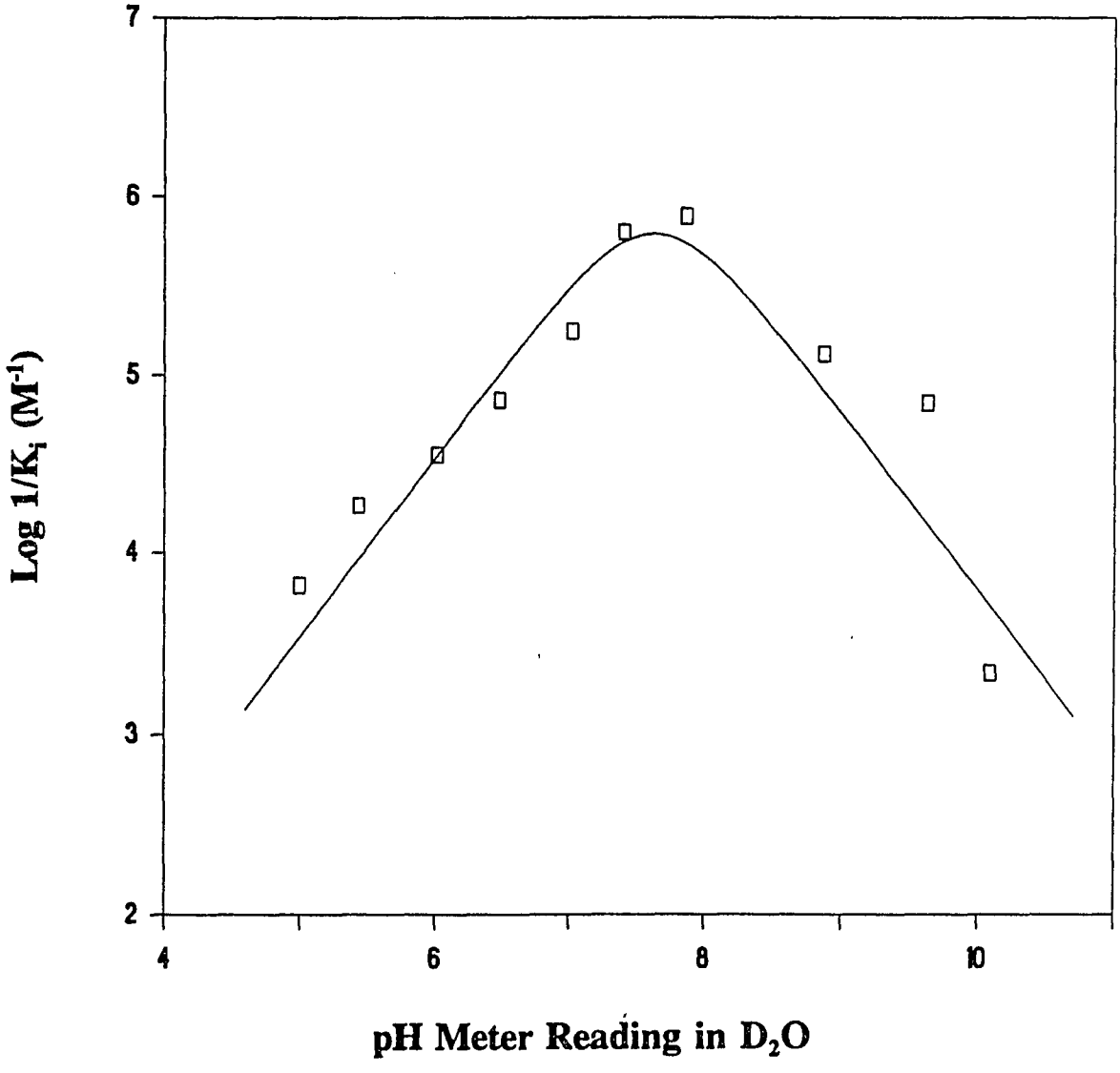

Fig.24 pH profile for the final inhibition of bovine thrombin by Ac-D-Phe-Pro-Arg in deuterium oxide buffer. The theoretical curve is drawn using pK_1 = 8.04($\pm$0.15), pK_2 = 7.22($\pm$0.20), optimum pH = 7.63($\pm$0.17) and K_i(optimum) = 1.63($\pm$0.334) μM.
Reaction conditions are given in the text.
(Data of Table XVIII Appendix A)

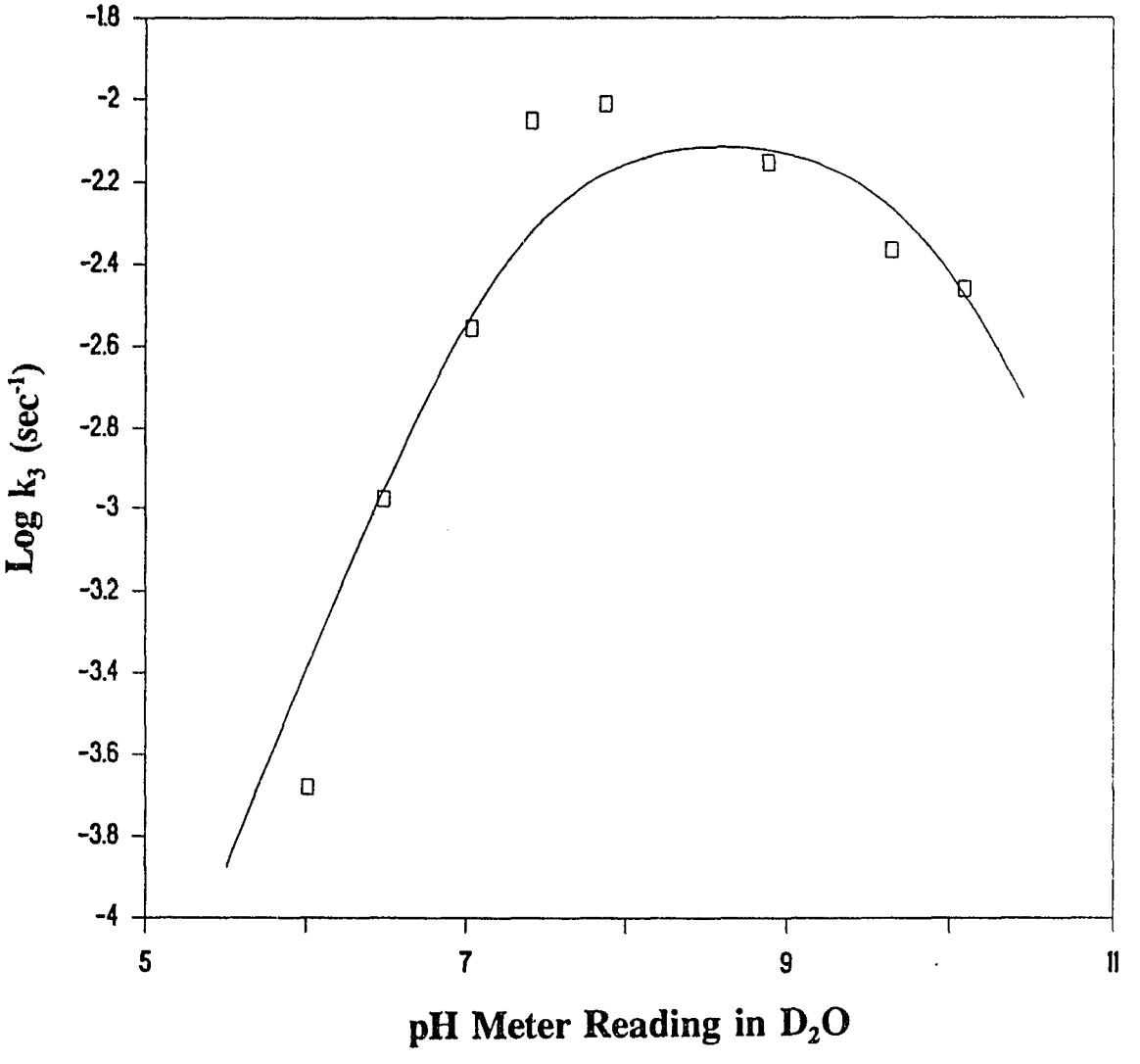

Fig.25 pH profile for the transition from initial inhibition to final inhibition of bovine thrombin by Ac-D-Phe-Pro-Arg in deuterium oxide buffer. k_3 is the first-order rate constant for the transition from the loose enzyme-inhibitor complex to the tight complex. The theoretical curve is drawn using $pK_1 = 7.30(\pm 0.15)$, $pK_2 = 9.90(\pm 0.20)$,
optimum pH = $8.60(\pm 0.17)$ and $k_3(Lim) = 8.48 \times 10^{-3}(\pm 9.73 \times 10^{-4})$ sec^{-1}.
Reaction conditions are given in the text.
(Data of Table XIX Appendix A)

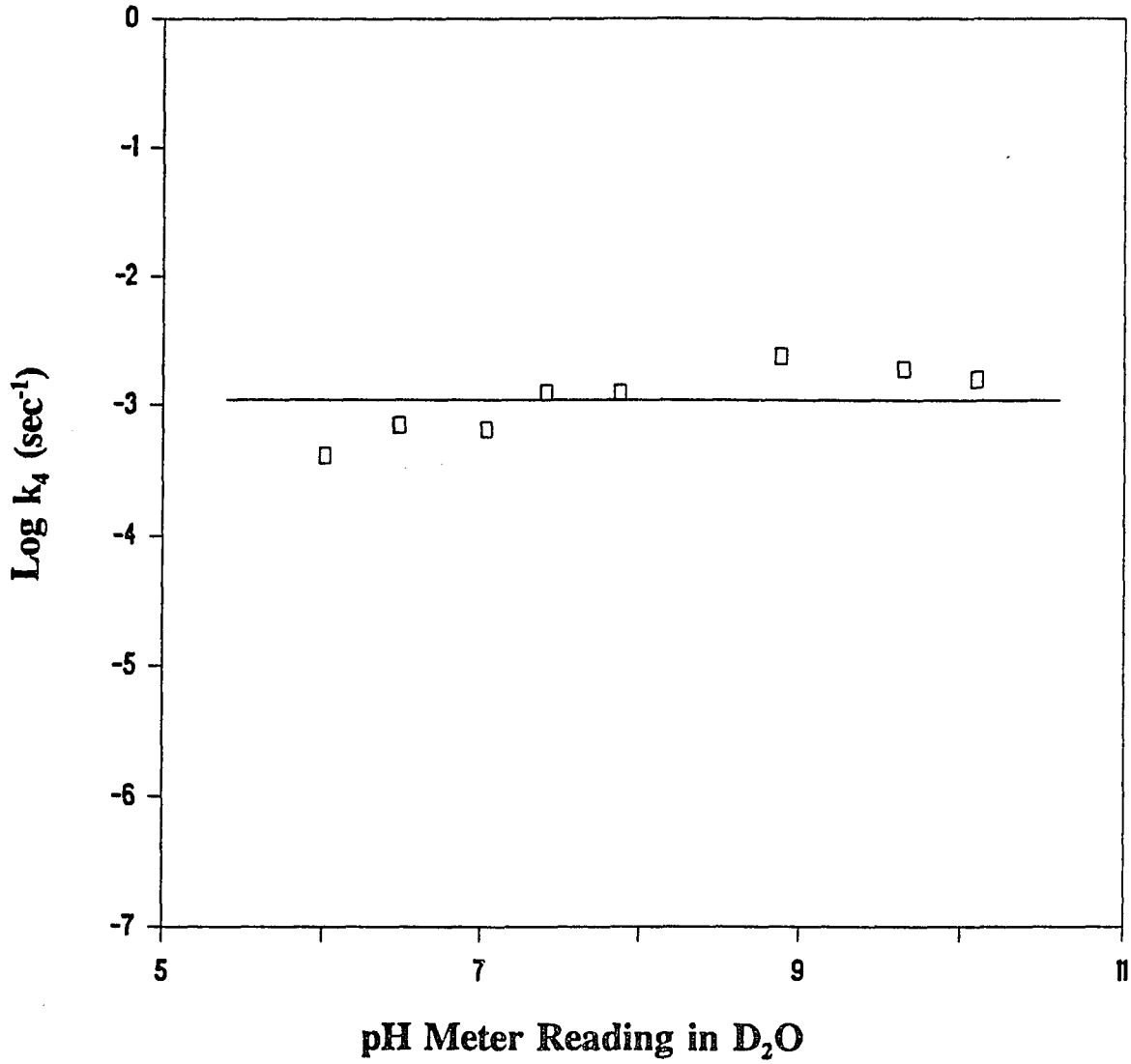

Fig.26 pH profile for the transition from final inhibition to initial inhibition of bovine thrombin by Ac-D-Phe-Pro-Arg in deuterium oxide buffer. k_4 is the first-order rate constant for the transition from the tight enzyme-inhibitor complex to the loose complex. The theoretical curve is drawn using slope = 0 and average $k_4 = 1.29 \times 10^{-3} (\pm 5.75 \times 10^{-4})$ sec^{-1}.
Reaction conditions are given in the text.
(Data of Table XX Appendix A)

Table II Deuterium Isotope Effect on the

Inhibition of Bovine Thrombin by Ac-D-Phe-Pro-Arg [a]

Solvent	$K_{i(initial)}$(Lim) (M)	$K_{i(final)}$(Opt.) (M)	k_3(Lim) (sec^{-1})	k_4(Average) (sec^{-1})
D_2O	9.09×10^{-6} ($\pm1.95\times10^{-6}$)	1.63×10^{-6} ($\pm3.34\times10^{-7}$)	8.48×10^{-3} ($\pm9.73\times10^{-4}$)	1.29×10^{-3} ($\pm5.75\times10^{-4}$)
H_2O	9.52×10^{-6} ($\pm1.05\times10^{-6}$)	1.32×10^{-6} ($\pm2.29\times10^{-7}$)	2.44×10^{-2} ($\pm2.88\times10^{-3}$)	8.80×10^{-4} ($\pm2.05\times10^{-4}$)

[a] Reaction conditions are given in the text.

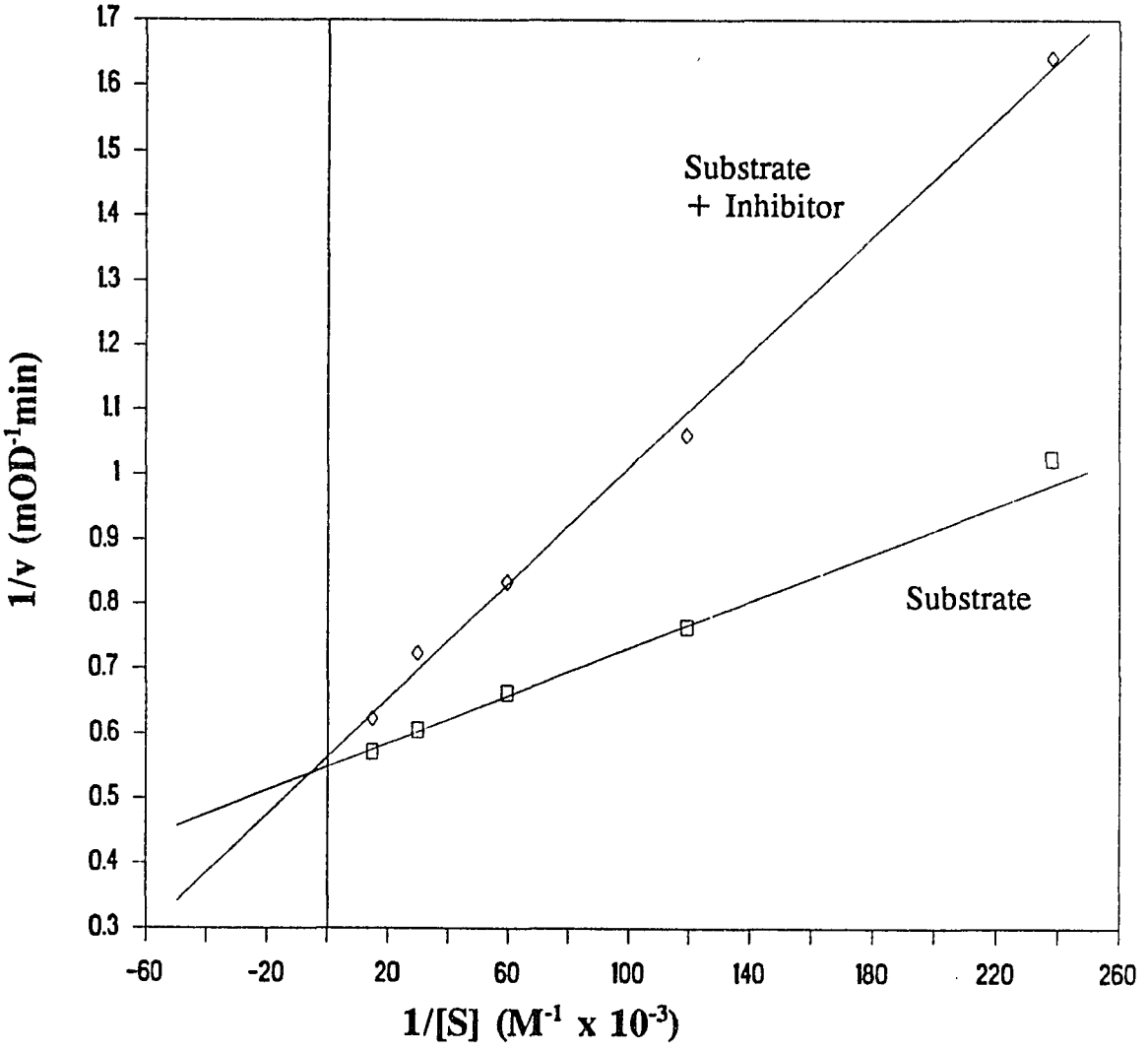

Fig.27 Inhibition of bovine thrombin by Z-D-Phe-Pro-boroMPG at pH 7.4. [inhibitor] = 3.15×10^{-8} M, the substrate was D-Phe-Pipecolyl-Arg-*p*NA. K_i = 21.6($\pm$2.34) nM, K_m = 3.32($\pm$0.151) μM. Reaction conditions are given in the text. (Data of Table XXI Appendix A)

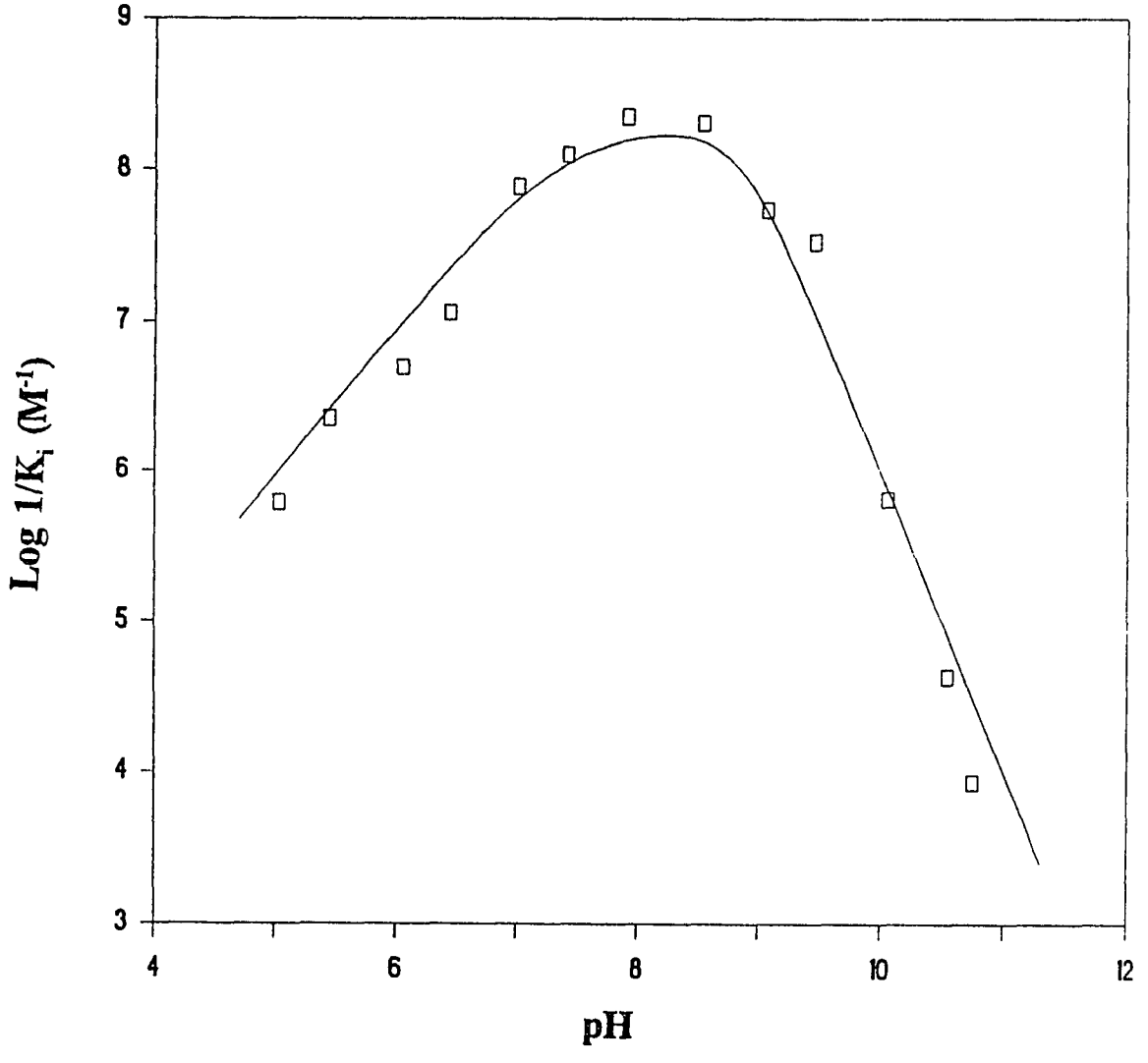

Fig.28 pH profile for inhibition of bovine thrombin by Z-D-Phe-Pro-boroMPG. The theoretical curve is drawn using $pK_1 = 7.33(\pm 0.15)$, a double ionization $pK_2 = 9.40(\pm 0.15)$, optimum pH = $8.25(\pm 0.15)$ and $K_i(Lim) = 5.00 \times 10^{-9}(\pm 1.70 \times 10^{-9})$ M.
Reaction conditions are given in the text.
(Data of Table XXII Appendix A)

amino-5-methoxypentanoic acid, also shows competitive inhibition on bovine thrombin (Fig.29). It inhibits rapidly and reversibly without slow-binding component.

The inhibition pH profile for N-(Z-D-Phe-Pro)-2-amino-5-methoxypentanoic acid (Fig.30) not only exhibits the two pKs of thrombin but also shows a pK of the enzyme-inhibitor complex (pK_3 of 7.05). The ionization of the binding complex observed here does not exist in the case of Z-D-Phe-Pro-boroMPG inhibition.

While the optimal pH values for the inhibition of bovine thrombin by the peptide boroMPG and its peptide carboxylate analog are similar (near pH 8.3), the latter has a limiting K_i of 0.167 mM which is about 30,000-fold higher than that for the peptide boroMPG (Ki(Lim) = 5 nM). The results clearly demonstrate that the high binding affinity of the peptide boronic acid results from the boronic acid moiety.

Selectivity of the Peptide Boronic Acids

In order to compare the properties of Ac-D-Phe-Pro-boroArg and Z-D-Phe-Pro-boroMPG, their inhibitory effects on other serine proteases related to the blood coagulation cascade were determined at pH 7.4 (Appendix C). The kinetic constants measured using initial rate data are presented Table III. The selectivity of the two inhibitors are compared in Fig.31. Both peptidyl boronic acids exhibit prompt inhibition on thrombin with similar potency. However, a large difference was observed between the boroMPG and the boroArg in the inhibition of plasmin and urokinase, the two enzymes involved in the hydrolysis of blood clots. Since Ac-D-Phe-Pro-boroArg not only strongly inhibits thrombin but also shows significant binding affinity to plasmin and urokinase, the boroArg peptide may act to inhibit both clot formation and clot

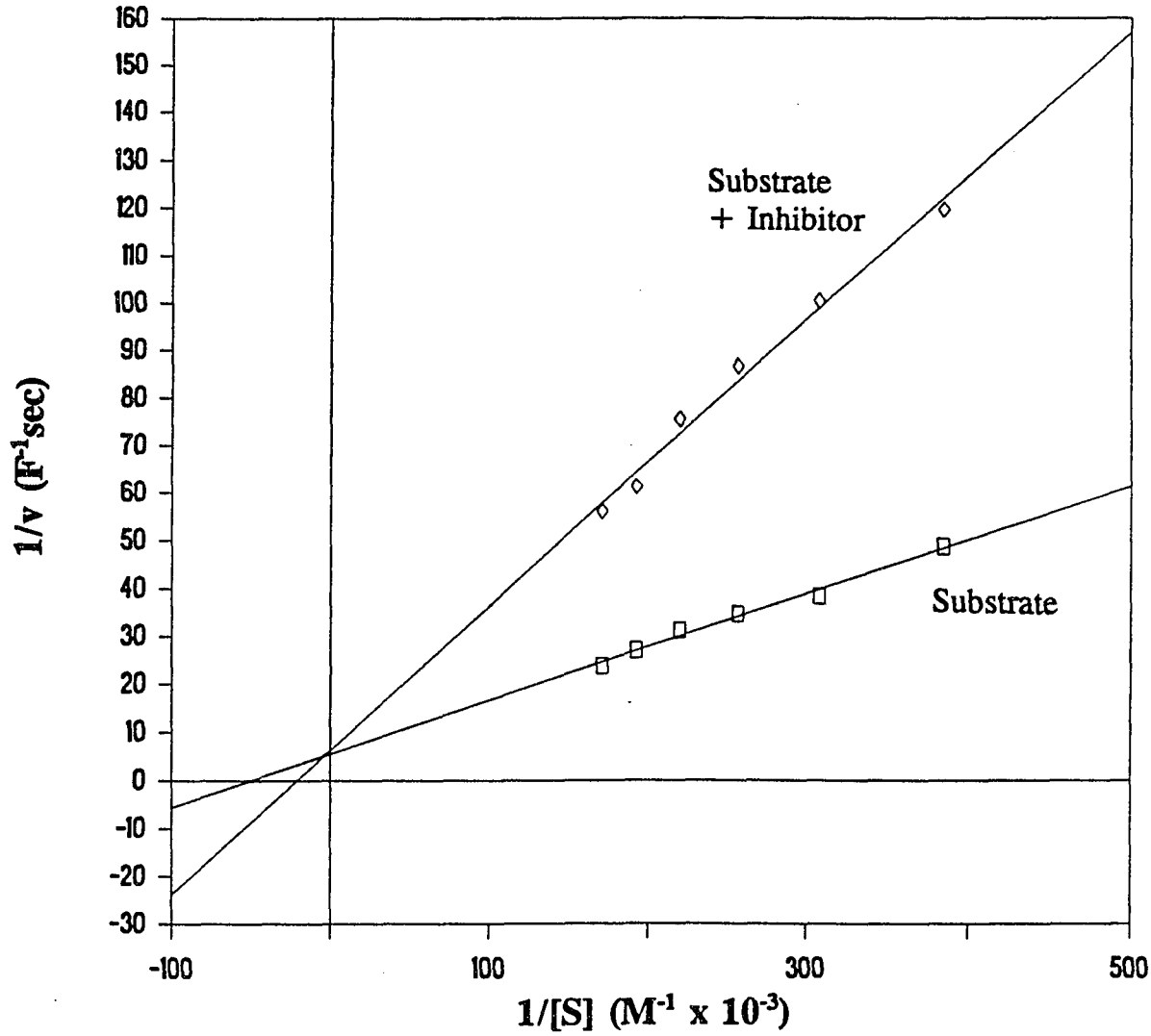

Fig.29 Inhibition of bovine thrombin by N-(Z-D-Phe-Pro)-2-amino-5-methoxypentanoic acid at pH 7.1. [inhibitor] = 4.06×10^{-4} M, the substrate was N-t-Boc-Valyl-Prolyl-Arginine-7-AMC. K_i = 0.237($\pm$0.0372) mM, K_m = 19.9($\pm$5.88) μM. Reaction conditions are given in the text. (Data of Table XXIII Appendix A)

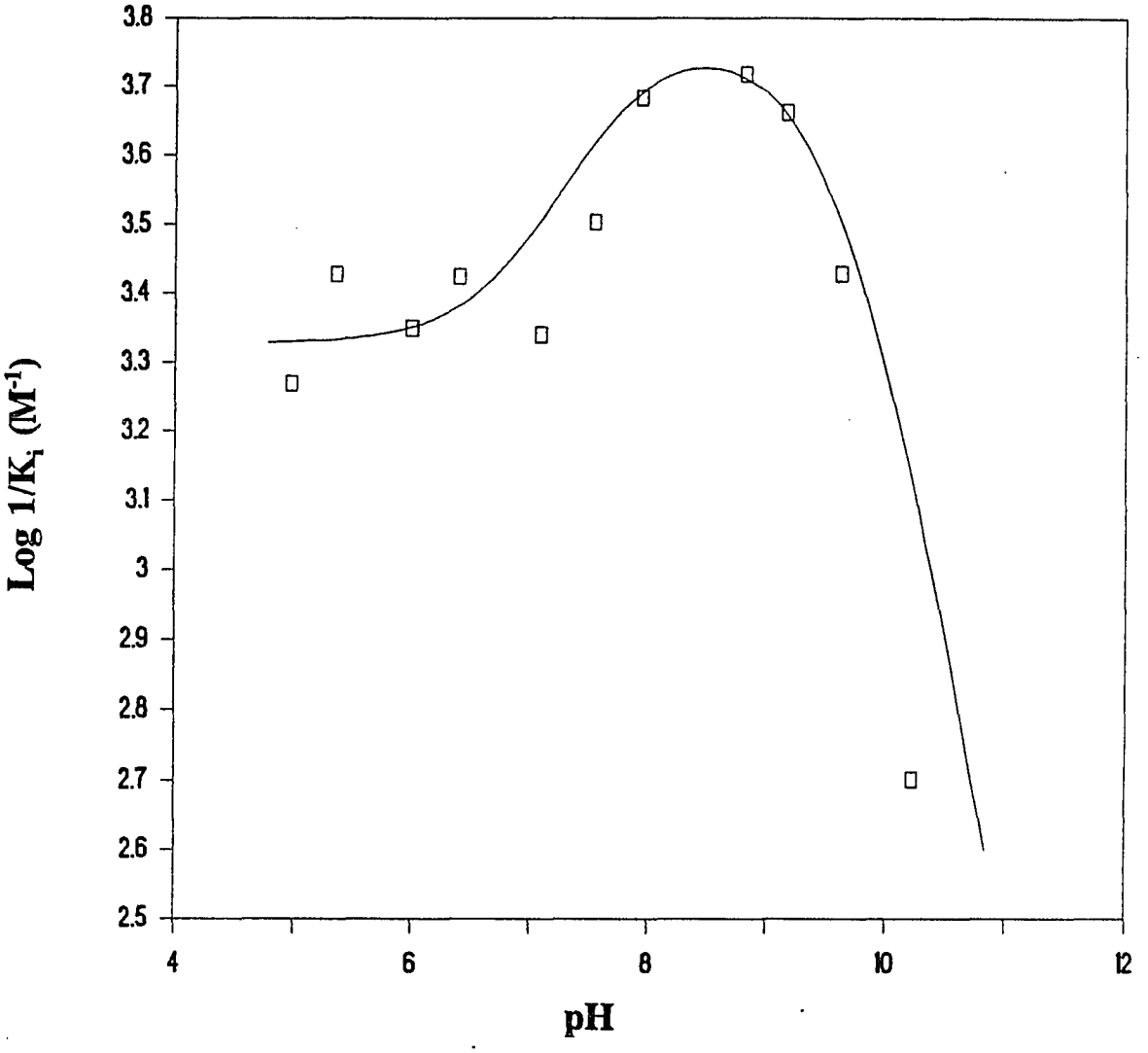

Fig.30 pH profile for inhibition of bovine thrombin by N-(Z-D-Phe-Pro)-2-amino-5-methoxypentanoic acid. The theoretical curve is drawn using $pK_1 = 7.50(\pm 0.25)$, $pK_2 = 9.68(\pm 0.20)$, $pK_3 = 7.05(\pm 0.20)$, optimum pH = $8.48(\pm 0.22)$ and $K_i(Lim) = 1.67 \times 10^{-4}(\pm 1.28 \times 10^{-5})$ M. Reaction conditions are given in the text.
(Data of Table XXIV Appendix A)

Table III Inhibition of Plasma Serine Proteases

by Peptide Boronic Acids at pH 7.4 [a]

Enzyme	Inhibitor	Inhibition Type	K_i(initial)
Thrombin	Ac-D-Phe-Pro-boroArg	competitive	5.48×10^{-9} M ($\pm9.26\times10^{-10}$)
	Z-D-Phe-Pro-boroMPG	competitive	2.16×10^{-8} M ($\pm2.34\times10^{-9}$)
Factor Xa	Ac-D-Phe-Pro-boroArg	competitive	5.88×10^{-8} M ($\pm8.85\times10^{-9}$)
	Z-D-Phe-Pro-boroMPG	competitive	1.23×10^{-5} M ($\pm1.97\times10^{-6}$)
Kallikrein	Ac-D-Phe-Pro-boroArg	competitive	8.11×10^{-7} M ($\pm1.25\times10^{-7}$)
	Z-D-Phe-Pro-boroMPG	competitive	7.73×10^{-5} M ($\pm2.00\times10^{-5}$)
Urokinase	Ac-D-Phe-Pro-boroArg	competitive	1.08×10^{-8} M ($\pm1.56\times10^{-9}$)
	Z-D-Phe-Pro-boroMPG	competitive	2.75×10^{-5} M ($\pm5.30\times10^{-6}$)
Plasmin	Ac-D-Phe-Pro-boroArg	competitive	2.25×10^{-8} M ($\pm3.16\times10^{-9}$)
	Z-D-Phe-Pro-boroMPG	mixed inhibition	2.37×10^{-5} M ($\pm3.90\times10^{-6}$) (from slope)
			2.49×10^{-6} M ($\pm2.24\times10^{-7}$) (from 1/v intercept)

[a] Reaction conditions are given in the text.

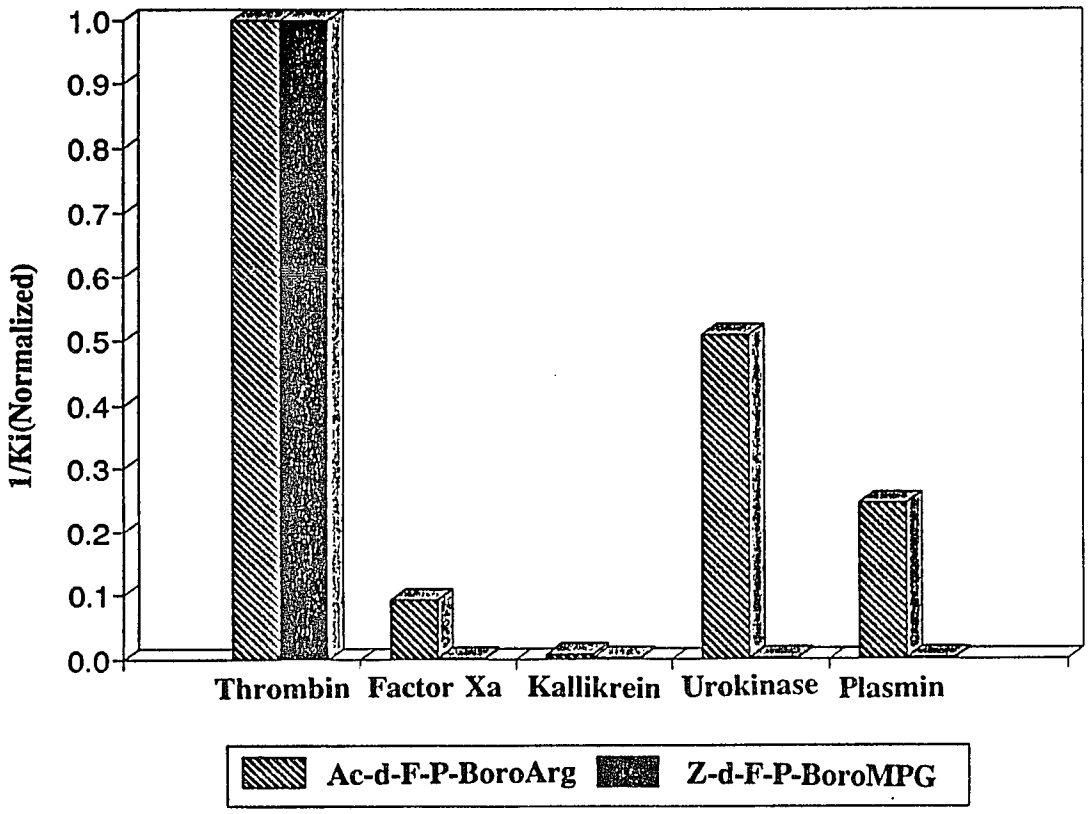

Fig.31 Inhibition of plasma serine proteases by peptide boronic acids at pH 7.4. Reaction conditions are given in the text.
(Data of Table III Part I)

dissolution. In contrast, Z-D-Phe-Pro-boroMPG acts only as an anticoagulant. It clearly has much higher selectivity than Ac-D-Phe-Pro-boroArg in inhibiting thrombin over other hemostatic coagulation factors.

pH-Dependent Inhibition of Bovine Thrombin by N^{α}-(2-naphthalenesulfonylglycyl)-4-amidino-D,L-phenylalaninepiperidide

N^{α}-(2-naphthalenesulfonylglycyl)-4-amidino-D,L-phenylalaninepiperidide (NAPAP) is a peptide carboxamide which was first studied by Stürzebecher *et al*[41]. This compound competitively inhibits thrombin (Fig.32) and binds in a pH-dependent manner (Fig.33). The best binding is at pH 8.50 with the limiting K_i of 3 nM.

The presence of the pK_1 of 7.15 demonstrates that the active site histidine side chain must be deprotonated for the inhibitor to bind. In the crystal structure for the NAPAP-thrombin complex[43,76], the active site's histidine side chain is bound to the inhibitor's piperidide group. Protonation of the histidine clearly destroys this association. This explanation has also been applied to the differential binding behavior of substrates[70].

The alkaline part of the profile appears to be a composite of the enzyme's pK_2 near 10 and the pK resulting from ionization of the inhibitor's sulfonamide NH group. This is suggested by the good fit to the slope of -2 in the theoretical curve used. The sulfonamide pK, measured by spectrophotometric titration at 247 nm (Fig.34), is 9.44. This value is compatible to the value of 9.9 previously determined for L-1-chloro-3-tosylamido-4-phenyl-2-butanone (TPCK)[49], which, while a different compound, also contains the ionizable aryl sulfonamide NH group.

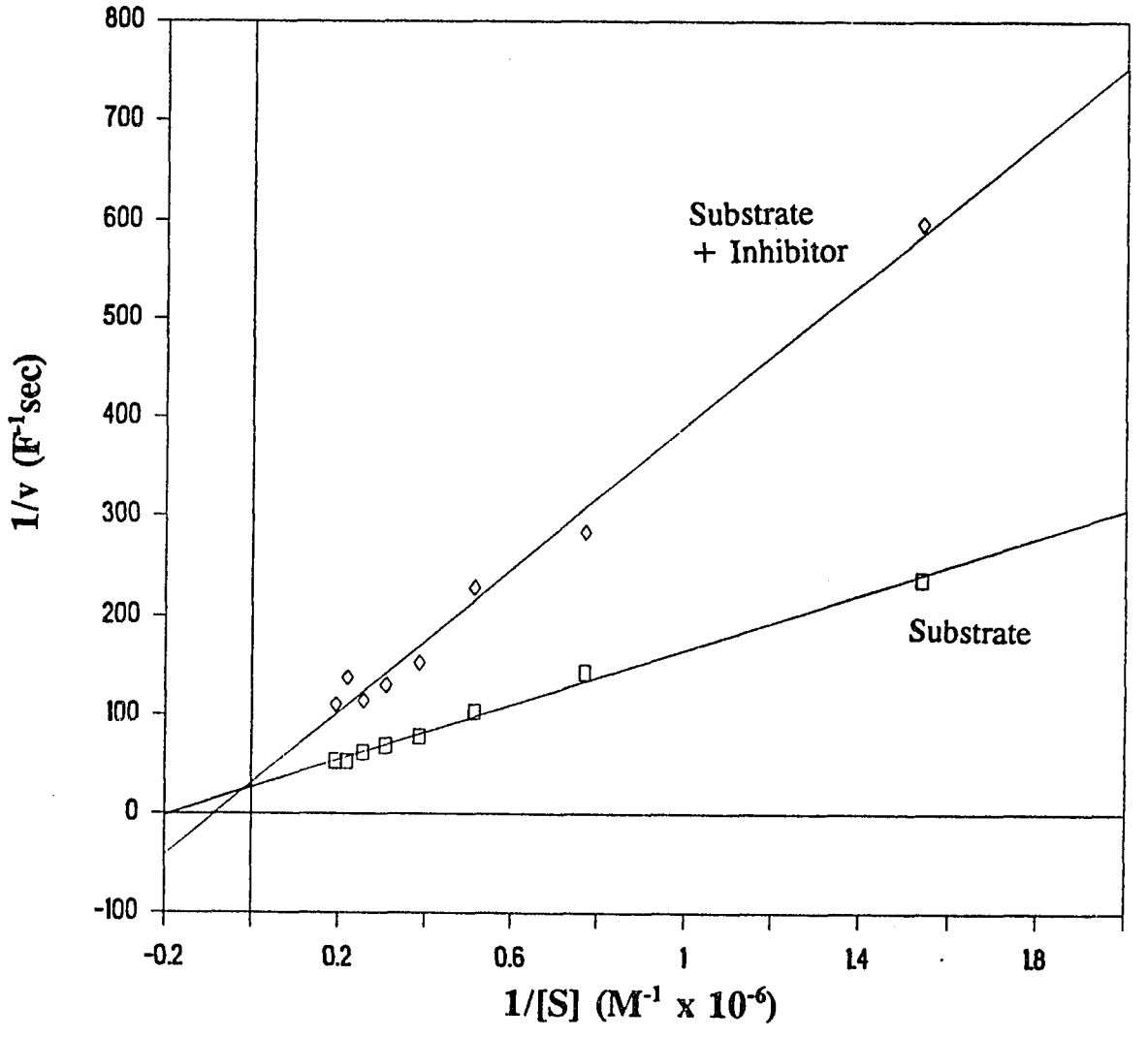

Fig.32 Inhibition of bovine thrombin by N^{α}-(2-naphthalenesulfonylglycyl)-4-amidino-D,L-phenylalaninepiperidide (NAPAP) at pH 7.8.
[inhibitor] = 4.0×10^{-9} M, the substrate was N-t-Boc-Valyl-Prolyl-Arginine-7-AMC. K_i = 2.52($\pm$0.285) nM, K_m = 5.36($\pm$1.50) μM.
Reaction conditions are given in the text.
(Data of Table XXV Appendix A)

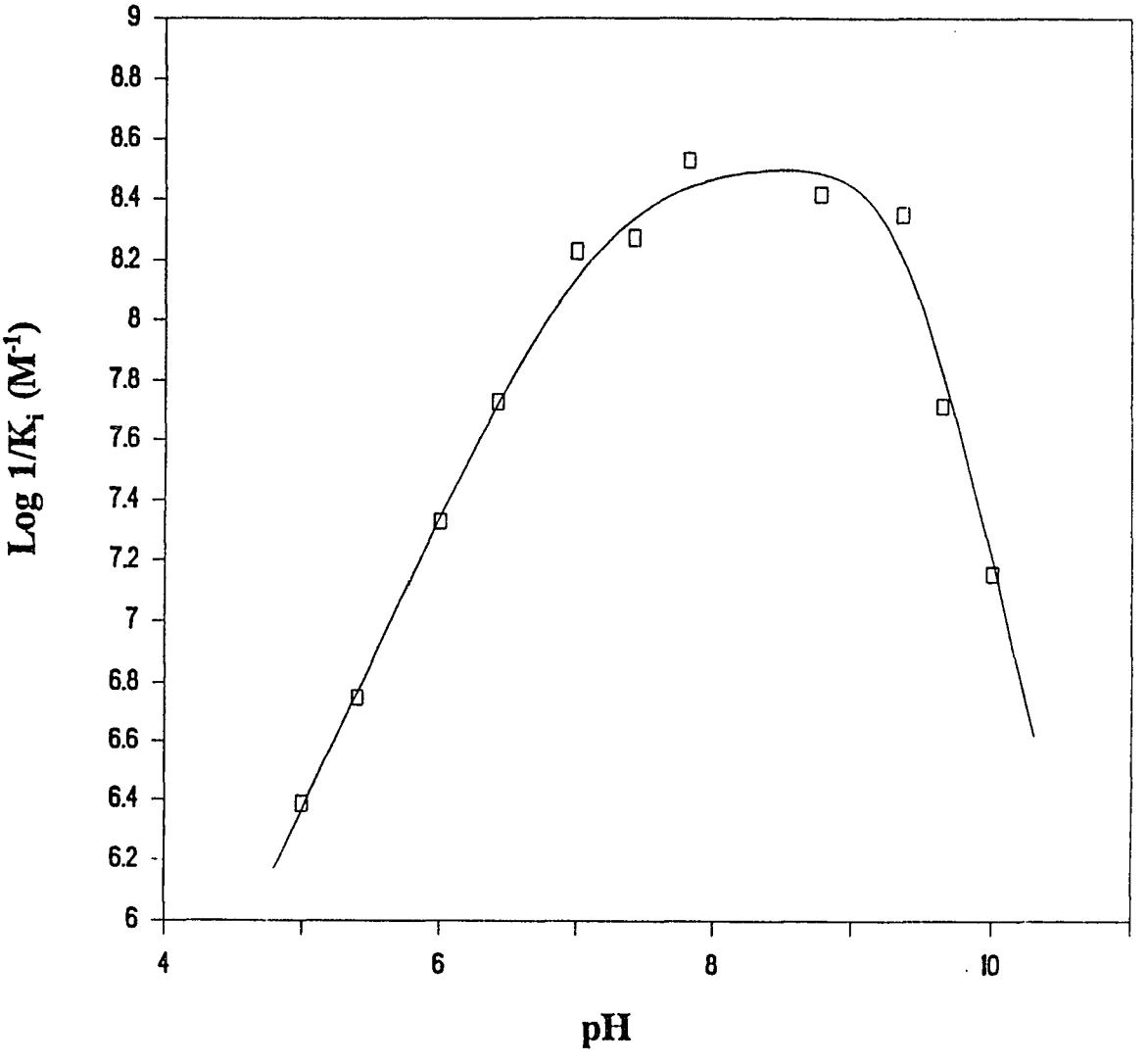

Fig.33 pH profile for inhibition of bovine thrombin by N^{α}-(2-naphthalenesulfonylglycyl)-4-amidino-D,L-phenylalaninepiperidide (NAPAP). The theoretical curve is drawn using $pK_1 = 7.15(\pm 0.05)$, a double ionization $pK_2 = 9.45(\pm 0.10)$, optimum pH = $8.50(\pm 0.07)$ and $K_i(Lim) = 3.00(\pm 0.42)$ nM. Reaction conditions are given in the text. (Data of Table XXVI Appendix A)

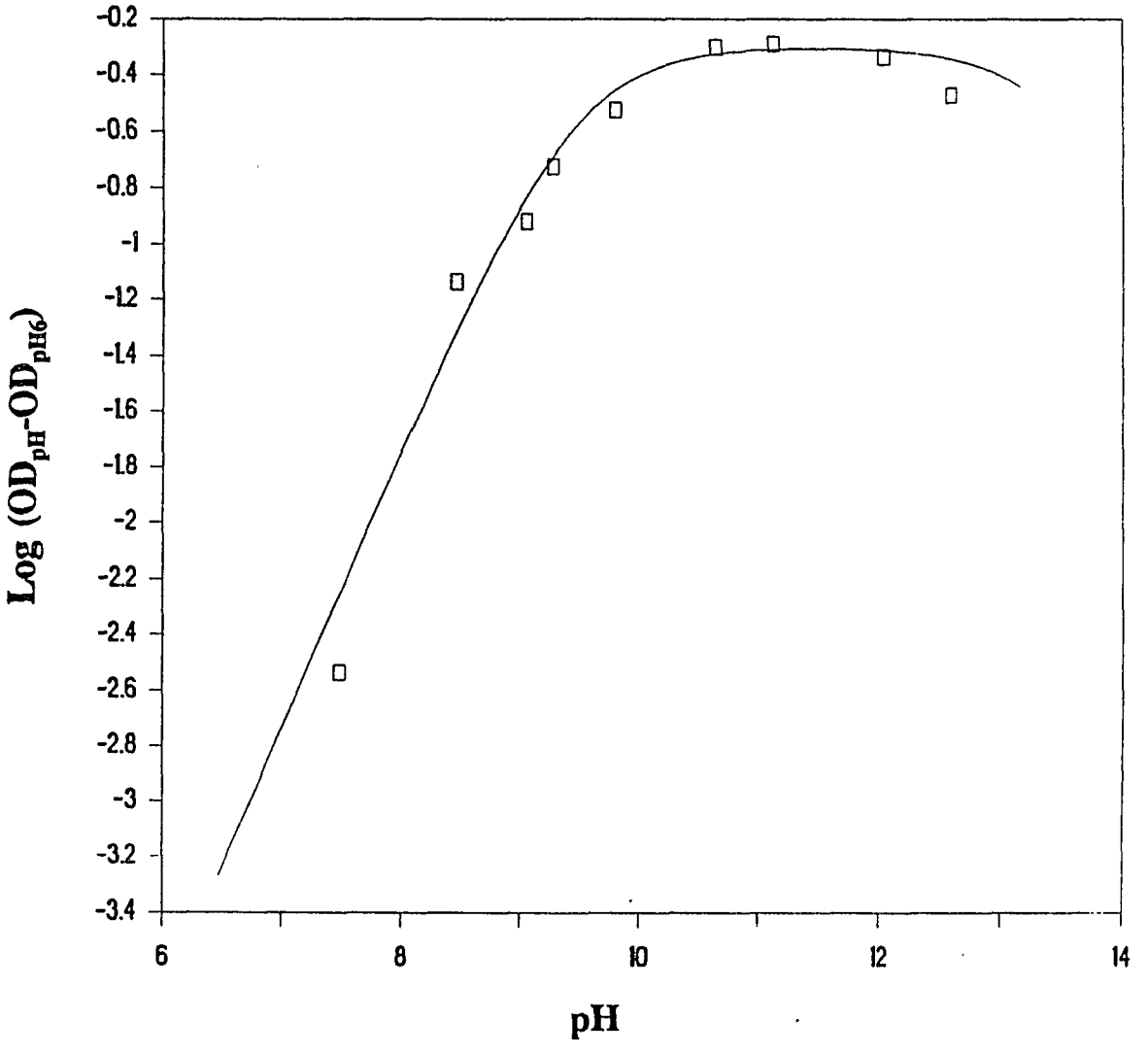

Fig.34 Spectrophotometric titration of 91 μM N$^{\alpha}$-(2-naphthalenesulfonylglycyl)-4-amidino-D,L-phenylalaninepiperidide (NAPAP). The theoretical curve is drawn using pK = 9.44($\pm$0.20). Reaction conditions are given in the text.
(Data of Table XXVII Appendix A)

pH-Dependent Inhibition of Bovine Thrombin by Leupeptin

Ac-Leu-Leu-ArgH (leupeptin) shows mixed inhibition on thrombin (Fig.35). The pH profile of inhibition is seen in Fig.36. The pK_1 of 7.07 is clearly diagnostic for the active site, and the pK_2 of 9.34 is close to that observed in the substrate hydrolysis. Leupeptin shows optimal binding on thrombin at pH 8.20 with the limiting K_i of 3.17 μM.

In contrast, other peptide aldehyde-serine protease systems show no pronounced pH dependence near pH 7[72]. The pK of 7.07 seen here indicates that although mixed inhibition type was observed, leupeptin appears to bind to the enzyme's active site with binding depending on the neutral imidazole.

This pK may suggest that the hemiacetal, which should be anionic immediately after attack by the serine oxygen atom, remains so and forms an ion-pair with the active site imidazolium ion[72]. The other possibility is that leupeptin's aldehyde carbon atom forms a complex with the nitrogen atom of the active site imidazole. Such a complex could not readily form with the protonated imidazolium ion. Formaldehyde inhibits serine proteases via such a complex[73].

pH-Dependent Inhibition of Bovine Thrombin by Phenylarsonic Acid

Arsonic acids are potential transition state analog inhibitors studied by Glazer[74]. These compounds are believed to form a tetrahedral monoester to the active site serine OH group. Like boronic acids, arsonic acids reversibly esterify to alcohols. In contrast to boronic acids, arsonic acid are tetrahedral Brϕnsted acids. Arsonic acids are anionic throughout the physiological pH range.

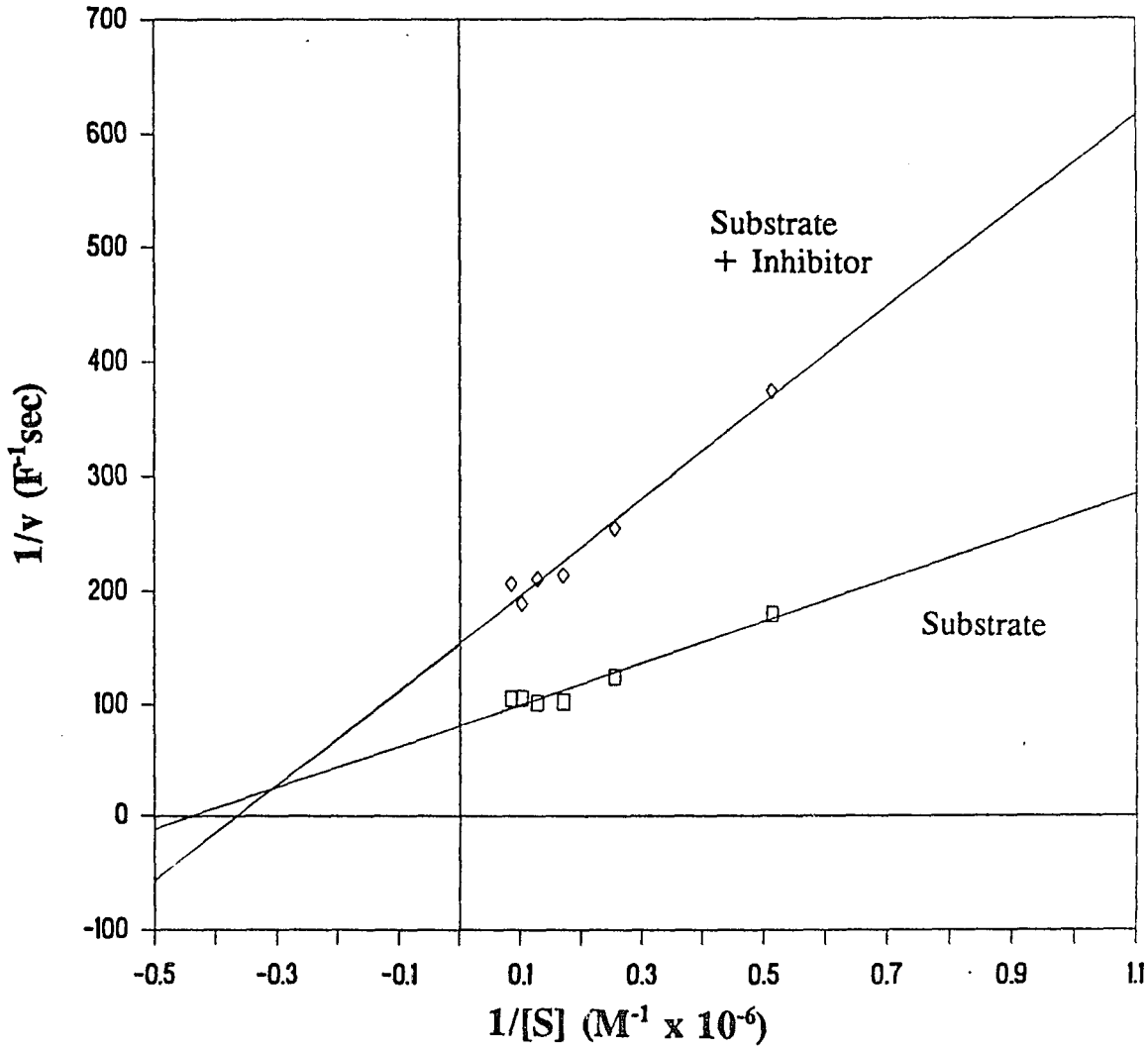

Fig.35 Inhibition of bovine thrombin by leupeptin (Ac-Leu-Leu-ArgH) at pH 7.8. [inhibitor] = 7.66×10^{-6} M, the substrate was N-t-Boc-Valyl-Prolyl-Arginine-7-AMC.K_i = 6.03($\pm$1.72) μM, K_m = 2.29($\pm$0.551) μM. Reaction conditions are given in the text.
(Data of Table XXVIII Appendix A)

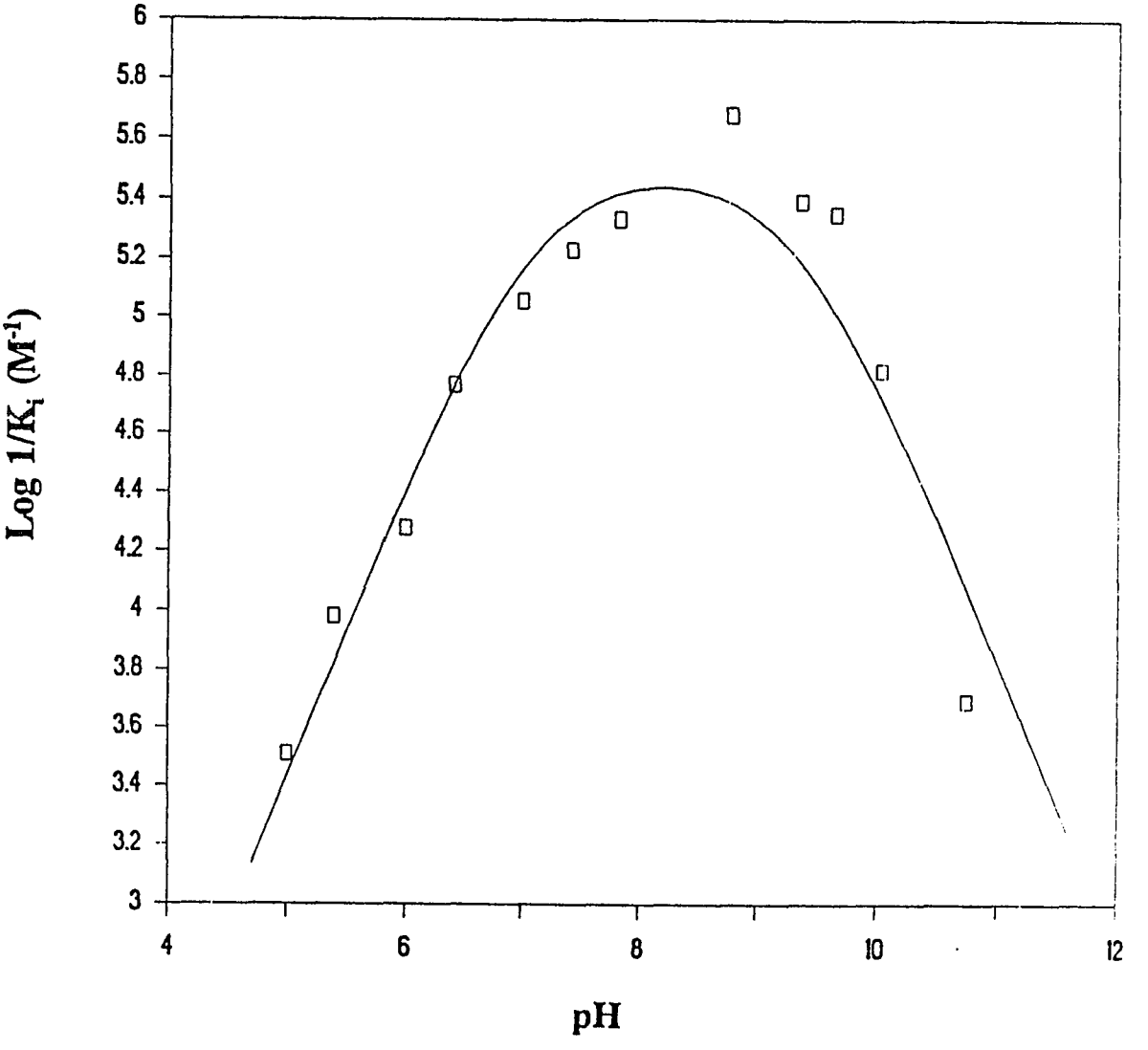

Fig.36 pH profile for inhibition of bovine thrombin by leupeptin (Ac-Leu-Leu-ArgH). The theoretical curve is drawn using $pK_1 = 7.07(\pm 0.10)$, $pK_2 = 9.34(\pm 0.20)$, optimum pH = $8.20(\pm 0.15)$ and $K_i(Lim) = 3.17(\pm 0.634)$ μM. Reaction conditions are given in the text. (Data of Table XXIX Appendix A)

Fig.37 shows that phenylarsonic acid exhibits competitive inhibition on thrombin. Unlike other inhibitors studied here, phenylarsonic acid shows optimal inhibition in acidic pH region with the limiting K_i of 3.77 mM (Fig.38). The inhibition pH profile clearly shows that the arsonic acid binds to thrombin with a pK of 7.37 and better binding is on the acid side of the pK. This is similar to the results obtained with arsonic acid inhibitions of trypsin and chymotrypsin, and shows that the anionic inhibitor cannot bind to the enzyme until the anionic active site is neutralized by protonation of the active site imidazole.

pH-Dependent Inhibition of Bovine Thrombin by 2,7-bis-(4-amidinobenzylidene)-cycloheptan-1-one

2,7-bis-(4-amidinobenzylidene)-cycloheptan-1-one is a known trypsin-like serine protease inhibitor[75]. It competitively inhibits thrombin[79]. The two positively charged diamidino groups in its molecular structure facilitate the binding of the inhibitor to the anionic active site of serine proteases.

The pH dependence of inhibition of bovine thrombin by 2,7-bis-(4-amidinobenzylidene)-cycloheptan-1-one is shown in Fig.39. The optimal inhibition is observed at pH 8.43 with the limiting K_i of 0.143 μM. pK_1 of 7.50 and pK_2 of 9.35 are the two pKs of thrombin seen in substrate kinetics. The pK_3 of 6.20 is a result of ionization of the enzyme-inhibitor complex.

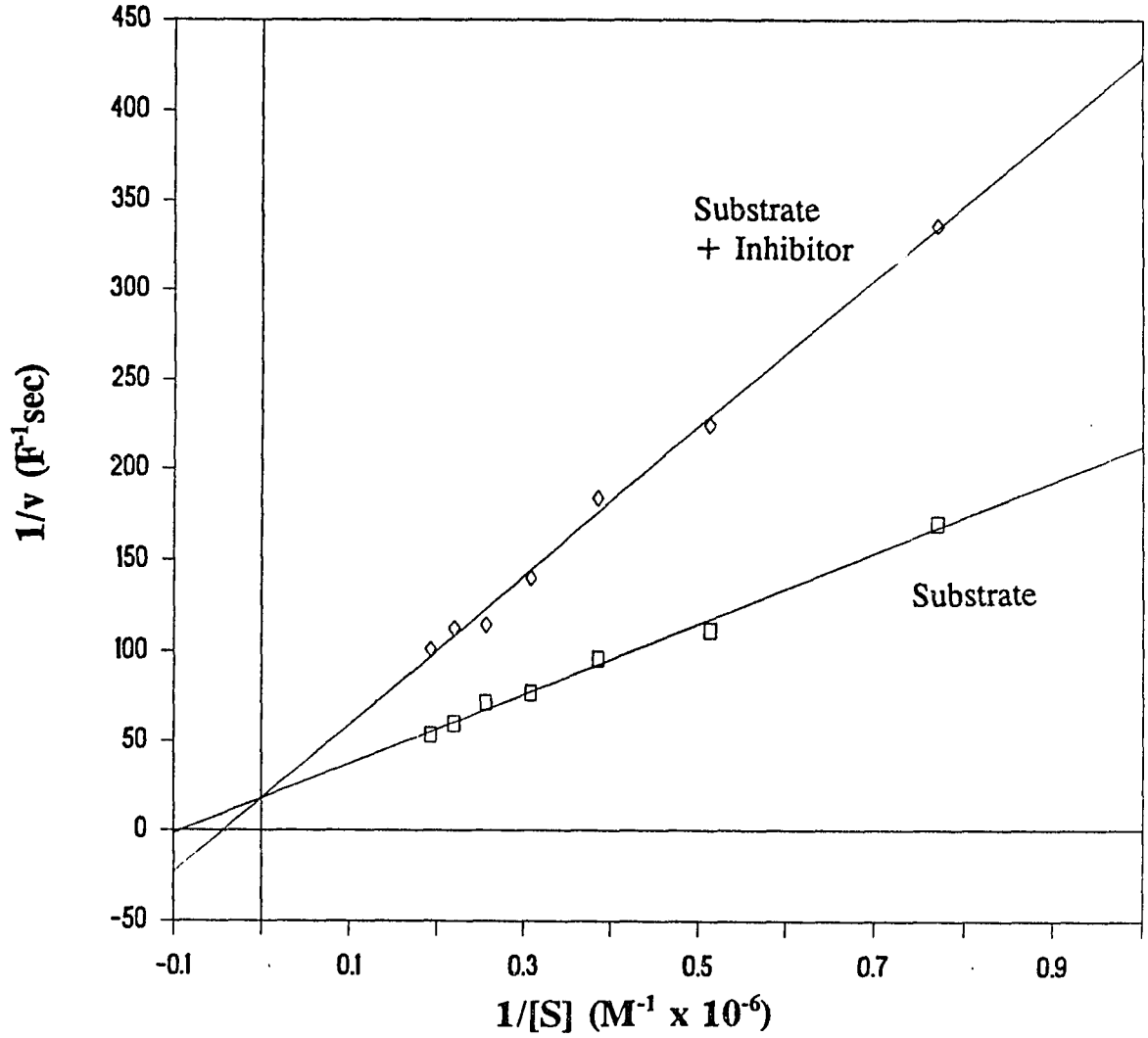

Fig.37 Inhibition of bovine thrombin by phenylarsonic acid at pH 6.0. [inhibitor] = 3.71×10^{-3} M, the substrate was N-t-Boc-Valyl-Prolyl-Arginine-7-AMC. K_i = 3.32($\pm$0.406) mM, K_m = 10.9($\pm$3.49) μM. Reaction conditions are given in the text.
(Data of Table XXX Appendix A)

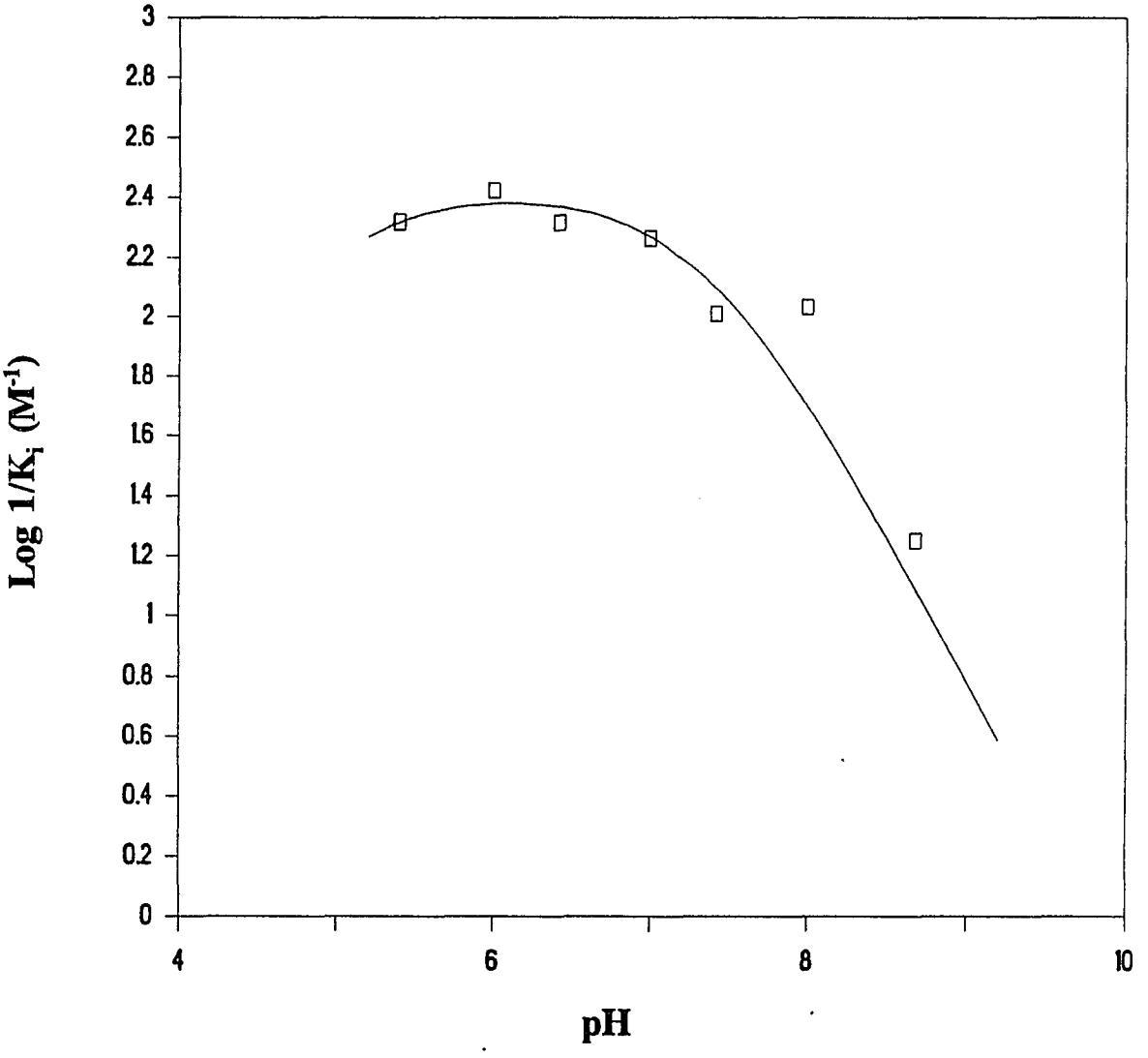

Fig.38 pH profile for inhibition of bovine thrombin by phenylarsonic acid. The theoretical curve is drawn using pK = 7.37($\pm$0.30) and K_i(Lim) = 3.77($\pm$0.302) mM. Reaction conditions are given in the text. (Data of Table XXXI Appendix A)

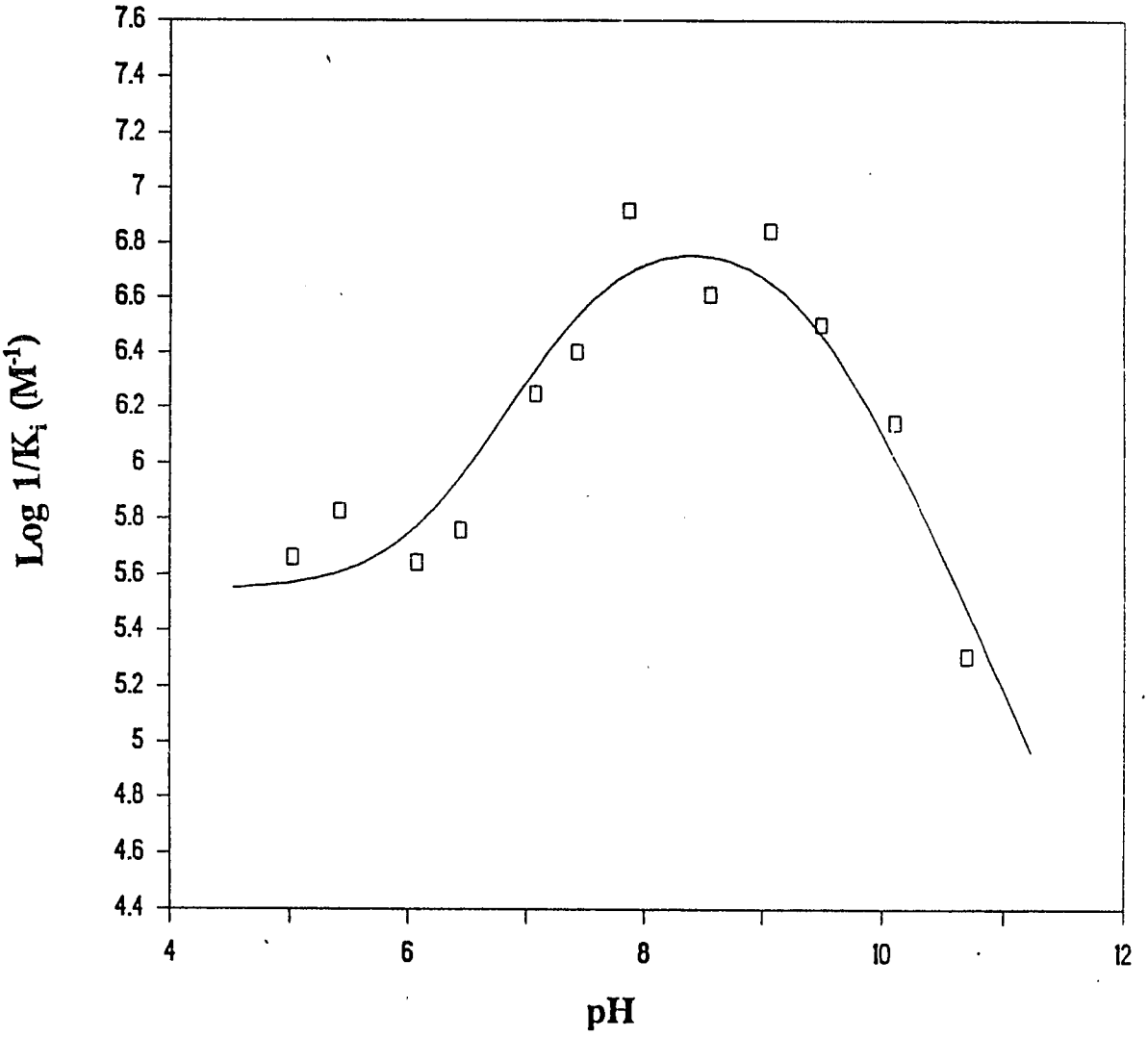

Fig.39 pH profile for inhibition of bovine thrombin by 2,7-bis-(4-amidinobenzylidene)-cycloheptan-1-one.
The theoretical curve is drawn using $pK_1 = 7.50(\pm 0.20)$, $pK_2 = 9.35(\pm 0.15)$, $pK_3 = 6.20(\pm 0.20)$, optimum pH $= 8.43(\pm 0.17)$ and $K_i(Lim) = 0.143(\pm 0.043)$ μM.
Reaction conditions are given in the text.
(Data of Table XXXII Appendix A)

CONCLUSIONS

Bovine thrombin exhibits the active site pK near 7 common to serine proteases. This pK is shown in pH profiles for all of the substrates and inhibitors studied here. For most serine proteases, the pK near 7 is reflected in k_{cat}. Such is the case for bovine thrombin catalyzed hydrolysis of N-t-Boc-Valyl-Prolyl-Arginine-7-AMC. For the chromogenic substrate D-Phe-Pipecolyl-Arg-*p*NA, the pK of 7 controls K_m while k_{cat} is less dependent on pH. The pH inhibition profiles are also governed by the enzyme's pK near 7 suggesting the importance of the active site imidazole in these inhibitors' binding.

In the cases of thrombin inhibition by peptidyl boronic acids, bovine thrombin is a subject to slow inhibition by both Ac-D-Phe-Pro-boroArg and Ac-D-Phe-Pro-Arg. The transition from fast-binding mode to slow-binding mode involves proton transfer whereas the reverse conversion is independent of pH. Z-D-Phe-Pro-boroMPG and N-(Z-D-Phe-Pro)-2-amino-5-methoxypentanoic acid on the other hand only exhibit fast inhibition on bovine thrombin. Therefore the slow inhibition effect is a result of the peptide sequence. It is not due to the presence of boronic acid group. The boronate moieties of the peptides exceedingly improve the inhibitory potency by acting as tight-binding tetrahedral transition state analogs.

Based on the crystallographic analyses for the structures of complexes formed between boronic acid inhibitors and other serine proteases[30,56-58,80], the mechanism of the association of the peptidyl boronic acids with bovine thrombin is proposed in Fig.40. The model suggests that the trigonal boronic acid moieties of the inhibitors esterify to the active site serine residue forming the covalent tetrahedral boron adducts which resemble

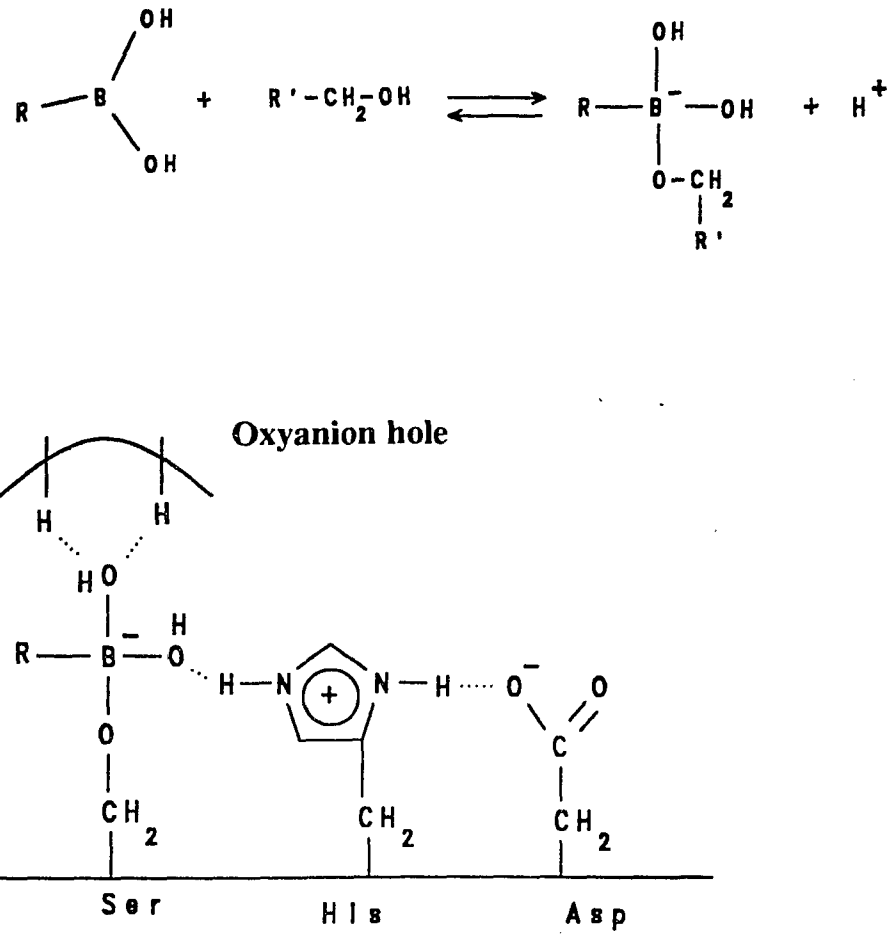

Fig.40 Scheme for a possible interaction of inhibitory peptidyl boronic acid with thrombin active site.

the tetrahedral intermediates generated on the reaction pathway for substrate hydrolysis. The esterification is associated with the proton transfer from the active site serine hydroxyl group to the active site histidine. This could explain the existence of the histidine pK in the inhibition pH profiles of the peptidyl boronic acids studied here.

In the tetrahedral boronic acid adduct, one boron hydroxyl group hydrogen bonds to the catalytic histidine side chain and the other OH is stabilized in the oxyanion hole. According to the tetrahedral covalent radii[77], the calculated B-O bond length is 1.54 Å. Based on this bond length, in a tetrahedral boron adduct, the active site serine oxygen would be 3.14 Å from the boron oxygen lying in the oxyanion hole. In the crystal structure of the complex formed between mutant α-lytic protease (Met 213 replaced by Ala) and methoxysuccinyl-Ala-Ala-Pro-Norleucine boronic acid[80], this distance is 2.46 Å. The covalent bond between O_τ of the catalytic Ser-195 and the inhibitor's boron atom in this complex is 1.61 Å. Similarly, in a purely tetrahedral transition state structure of peptide bond hydrolysis, the calculated C-O bond length is 1.43 Å, the expected distance between the active site serine oxygen to the oxyanion is 2.71 Å. According to the crystallographic analysis data for D-Phe-Pro-Arg-CH_2Cl-human thrombin complex[76], the covalent linkage between the active site serine O_τ and the inhibitor's ketone carbonyl carbon is 1.48 Å. The serine oxygen is 2.14 Å to the oxyanion. These results clearly indicate that the boron tetrahedral adduct can function as an approximate analog for the transition state intermediate of substrate hydrolysis.

Based on the crystal structure of the complex formed between human thrombin and D-Phe-Pro-Arg-CH_2Cl[76], the binding model of D-Phe-Pro-boroArg in thrombin active site is derived. As presented in Fig.41, the positively charged P_1 arginine side chain

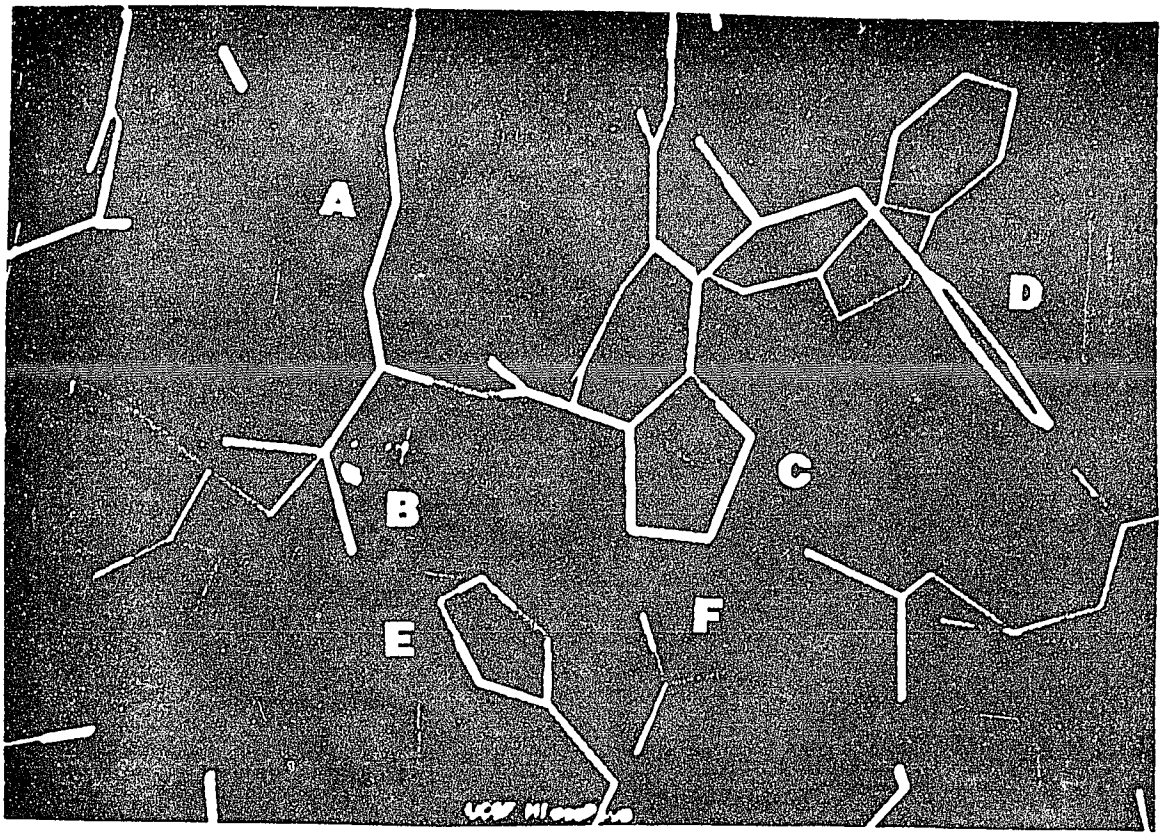

Fig.41 A possible binding model of Ac-D-Phe-Pro-boroArg in the active site of human thrombin.(derived from the X-ray crystal structure of the thrombin complex formed with D-Phe-Pro-Arg-CH_2Cl reported in ref.76) A is the inhibitor's boroarginine side chain. B is the boroarginine boron atom esterified to the active site serine hydroxyl group. C is the inhibitor's proline. D is the inhibitor's D-phenylalanine. E is the imidazole of the catalytic histidine. F is the carboxylate of the active site aspartate.

binds into the specific pocket forming ion pair with the negatively charged carboxylic group of aspartate located at the base of the pocket. P_2-residue proline and P_3-residue D-phenylalanine are situated in a hydrophobic binding area surrounded by the apolar amino acid side chains. The active site serine oxygen is covalently connected to the inhibitor's boron atom. The formation of the tetrahedral boron adduct is facilitated by the neutral imidazole in the catalytic center.

In the crystal structure of NAPAP-thrombin complex[76] (Fig.42), the *p*-amidinophenylalanine moiety occupies the specific pocket; the naphthyl group binds at the hydrophobic P_3 site; the piperidine ring at the P_2 position is tightly packed between the naphthyl moiety and the active site histidine. The carbonyl group of amidinophenylalanine (the presumed scissile peptide bond of NAPAP) is located too far away from the active site serine (> 4 Å) to form a covalent bond. The oxyanion hole is not directly used by NAPAP. Its carbonyl oxygen is stabilized by a water molecule which is hydrogen bonded to a further water in this case.

The binding mode of NAPAP in thrombin active site clearly shows that there is an important hydrophobic interaction between the piperidine ring of the inhibitor and the active site imidazole. The distance between the two nearly parallel groups is 3.5 Å[76]. The pH dependent K_i profile of NAPAP suggests that the association of histidine side chain with the inhibitor's piperidine group is abolished by imidazole protonation. A possible explanation for this observation is presented in Fig.43. The piperidine amide group of NAPAP exists in two resonance forms, A and B. The positive charge on the amide nitrogen in the B form clearly requires a deprotonated neutral imidazole ring for the hydrophobic interaction.

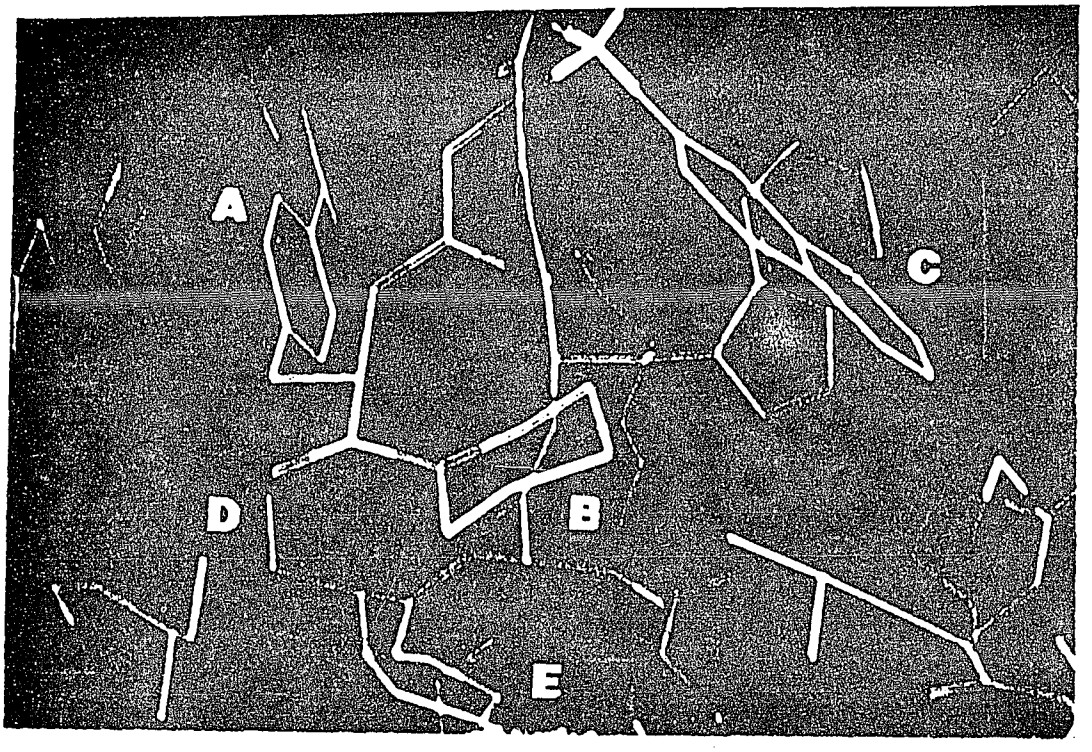

Fig.42 X-ray crystal structure of the active site region of the NAPAP-human thrombin complex. (from ref.76)
A is NAPAP's *p*-amidinophenylalanine moiety. B is NAPAP's piperidine ring. C is NAPAP's naphthyl group. D is the active site serine hydroxyl. E is the imidazole of the active site histidine.

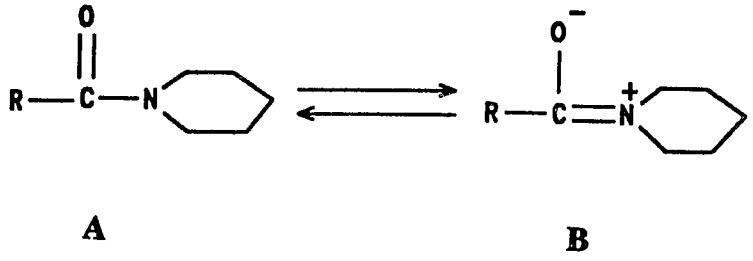

A B

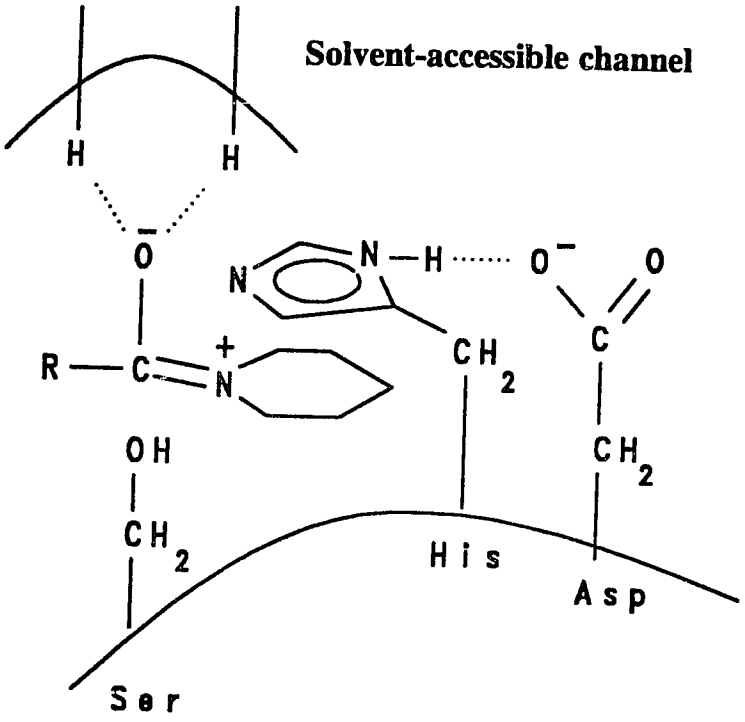

Fig.43 Scheme for a possible interaction of NAPAP with thrombin active site.

Inhibition of serine proteases by aldehydes and ketones is well known[36-39]. NMR[39,78] and X-ray[9,76] studies have provided evidence to support the formation of a hemiacetal or a hemiketal with the active site serine residue.

In the present study, the pK near 7 observed in the pH dependencies of K_i for leupeptin and 2,7-bis-(4-amidinobenzylidene)-cycloheptan-1-one suggests that the deprotonated histidine which participates in the transition state of substrate hydrolysis is essential for these inhibitors' association to the active site of thrombin. These results are quite different from that observed in the inhibition of chymotrypsin by its specific aldehyde, N-benzoyl-L-phenylalaninal, where the lack of a significant pH dependency in K_i near pH 7 suggests the presence of a neutral hemiacetal adduct in chymotrypsin active site[72].

Based on the experimental results obtained here, the possible mechanisms for the formations of hemiacetal and hemiketal in the inhibition of bovine thrombin by leupeptin and 2,7-bis-(4-amidinobenzylidene)-cycloheptan-1-one are proposed in Fig.44 and Fig.45 respectively. In both cases, the inhibition pH profiles support the idea that the enzyme-inhibitor complexes exist mainly as tetrahedral oxyanions, not as protonated neutral species. The active site imidazole is intimately involved in the inhibitors' binding. It contributes to the stabilization of the negative charged adducts. The anionic tetrahedral hemiacetal and hemiketal have no substantial differences in structure and charge from the transition state in thrombin-catalyzed substrate hydrolysis.

Inhibition of serine proteases by phenylarsonic acids is believed due to the esterification of the arsonic acid to the active site serine hydroxyl group[74]. Unlike the boronic acid, aldehyde and ketone inhibitors, which form tetrahedral adducts with serine

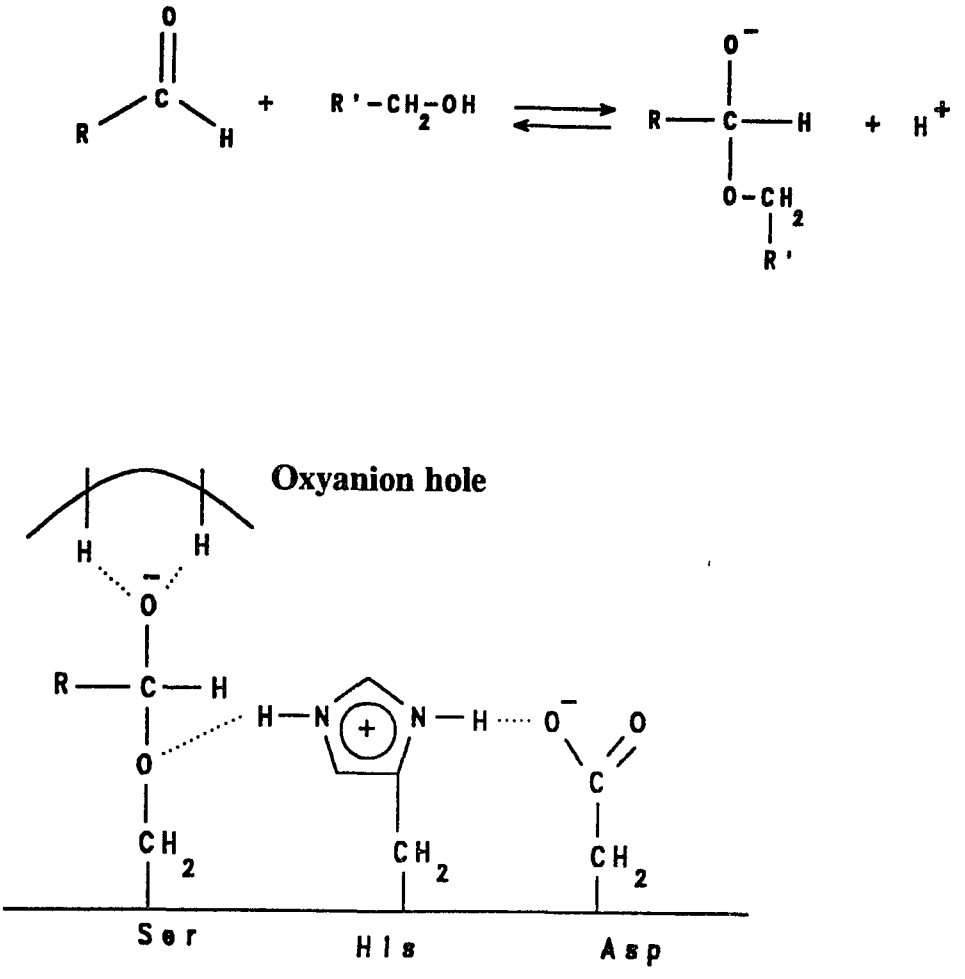

Fig.44 Scheme for a possible interaction of leupeptin with thrombin active site.

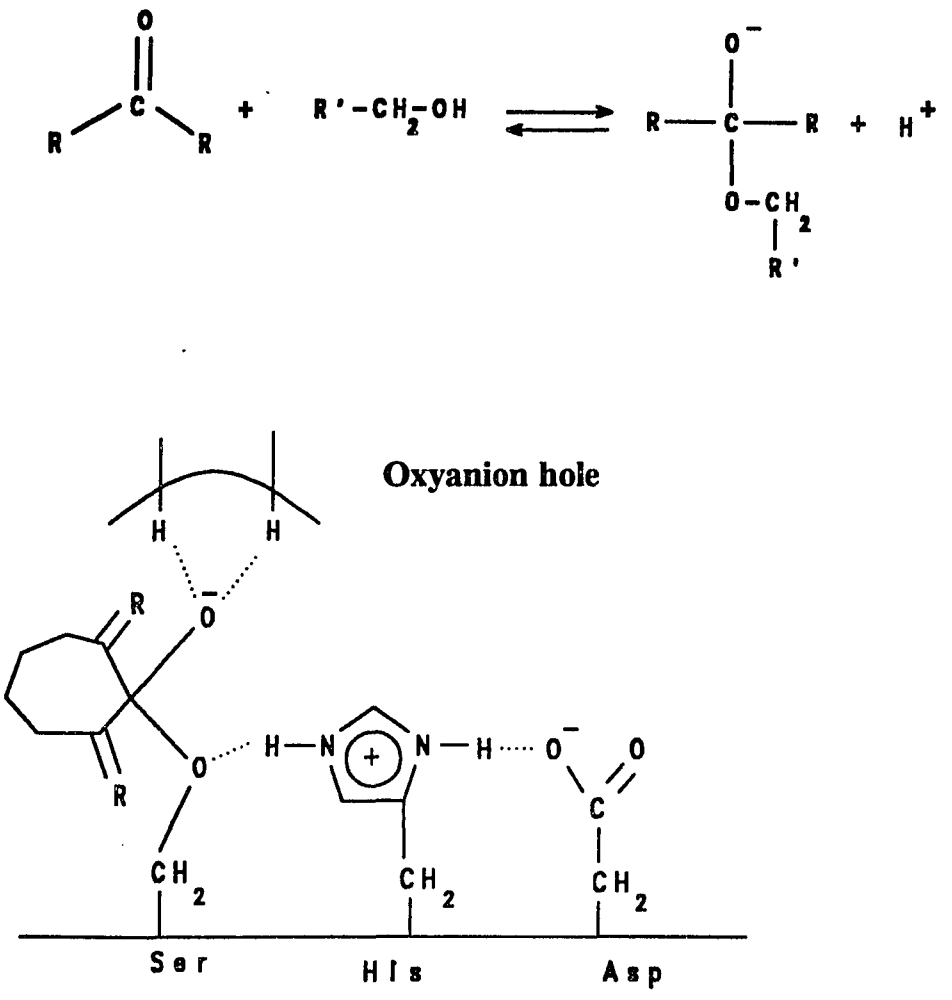

Fig.45 Scheme for a possible interaction of 2,7-bis-(4-amidinobenzylidene)-cycloheptan-1-one with thrombin active site.

hydroxyl directly from their trigonal configurations, the arsonic acid monoester formation proceeds by a pentacoordinate intermediate (Fig.46).

Although the arsenical ester formed in the enzyme active site is in a transition state-like tetrahedral configuration, its structure is significantly different from the transition state intermediate. According to the tetrahedral covalent radii[77], the As-O bond length is 1.84 Å while the C-O bond length in transition state is 1.43 Å. In the arsenical tetrahedral structure, the calculated distance between the active site serine oxygen to the oxygen situated in the oxyanion hole is 4.49 Å. In the transition state, based on the covalent radii[77], the serine hydroxyl is 2.71 Å away from the oxyanion. It is clear that the size of arsenical tetrahedral structure is much larger compared to the carbon tetrahedral transition state. This may be one reason for the observed poor binding affinity of phenylarsonic acid to thrombin active site.

While the neutral inhibitors used here show higher affinity to thrombin on the alkaline side of histidine pK, the anionic compound tested binds more poorly in alkaline pH values. The binding of phenylarsonate to the active site is clearly blocked by the active site's anionic charge at pH values above seven. The reverse pH-K_i profile suggests that the binding of the inhibitor requires the existence of a protonated imidazole at the active site of thrombin (Fig.46).

These results suggest that future work on thrombin inhibitors should not emphasize anionic inhibitors that are repelled from the active site at physiological pH values.

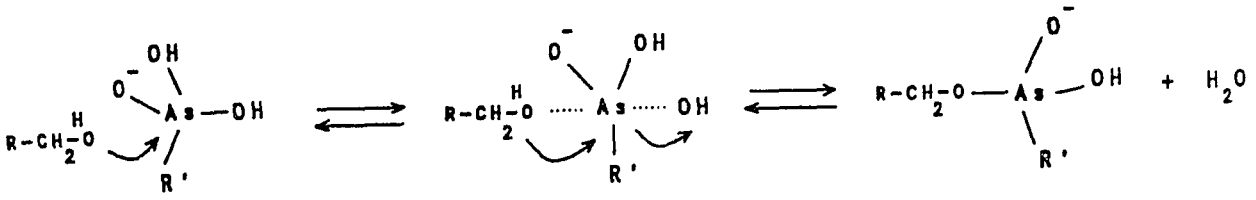

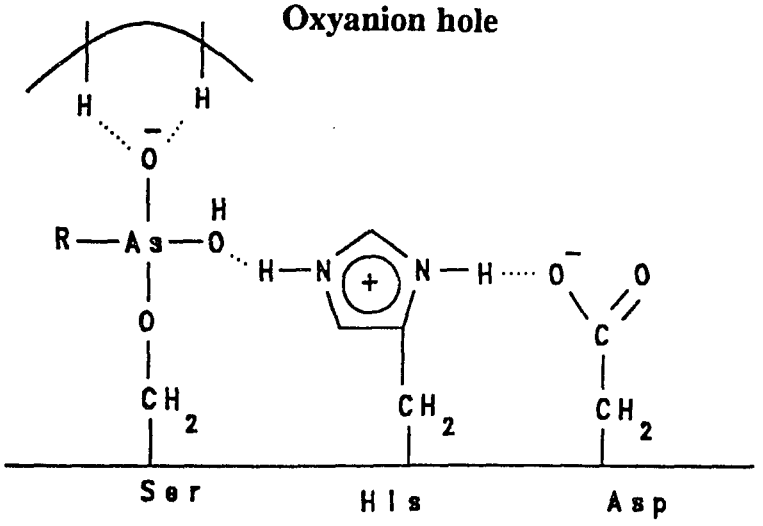

Fig.46 Scheme for a possible interaction of phenylarsonic acid with thrombin active site.

PART II

BIOMIMETRIC CATALYSIS: BORON ACIDS ACCELERATE THE FORMATION OF SALICYLALDOXIME AND SALICYLALDEHYDE PHENYLHYDRAZONE

INTRODUCTION

The boron family of acids, including boric, boronic, and borinic acids have acquired particular attention of chemists due to their Lewis acid character. Boron atom in these acids has one vacant orbital which is available for the formation of a fourth covalent bond with electron donor. They ionize to form tetrahedral boronate anions by addition of a hydroxyl group from water[1].

$$R\text{-}B(OH)_2 + H_2O \rightleftharpoons R\text{-}B(OH)_3^- + H^+$$

This mode of ionization enables their rapid and reversible esterification to alcohols[2-8]. The associations of boric acid and substituted benzeneboronic acids with polyols, dicarboxylic acids and hydroxy acids have been studied by temperature-jump relaxation kinetics[3-8]. The dissociation constants of these reactions are in the millimolar to micromolar range.

The reversible complexation of boronic acids with various ligands has led to their applications in several aspects. One is the use of boronic acids in studies of hydrolytic enzymes, where boronates function as potent transition state analog inhibitors as demonstrated in the first part of this dissertation.

Another utility of these acids is in affinity chromatography, where boronic acids can be coupled to solid matrices and then be used to separate biological interesting enzymes[9-11] and diol-containing compounds[12-14].

Catalysis by the boron family of acids has also been an interesting subject in

enzyme model studies[15-27]. Unlike the common model systems based on oligomeric or polymeric substance[28-38], these acids are simple and small molecules that exhibit reversible enzyme-like binding to their substrates prior to the catalytic steps.

Boric acid has been found to be a good catalyst in several investigations. Peer and coworkers observed that boric acid catalyzes the formation of *o*-(hydroxymethyl)-phenol from the reaction between formaldehyde and phenol[15-16].

Capon and Ghosh reported the greatly enhanced hydrolysis rate of phenyl salicylate in borate buffers[20]. Okuyama *et al.* demonstrated that borate accelerates the hydrolysis of S-butyl 2-hydroxy-2-phenylthioacetates by a factor of about 80 at pH 9.0[21]. The remarkable catalytic effect of boric acid has also been shown on the formation and hydrolysis of hydroxyl group containing imines[22-25].

Boronic acids possess much higher binding affinity to various alcohols than boric acid[7]. This property ensures boronic acids to function as better catalysts.

In the earlier experiments done by Letsinger *et al.*, It was observed that 8-quinolineboronic acid effectively accelerates the hydrolysis of chloroethanol to ethyleneglycol[17]. This boronic acid was also found to be cis-trans stereoselective in the hydrolytic reactions of chloroalcohols[18]. Letsinger and Macheon also used boronoarylbenzimidazole as a catalyst to facilitate the formation of ethers from choroethanol in butanol solution[19].

In recent years, Rao and Philipp have studied the boronic acid catalyzed hydrolysis of salicylaldehyde imines[26]. These reactions clearly display Michaelis-Menten kinetics. Binding of the substrate is controlled by the boronic acid ionization with catalytic activity depending on the trigonal neutral boronic acids. The binding constants

are improved by electron-withdrawing substituents on the benzeneboronic acids, whereas the catalytic constants have no pH or electronic dependencies. The mechanism of this catalysis is likely to be an intramolecular transfer of a boron-coordinated hydroxide ion within a borate-substrate complex.

Based on the patent literature describing the boric acid catalyzed mandelonitrile hydrolysis to form mandelamide[39], Rao and Philipp also investigated the mechanism of mandelonitrile hydrolysis using substituted benzeneboronic acids[27]. Their experiment showed that the hydrolysis rate of mandelonitrile to mandelamide increases continuously with increasing concentration of benzeneboronic acid. On the other hand, benzonitrile, which lacks a hydroxyl group adjacent to the nitrile, is not affected by the presence of boronic acids suggesting that the hydrolysis of mandelonitrile depends on the complexation of boronic acids to the hydroxyl group of mandelonitrile.

Rao and Philipp's works clearly demonstrated that boronic acids are more effective catalysts than boric acid. Due to the commercial availability of various substituted boronic acids, the boron family of acids provides a useful model system for the study of catalytic mechanisms.

In the present project, the catalytic effects of boric, boronic and borinic acids on the formation of salicylaldoxime from salicylaldehyde and hydroxylamine in aqueous solution have been studied (Scheme I).

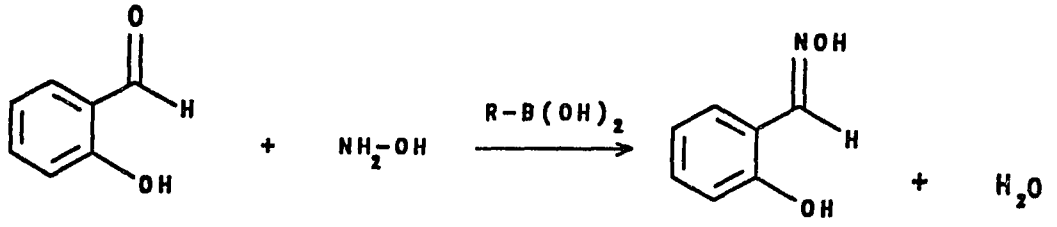

Scheme I

This reaction system involves three steps as shown in Scheme II,

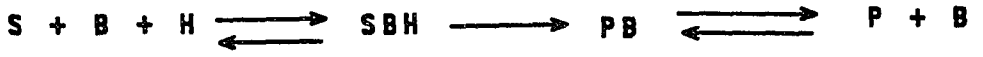

Scheme II

where S represents salicylaldehyde, B represents boronic acid, H represents hydroxylamine, P represents the product, salicylaldoxime.

The first step is the association of salicylaldehyde, boronic acid and hydroxylamine to form the productive ternary complex (SBH). In the second step, the chemical conversion of this ternary complex leads to the formation of the reaction product, salicylaldoxime, which is bound to boronic acid in the binary complex (PB). In the third step, the dissociation of boronic acid from the binary complex releases the free product and regenerates the catalyst, boronic acid. Like enzyme catalyzed reactions, all steps equilibrate rapidly relative to the step of the chemical conversion.

In order to understand the mechanisms of this enzyme model system, pH dependent kinetics were performed using a variety of different boron acids. The

complexation of salicylaldoxime with boron acids was deduced from the UV spectral analysis. The dissociation constants of these complexes were determined in comparison with other salicylaldehyde derivatives.

In this project, it also has been found that boronic acids exhibit similar catalytic function on the formation of salicylaldehyde phenylhydrazone (Scheme III). The pH dependencies and the electronic substituent effect of this reaction were investigated using 3,5-bis(trifluoromethyl)benzeneboronic acid, benzeneboronic acid and various phenylhydrazine derivatives.

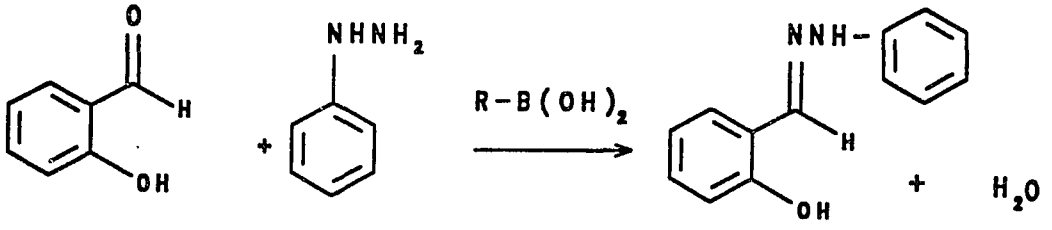

Scheme III

Based on the data collected here, the linear free energy relationships of the catalysts were established. Chemical mechanisms involved in these reactions are proposed.

EXPERIMENTAL

Materials

Acetate, phosphate and bicarbonate buffers of 0.1 M ionic strength were prepared according to buffer formulas given in the *Biochemists' Handbook*[40]. They were made from reagent grade chemicals and deionized water or deuterium oxide which was purchased from Cambridge Isotope Laboratories.

Salicylaldehyde was purchased from Sigma. A 0.016 M stock solution was made in deionized water. *p*-Hydroxybenzaldehyde and *m*-hydroxybenzaldehyde were purchased from Sigma. Stock solutions of 0.17 M were initially made in dimethylsulfoxide. They were further diluted in deionized water to the finial stock concentration of 1.7 mM.

Hydroxylamine hydrochloride was purchased from Fisher Scientific. A 0.16 M stock solution was made in deionized water. Methoxylamine hydrochloride was purchased from Aldrich. A stock solution of 0.17 M was made in deionized water. Phenylhydrazine was purchased from Aldrich. The stock solution of 0.33 M phenylhydrazine hydrochloride was made in deionized water together with 0.5 M hydrochloric acid. 4-Chlorophenylhydrazine hydrochloride, 4-fluorophenylhydrazine hydrochloride and 4-hydrazinobenzoic acid were purchased from Aldrich. 0.21 M stock solutions of these were made in dimethylsulfoxide. 4-Methoxyphenylhydrazine hydrochloride was purchased from Lancaster. A stock solution of 0.23 M was made in dimethylsulfoxide.

Salicylaldoxime was purchased from Sigma. A 0.011 M stock solution was made in deionized water. Salicylamide was purchased from Eastman Organic Chemicals. A stock solution of 0.018 M was made in deionized water. Salicylhydroxamic acid and salicyloylhydrazide were purchased from Sigma. 8.6 mM stock solutions of these were

made in dimethylsulfoxide.

Boric acid was purchased from Fisher Scientific. A 0.85 M stock solution was made in deionized water. Diphenylborinic anhydride was purchased from Aldrich. A stock solution of 0.17 M diphenylborinic acid was made in dimethylsulfoxide.

Benzeneboronic acid and 4-bromobenzeneboronic acid were purchased from Aldrich. A 0.67 M stock solution of the former and a 0.48 M stock solution of the latter were made in dimethylsulfoxide. 3,5-Bis(trifluoromethyl)benzeneboronic acid was purchased from Alfa. A stock solution of 0.11 M was made in dimethylsulfoxide. 4-Chloro-benzeneboronic acid, 4-fluorobenzeneboronic acid, 4-methoxybenzeneboronic acid, 3-chloro-4-fluorobenzeneboronic acid, 3,5-dichlorobenzeneboronic acid and 2,4-dichlorobenzeneboronic acid were purchased from Lancaster. Stock solutions of these were made in dimethylsulfoxide ranging from 0.2 M to 0.6 M.

Methods

Kinetic measurements. All reactions were conducted at 25.5°C on a Perkin Elmer double beam UV/VIS spectrometer. Typical assay mixtures contained 1 ml of buffer, 5-50 μl of a boronic acid stock solution, 5-70 μl of 0.16 M hydroxylamine hydrochloride (or 5-40 μl stock solution of phenylhydrazine or its derivatives) and 5-10 μl of 0.016 M salicylaldehyde. The reactions were initiated by the addition of salicylaldehyde into a quartz cuvette containing the reaction mixture. The spontaneous reactions were carried out in the absence of any boron acids.

The rate of spontaneous and boric or boronic acid catalyzed formation of salicylaldoxime was determined at 304 nm in various pH buffers of 0.1 M ionic strength.

When diphenylborinic acid was used, the reaction was followed at 340 nm (pH 6.0-7.5), 350 nm (pH < 6.0) and 385 nm (pH > 7.5). At pH 6.4, the generation of *m*-hydroxybenzaldehyde oxime and *p*-hydroxybenzaldehyde oxime was observed at 325 nm and 290 nm respectively.

The formation of salicylaldehyde O-methyloxime was assayed at 304 nm with boric, boronic and diphenylborinic acids under same the conditions as for salicylaldoxime formation. When *m*-hydroxybenzaldehyde or *p*-hydroxybenzaldehyde was used in place of salicylaldehyde, the rate of the O-methyloxime formation was determined at 325 nm and 290 nm respectively at pH 6.4.

In the hydrazone formation reactions, the time-dependent absorbance changes were followed at 350 nm for salicylaldehyde phenylhydrazone, 370 nm for salicylaldehyde 4-methoxyphenylhydrazone and salicylaldehyde 4-chloro-phenylhydrazone, 360 nm for salicylaldehyde 4-fluorophenylhydrazone and 380 nm for salicylaldehyde 4-carboxyphenylhydrazone. In the case of *meta* or *para* hydroxybenzaldehyde phenylhydrazone formation, 340 nm was used for the kinetic assay.

The pH of reaction solutions was measured on a Radiometer PHM62 immediately after completion of each reaction. The reaction rate constants obtained in the presence of boron acids were corrected for spontaneous formation by subtracting the spontaneous rate constant from the catalyzed rate constant at each pH. Linear regression data analysis was performed on a Lotus-123 spreadsheet. pH profiles were generated in the same way as described in part I of this dissertation.

Kinetics in deuterium oxide. The kinetic measurements in deuterium oxide

buffers were performed essentially same as in water. The pH of deuterium oxide solutions was reported as the value directly read on the pH meter without correction for the deviation near 0.4 caused by deuterium oxide[41-42]. This procedure minimizes the change in observed pK values.

Determination of the dissociation constants. The complexation between boron acids and salicylaldoxime was observed in various pH buffers of 0.1 M ionic strength at 25.5°C. The UV spectra of salicylaldoxime in the presence of boron acids were compared with those obtained in their absence.

At fixed concentration of salicylaldoxime (0.11 mM), the net absorbance increase at particular wavelength (340 nm or 330 nm) was determined at different concentrations of boron acids. The dissociation constant values (K_{diss}) were calculated from the slope of the plot of absorbance/[boron acid] versus absorbance (Eadie-Hofstee plot). In the same way, the complexation of diphenylborinic acid with other salicylaldehyde derivatives (salicyloylhydrazide, salicylhydroxamic acid, salicylamide) at pH 6.6 was also studied. In the presence of various levels of diphenylborinic acid, their binding constants were determined at 340 nm with 8.7×10^{-5} M salicyloyl hydrazide, 355 nm with 8.6×10^{-5} M salicylhydroxamic acid, 330 nm with 1.85×10^{-4} M salicylamide.

Salicylaldoxime and salicylaldoxime diphenylborinic acid complex were subjected to spectrophotometric titration. This was done by taking the spectra of 0.11 mM salicylaldoxime or its diphenylborinic acid complex in 0.1 M buffers of various pH from 190 nm to 600 nm. The titration curves of salicylaldoxime and the complex were generated respectively by plotting the ratios of OD_{350nm}/OD_{304nm} and OD_{310nm}/OD_{340nm} as a function of pH.

RESULTS AND DISCUSSION

Formation of Salicylaldoxime

Characterization of kinetic mechanism. The formation of salicylaldoxime was studied by varying one reactant concentration and keeping the others constant. As seen in Fig.1 and Fig.2, the spontaneous reaction rate increased linearly with both hydroxylamine and salicylaldehyde concentrations. This suggests that the spontaneous formation of salicylaldoxime follows a second-order kinetic mechanism. In the presence of 3,5-bis(trifluoromethyl)benzeneboronic acid, the most effective boronic acid used in this study, a linear dependence of the reaction rate was also observed on the concentration of the boronic acid, hydroxylamine and salicylaldehyde (Fig.3, 4, 5). The results indicate a third-order kinetic mechanism for the boronic acid catalyzed salicylaldoxime formation reaction.

When diphenylborinic acid was used as a catalyst, the reaction rate displayed a hyperbolic dependence on both the borinic acid and hydroxylamine concentrations (Fig.6, 7). These hyperbolic curves are similar to those observed in enzyme-catalyzed reactions. At low reactant concentration level (linear region of the hyperbolic curves) this reaction also follows a third-order kinetic mechanism (Fig.6, 7, 8). Fig.9 and Fig.10 present Eadie-Hofstee plots for the effects of diphenylborinic acid concentration and hydroxylamine concentration on the rate of salicylaldoxime formation. K_m and k_{cat} were calculated from the slope and y-intercept of these linear plots[56].

Effect of pH on the formation of salicylaldoxime. The logarithm of the second-order rate constants (k_2) for the spontaneous formation of salicylaldoxime is plotted as

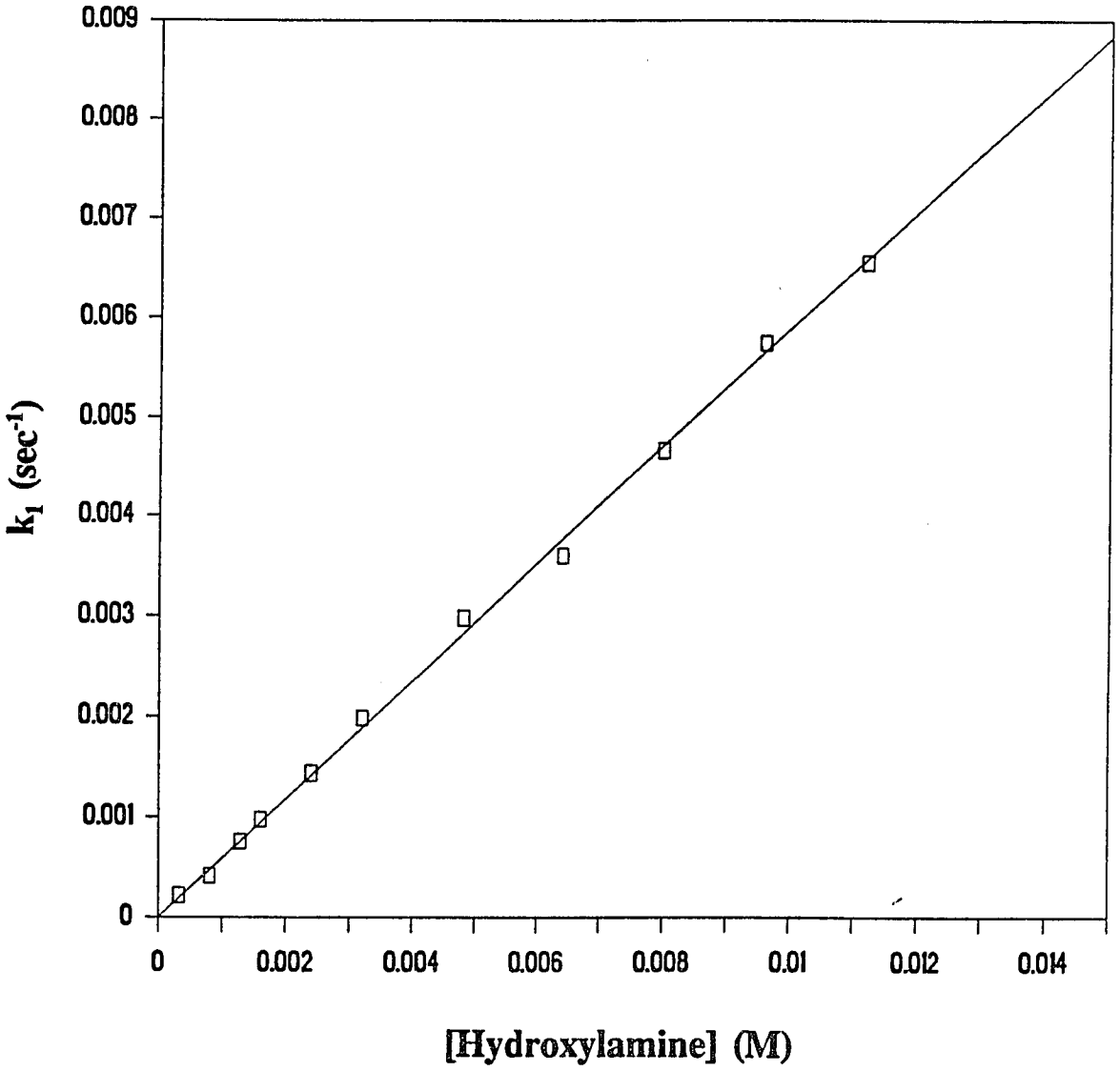

Fig.1 Effect of hydroxylamine concentration on the rate of spontaneous formation of salicylaldoxime in pH 6.0 0.1 M phosphate buffer, 25.5°C.
[salicylaldehyde] = 0.160 mM.
k_1 refers to the pseudo-first-order rate constant.
The second-order rate constant (k_2 = slope) is
$0.5891(\pm 4.72 \times 10^{-3})$ M^{-1} sec^{-1}.
(Data of Table I Appendix D)

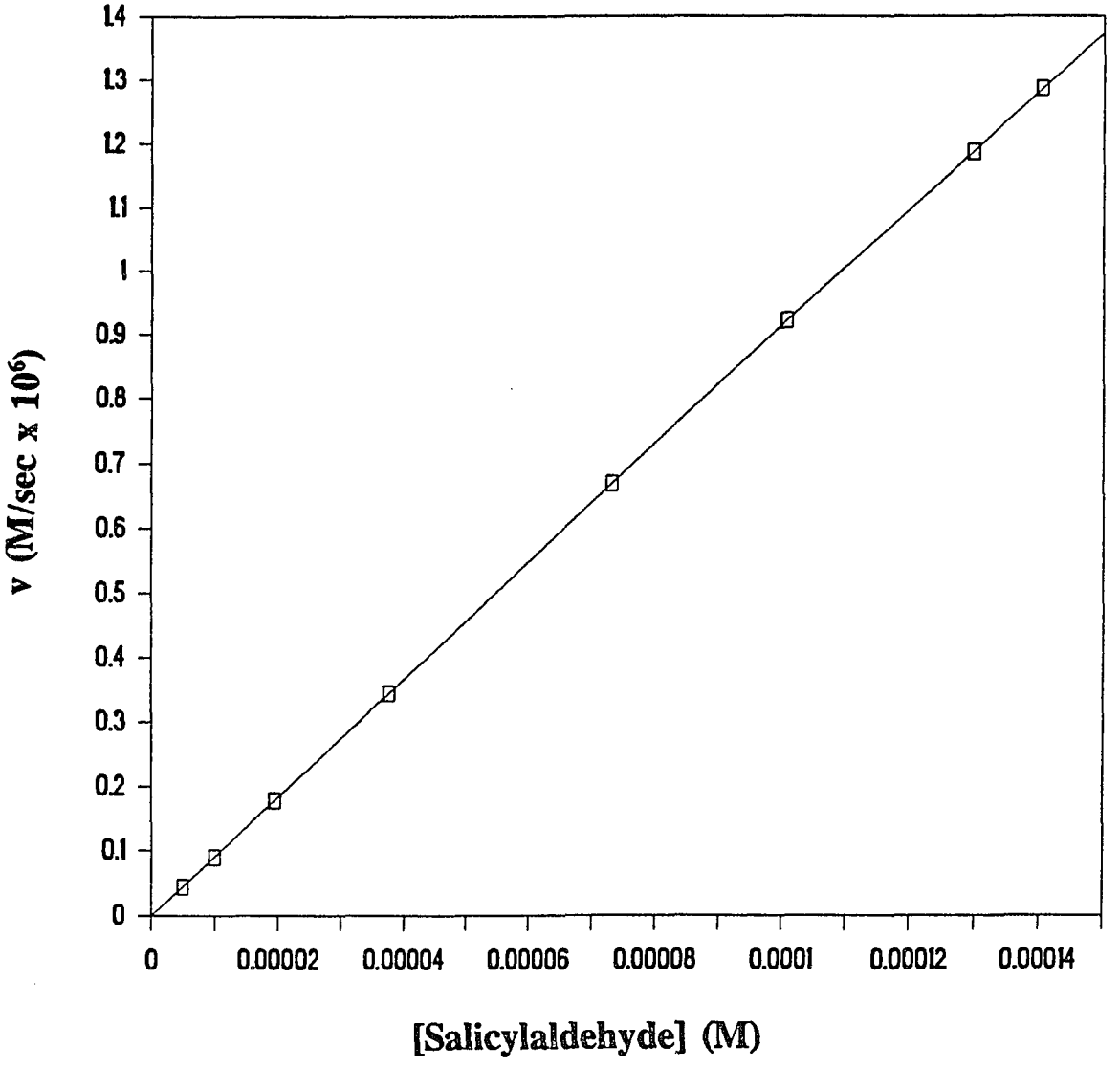

Fig.2 Effect of salicylaldehyde concentration on the rate of spontaneous formation of salicylaldoxime in pH 6.0 0.1 M phosphate buffer, 25.5°C. [hydroxylamine] = 16.0 mM. v refers to the initial rate. The second-order rate constant (k_2 = slope/[hydroxylamine]) is $0.572(\pm 5.02 \times 10^{-5})$ M^{-1} sec^{-1}.
(Data of Table II Appendix D)

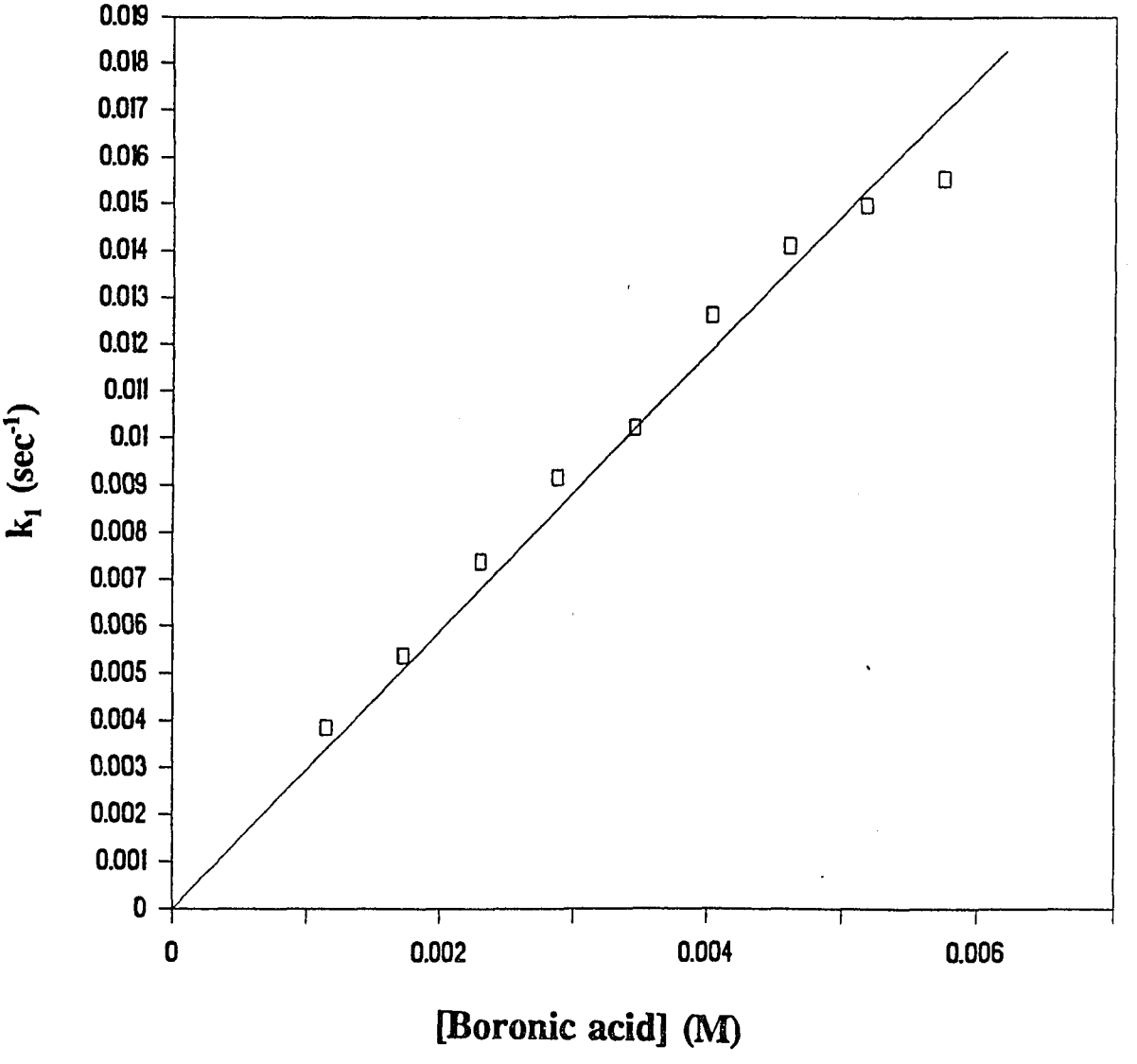

Fig.3 Effect of 3,5-bis(trifluoromethyl)benzeneboronic acid concentration on the rate of salicylaldoxime formation in pH 6.0 0.1 M phosphate buffer, 25.5°C. [salicylaldehyde] = 0.160 mM, [hydroxylamine] = 0.800 mM. k_1 refers to the pseudo-first-order rate constant. The third-order rate constant (k_3 = slope/[hydroxylamine]) is 3686($\pm$79.5) M^{-2} sec^{-1}. (Data of Table III Appendix D)

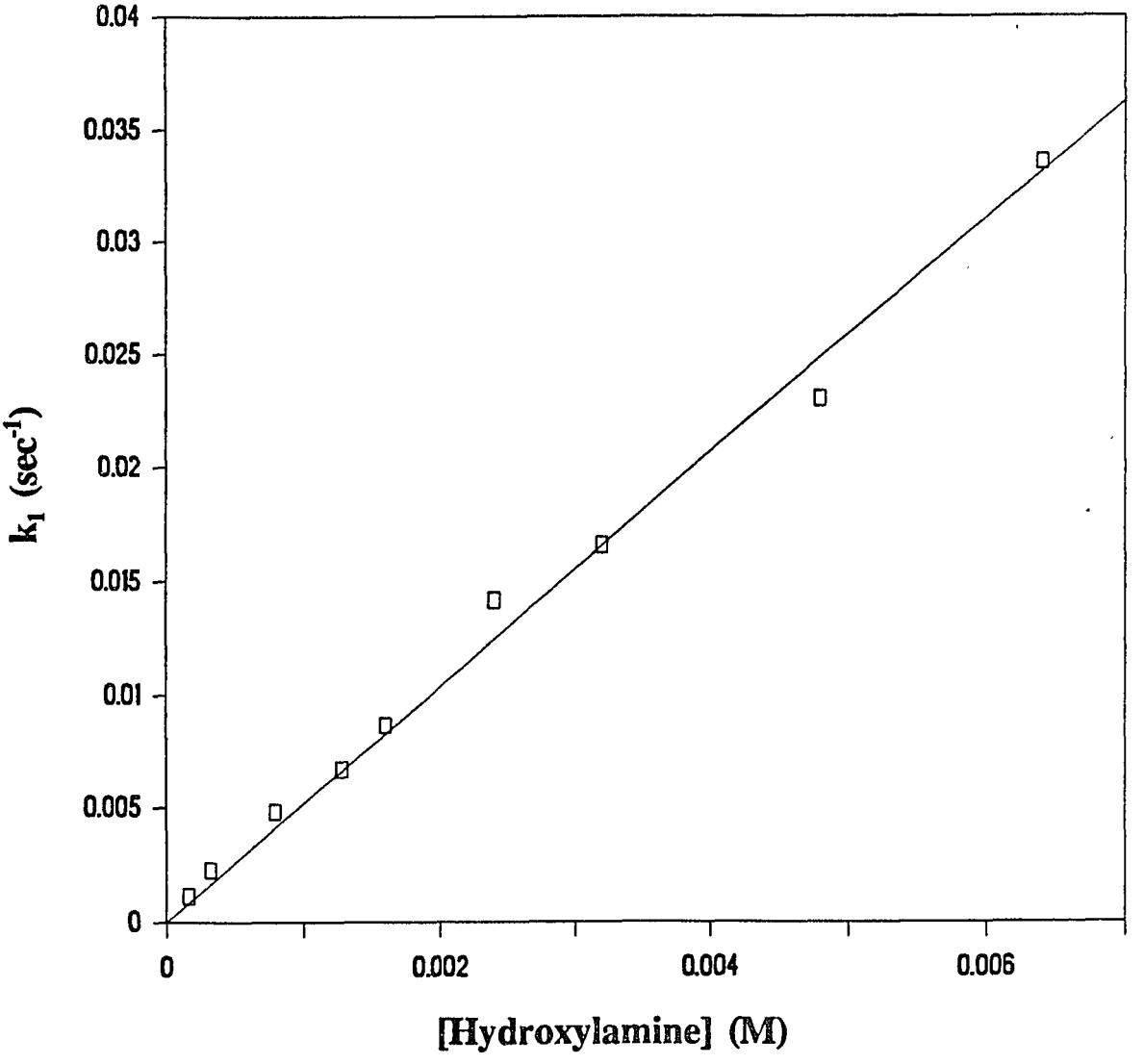

Fig.4 Effect of hydroxylamine concentration on the rate of 3,5-bis(trifluoromethyl)benzeneboronic acid catalyzed formation of salicylaldoxime in pH 6.0 0.1 M phosphate buffer, 25.5°C.
[salicylaldehyde] = 0.160 mM, [boronic acid] = 1.18 mM.
k_1 refers to the pseudo-first-order rate constant. The third-order rate constant (k_3 = slope/[boronic acid]) is 4384($\pm$90.0) M^{-2} sec^{-1}.
(Data of Table IV Appendix D)

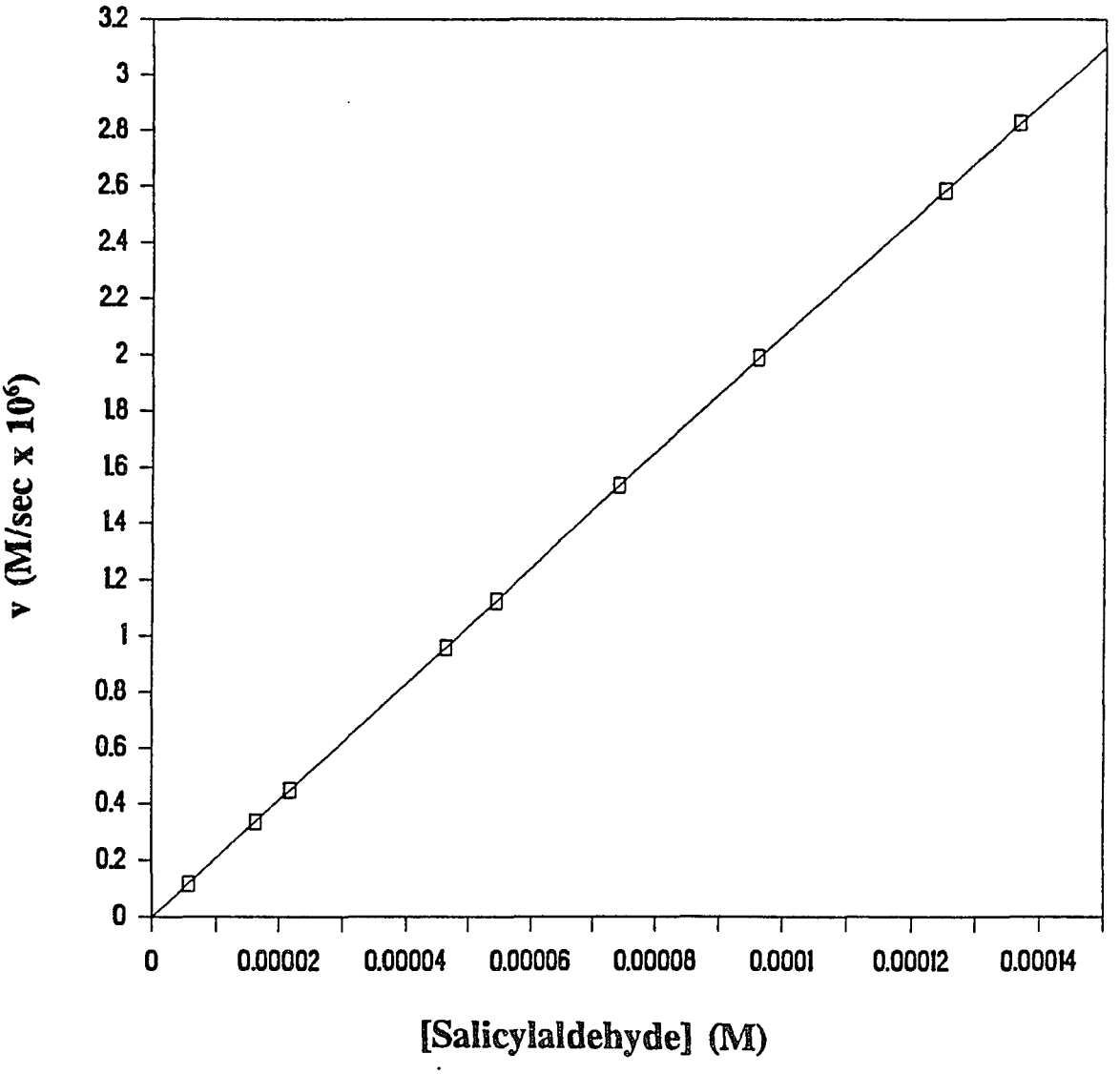

Fig.5 Effect of salicylaldehyde concentration on the rate of 3,5-bis(trifluoromethyl)benzeneboronic acid catalyzed formation of salicylaldoxime in pH 6.0 0.1 M phosphate buffer, 25.5°C. [boronic acid] = 2.30 mM, [hydroxylamine] = 1.66 mM. v refers to the initial rate. The third-order rate constant (k_3 = slope/([boronic acid]x[hydroxylamine])) is 5415($\pm$0.746) M^{-2} sec^{-1}.
(Data of Table V Appendix D)

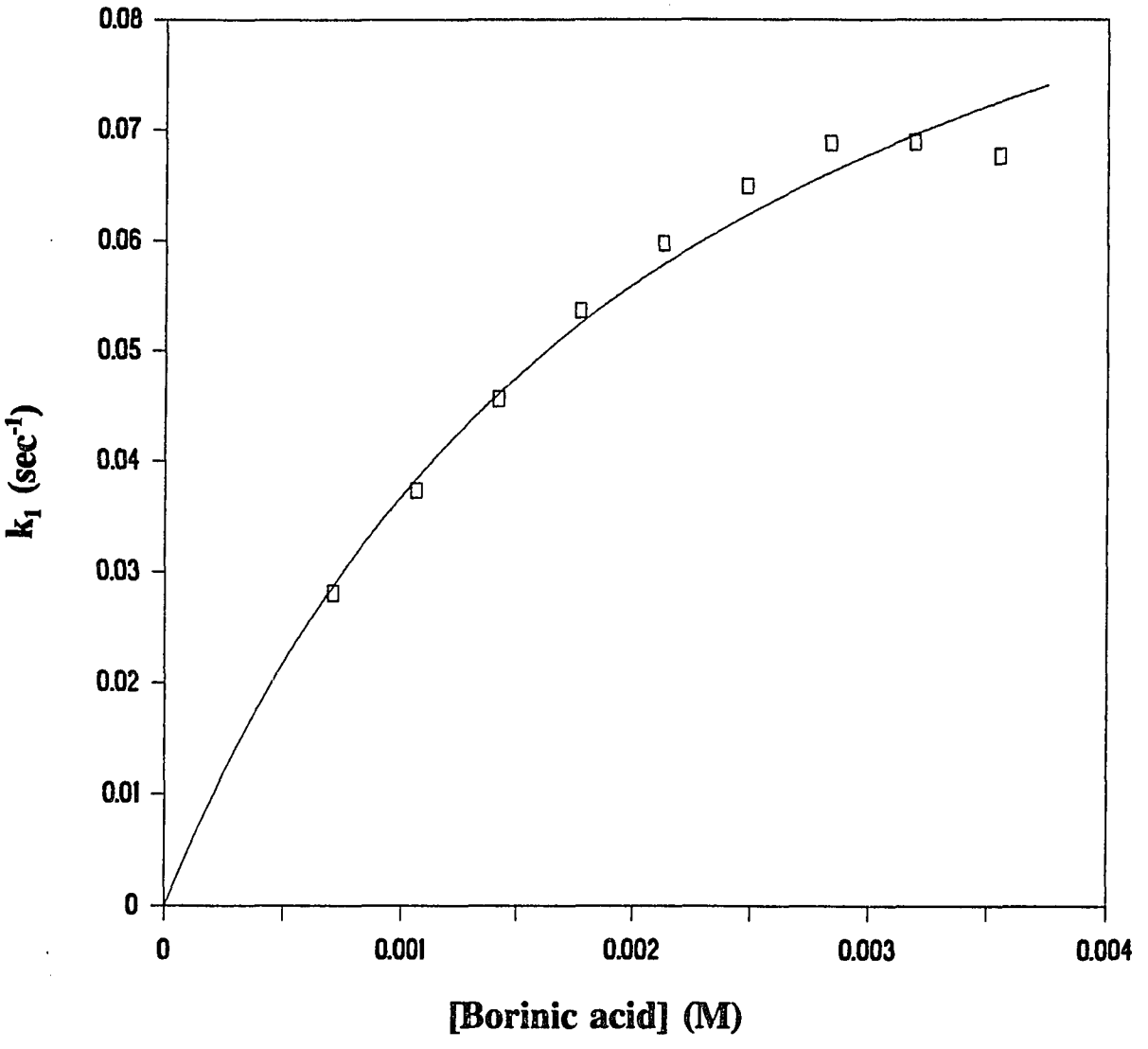

Fig.6 Effect of diphenylborinic acid concentration on the rate of salicylaldoxime formation in pH 6.5 0.1 M phosphate buffer, 25.5°C. [hydroxylamine] = 1.71 mM, [salicylaldehyde] = 0.160 mM.
k_1 refers to the pseudo-first-order rate constant.
(Data of Table VI Appendix D)

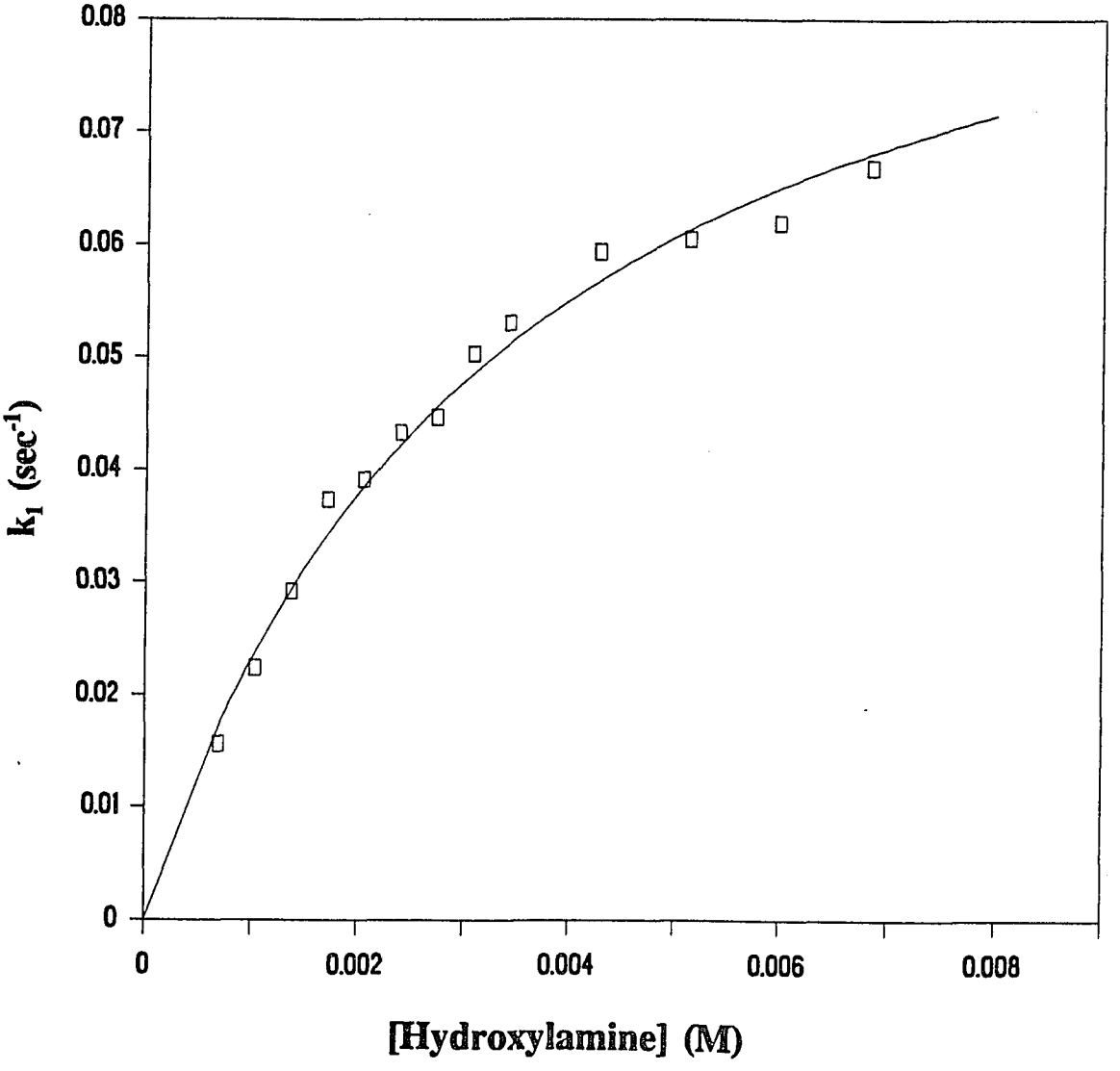

Fig.7 Effect of hydroxylamine concentration on the rate of diphenylborinic acid catalyzed formation of salicylaldoxime in pH 6.5 0.1 M phosphate buffer, 25.5°C.
[borinic acid] = 1.06 mM, [salicylaldehyde] = 0.160 mM.
k_1 refers to the pseudo-first-order rate constant.
(Data of Table VII Appendix D)

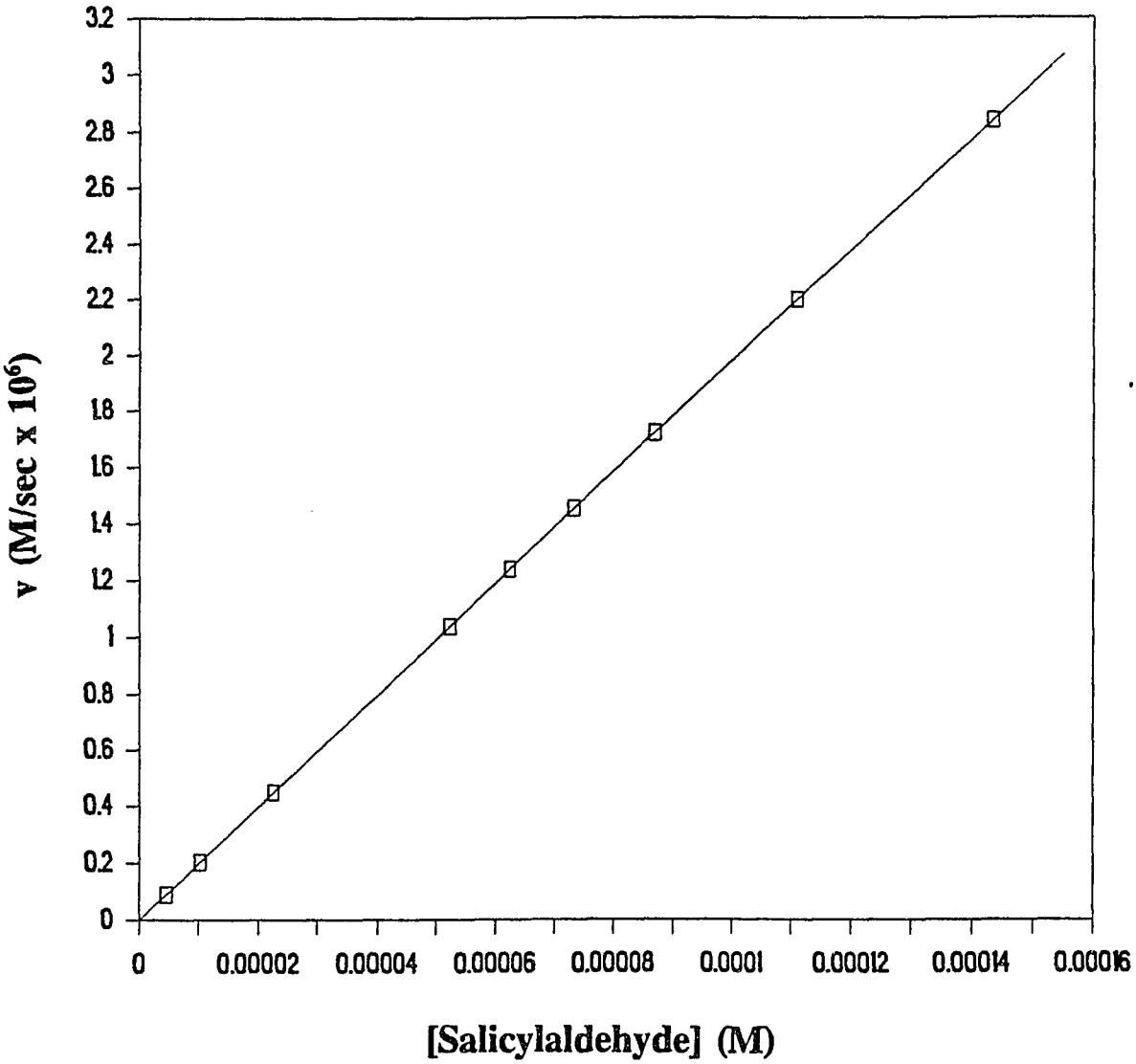

Fig.8 Effect of salicylaldehyde concentration on the rate of diphenylborinic acid catalyzed formation of salicylaldoxime in pH 6.5 0.1 M phosphate buffer, 25.5°C. [borinic acid] = 1.06 mM, [hydroxylamine] = 0.856 mM. v refers to the initial rate. The third-order rate constant (k_3 = slope/([borinic acid]x[hydroxylamine])) is $2.18 \times 10^4 (\pm 1.45)$ M^{-2} sec^{-1}.
(Data of Table VIII Appendix D)

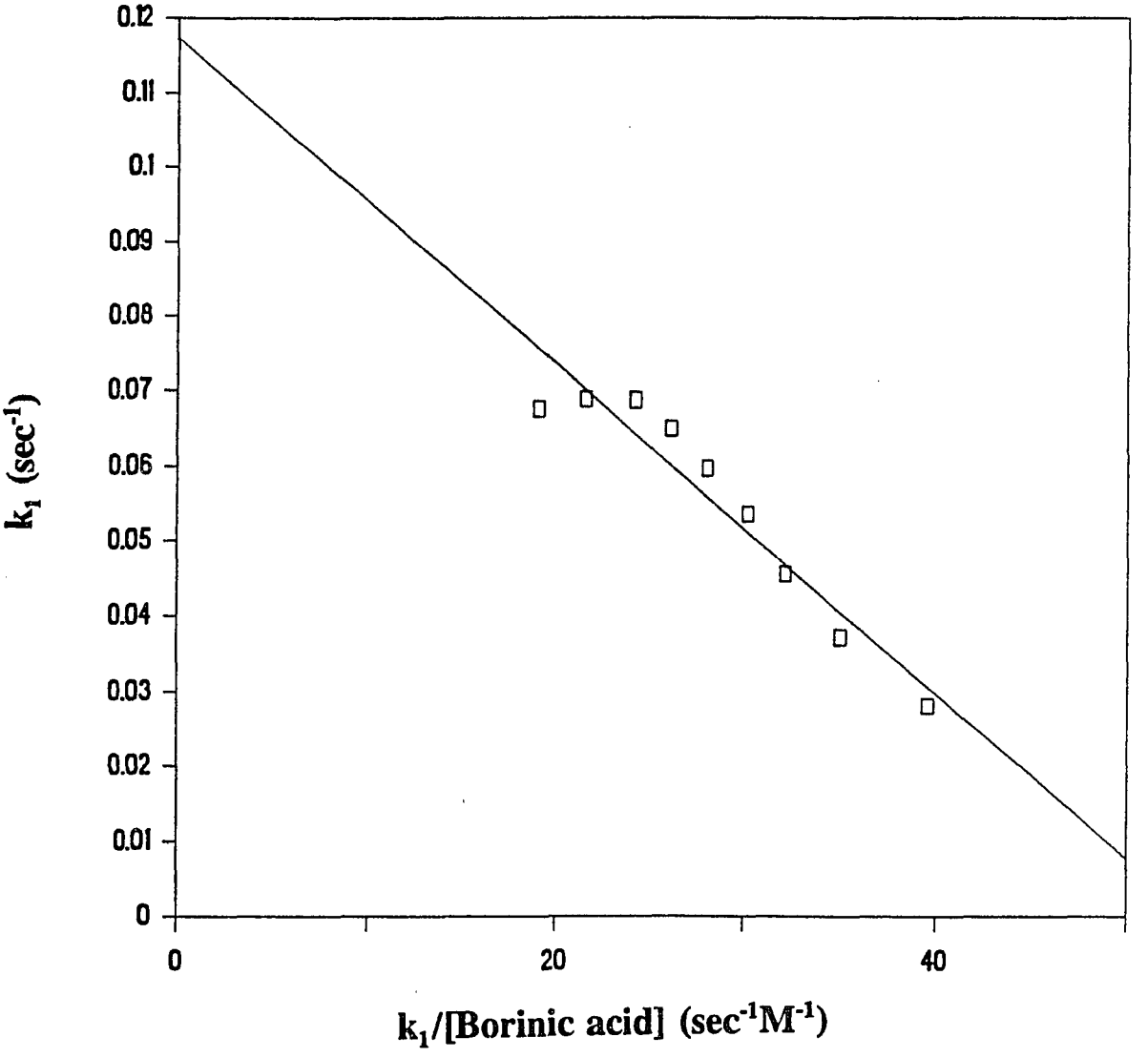

Fig.9 Eadie-Hofstee plot for the effect of diphenylborinic acid concentration on the rate of salicylaldoxime formation in pH 6.5 0.1 M phosphate buffer, 25.5°C. [hydroxylamine] = 1.71 mM, [salicylaldehyde] = 0.160 mM.
k_1 refers to the pseudo-first-order rate constant.
K_m = 2.19(±0.249) mM, k_{cat} = 0.117(±4.61x10^{-3}) sec^{-1}.
(Data of Table VI Appendix D)

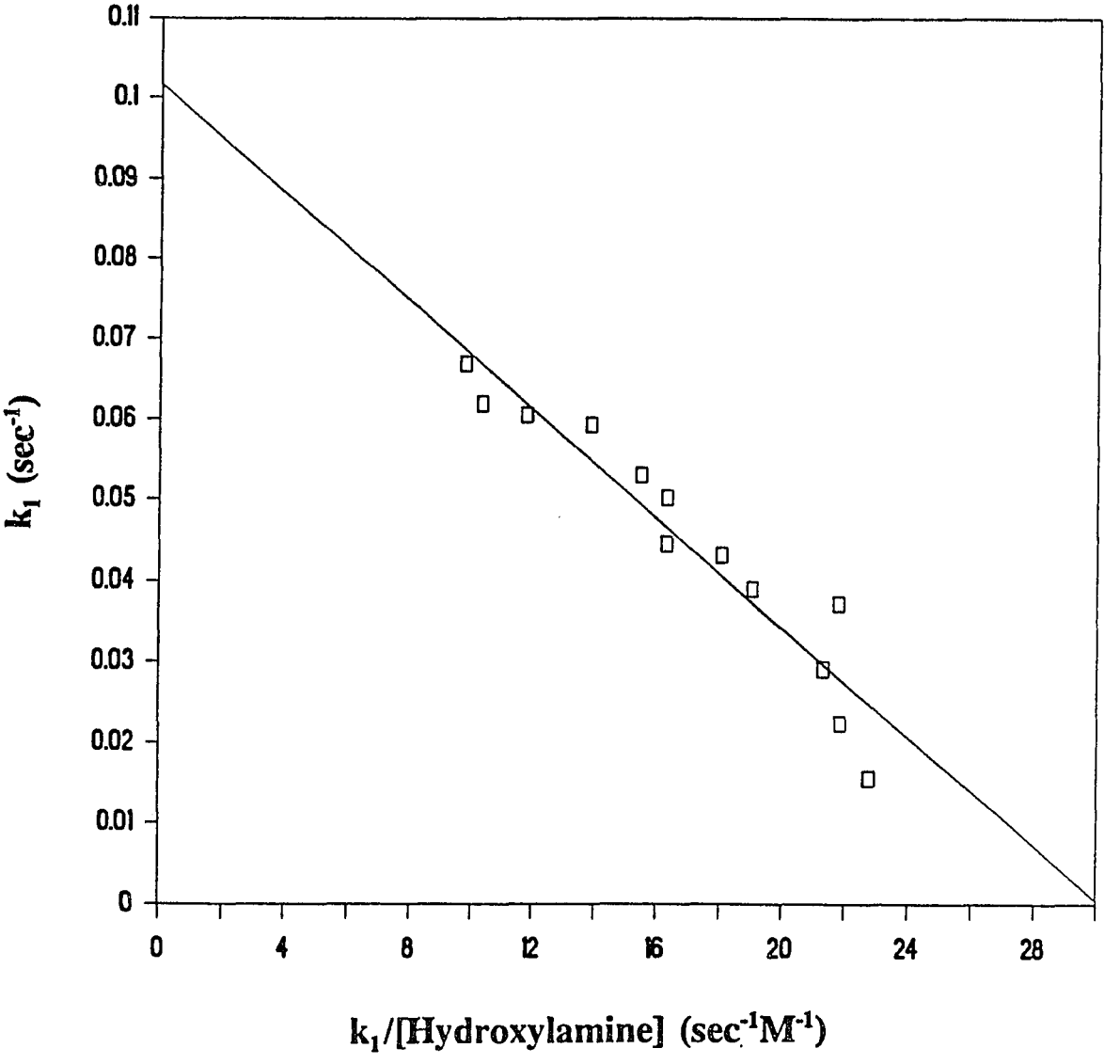

Fig.10 Eadie-Hofstee plot for the effect of hydroxylamine concentration on the rate of diphenylborinic acid catalyzed formation of salicylaldoxime in pH 6.5 0.1 M phosphate buffer, 25.5°C.
[borinic acid] = 1.06 mM, [salicylaldehyde] = 0.160 mM.
k_1 refers to the pseudo-first-order rate constant.
K_m = 3.37(±0.331) mM, k_{cat} = 0.102(±5.135x10^{-3}) sec^{-1}.
(Data of Table VII Appendix D)

a function of pH in Fig.11. The pH dependence suggests that specific acid catalysis is involved in this reaction system. The pK of 5.90 observed in the pH profile reflects the ionization of hydroxylamine[43], which functions in its neutral form as an active nucleophile. In the low pH region where the second-order rate constant is independent of pH, the increase on the concentration of the active form of the carbonyl group of salicylaldehyde ($>C=OH^+$) is balanced by the protonation of hydroxylamine. This results in the plateau observed in the acidic part of the pH profile. At the pH values above the pK of hydroxylamine, the nucleophile mainly exists in its active neutral form, but the concentration of $>C=OH^+$ decreases with increasing pH, therefore the rate constant decreases linearly with increasing pH. In the high pH range in which the carbonyl group is more completely in its neutral form $>C=O$, a different mechanism must become predominant. Thus, the observed rate constant becomes independent of pH.

The pH profile of the third-order rate constant (k_3) of 3,5-bis(trifluoromethyl)-benzeneboronic acid catalyzed salicylaldoxime formation is bell shaped with pK_1 of 6.06 and pK_2 of 6.74 (Fig.12). The optimum catalytic activity was observed at pH 6.40 with the limiting third-order rate constant of 1.149×10^4 M^{-2} sec^{-1}. In order to determine the origin of the pKs observed in this pH dependence, other benzeneboronic acids which have different ionization pKs (see Appendix E Table I) were selected for the pH study. Like 3,5-bis(trifluoromethyl)benzeneboronic acid, salicylaldoxime formation catalyzed by other boronic acids uniformly displayed similar pH dependence with pK_1 around 6 and pK_2 around 7 (Appendix E). The experimental results suggest that only the unionized neutral forms of the boronic acids are catalytically active. These benzeneboronic acids share a common catalytic mechanism in this reaction system. While the pK_1 observed in

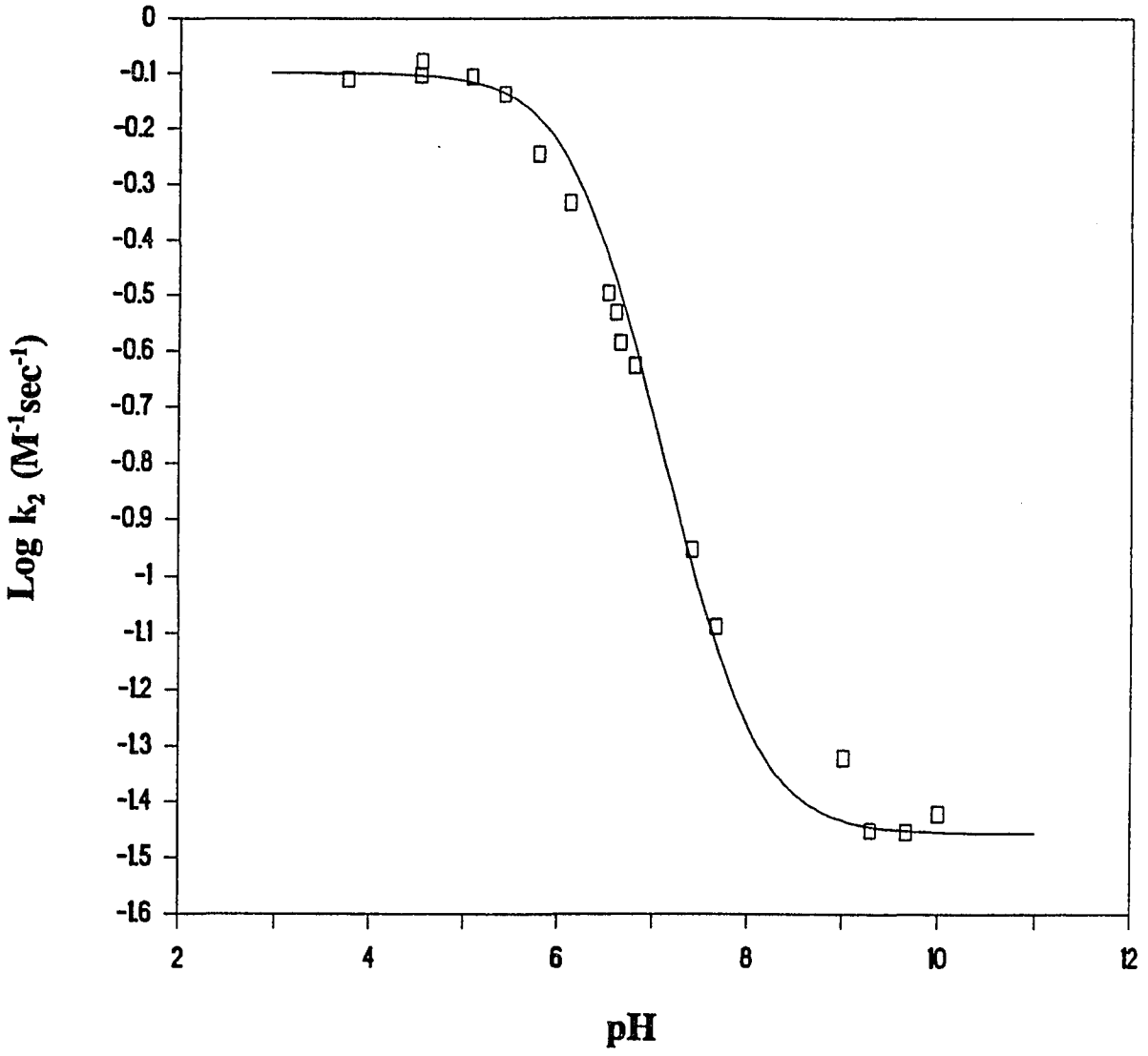

Fig.11 pH profile of spontaneous formation of salicylaldoxime in 0.1 M buffers, 25.5°C. pK = 5.90(±0.15).
In acidic region, k_2 (Lim) = 0.798(±0.092) M^{-1} sec^{-1}.
In alkali, k_2 (Lim) = $3.50x10^{-2}$(±$3.0x10^{-3}$) M^{-1} sec^{-1}.
k_2 refers to the second-order rate constant.
(Data of Table IX Appendix D)

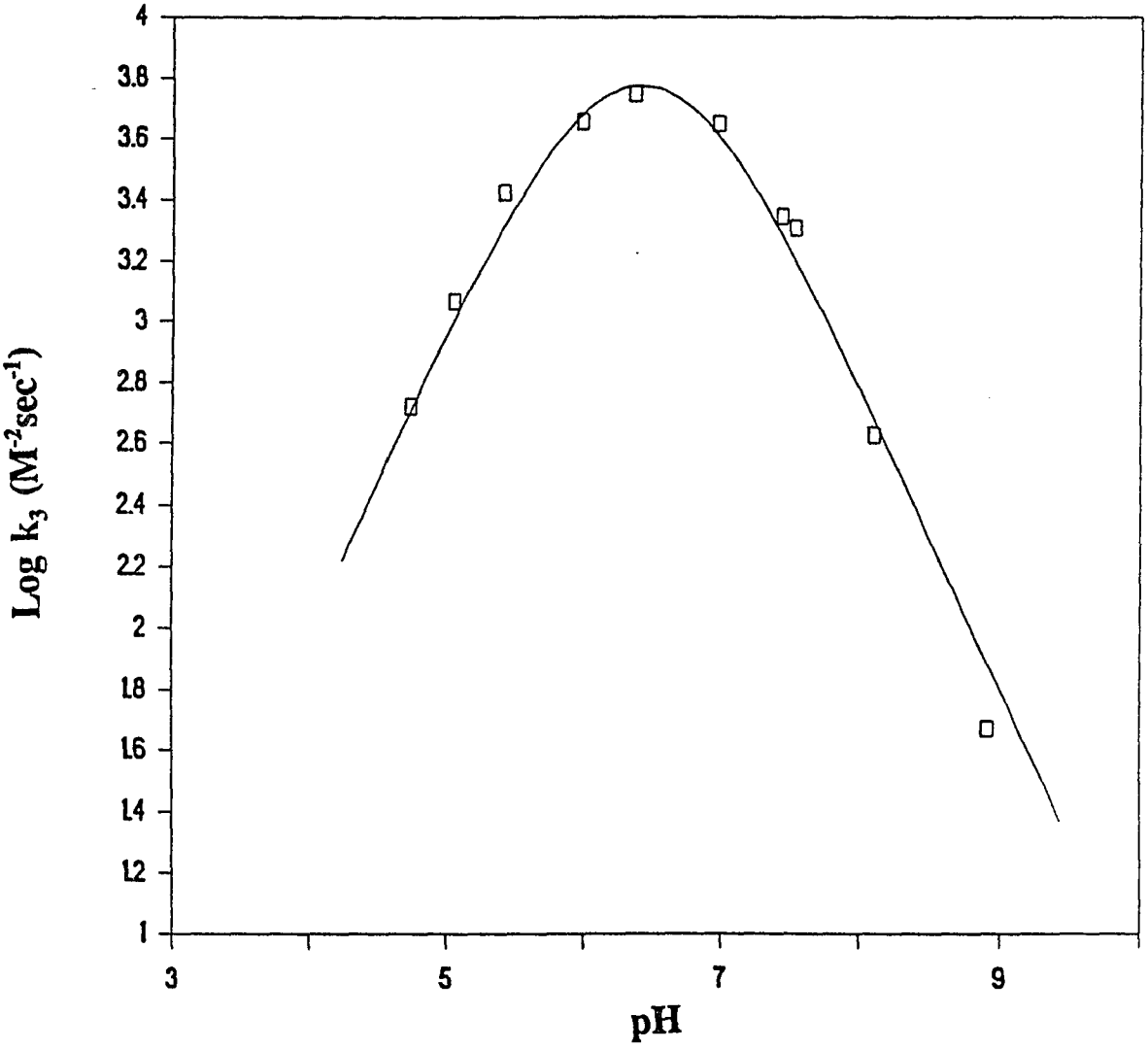

Fig.12 pH profile of 3,5-bis(trifluoromethyl)benzeneboronic acid catalyzed formation of salicylaldoxime in 0.1 M buffers, 25.5°C.
$pK_1 = 6.06(\pm 0.05)$, $pK_2 = 6.74(\pm 0.10)$, optimum pH = $6.40(\pm 0.07)$,
k_3 (Lim) = $1.149 \times 10^4(\pm 2.417 \times 10^3)$ M^{-2} sec^{-1}.
k_3 refers to the third-order rate constant.
(Data of Table X Appendix D)

Similar pH profiles for other boronic acids are in Appendix E

these pH profiles reflects the ionization of hydroxylamine, the pK_2 may have different origins. Since the phenol group of salicylaldehyde has a pK of 6.79[44], in the catalysis of boronic acids which have ionization pKs near 7, (like the cases of 3,5-bis(trifluoro-methyl)benzeneboronic acid and 3,5-dichlorobenzeneboronic acid in this study,) the pK_2 may relate to the inability of the ionized phenol anion to complex to the negative tetrahedral boronic acids. Another possible origin for the pK_2 is presumably the ionization of the amino group in the ternary complex (Scheme IV structure A). This could explain the common pK_2 around 7 observed in the pH dependencies of the oxime formation catalyzed by the benzeneboronic acids with ionization pK higher than 7.

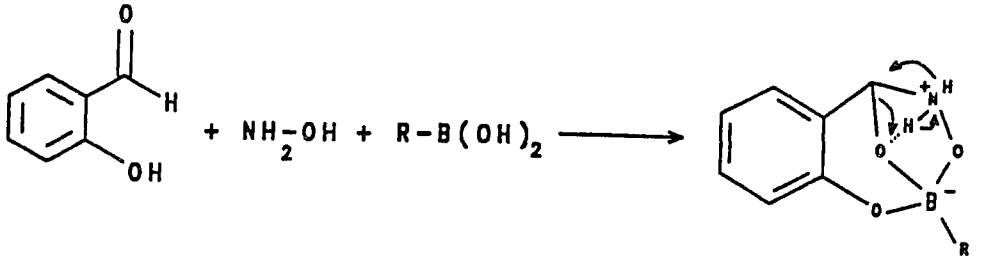

A

Scheme IV

A bell-shaped pH dependence was also observed for the boric acid catalyzed formation of salicylaldoxime (Fig.13). Boric acid catalysis was optimal at pH 7.35 with the limiting third-order rate constant of 75.5 M^{-2} sec^{-1}. The pK_1 of 6.10 is close to the pK of hydroxylamine. The pK_2 of 8.60 perhaps is due to the ionization of boric acid[8]. The pH profile indicates that neutral boric acid prefers the ionized phenol group of salicylaldehyde for binding in its catalysis.

In the case of diphenylborinic acid catalyzed salicylaldoxime formation, the pH dependence (Fig.14) is quite different from those observed in the cases of boronic acid

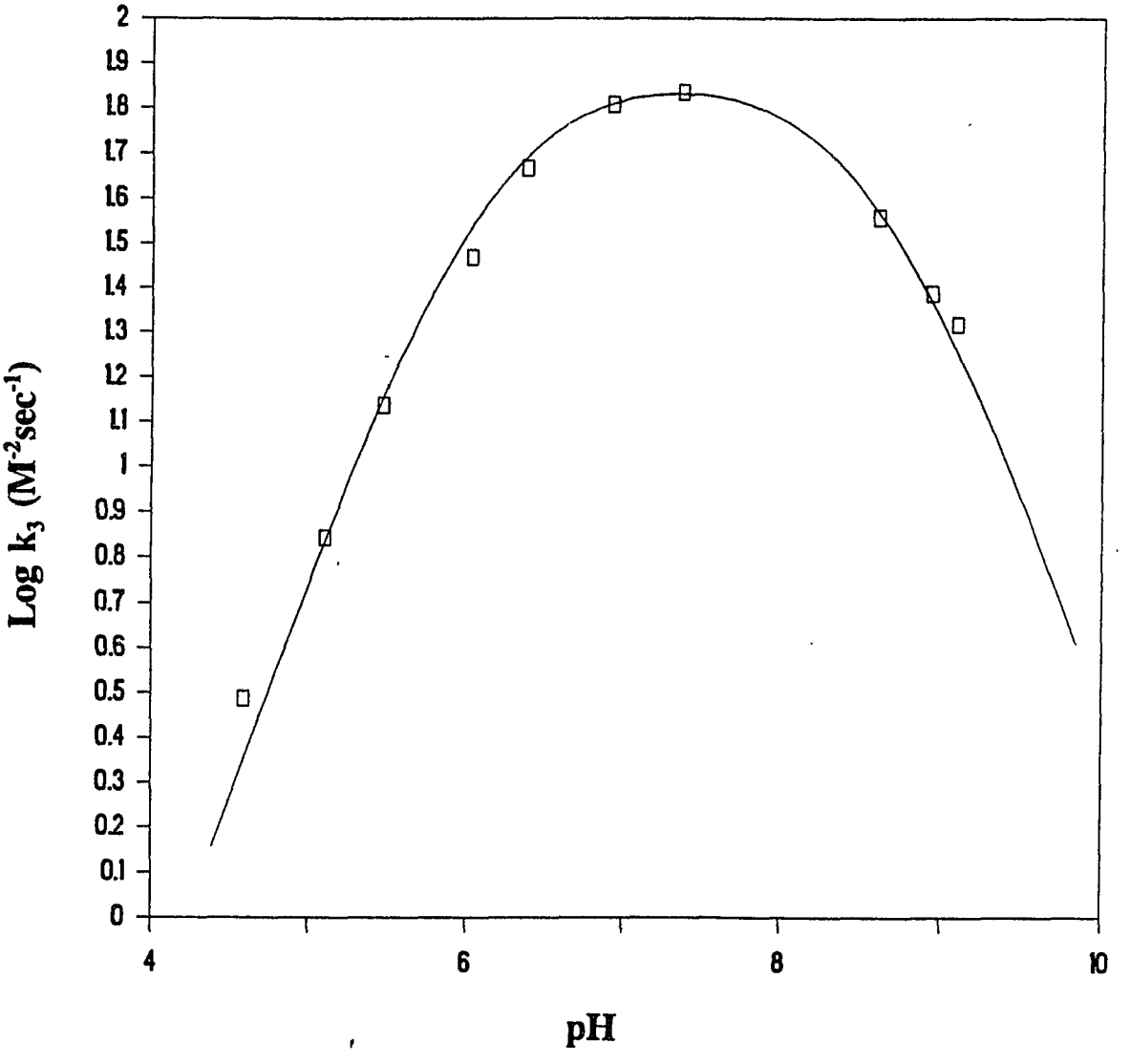

Fig.13 pH profile of boric acid catalyzed formation of salicylaldoxime in 0.1 M buffers, 25.5°C. pK_1 = 6.10(±0.05), pK_2 = 8.60(±0.05), optimum pH = 7.35(±0.05), k_3 (Lim) = 75.5(±1.49) M^{-2} sec^{-1}.
k_3 refers to the third-order rate constant.
(Data of Table XI Appendix D)

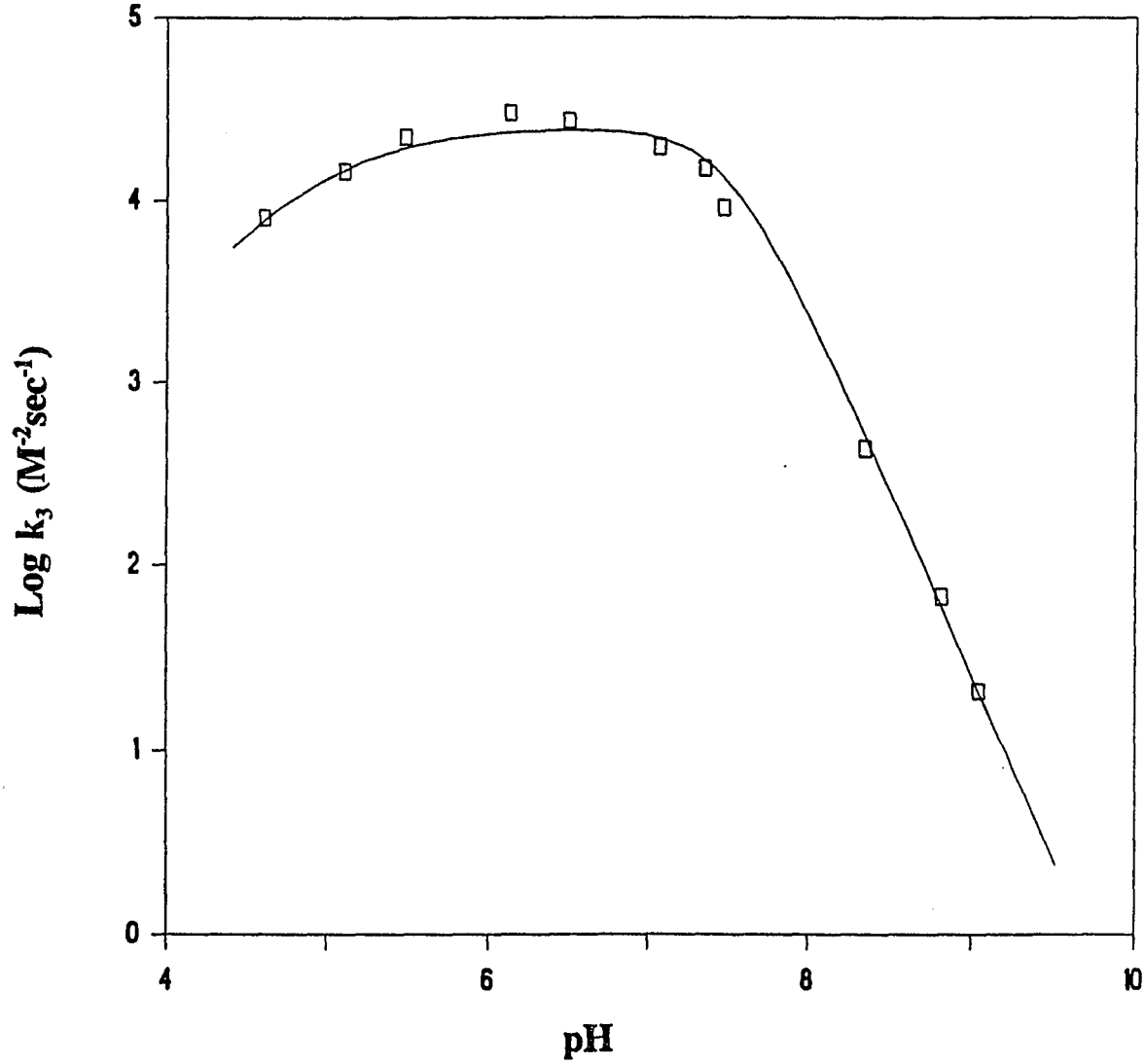

Fig.14 pH profile of diphenylborinic acid catalyzed formation of salicylaldoxime in 0.1 M buffers, 25.5°C.
Double-ionization pK (average) = 7.50($\pm$0.05),
k_3 (Lim) = $2.50 \times 10^4 (\pm 1.93 \times 10^3)$ M^{-2} sec^{-1}.
k_3 refers to the third-order rate constant.
(Data of Table XII Appendix D)

catalysis. This pH profile shows double-proton ionization with the average pK of 7.50. The limiting third-order rate constant is 2.50×10^4 M^{-2} sec^{-1}. Since the pK of diphenylborinic acid is 6.2[45], the pH dependence suggests that diphenylborinic acid is catalytically active in both ionized and unionized forms. The catalytic mechanism involved in this case is clearly different from those used by boric and boronic acids.

Effect of substituents of benzeneboronic acid on the formation of salicylaldoxime. In order to determine the influence of Hammett σ on the catalytic effectiveness of boronic acid, the logarithm values of the limiting third-order rate constants obtained from the pH profiles of salicylaldoxime formation catalyzed by various substituted benzeneboronic acids are plotted as a function of substituent constants in Fig.15. In this plot, all the boronic acids fall on a straight line with a slope of +1.51 suggesting that benzeneboronic acids with electron-withdrawing substituents are better catalysts than those with electron-donating substituents.

Solvent deuterium isotope effect on the formation of salicylaldoxime. The purpose of this experiment is to determine if proton transfer is involved in the rate-determining step of the reaction. The pH profiles of spontaneous, boric acid, 3,5-bis-(trifluoromethyl)benzeneboronic acid and diphenylborinic acid catalyzed salicylaldoxime formation in deuterium oxide are similar to those obtained in water (Appendix F). However, lower reaction rate constants were observed in deuterium oxide (Table I). Since the ratios of k_H/k_D are greater than one, it may be concluded that proton transfer is involved in the rate determining step of salicylaldoxime formation.

Effect of pH on the formation of salicylaldehyde O-methyloxime. In an effort to investigate the function of OH group of hydroxylamine in the boron acid catalyzed

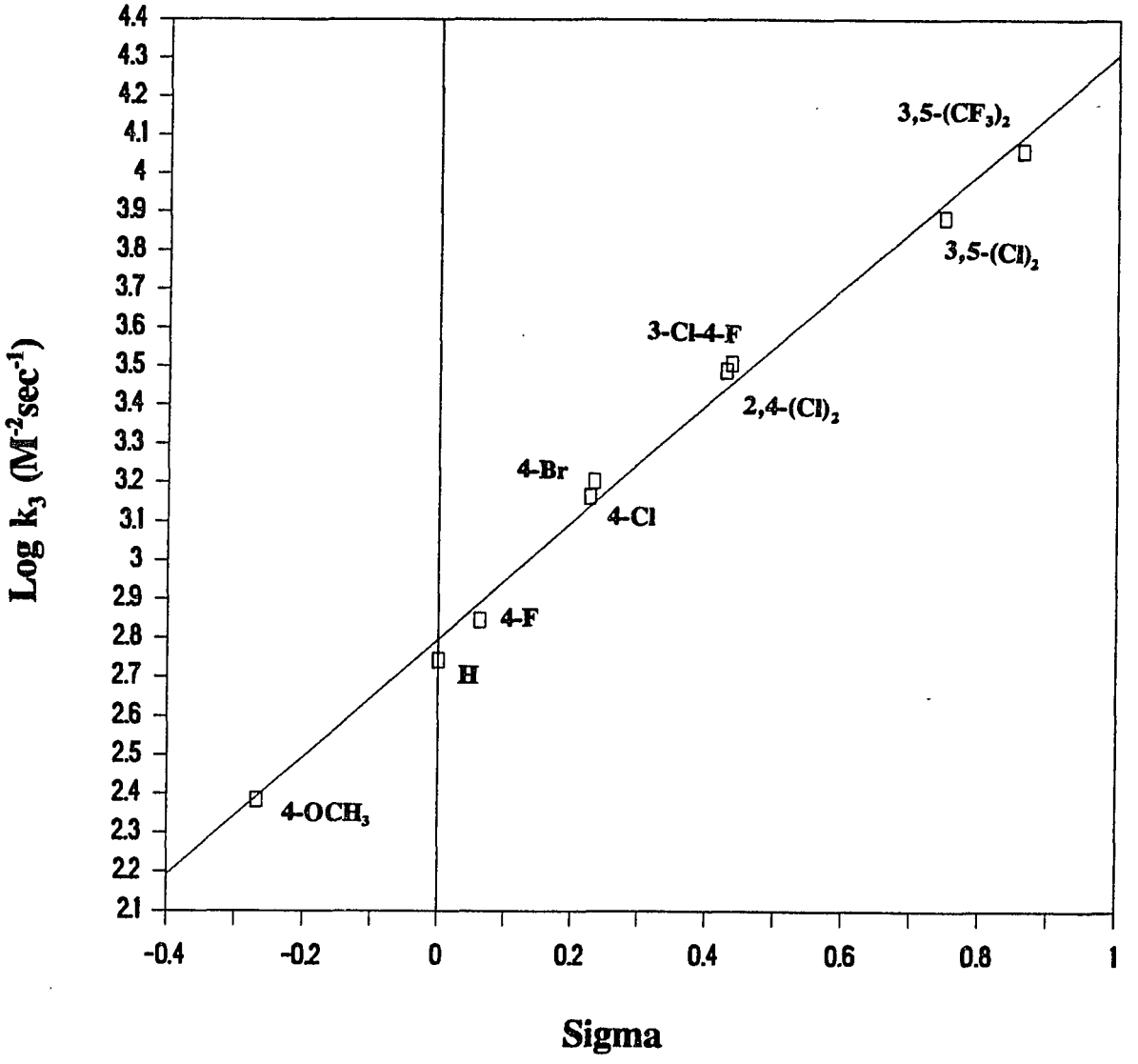

Fig.15 Hammett plot relating log k_3 (Lim) and *sigma* for the formation of salicylaldoxime catalyzed by substituted benzeneboronic acids in 0.1 M buffer, 25.5°C. The value of *rho* is $+1.51 \pm 0.048$.
k_3 refers to the third-order rate constant.
(Data of Table XIII Appendix D)

Table I

Solvent Deuterium Isotope Effect

on the Formation of Salicylaldoxime at 25.5°C

boron acid	k_3 (Lim.in H_2O) (M^{-2} sec^{-1})	k_3 (Lim.in D_2O) (M^{-2} sec^{-1})	k_{3H}/k_{3D} (Lim.)
boric acid	75.54 (±1.49)	50.24 (±2.62)	1.50 (±0.114)
3,5-bis(trifluoro-methyl)benzene-boronic acid	$1.15x10^4$ ($\pm 2.42x10^3$)	$5.84x10^3$ ($\pm 6.59x10^2$)	1.97 (±0.717)
diphenyl-borinic acid	$2.50x10^4$ ($\pm 1.93x10^3$)	$1.30x10^4$ ($\pm 2.00x10^3$)	1.92 (±0.525)

spontaneous (Opt.pH 4.00)	k_2 (Lim. in H_2O) (M^{-1} sec^{-1})	k_2 (Lim. in D_2O) (M^{-1} sec^{-1})	k_{2H}/k_{2D} (Lim.)
	0.798 (±0.092)	0.400 (±0.030)	1.995 (±0.410)

formation of salicylaldoxime, methoxylamine (NH_2-OCH_3) was used to substitute hydroxylamine in the oxime formation reaction. Unlike the case of salicylaldoxime formation, boric, boronic and diphenylborinic acids display the same type of pH dependence in the catalysis for the formation of salicylaldehyde O-methyloxime (Fig.16, 17, 18). These pH profiles are governed by single proton ionizations corresponding to the pKs of boron acids. This suggests that neutral trigonal boron acids are the effective catalysts. Since methoxylamine has a pK of 4.6[49], the pK_1 of 4.85 exhibited in the pH profile of 4-bromobenzeneboronic acid (Fig.17) may relate to the ionization of that nucleophile. This pK was not clearly observed in all the cases studied here. The pH dependencies observed here are consistent with those found in the boronic acid catalyzed hydrolysis of the imine formed from salicylaldehyde and an amino acid[26]. This indicates that salicylaldehyde O-methyloxime formation may share an identical catalytic mechanism with such imine hydrolyses.

When the limiting third-order rate constant, k_3(Lim), for a boron acid catalyzed reaction is compared to the spontaneous second-order rate constant (k_2) which is taken at the pH where optimal catalysis is observed, the ratio of k_2/k_3(Lim) reflects the binding affinity of the catalyst in the transition state of the catalytic complex[46], the lower the value, the higher the catalytic effectiveness.

Table II summarizes the values of limiting k_3 and k_2/k_3(Lim) determined for the formation of salicylaldoxime and salicylaldehyde O-methyloxime with different boron acids. It is clear that the effectiveness of boric and boronic acids in the catalysis of salicylaldoxime formation is at least 5-fold better than in the case of O-methyloxime formation. Diphenylborinic acid on the other hand, exhibits similar catalytic effect in

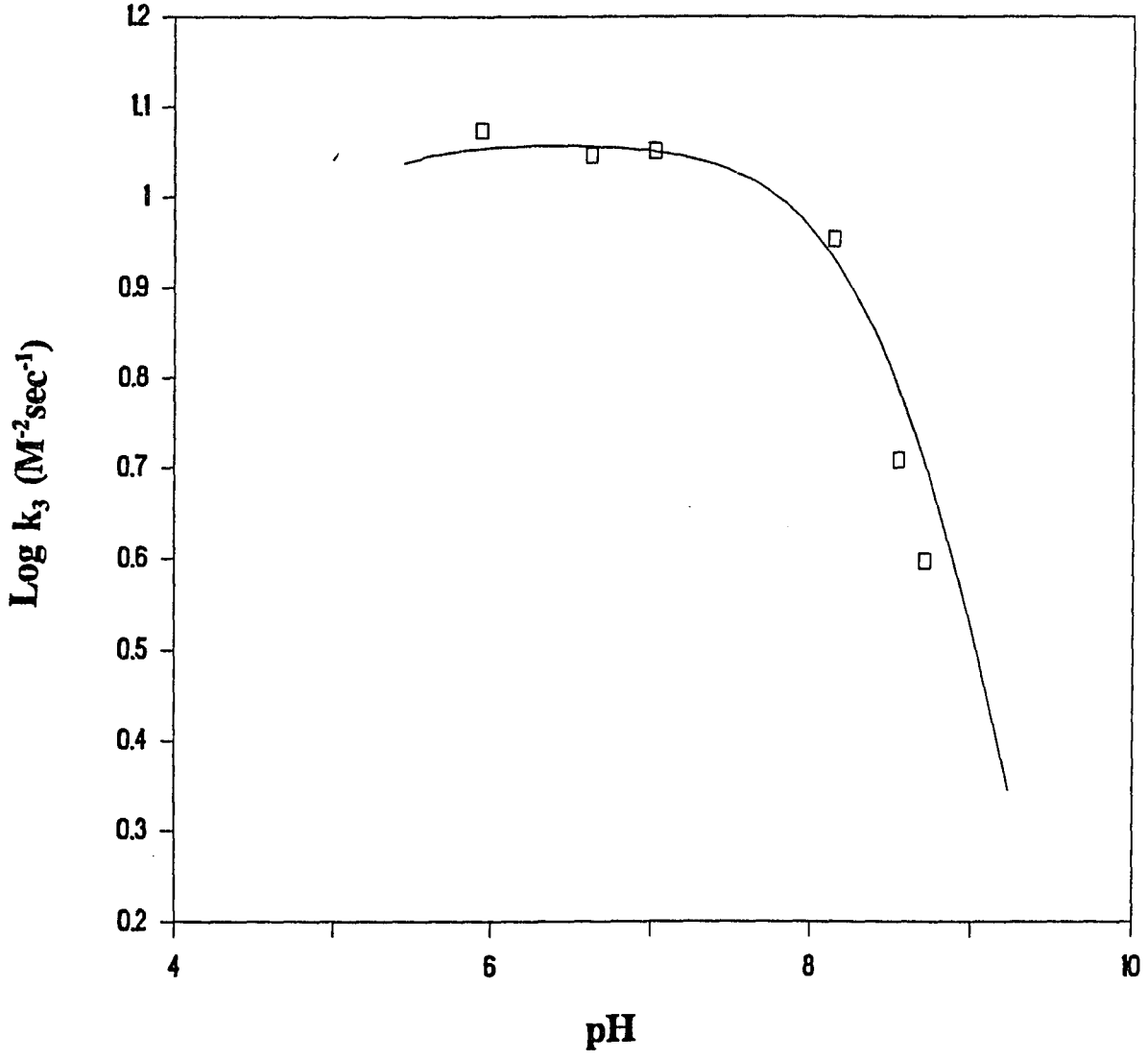

Fig.16 pH profile of boric acid catalyzed formation of salicylaldehyde O-methyloxime in 0.1 M buffers, 25.5°C.
pK = 8.60(±0.15), k_3 (Lim) = 11.54(±0.254) M^{-2} sec^{-1}.
k_3 refers to the third-order rate constant.
(Data of Table XIV Appendix D)

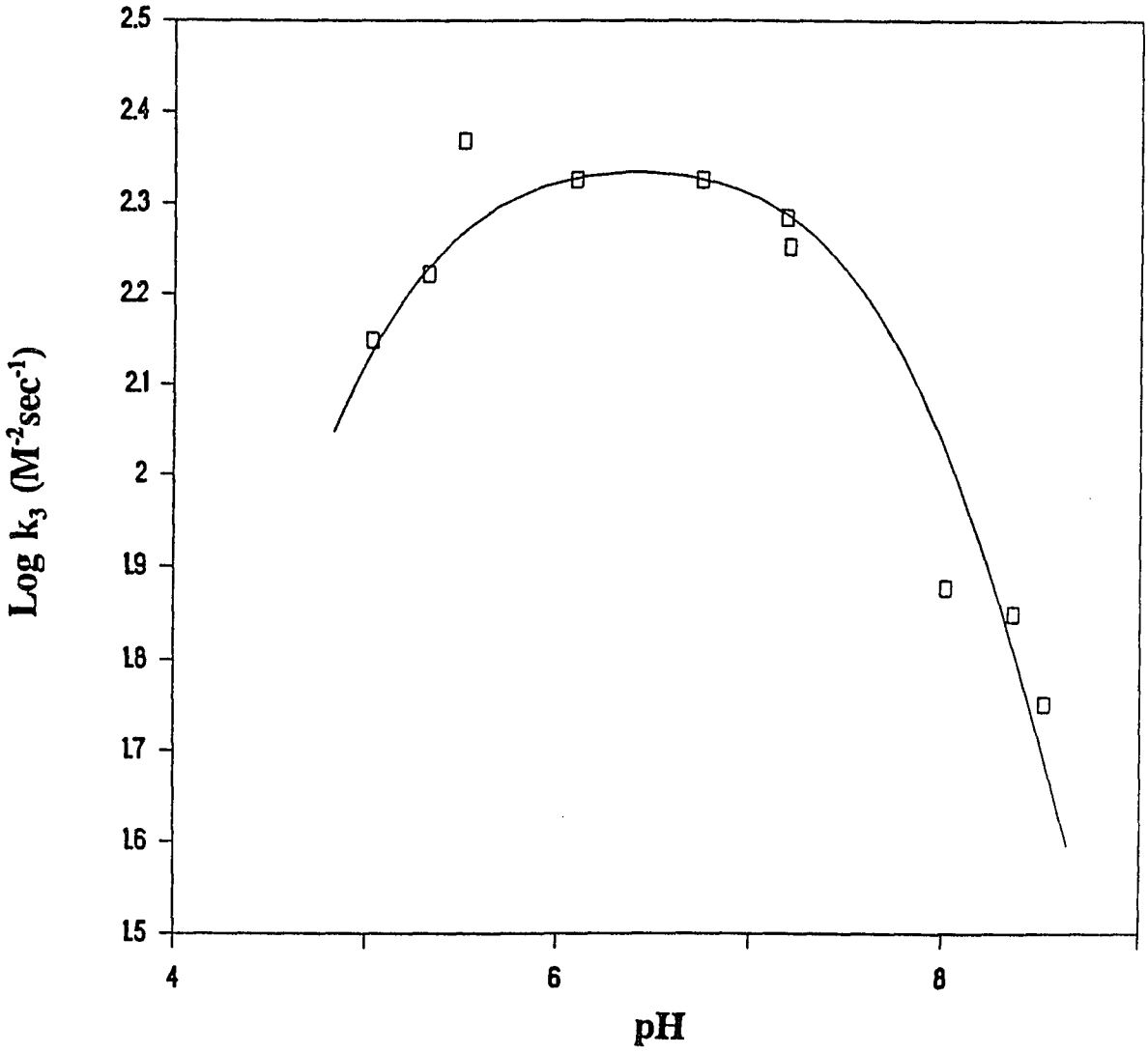

Fig.17 pH profile of 4-bromobenzeneboronic acid catalyzed formation of salicylaldehyde O-methyloxime in 0.1 M buffers, 25.5°C. $pK_1 = 4.85(\pm 0.05)$, $pK_2 = 7.95(\pm 0.10)$, optimum pH = $6.40(\pm 0.07)$, k_3 (Lim) = $2.28 \times 10^2(\pm 8.02)$ M^{-2} sec^{-1}. k_3 refers to the third-order rate constant. (Data of Table XV Appendix D)

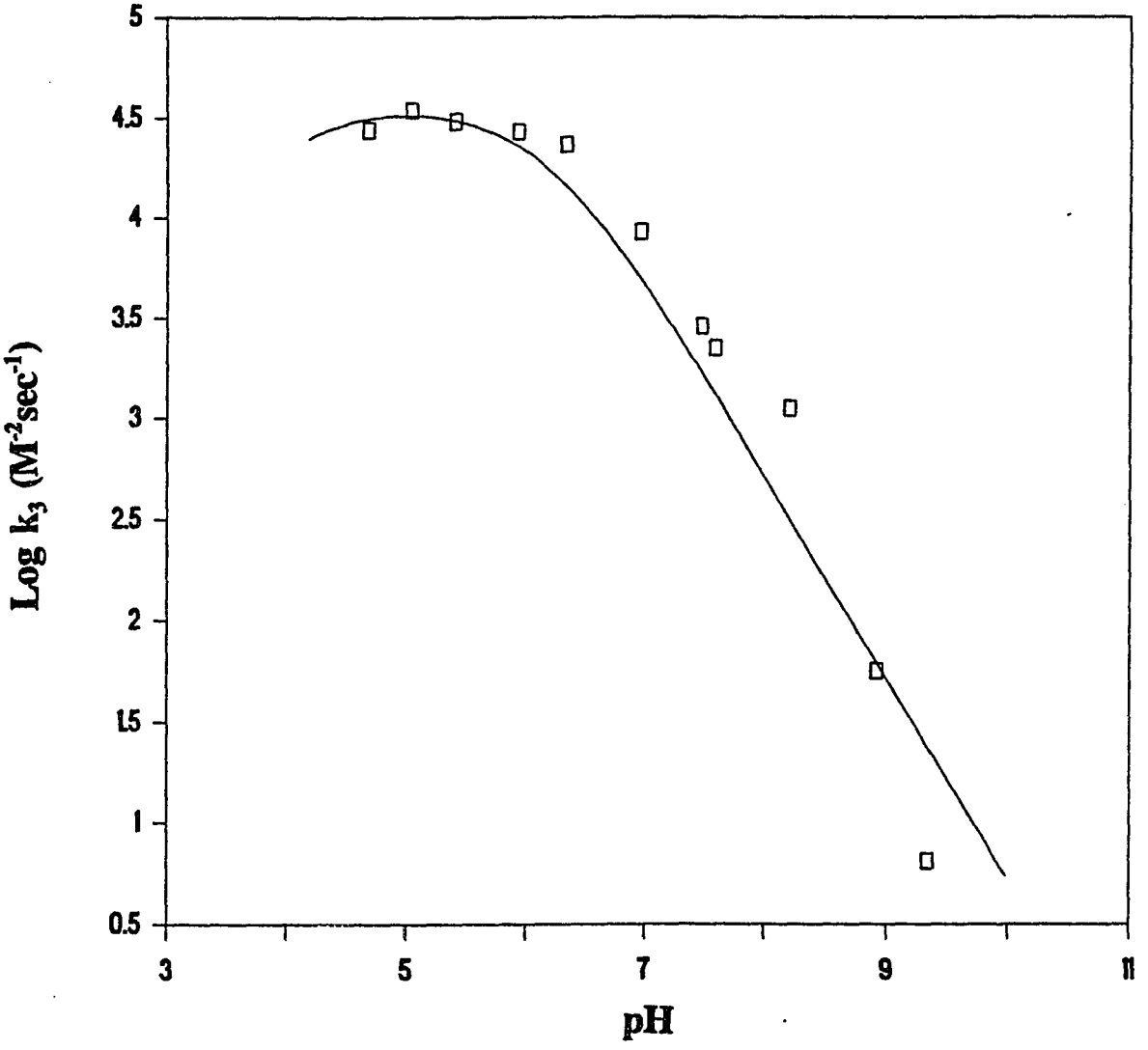

Fig.18 pH profile of diphenylborinic acid catalyzed formation of salicylaldehyde O-methyloxime in 0.1 M buffers, 25.5°C.
pK = 6.14(±0.20), k_3 (Lim) = $3.73x10^4(\pm 5.38x10^3)$ M^{-2} sec^{-1}.
k_3 refers to the third-order rate constant.
(Data of Table XVI Appendix D)

Table II

Comparison of the Kinetic Constants for the Formation of Salicylaldoxime and Salicylaldehyde O-Methyloxime Catalyzed by Boron Acids at 25.5°C

boron acid	k_3(Lim.) (M^{-2} sec^{-1}) (oxime)	k_3(Lim.) (M^{-2} sec^{-1}) (O-methyloxime)	k_2/k_3(Lim.)* (M) (oxime)	k_2/k_3(Lim.)* (M) (O-methyloxime)
boric acid	75.54 ($\pm$1.49)	11.54 ($\pm$0.254)	1.513×10^{-3} ($\pm3.04\times10^{-5}$)	1.74×10^{-2} ($\pm3.92\times10^{-4}$)
benzeneboronic acid	5.546×10^{2} ($\pm$93.4)	76.98 ($\pm$2.70)	5.715×10^{-4} ($\pm1.16\times10^{-4}$)	7.84×10^{-3} ($\pm2.85\times10^{-4}$)
4-bromobenzene-boronic acid	1.602×10^{3} ($\pm$361.3)	2.28×10^{2} ($\pm$8.02)	2.38×10^{-4} ($\pm6.93\times10^{-5}$)	1.139×10^{-3} ($\pm4.15\times10^{-5}$)
3,5-bis(trifluoro-methyl)benzene-boronic acid	1.149×10^{4} ($\pm2.417\times10^{3}$)	2.266×10^{3} ($\pm3.56\times10^{2}$)	3.71×10^{-5} ($\pm9.88\times10^{-6}$)	1.69×10^{-4} ($\pm3.15\times10^{-5}$)
diphenyl-borinic acid	2.497×10^{4} ($\pm1.93\times10^{3}$)	3.731×10^{4} ($\pm5.38\times10^{3}$)	1.44×10^{-5} ($\pm1.205\times10^{-6}$)	3.30×10^{-5} ($\pm5.56\times10^{-6}$)

* k_2 for each boron acid is taken at the pH which gives optimal k_3

both cases.

The experimental results suggest that hydroxylamine and methoxylamine follow different mechanisms in the boron acid catalyzed oxime formations. The OH group of hydroxylamine may play an important role in the boron acid catalysis.

Comparison of salicylaldehyde, *p*-hydroxybenzaldehyde and *m*-hydroxybenzaldehyde on the oxime formation. Using *p*-hydroxybenzaldehyde and *m*-hydroxybenzaldehyde instead of salicylaldehyde, the oxime formation reactions from hydroxylamine, methoxylamine and these salicylaldehyde isomers were studied at pH 6.4. Table III, Table IV and Table V present the kinetic data determined for boron acid catalyzed oxime formation reactions. The data in Table III, IV demonstrate that the boron acids not only accelerate the formation of salicylaldoxime but also accelerate the formation of *m*-hydroxybenzaldehyde oxime and *p*-hydroxybenzaldehyde oxime. However, in cases of the *para* and *meta* isomers, the boron acids displayed much lower catalytic effects than in the case of salicylaldehyde. This indicates the important function of the *ortho* phenolic OH group of salicylaldehyde in the catalyses.

In the *para* and *meta* hydroxybenzaldehyde O-methyloxime formation reactions, the boronic acid has no effect in the reaction (Table V). The data further support the idea that both the *ortho* phenolic group of salicylaldehyde and the OH group of hydroxylamine are involved in the boron acid catalyzed formation of salicylaldoxime.

Complexation between Boron Acids and Salicylaldoxime

Spectrophotometric titration of salicylaldoxime. The UV spectra of

Table III

Comparison of Salicylaldehyde, *m*-Hydroxybenzaldehyde and *p*-Hydroxybenzaldehyde on the Oxime Formation Reaction Catalyzed by 3,5-Bis(trifluoromethyl)benzeneboronic acid [a]

aldehyde	k_2 (M^{-1} sec^{-1})	k_3 (M^{-2} sec^{-1})	k_2/k_3 (μM)
salicyl-aldehyde	0.2527 ($\pm 4.05 \times 10^{-4}$)	3822 (± 3.35)	66.12 (± 0.164)
m-hydroxy-benzaldehyde	0.3661 ($\pm 1.47 \times 10^{-3}$)	99.92 (± 1.61)	3664 (± 75.03)
p-hydroxy-benzaldehyde	0.0834 ($\pm 1.05 \times 10^{-4}$)	109.2 (± 0.372)	763.6 (± 3.58)

[a] Conditions: 0.1 M phosphate buffer, pH 6.4, 25.5°C.

Table IV

Comparison of Salicylaldehyde, *m*-Hydroxybenzaldehyde and *p*-Hydroxybenzaldehyde on the Oxime Formation Reaction Catalyzed by Diphenylborinic acid [a]

aldehyde	k_2 (M^{-1} sec^{-1})	k_3 (M^{-2} sec^{-1})	k_2/k_3 (μM)
salicyl-aldehyde	0.2527 ($\pm 4.05 \times 10^{-4}$)	22600 (± 41.8)	11.18 (± 0.0387)
m-hydroxy-benzaldehyde	0.3661 ($\pm 1.47 \times 10^{-3}$)	3533 (± 13.8)	103.6 (± 0.822)
p-hydroxy-benzaldehyde	0.0834 ($\pm 1.05 \times 10^{-4}$)	1767 (± 2.58)	47.19 (± 0.129)

[a] Conditions: 0.1 M phosphate buffer, pH 6.4, 25.5°C.

Table V

Comparison of Salicylaldehyde, *m*-Hydroxybenzaldehyde and *p*-Hydroxybenzaldehyde on the O-Methyloxime Formation Reaction at 25.5°C, pH 6.4, Catalyzed by 3,5-Bis(trifluoromethyl)benzeneboronic acid

p-Hydroxy-benzaldehyde (μM)	Methoxylamine (mM)	Boronic acid (mM)	k_1 * (sec^{-1})
91.0	19.5	0.000	4.94×10^{-4} ($\pm 1.31 \times 10^{-7}$)
91.0	19.5	2.54	5.15×10^{-4} ($\pm 7.27 \times 10^{-7}$)
m-Hydroxy-benzaldehyde (μM)	Methoxylamine (mM)	Boronic acid (mM)	k_1 * (sec^{-1})
101.1	19.5	0.000	1.62×10^{-3} ($\pm 5.23 \times 10^{-6}$)
101.1	19.5	2.54	1.63×10^{-3} ($\pm 2.57 \times 10^{-6}$)
Salicyl-aldehyde (μM)	Methoxylamine (mM)	Boronic acid (mM)	k_1 * (sec^{-1})
160	1.67	0.000	2.54×10^{-4} ($\pm 9.69 \times 10^{-8}$)
160	1.67	2.54	7.67×10^{-3} ($\pm 6.80 \times 10^{-6}$)

* k_1 refers to the pseudo-first-order rate constant.

salicylaldoxime in different pH buffers are shown in Fig.19. Salicylaldoxime has a absorption band at 304 nm. This band shifts to 340 nm when pH > 9.0 indicating the ionization of the phenol group in salicylaldoxime. In order to determine the ionization pK, the ratios of OD_{350nm}/OD_{304nm} are plotted as a function of pH in Fig.20. The pK value for the ionization of the phenol group is 9.0 which is consistent with the values reported in the literature[52-53,55].

pH dependence of complexation between diphenylborinic acid and salicylaldoxime. In this experiment, the association of diphenylborinic acid to salicylaldoxime was studied in different pH buffers. Fig.21, Fig.22 and Fig.23 show the UV spectra obtained at pH 4.67, pH 6.58 and pH 9.06. As seen in these spectra, addition of diphenylborinic acid causes the salicylaldoxime band at 304 nm to diminish with simultaneous appearance of a new band around 340 nm. Since diphenylborinic acid has no absorption band in this region, the spectral changes result from the complexation between the borinic acid and salicylaldoxime.

The spectrophotometric titration of the salicylaldoxime-diphenylborinic acid complex shows two pKs (Fig.24). As illustrated in Scheme V, the pK_1 of 5.85 presumably controls the protonation of the phenol oxygen in the complex while pK_2 of 9.70 perhaps reflects the ionization of the complex's imine group. The complex structure presented here is consistent with that reported in the literature[54].

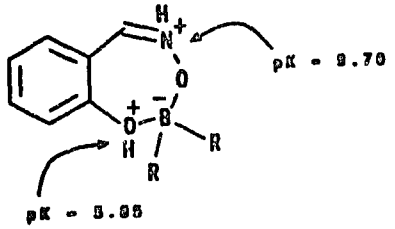

Scheme V

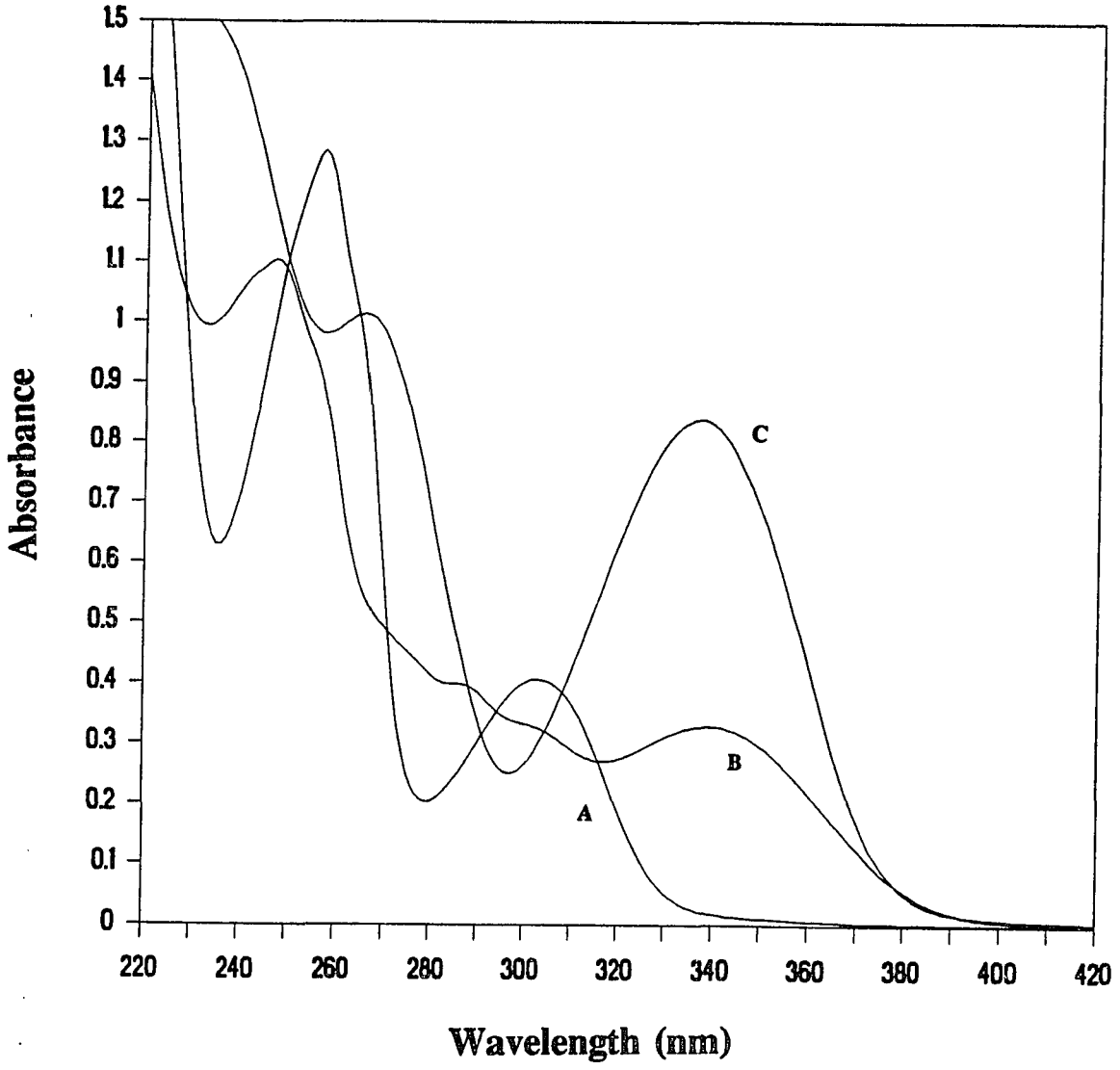

Fig.19 VU spectra of salicylaldoxime (0.1097 mM) in various pH buffer, 25.5°C.
Curve A is salicylaldoxime (peak at 304 nm) at pH 6.58,
Curve B is salicylaldoxime (peak at 340 nm) at pH 9.06,
Curve C is salicylaldoxime (peak at 340 nm) at pH 12.63.

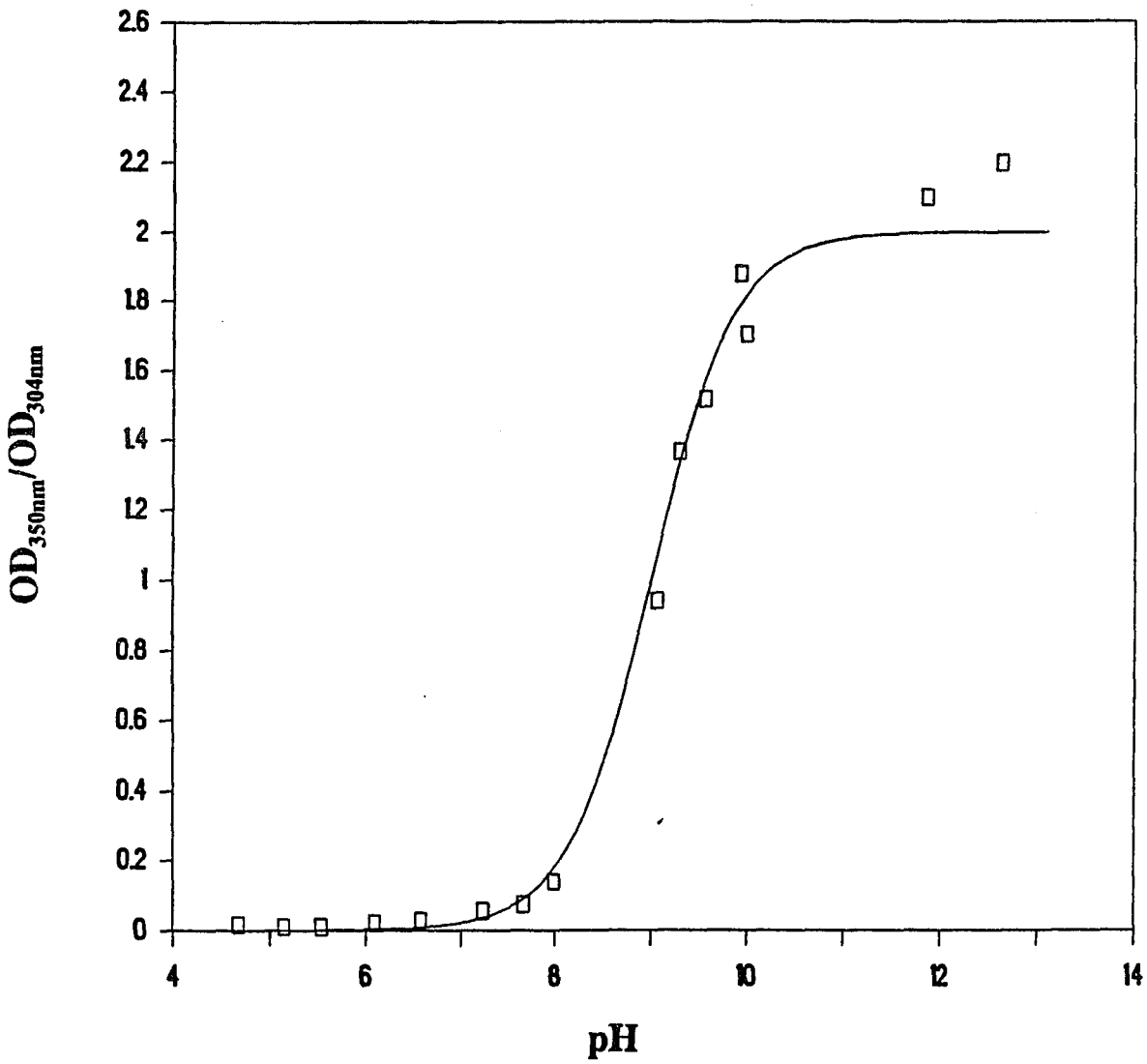

Fig.20 Spectrophotometric titration of salicylaldoxime (0.1097 mM) at 25.5°C. pK = 9.0(±0.05). (Data of Table XVII Appendix D)

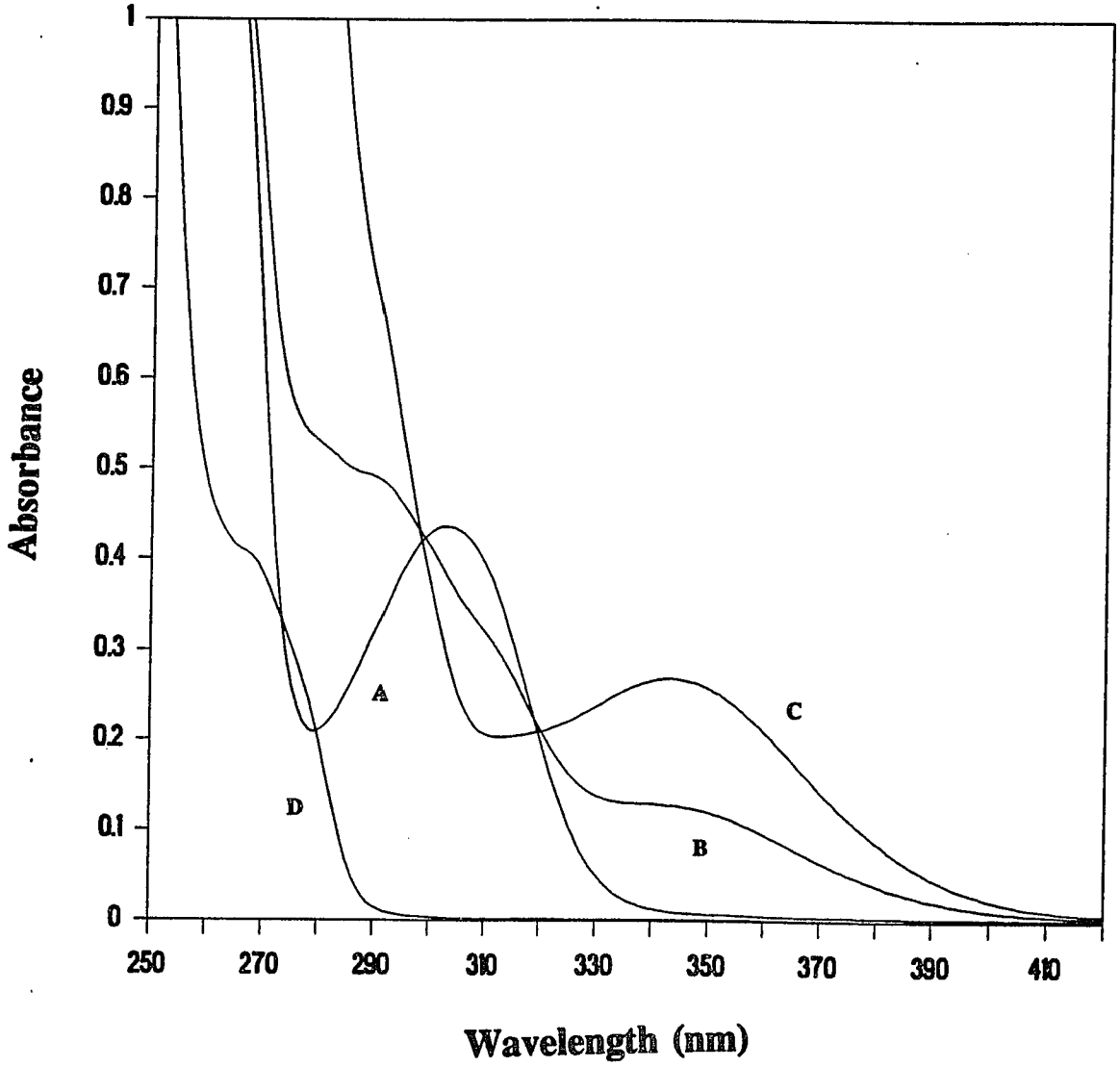

Fig.21 UV spectra of complexation between diphenylborinic acid and salicylaldoxime (0.1097 mM) in pH 4.67 0.1 M buffer, 25.5°C.
Curve A is salicylaldoxime (peak at 304 nm),
Curve B is salicylaldoxime with 0.171 mM borinic acid,
Curve C is salicylaldoxime with 1.03 mM borinic acid
(peak of the complex is at 344 nm),
Curve D is 0.343 mM diphenylborinic acid.

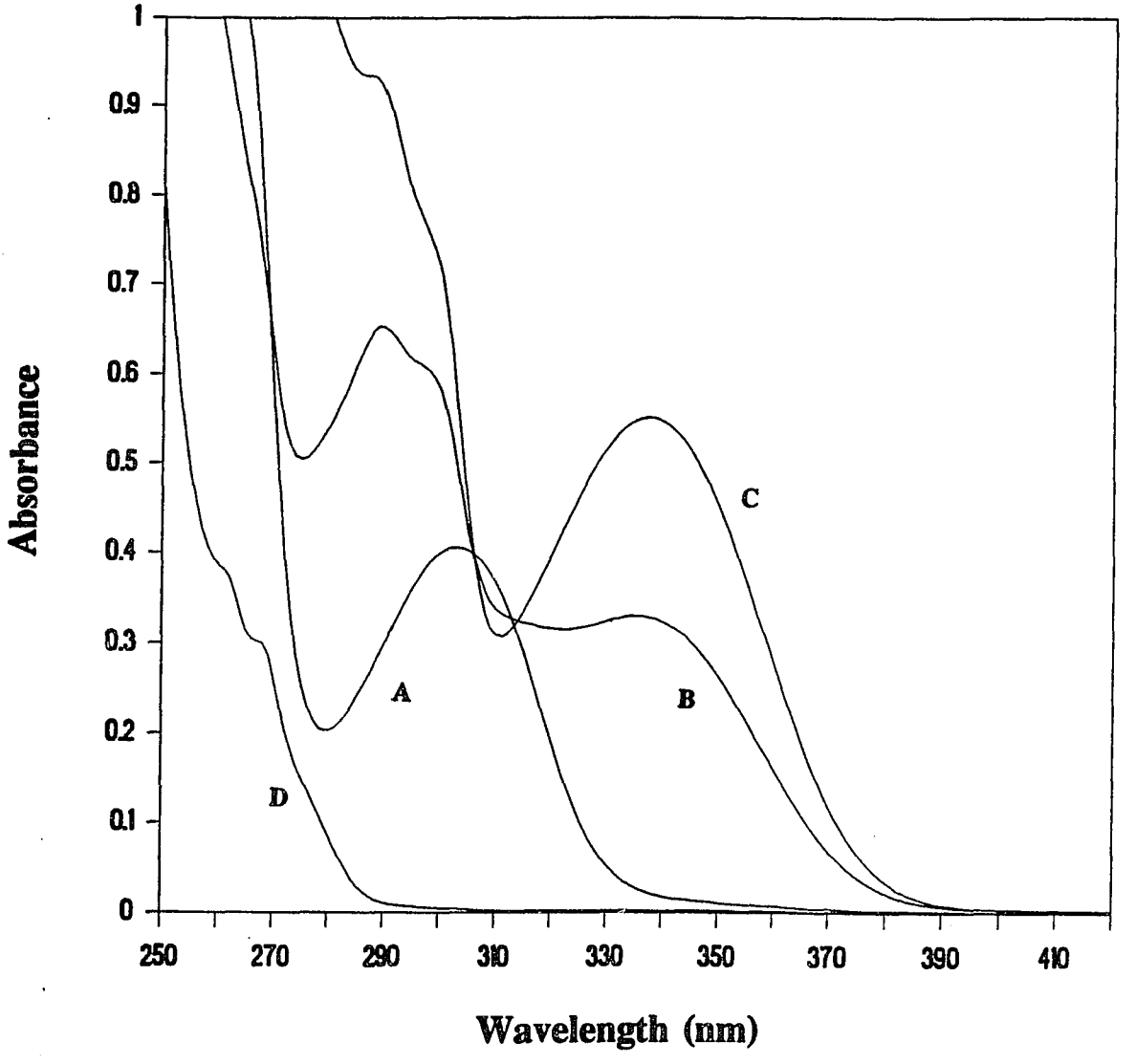

Fig.22 UV spectra of complexation between diphenylborinic acid and salicylaldoxime (0.1097 mM) in pH 6.58 0.1 M buffer, 25.5°C.
Curve A is salicylaldoxime (peak at 304 nm),
Curve B is salicylaldoxime with 0.103 mM borinic acid,
Curve C is salicylaldoxime with 1.20 mM borinic acid
(peak of the complex is at 338 nm),
Curve D is 0.343 mM diphenylborinic acid.

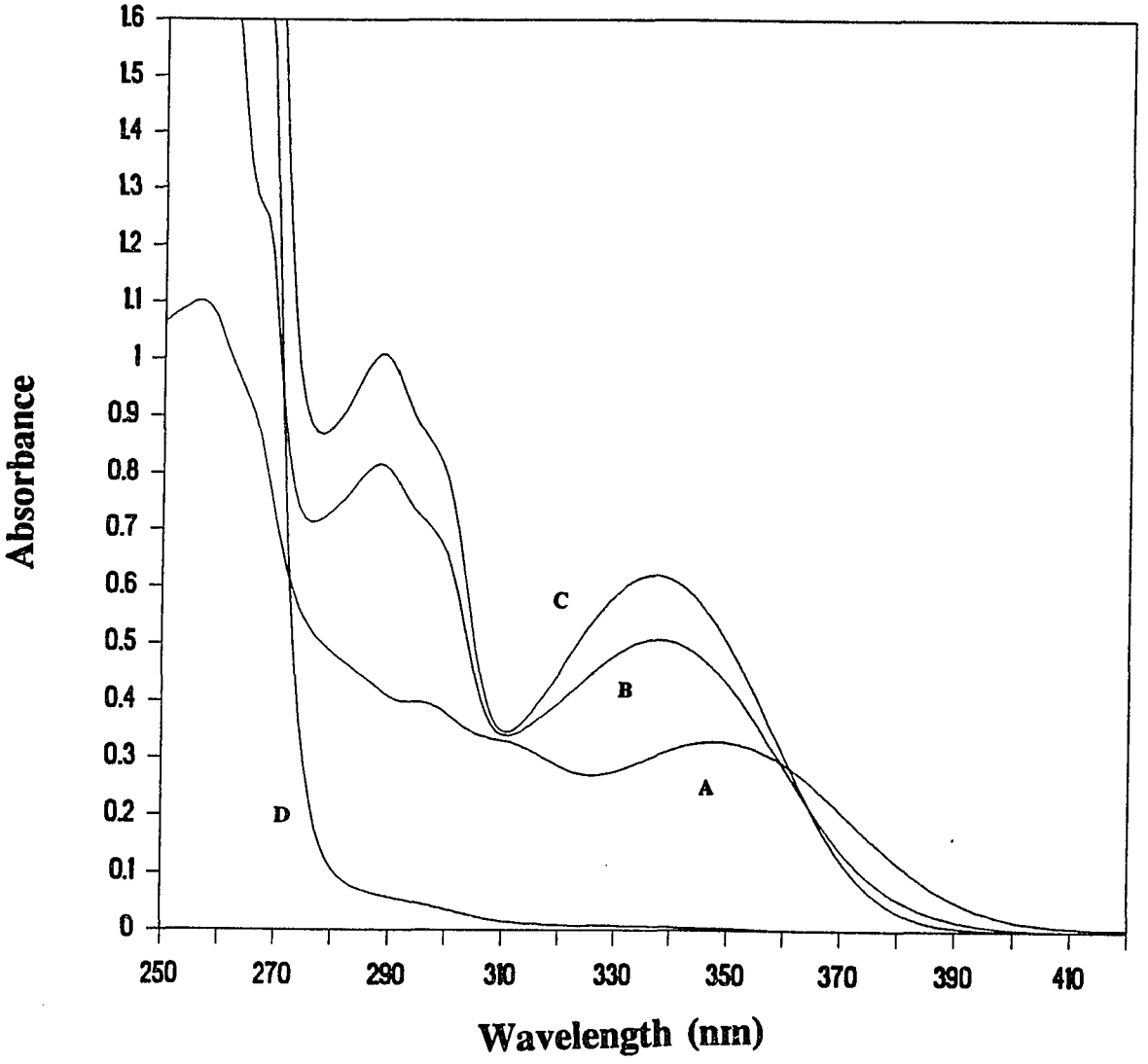

Fig.23 UV spectra of complexation between diphenylborinic acid and salicylaldoxime (0.1097 mM) in pH 9.06 0.1 M buffer, 25.5°C.
Curve A is salicylaldoxime (peak at 350 nm),
Curve B is salicylaldoxime with 1.03 mM borinic acid,
Curve C is salicylaldoxime with 2.75 mM borinic acid
(peak of the complex is at 338 nm),
Curve D is 2.75 mM diphenylborinic acid.

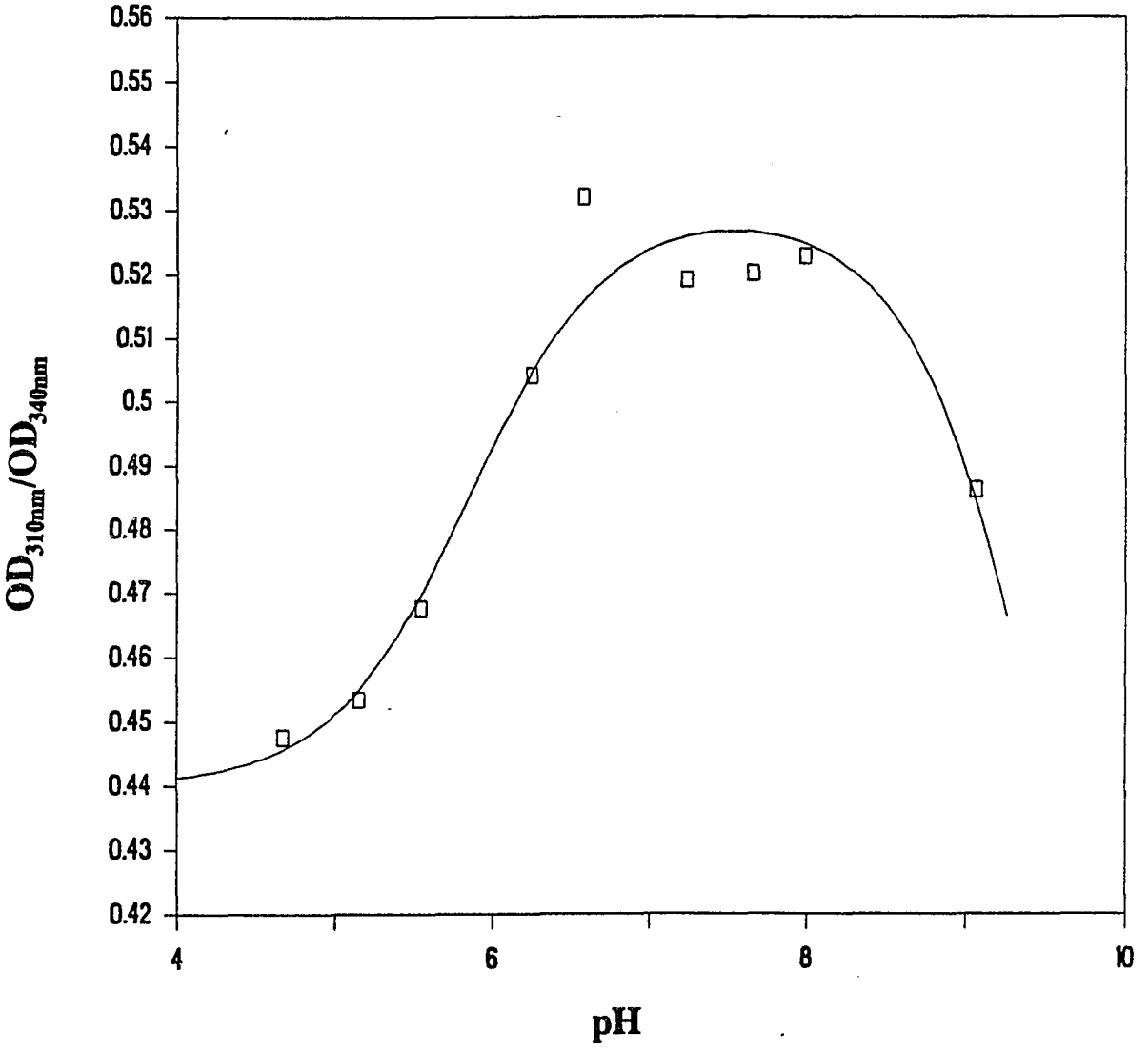

Fig.24 Spectrophotometric titration of salicylaldoxime-diphenylborinic acid complex at 25.5°C. $pK_1 = 5.85(\pm 0.05)$, $pK_2 = 9.70(\pm 0.10)$. (Data of Table XVIII Appendix D)

Fig.25 shows the hyperbolic curve observed when the values of net absorbance increase at 340 nm were plotted as a function of diphenylborinic acid concentrations. This relationship is linearized in Fig.26 by replotting OD_{340nm}/[borinic acid] versus OD_{340nm} (Eadie-Hofstee plot). From the slopes of this type of linear plots the dissociation constants (K_{diss}) of diphenylborinic acid to salicylaldoxime were determined at various pH values.

The pH profile of K_{diss} (Fig.27) shows optimal binding at pH 7.27 with a limiting K_{diss} value of 50.0 μM. In the acidic region the limiting K_{diss} is 0.30 mM. The pK_1 of 6.20 reflects the ionization of diphenylborinic acid[45]. The pK_2 of 8.40 is close to the pK value for the ionization of the phenol group of salicylaldoxime. The pK_3 of 5.40 perhaps originates from the ionization of the oxime-diphenylborinic acid complex. The pH dependence suggests that both the unionized and ionized borinic acid form complexes with salicylaldoxime. It is clear that the ionized borinic acid displays higher binding affinity.

Complexation between salicylaldoxime and boric, boronic acids. As demonstrated in Fig.28, 29, boric and boronic acids also complex with salicylaldoxime resulting in a new absorption band around 320 nm. The complexation was studied by varying the concentration of boronic acid at fixed concentration of salicylaldoxime for K_{diss} determination.

Fig.30 shows that the pH dependence of complexation between benzeneboronic acid and salicylaldoxime is controlled by two pKs. While pK_1 of 9.2 reflects the ionization of benzeneboronic acid[50], the pK_2 of 8.2 perhaps relates to the ionization of phenol group of the oxime. The pH profile suggests a better complexation between ionized

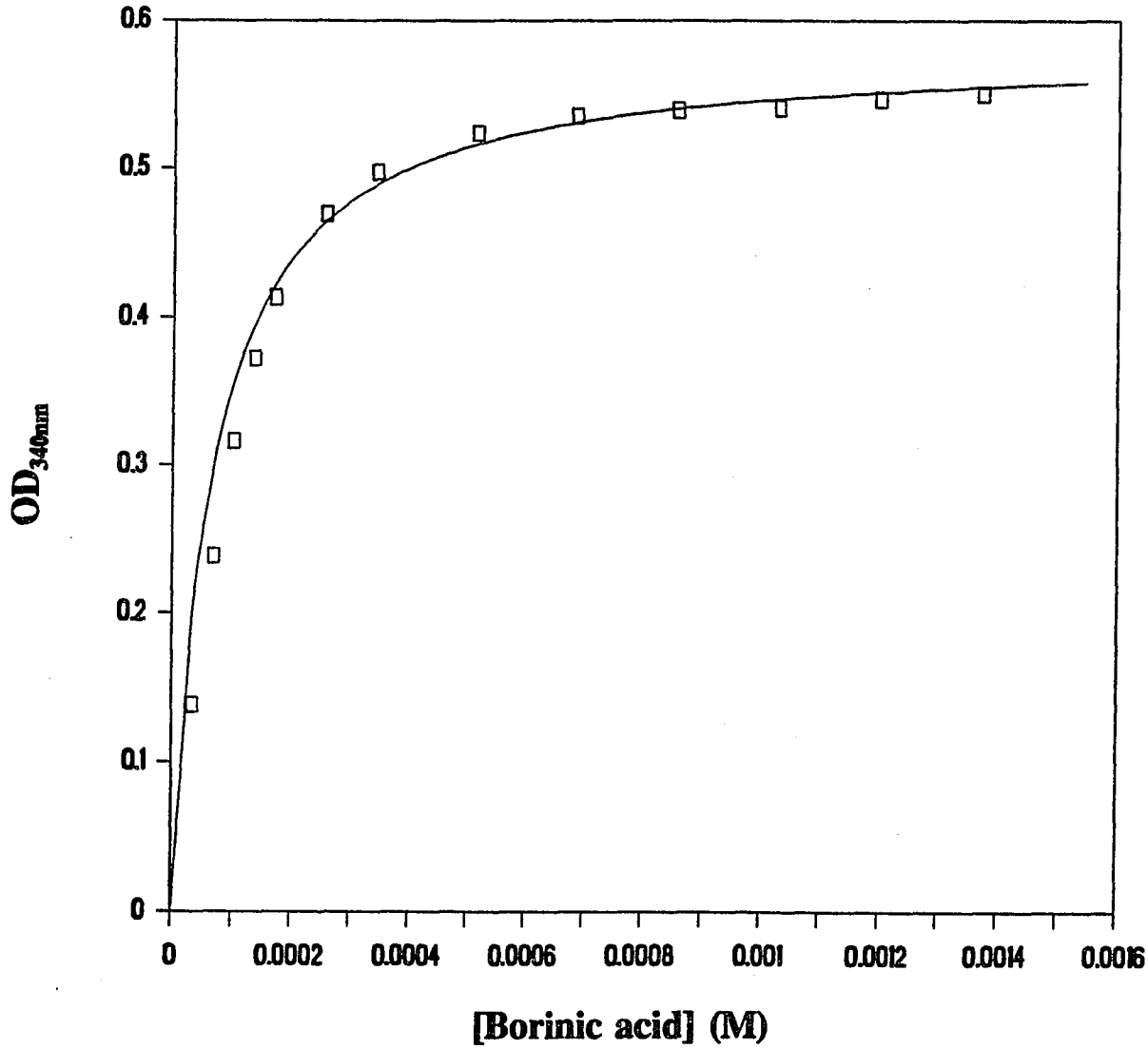

Fig.25 Effect of diphenylborinic acid concentration on the complexation between diphenylborinic acid and salicylaldoxime (0.1097 mM) in pH 6.58 0.1 M buffer, 25.5°C.
(Data of Table XIX Appendix D)

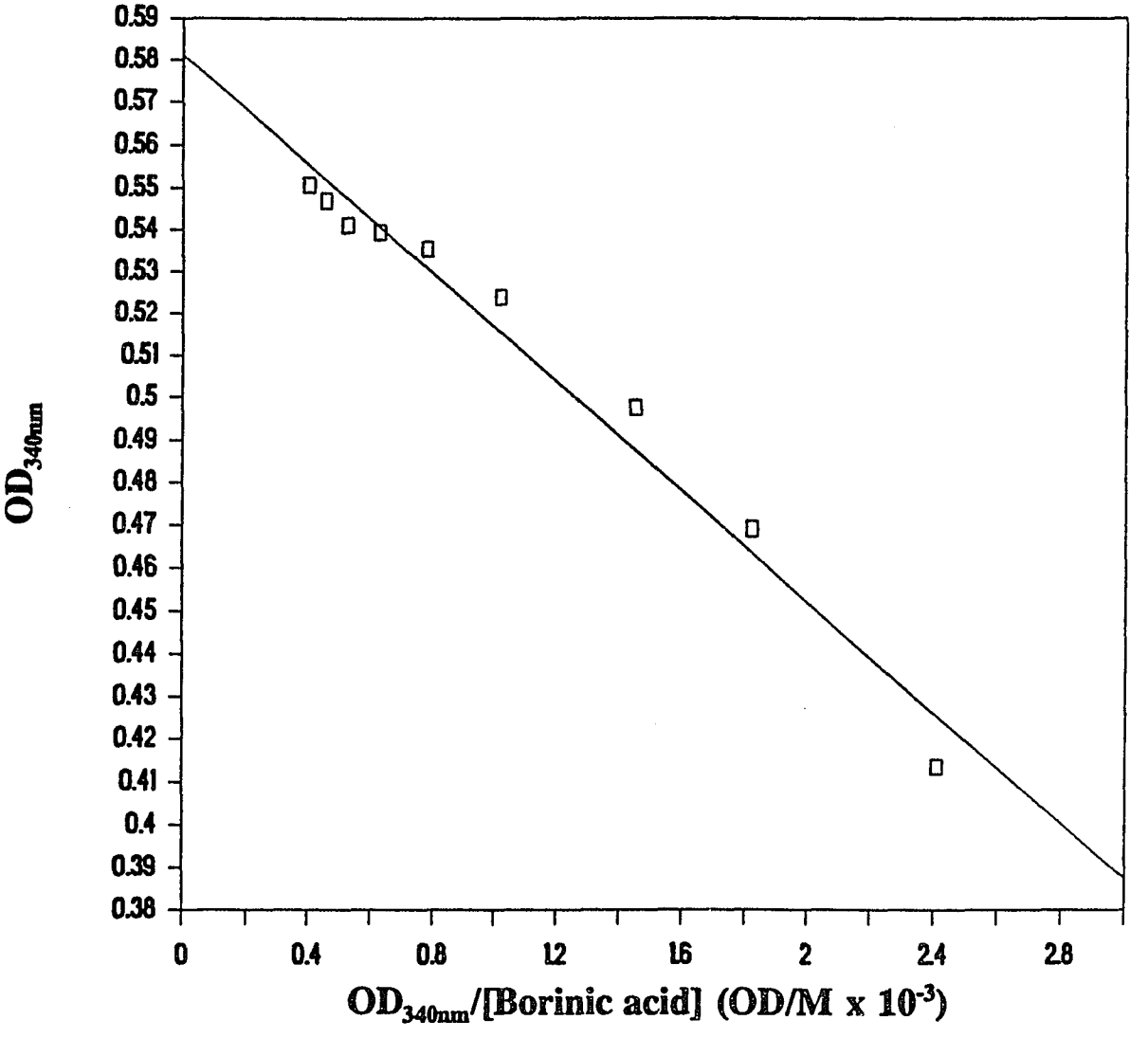

Fig.26 Eadie-Hofstee plot for the complexation between diphenylborinic acid and salicylaldoxime (0.1097 mM) in pH 6.58 0.1 M buffer, 25.5°C. K_{diss} = 64.6(±4.07) μM.
(Data of Table XIX Appendix D)

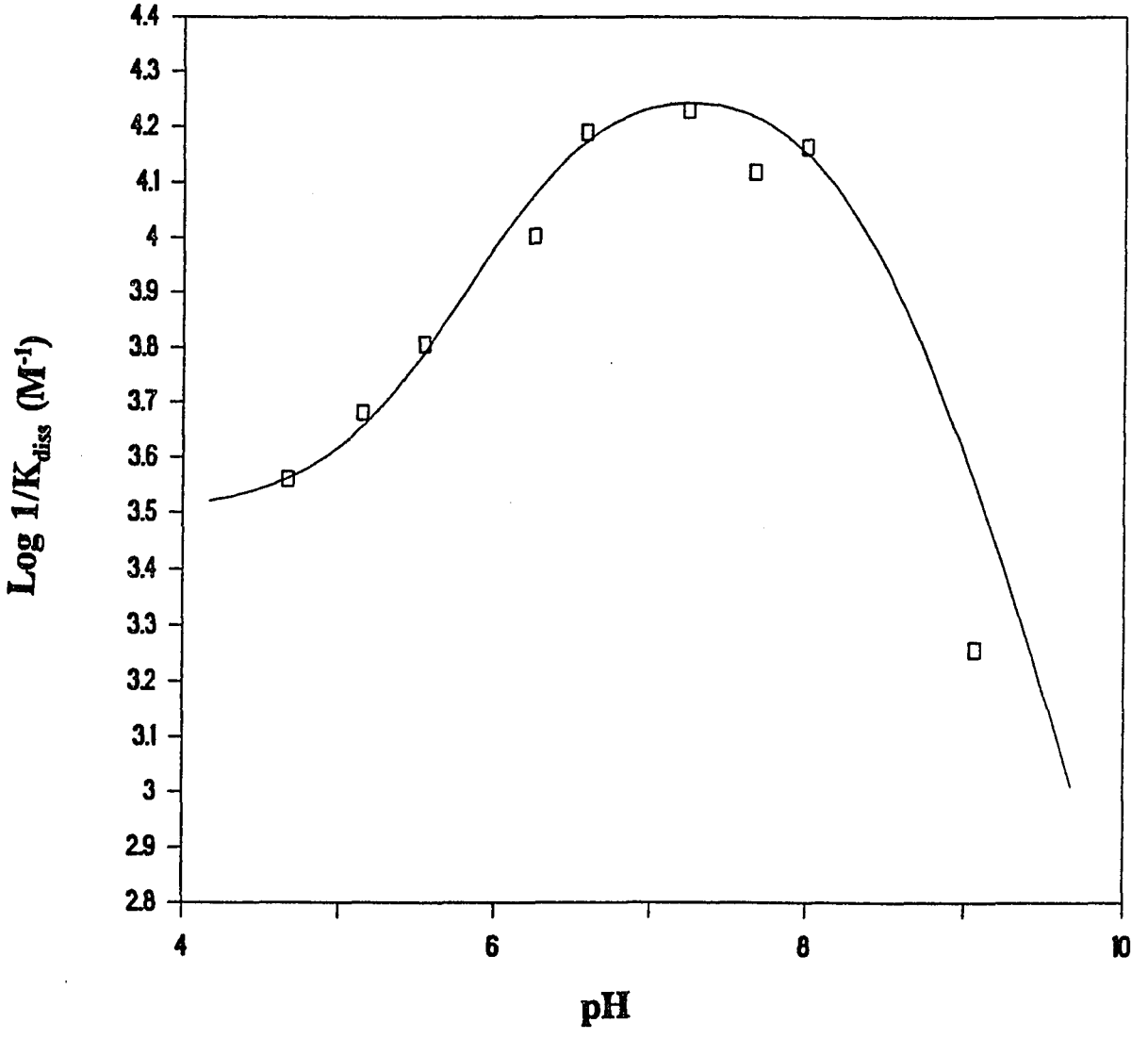

Fig.27 pH profile of diphenylborinic acid complexation with salicylaldoxime in 0.1 M buffers, 25.5°C.
pK_1 = 6.20(±0.10), pK_2 = 8.40(±0.25), pK_3 = 5.40(±0.05), optimum pH = 7.27(±0.17), limiting K_{diss} = 50.0(±5.55) μM. Limiting K_{diss} = 0.30(±0.03) mM in acidic region.
(Data of Table XX Appendix D)

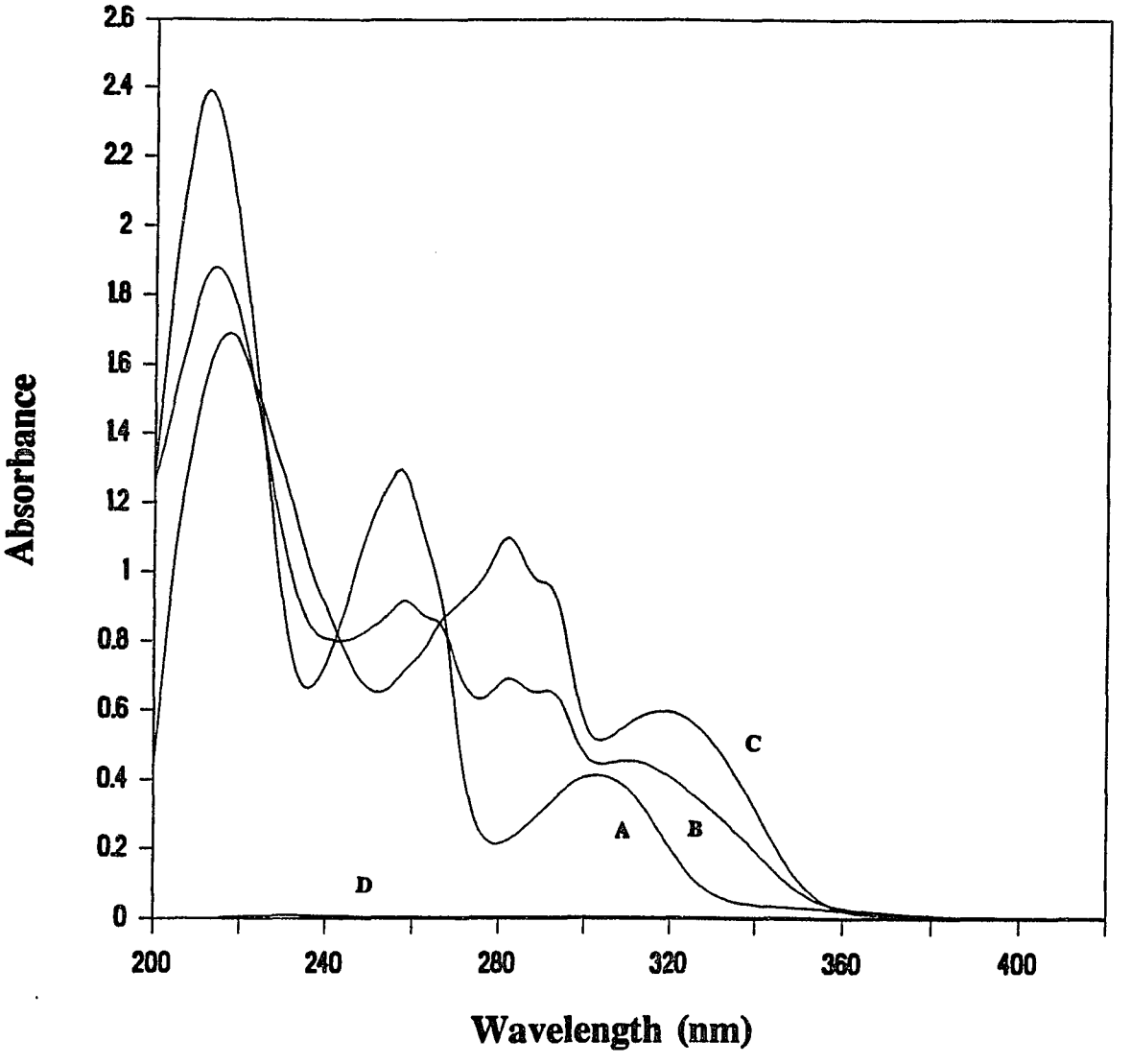

Fig.28 UV spectra of complexation between boric acid and salicylaldoxime (0.1097 mM) in pH 7.80 0.1 M buffer, 25.5°C.
Curve A is salicylaldoxime (peak at 304 nm),
Curve B is salicylaldoxime with 67.6 mM boric acid,
Curve C is salicylaldoxime with 0.338 M boric acid
(peak of the complex is at 320 nm),
Curve D is 0.135 M boric acid.

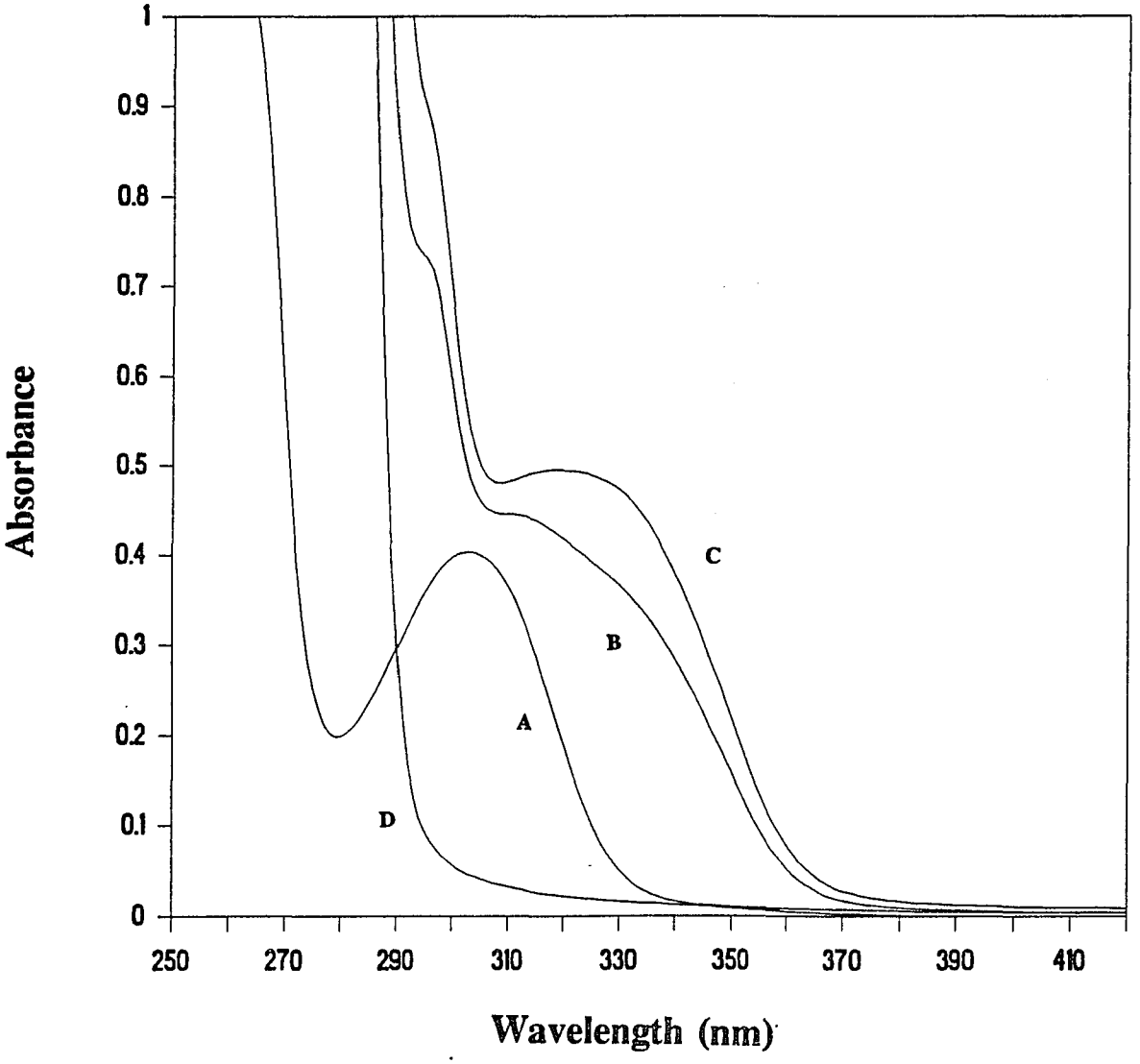

Fig.29 UV spectra of complexation between 2,4-dichlorobenzeneboronic acid and salicylaldoxime (0.1097 mM) in pH 6.60 0.1 M buffer, 25.5°C.
Curve A is salicylaldoxime (peak at 304 nm),
Curve B is salicylaldoxime with 7.44 mM boronic acid,
Curve C is salicylaldoxime with 17.4 mM boronic acid
(peak of the complex is at 320 nm),
Curve D is 9.92 mM 2,4-dichlorobenzeneboronic acid.

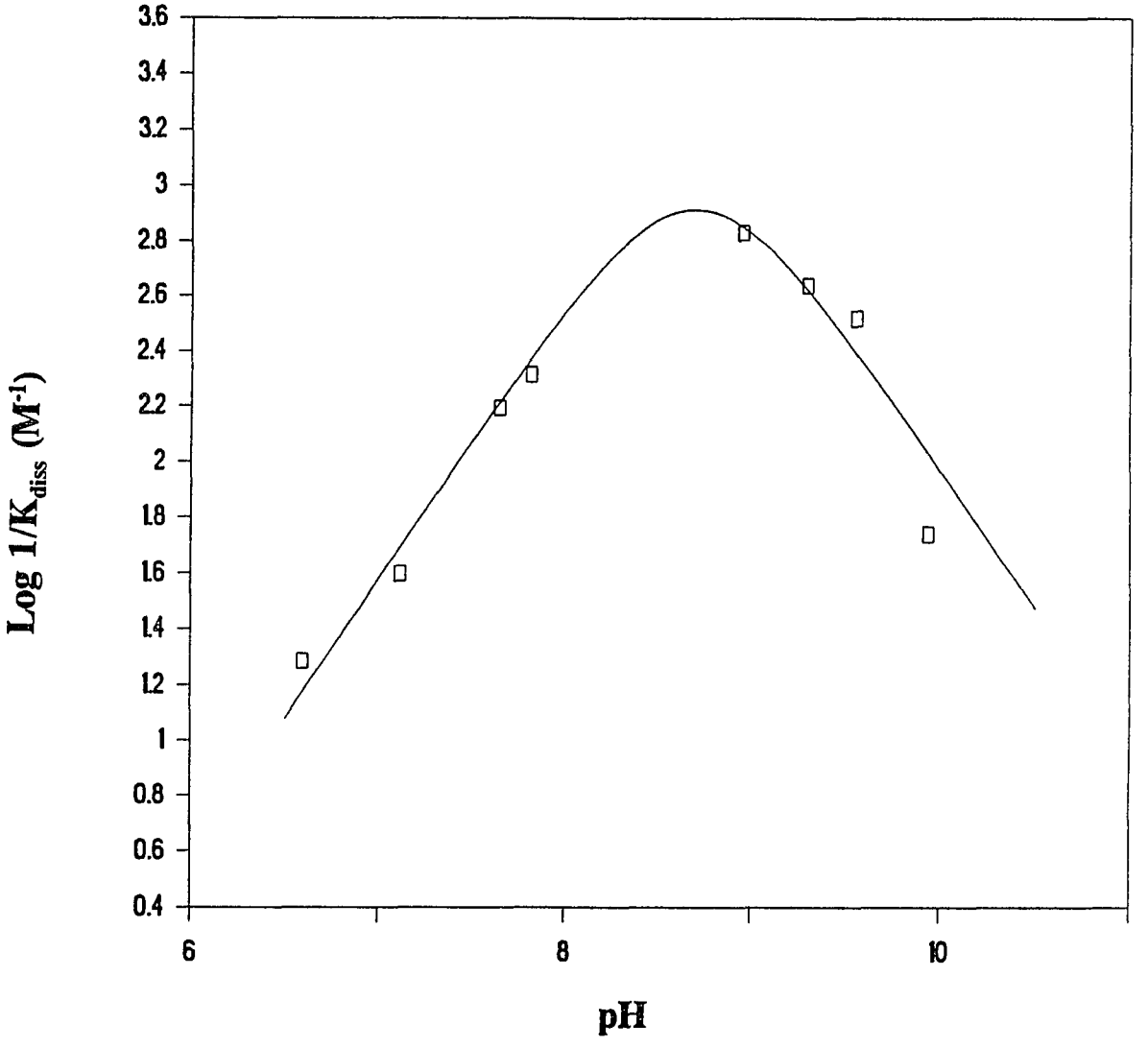

Fig.30 pH profile of benzeneboronic acid complexation with salicylaldoxime in 0.1 M buffers, 25.5°C.
$pK_1 = 9.20(\pm 0.05)$, $pK_2 = 8.20(\pm 0.10)$, optimum pH = $8.70(\pm 0.07)$, optimum $K_{diss} = 1.22(\pm 0.261)$ mM.
(Data of Table XXI Appendix D)

benzeneboronic acid and the protonated phenol group in the oxime. This binding pattern is consistent with that observed in the oxime-diphenylborinic acid complex. Another possible interpretation of the pH profile is that pK_1 originates from the ionization of phenolic group of salicylaldoxime and pK_2 originates from benzeneboronic acid. The association between the neutral boronic acid and salicylaldoxime is facilitated by the ionization of the phenol group in the oxime.

In order to determine the binding affinity of these catalysts to the product and compare the effect of substituents of benzeneboronic acid on the complexation, the dissociation constants of various substituted benzeneboronic acids for salicylaldoxime were determined at pH 6.6 (appendix H). This pH was chosen since benzeneboronic acids exhibit optimal catalysis for salicylaldoxime formation around pH 6.6. The dissociation constants are in millimolar range (Table VI). Fig.31 shows the Hammett plot relating log K_{diss} and *sigma*. In this plot, a straight line with a slope of -1.23 was obtained showing that benzeneboronic acids with electron-withdrawing substituents have a higher binding affinity to salicylaldoxime. These results are consistent with the binding pattern observed in boronic acid catalyzed hydrolysis of the imine formed from salicylaldehyde and an amino acid where binding was also improved by electron-withdrawing substituents on the catalysts[26].

Complexation between diphenylborinic acid and other salicylaldehyde derivatives. Fig.32 and Fig.33 show the UV spectra obtained when diphenylborinic acid complexes with salicyloylhydrazide and salicylamide. It is clear that the complexation causes similar spectral changes in these cases as seen in the case of salicylaldoxime. The diphenylborinate-salicyloylhydrazide complex and diphenylborinate-salicylamide complex

Table VI

Dissociation Constants for the Complexation of Salicylaldoxime with Substituted Benzeneboronic Acids at pH 6.6, 25.5°C

Boron acid	K_{diss} (M)
benzeneboronic acid	5.510×10^{-2} ($\pm 4.73 \times 10^{-3}$)
2,4-dichloro-benzeneboronic acid	4.560×10^{-3} ($\pm 1.82 \times 10^{-4}$)
3,5-dichloro-benzeneboronic acid	4.789×10^{-3} ($\pm 1.89 \times 10^{-4}$)
3-chloro-4-fluoro-benzeneboronic acid	7.802×10^{-3} ($\pm 3.56 \times 10^{-4}$)
4-bromobenzene-boronic acid	1.564×10^{-2} ($\pm 3.76 \times 10^{-4}$)
4-chlorobenzene-boronic acid	1.238×10^{-2} ($\pm 7.30 \times 10^{-4}$)
4-fluorobenzene-boronic acid	1.832×10^{-2} ($\pm 8.52 \times 10^{-4}$)
3,5-bis(trifluoro-methyl)benzene-boronic acid	2.843×10^{-3} ($\pm 1.38 \times 10^{-4}$)

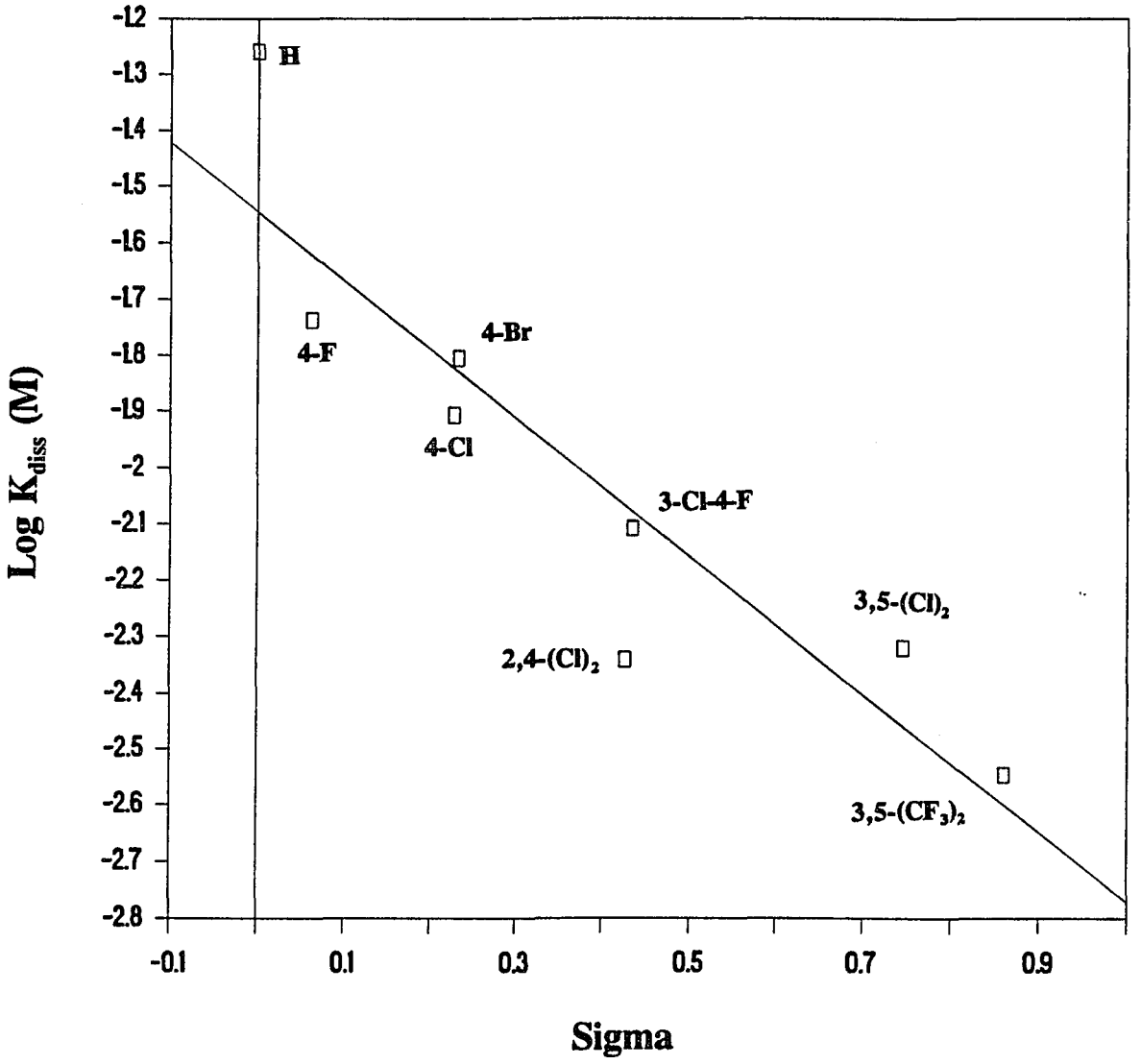

Fig.31 Hammett plot relating log K_{diss} and *sigma* for the complexation of salicylaldoxime with substituted benzeneboronic acids in pH 6.6 0.1 M buffer, 25.5°C. The value of *rho* is -1.23±0.225.
(Data of Table XXII Appendix D)

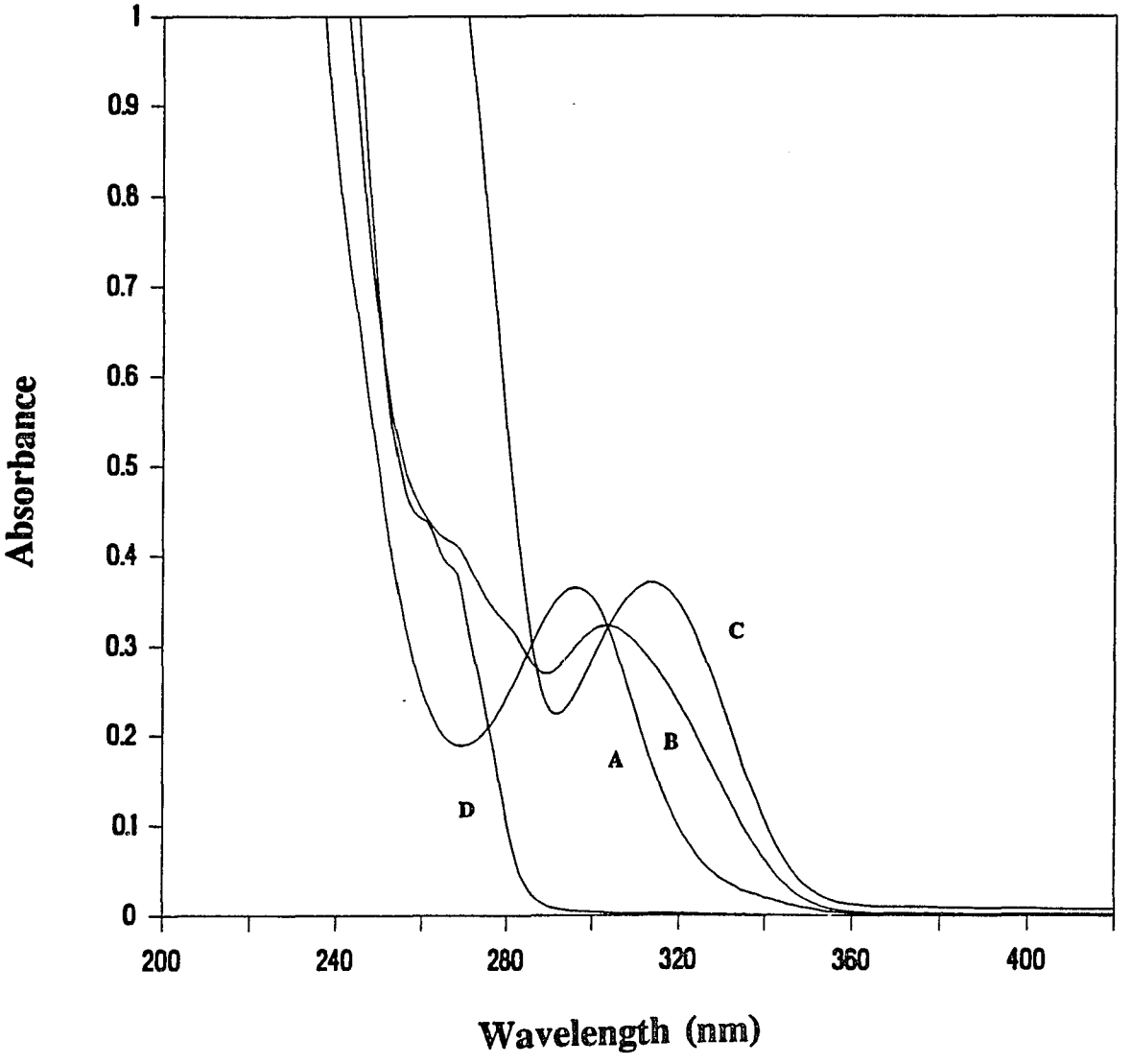

Fig.32 UV spectra of complexation between diphenylborinic acid and salicyloylhydrazide (87.4 μM) in pH 6.60 0.1 M buffer, 25.5°C.
Curve A is salicyloylhydrazide (peak at 295 nm),
Curve B is salicyloylhydrazide with 0.103 mM borinic acid,
Curve C is salicyloylhydrazide with 0.686 mM borinic acid
(peak of the complex is at 314 nm),
Curve D is 0.343 mM diphenylborinic acid.

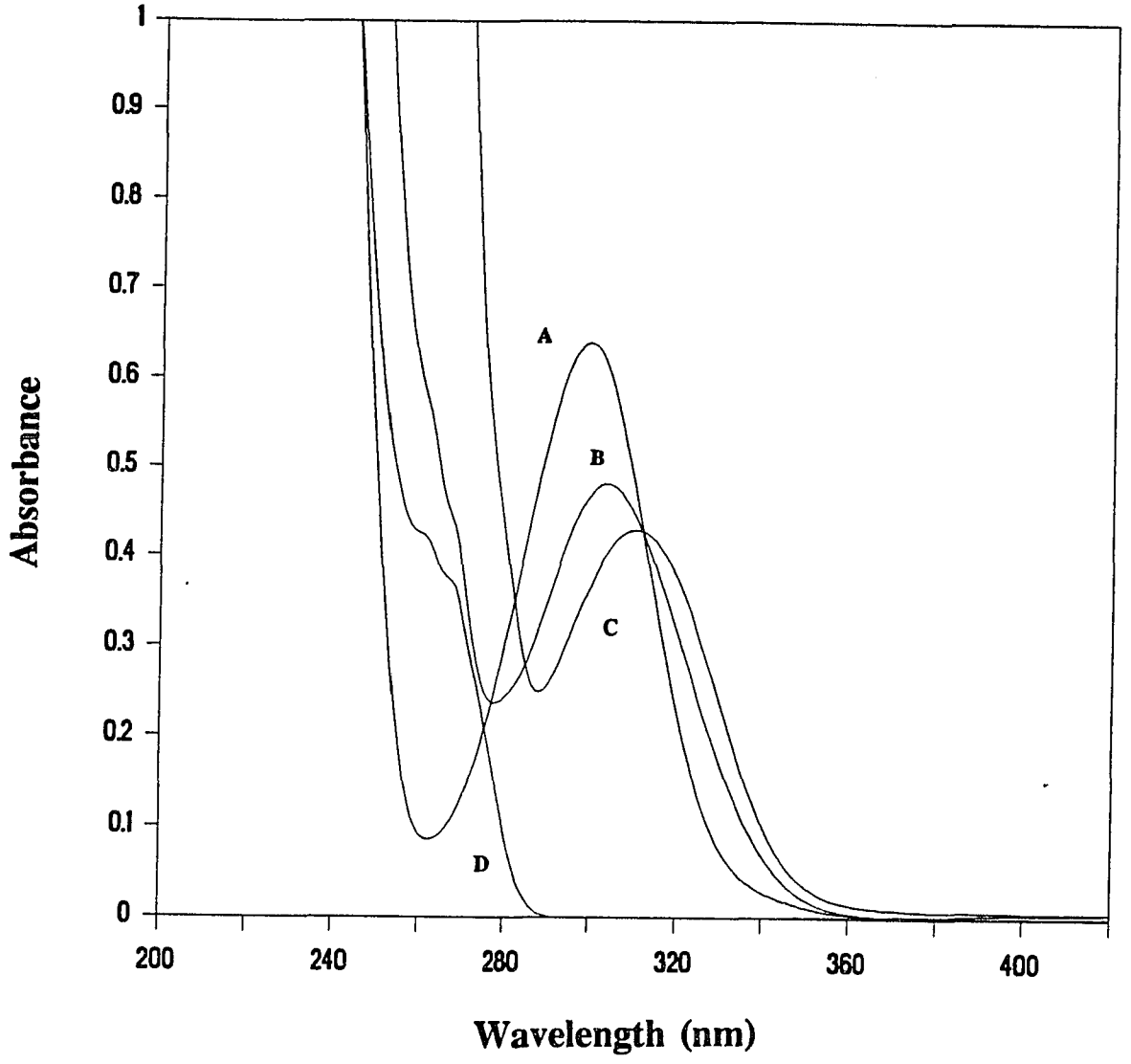

Fig.33 UV spectra of complexation between diphenylborinic acid and salicylamide (0.185 mM) in pH 6.60 0.1 M buffer, 25.5°C.
Curve A is salicylamide (peak at 300 nm),
Curve B is salicylamide with 0.322 mM borinic acid,
Curve C is salicylamide with 1.61 mM borinic acid
(peak of the complex is at 312 nm),
Curve D is 0.343 mM diphenylborinic acid.

displayed new absorption bands at 314 nm and 312 nm respectively.

The dissociation constants of diphenylborinic acid to salicylamide, salicylhydroxamic acid and salicyloylhydrazide were determined at pH 6.6 (appendix I). This was done in order to compare diphenylborinic acid's binding affinity to salicylaldoxime with that towards structurally related salicylaldehyde derivatives. These results are summarized in Table VII. Among these compounds, salicylaldoxime shows the highest affinity to diphenylborinic acid.

Comparison of Boric, Boronic and Borinic Acids on the Formation and Complexation of Salicylaldoxime

The differences of the effects of boric acid, benzeneboronic acids and diphenylborinic acid on the formation of salicylaldoxime are shown in Table VIII. The limiting third-order rate constant for each boron acid catalyzed salicylaldoxime formation is compared with the corresponding second-order rate constant of the spontaneous reaction at the pH where optimal catalysis was observed. The limiting third-order rate constants are also compared with the optimum second-order rate constant of the spontaneous oxime formation. The values of the ratio of k_2/k_3 which reflect the binding affinities of catalysts in their transition state of the catalytic complexes[46] clearly indicate that the borinic acid and benzeneboronic acids are more effective catalysts than boric acid.

Diphenylborinic acid exhibits best catalytic effect in this reaction system. The saturation kinetics observed in this case allow the determination of k_{cat} and K_m for diphenylborinic acid in the salicylaldoxime formation. These data are listed in Table IX.

Table VII

Comparison of Salicylaldehyde Derivatives

on the Complexation with Diphenylborinic Acid [a]

compound	structure	K_{diss} (μM)
salicylaldoxime	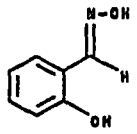	64.56 (±4.07)
salicyloyl-hydrazide	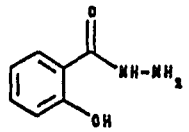	112.7 (±10.4)
salicyl-hydroxamic acid	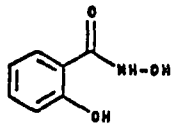	1058 (±49.1)
salicylamide	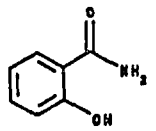	345.5 (±30.5)

[a] Conditions: 0.1 M phosphate buffer, pH 6.6, 25.5°C.

Table VIII

Kinetic Rate Constants for the Formation of Salicylaldoxime with Boric Acid, Substituted Benzeneboronic Acids, and Diphenylborinic Acid at 25.5°C [a]

boron acid	k_3 (Lim.) (M^{-2} sec^{-1})	k_2/k_3(Lim.) (M)	k_2(Opt.)/k_3(Lim.) (M)
boric acid	7.554×10^{1} (± 1.49)	1.513×10^{-3} ($\pm 3.04 \times 10^{-5}$)	1.056×10^{-2} ($\pm 1.45 \times 10^{-3}$)
benzeneboronic acid	5.546×10^{2} (± 93.4)	5.715×10^{-4} ($\pm 1.16 \times 10^{-4}$)	1.439×10^{-3} ($\pm 4.91 \times 10^{-4}$)
2,4-dichloro-benzeneboronic acid	3.083×10^{3} (± 551.5)	1.381×10^{-4} ($\pm 3.01 \times 10^{-5}$)	2.589×10^{-4} ($\pm 9.27 \times 10^{-5}$)
3,5-dichloro-benzeneboronic acid	7.681×10^{3} (± 2170)	5.252×10^{-5} ($\pm 2.07 \times 10^{-5}$)	1.039×10^{-4} ($\pm 5.76 \times 10^{-5}$)
3-chloro-4-fluoro-benzeneboronic acid	3.225×10^{3} (± 913.4)	1.251×10^{-4} ($\pm 4.94 \times 10^{-5}$)	2.474×10^{-4} ($\pm 1.38 \times 10^{-4}$)
4-bromobenzene-boronic acid	1.602×10^{3} (± 361.3)	2.380×10^{-4} ($\pm 6.93 \times 10^{-5}$)	4.982×10^{-4} ($\pm 2.19 \times 10^{-4}$)
4-chlorobenzene-boronic acid	1.463×10^{3} (± 192.6)	2.309×10^{-4} ($\pm 3.50 \times 10^{-5}$)	5.454×10^{-4} ($\pm 1.55 \times 10^{-4}$)
4-fluorobenzene-boronic acid	7.027×10^{2} (± 154)	4.809×10^{-4} ($\pm 1.35 \times 10^{-4}$)	1.136×10^{-3} ($\pm 4.86 \times 10^{-4}$)
3,5-bis(trifluoro-methyl)benzene-boronic acid	1.149×10^{4} (± 2416.6)	3.705×10^{-5} ($\pm 9.87 \times 10^{-6}$)	6.948×10^{-5} ($\pm 2.86 \times 10^{-5}$)
4-methoxybenzene-boronic acid	2.422×10^{2} (± 71.17)	1.309×10^{-3} ($\pm 5.45 \times 10^{-4}$)	3.296×10^{-3} ($\pm 1.91 \times 10^{-3}$)
diphenyl-borinic acid	2.497×10^{4} ($\pm 1.93 \times 10^{3}$)	1.440×10^{-5} ($\pm 1.21 \times 10^{-6}$)	3.197×10^{-5} ($\pm 6.67 \times 10^{-6}$)

[a] In k_2/k_3(Lim.), k_2 is taken at the pH of optimal catalysis.

Table IX

Kinetic Constants for the Formation of

Salicylaldoxime Catalyzed by Diphenylborinic Acid [a]

experiment	k_{cat} (sec^{-1})	K_m (mM)	k_{cat}/K_m ($M^{-1}sec^{-1}$)
dependence of k_1 [b] on the borinic acid concentration (Fig.6, Fig.9)	0.117 ($\pm 4.61 \times 10^{-3}$)	2.19 (± 0.249)	53.6 (± 9.23)
dependence of k_1 [b] on the hydroxylamine concentration (Fig.7, Fig.10)	0.102 ($\pm 5.14 \times 10^{-3}$)	3.37 (± 0.331)	30.1 (± 4.99)

[a] Conditions: 0.1 M phosphate buffer, pH 6.5, 25.5°C.

[b] k_1 refers to the pseudo-first-order rate constant.

Brønsted plots relating the boron acid pK values to logarithm of limiting third-order rate constants for the boron acid catalyzed formation of salicylaldoxime and salicylaldehyde O-methyloxime are shown in Fig.34. The two lines intersect near the pK of diphenylborinic acid.

In the case of salicylaldehyde O-methyloxime formation, boric acid, benzeneboronic acids and diphenylborinic acid fall on a single straight line with a slope of -1.11 showing that boron acids with lower pKs exhibit better catalysis. This is also consistent with the results observed in the boron acid catalyzed hydrolysis of the imine formed from salicylaldehyde and an amino acid[26]. The agreement of pH dependencies and the Brønsted plot indicates that these boron acids may share a common catalytic mechanism in the O-methyloxime formation and such imine hydrolyses[26].

The Brønsted plot of salicylaldoxime formation shows that all benzeneboronic acids fall on one straight line, deviations are observed for boric acid and diphenylborinic acid. It is clear that the different catalytic effects displayed by boric acid, benzeneboronic acids and diphenylborinic acid are not only related to the pKs of the boron acids but also directly related to the different number of aryl groups attached to the boron atom. The Brønsted plot suggests that the catalytic mechanisms involved in boric acid, benzeneboronic acids and diphenylborinic acid are different. This is also supported by the different types of pH dependencies observed in the boron acid catalysis.

The binding affinities of boric acid, benzeneboronic acids and diphenylborinic acid to salicylaldoxime are compared in Table X. 3,5-bis(trifluoromethyl)benzeneboronic acid and diphenylborinic acid are the two catalysts which display highest binding affinity to salicylaldoxime studied here. The Brønsted plot in Fig.35 shows that the dissociation

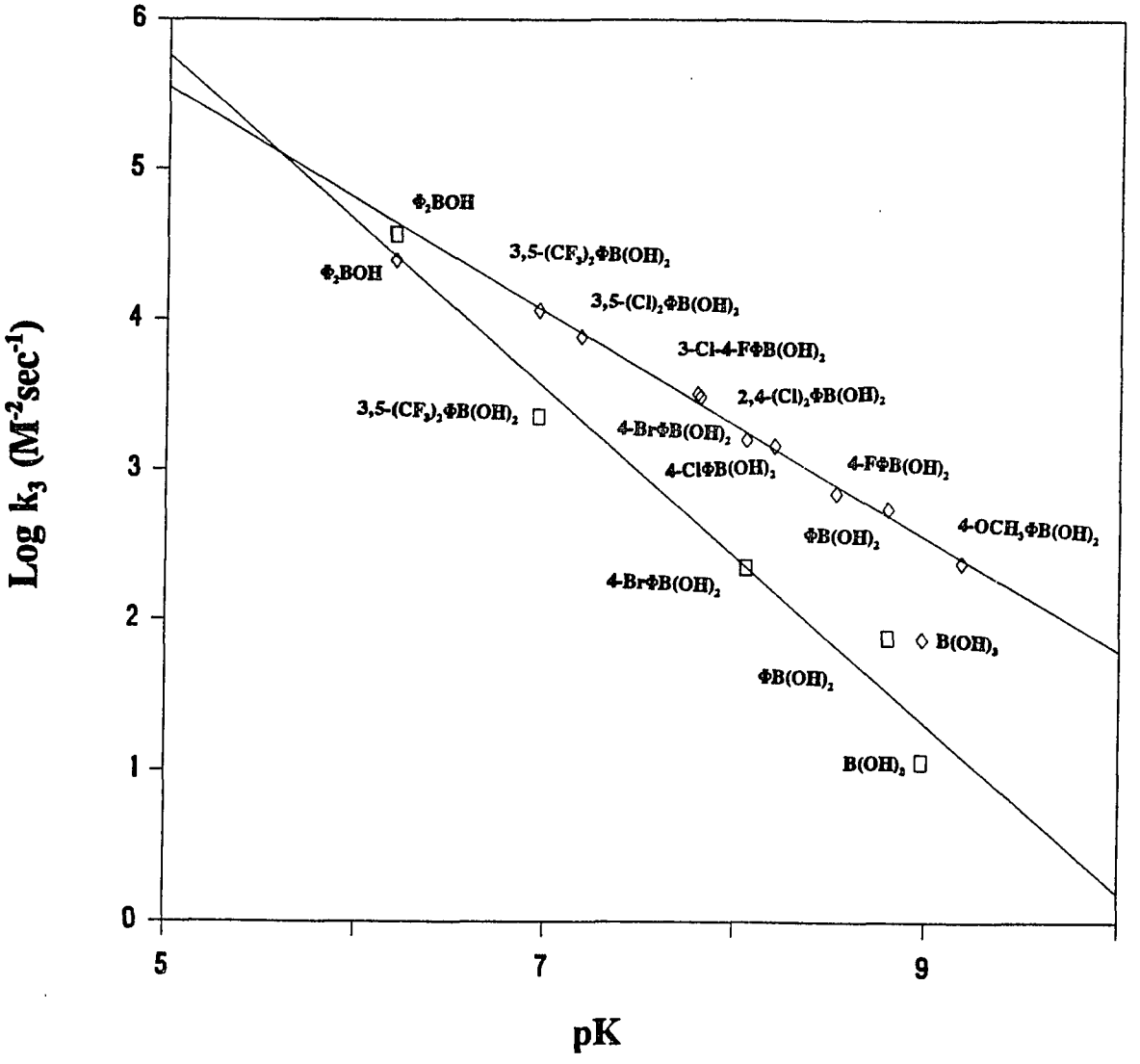

Fig.34 Brϕnsted plots relating boron acid pK values to log k_3 (Lim) for the formation of salicylaldoxime and salicylaldehyde O-methyloxime in 0.1 M buffer, 25.5°C. The slope for the O-methyloxime reaction (□), calculated using boric, boronic and borinic acid data, is -1.11±0.125. The slope for the oxime reaction (◊), calculated using boronic acid data, is -0.750±0.023. k_3 refers to the third-order rate constant.
(Data of Table XXIII Appendix D)

Table X

Dissociation Constants for the Complexation of Salicylaldoxime with Boric Acid, Substituted Benzeneboronic Acids, Diphenylborinic Acid [a]

Boron acid	K_{diss} (M)	pH
boric acid	9.360×10^{-2} ($\pm 7.33 \times 10^{-3}$)	7.8
	4.288×10^{-1} (± 0.1541)	6.8
benzeneboronic acid	5.510×10^{-2} ($\pm 4.73 \times 10^{-3}$)	6.6
2,4-dichloro-benzeneboronic acid	4.560×10^{-3} ($\pm 1.82 \times 10^{-4}$)	6.6
3,5-dichloro-benzeneboronic acid	4.789×10^{-3} ($\pm 1.89 \times 10^{-4}$)	6.6
3-chloro-4-fluoro-benzeneboronic acid	7.802×10^{-3} ($\pm 3.56 \times 10^{-4}$)	6.6
4-bromobenzene-boronic acid	1.564×10^{-2} ($\pm 3.76 \times 10^{-4}$)	6.6
4-chlorobenzene-boronic acid	1.238×10^{-2} ($\pm 7.295 \times 10^{-4}$)	6.6
4-fluorobenzene-boronic acid	1.832×10^{-2} ($\pm 8.52 \times 10^{-4}$)	6.6
3,5-bis(trifluoro-methyl)benzene-boronic acid	2.843×10^{-3} ($\pm 1.38 \times 10^{-4}$)	6.6
diphenyl-borinic acid	6.456×10^{-5} ($\pm 4.07 \times 10^{-6}$)	6.6
	5.902×10^{-5} ($\pm 1.83 \times 10^{-6}$)	7.2

[a] Conditions: 0.1 M phosphate buffer, 25.5°C.

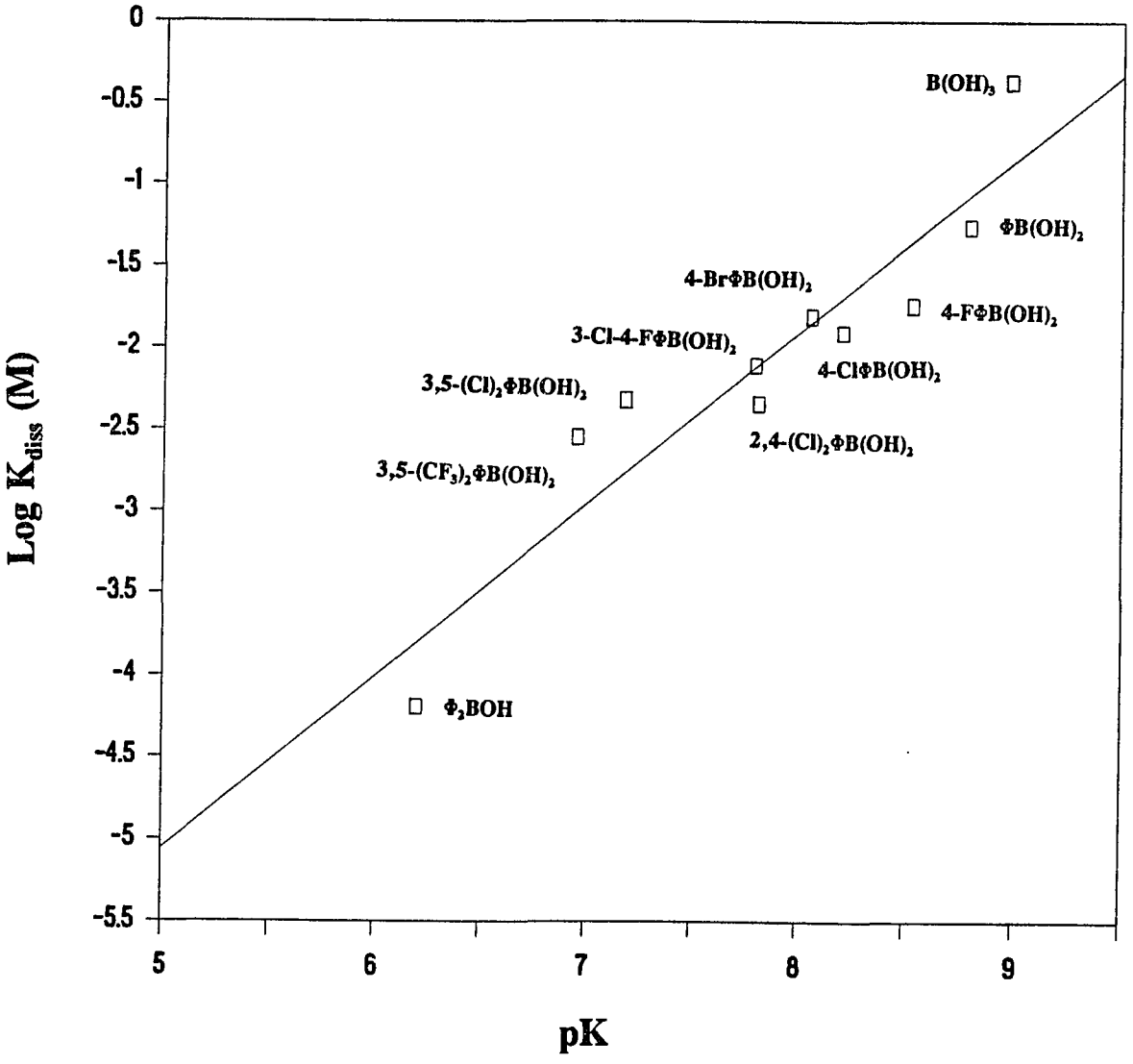

Fig.35 Brϕnsted plot relating boron acid pK values to log K_{diss} for the complexation of salicylaldoxime with boron acids in pH 6.6 0.1 M buffer, 25.5°C. The slope, calculated using boric, boronic and borinic acid data is $+1.05 \pm 0.14$.
(Data of Table XXIV Appendix D)

constants are governed by the pK of the boron acid. Thus, the different binding affinities observed for boric, boronic and diphenylborinic acids result from their different acidities. The Brϕnsted plot also suggests a similar complexation mechanism for these boron acids.

Comparison of the values of k_2/k_3 (binding constant in catalytic transition state Table VIII) with the dissociation constants of salicylaldoxime-boron acid complexes (listed in Table X) clearly shows that boric and benzeneboronic acids exhibit at least 10-fold higher affinity in their transition state catalytic complexes than in their salicylaldoxime-boron acid complexes. The binding affinities of diphenylborinic acid to the reaction product oxime and the transition state are similar.

Formation of Salicylaldehyde Phenylhydrazones

Effect of pH on the formation of salicylaldehyde phenylhydrazone. The spontaneous and the boronic acid catalyzed formation of salicylaldehyde phenylhydrazone was studied in the pH range 4.6 to 9.0. In the absence of boronic acid, the logarithm of the second-order rate constants decreased linearly with increasing pH (Fig.36). This indicates that the spontaneous salicylaldehyde phenylhydrazone formation involves specific acid (hydronium ion) catalysis.

Boronic acids exhibit an efficient catalytic effect on hydrazone formation reactions. Fig.37 shows the pH dependence of salicylaldehyde phenylhydrazone formation catalyzed by 3,5-bis(trifluoromethyl)benzeneboronic acid. The pH profile is quite similar to that observed in the case of salicylaldoxime formation. The boronic acid displayed optimal catalysis at pH 6.20 with limiting third-order rate constant of 2.54×10^4 M^{-2} sec^{-1}.

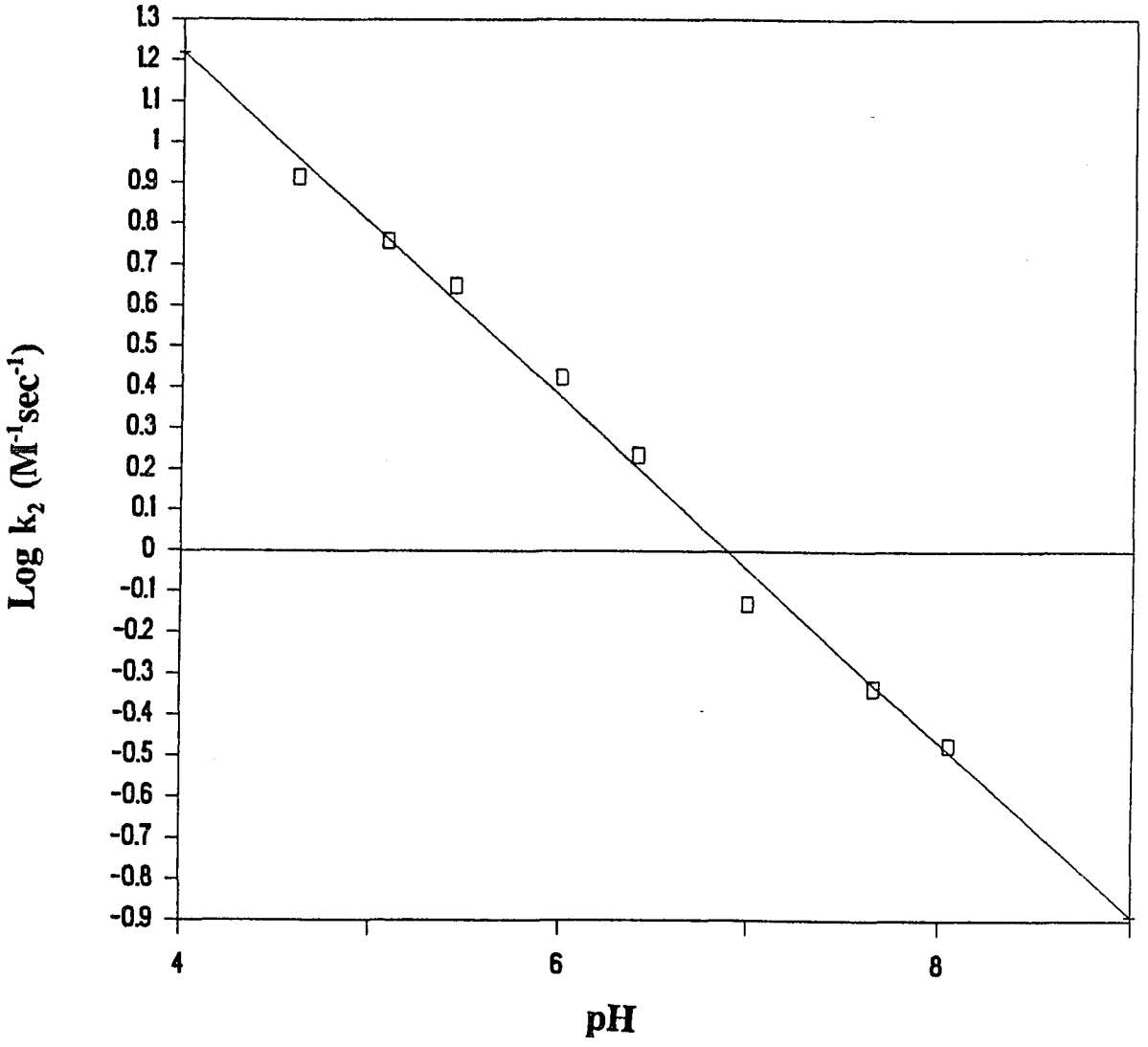

Fig.36 pH profile of spontaneous formation of salicylaldehyde phenylhydrazone in 0.1 M buffers, 25.5°C.
Slope is -0.422(±0.0149).
k_2 refers to the second-order rate constant.
(Data of Table XXV Appendix D)

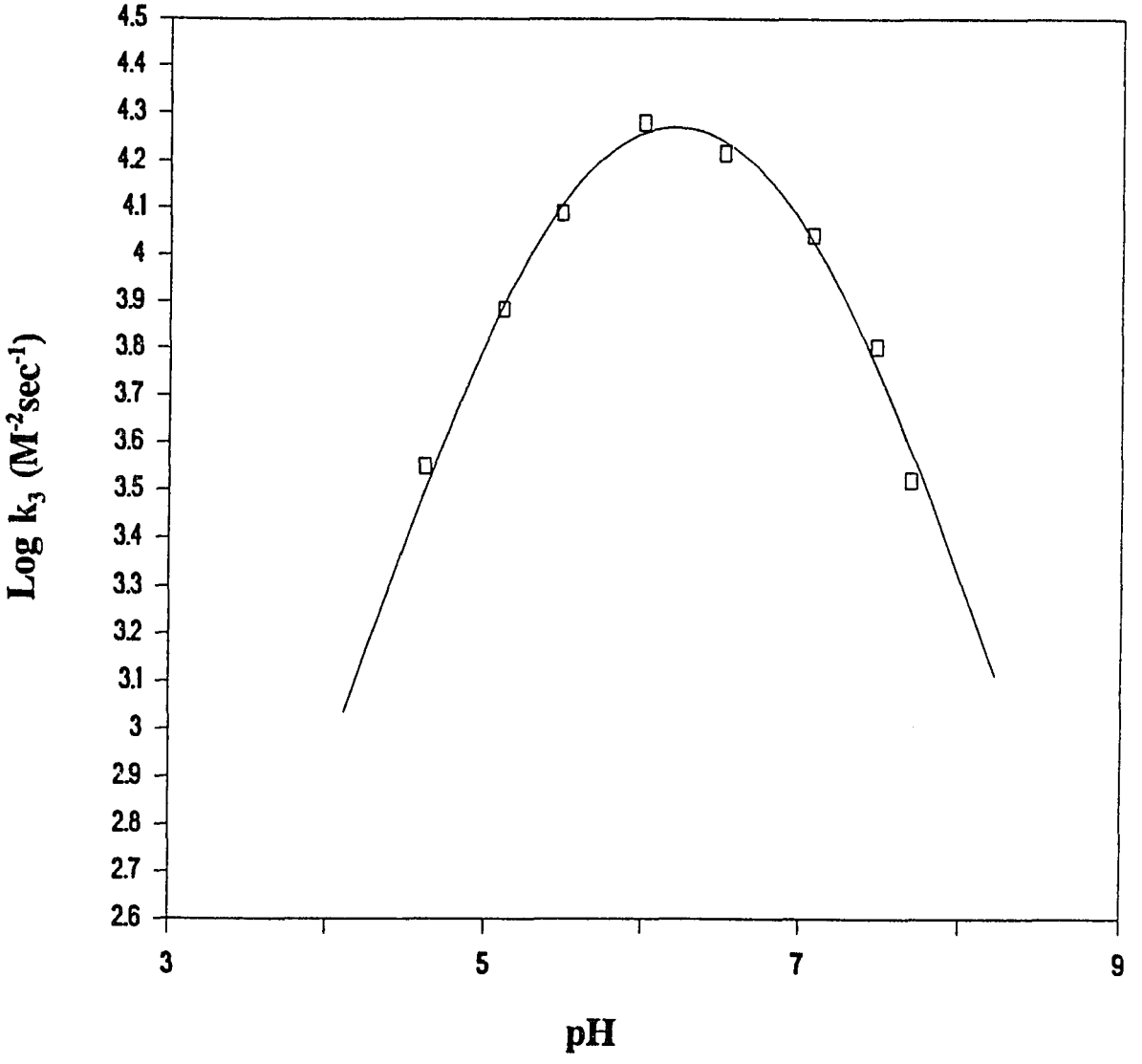

Fig.37 pH profile of 3,5-bis(trifluoromethyl)benzeneboronic acid catalyzed formation of salicylaldehyde phenylhydrazone in 0.1 M buffers, 25.5°C.
$pK_1 = 5.46(\pm 0.05)$, $pK_2 = 6.94(\pm 0.05)$, optimum pH = $6.20(\pm 0.05)$,
k_3 (Lim) = $2.54 \times 10^4(\pm 1.485 \times 10^3)$ M^{-2} sec^{-1}.
k_3 refers to the third-order rate constant.
(Data of Table XXVI Appendix D)

The corresponding optimum k_2/k_3 (binding constant in catalytic transition state) is $7.68x10^{-5}$ M. The pK_1 of 5.46 is presumably due to the ionization of phenylhydrazine[47] indicating that the nucleophile is active in its neutral form. The pK_2 of 6.94 reflects either the ionization of phenolic hydroxyl group in the salicylaldehyde or the ionization of the boronic acid. This pK was also seen in the case of salicylaldoxime formation.

Fig.38 shows the pH profile of benzeneboronic acid catalysis for the salicylaldehyde phenylhydrazone formation. While the pK_1 of 5.15 reflects the ionization of phenylhydrazine, the pK_2 of 7.75 is lower than the pK of benzeneboronic acid (pK = 8.8[50]). It perhaps originates from the ionization of the ternary complex (structure A) formed in the catalysis as illustrated in Scheme VI. In the case of 3,5-bis(trifluoromethyl)benzeneboronic acid, the low pK value of the boronic acid results in the pK of the ternary complex invisible in the pH profile. The pH dependencies observed here suggest that boronic acids are catalytically active in their neutral trigonal configurations.

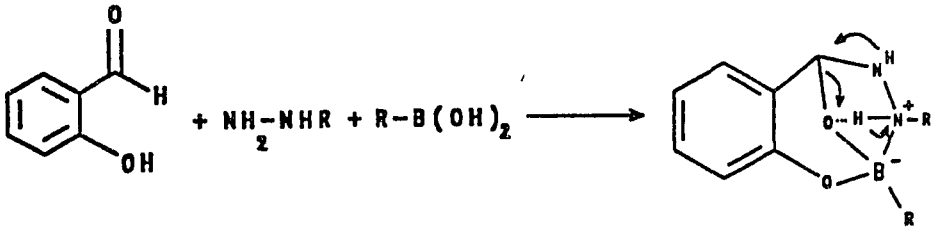

A

Scheme VI

Solvent deuterium isotope effect on the formation of salicylaldehyde phenylhydrazone. Although the pH profiles of spontaneous and 3,5-bis(trifluoromethyl)benzeneboronic acid catalyzed formation of salicylaldehyde phenylhydrazone in deuterium oxide are similar to those obtained in water (Fig.39,

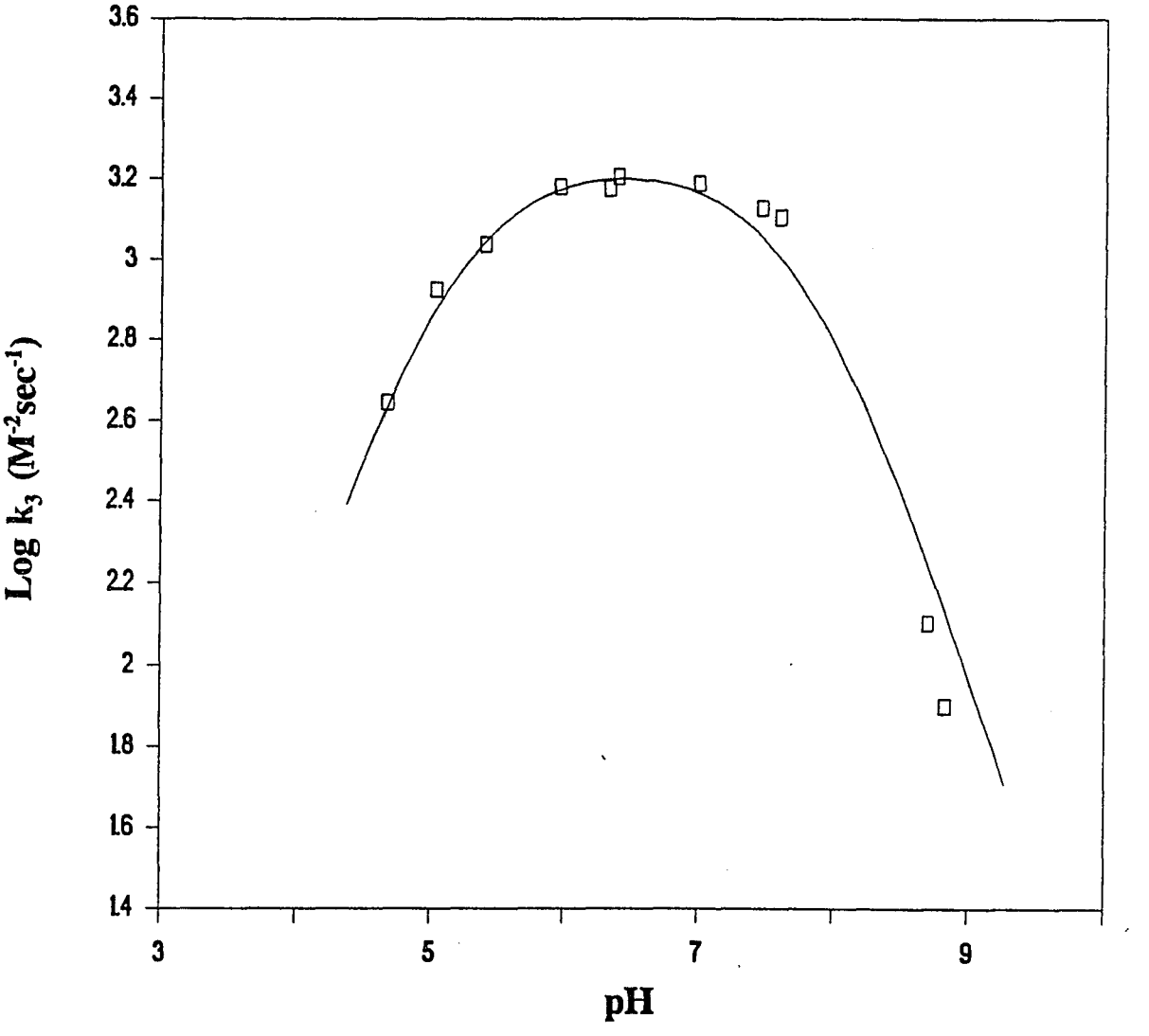

Fig.38 pH profile of benzeneboronic acid catalyzed formation of salicylaldehyde phenylhydrazone in 0.1 M buffers, 25.5°C.
$pK_1 = 5.15(\pm 0.05)$, $pK_2 = 7.75(\pm 0.15)$, optimum pH = $6.45(\pm 0.10)$
k_3 (Lim) = $1.75 \times 10^3(\pm 66.2)$ M^{-2} sec^{-1}.
k_3 refers to the third-order rate constant.
(Data of Table XXVII Appendix D)

40), the reaction rates were slower in deuterium oxide. The ratio of the limiting third-order rate constants, k_H/k_D, is 2.18($\pm$0.2935) indicating that proton transfer is involved in the rate determining step.

Effect of substituents of phenylhydrazine on the formation of salicylaldehyde phenylhydrazones. This experiment was done in order to study the influence of substituents of reactant on the hydrazone formation reaction. At pH 6.0, the kinetic rate constants were determined for both spontaneous and 3,5-bis(trifluoromethyl)-benzeneboronic acid catalyzed hydrazone formation with various substituted phenylhydrazines.

As seen in Fig.41, in the presence of 3,5-bis(trifluoromethyl)benzeneboronic acid, the Hammett plot is a straight line with a slope close to zero (+0.05). This plot suggests that the third-order rate constant of the boronic acid catalyzed hydrazone formation is independent of electronic effects due to the substituents on the reactant, phenylhydrazine.

When the values of logarithm of second-order rate constant for spontaneous hydrazone formation were plotted as a function of substituent constants, the plot is also linear with a slope of +0.36 (Fig.42). Although this slope is larger than the one observed in the 3,5-bis(trifluoromethyl)benzeneboronic acid catalyzed reaction, the result indicates that substituents on phenylhydrazine have little influence on the rate of spontaneous salicylaldehyde phenylhydrazone formation.

Comparison of salicylaldehyde, *p*-hydroxybenzaldehyde and *m*-hydroxy-benzaldehyde on the phenylhydrazone formation. The catalytic effect of 3,5-bis(trifluoromethyl)benzeneboronic acid on the formations of *p*-hydroxybenzaldehyde phenylhydrazone and *m*-hydroxybenzaldehyde phenylhydrazone were studied at pH 6.0.

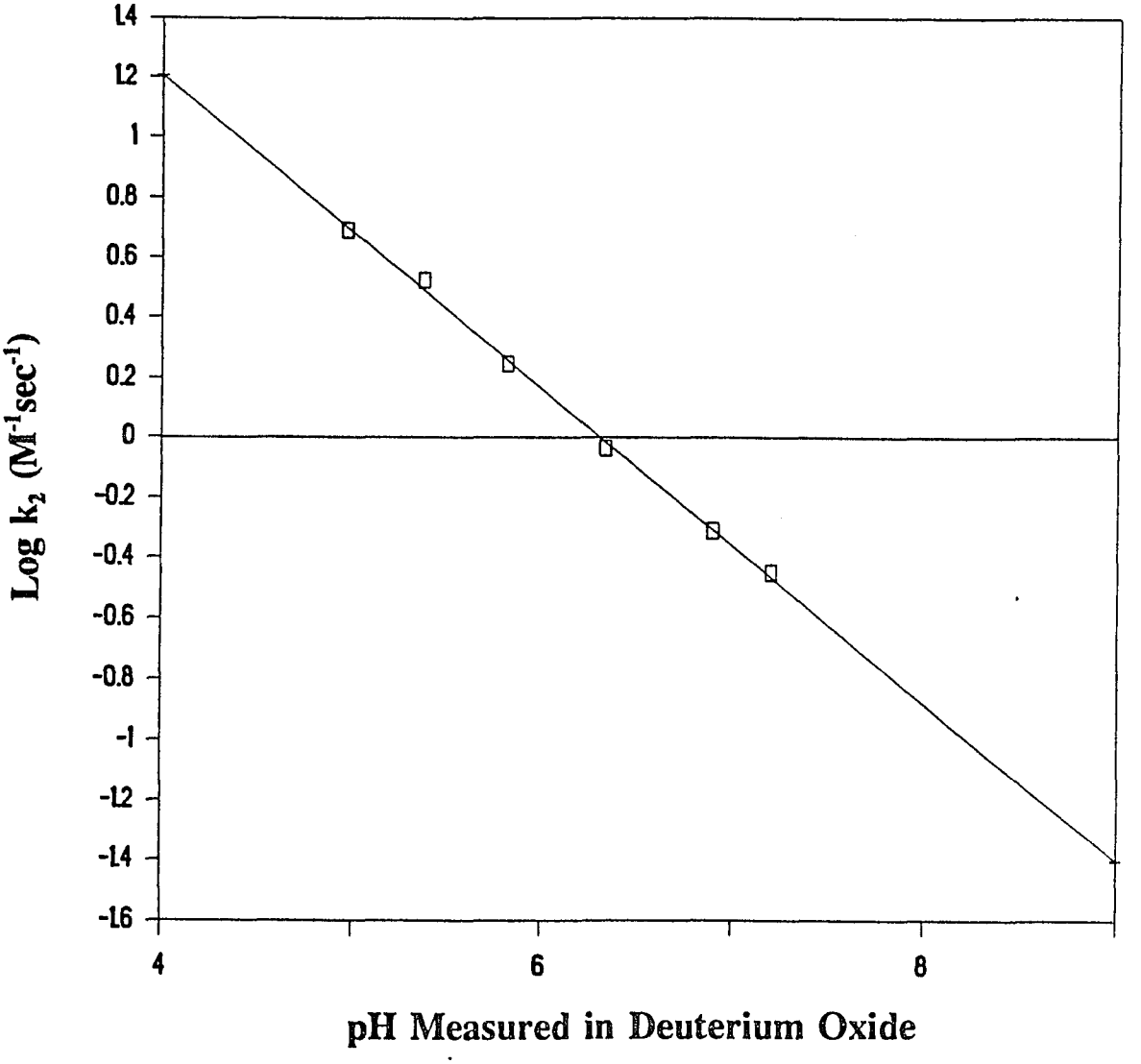

Fig.39 pH profile of spontaneous formation of salicylaldehyde phenylhydrazone in 0.1 M deuterium oxide buffers, 25.5°C.
Slope is -0.522(±0.0114).
k_2 refers to the second-order rate constant.
(Data of Table XXVIII Appendix D)

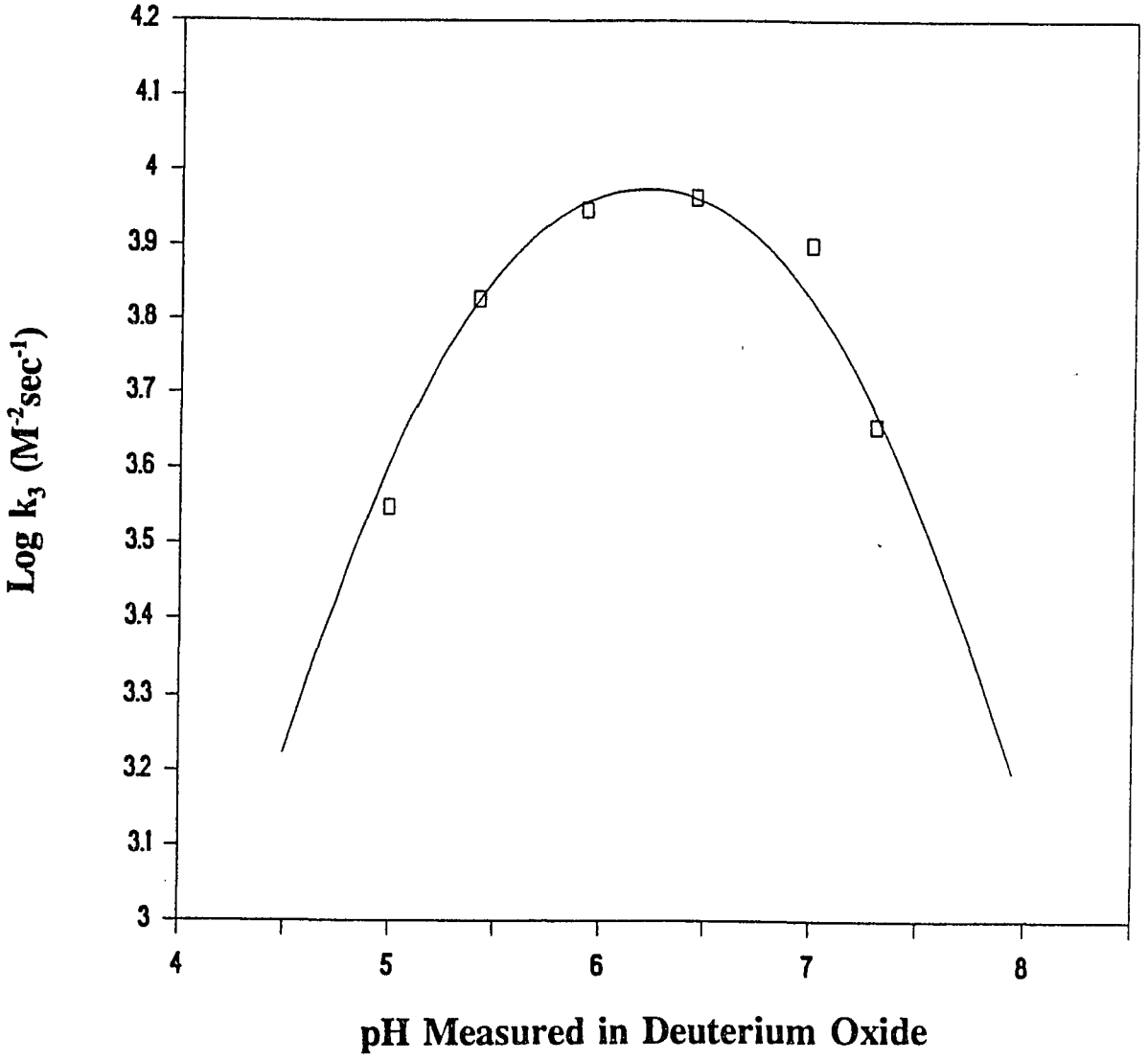

Fig.40 pH profile of 3,5-bis(trifluoromethyl)benzeneboronic acid catalyzed formation of salicylaldehyde phenylhydrazone in 0.1 M deuterium oxide buffers, 25.5°C.
$pK_1 = 5.27(\pm 0.05)$, $pK_2 = 7.13(\pm 0.10)$, optimum pH = $6.20(\pm 0.07)$,
k_3 (Lim) = $1.16 \times 10^4(\pm 7.73 \times 10^2)$ M^{-2} sec^{-1}.
k_3 refers to the third-order rate constant.
(Data of Table XXIX Appendix D)

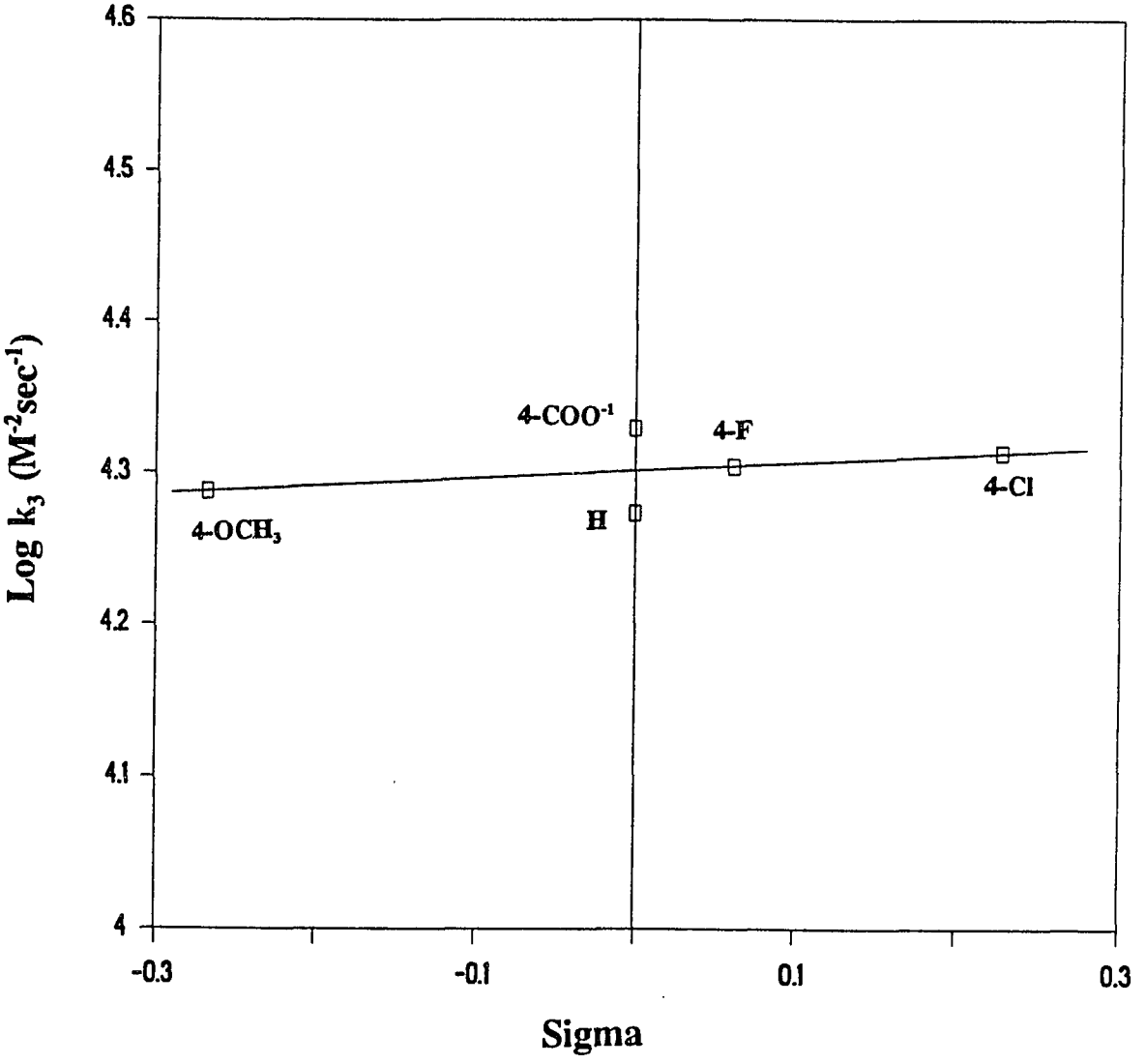

Fig.41 Hammett plot relating log k_3 and *sigma* for the 3,5-bis(trifluoromethyl)benzeneboronic acid catalyzed formation of salicylaldehyde phenylhydrazone with substituted phenylhydrazines in pH 6.0 0.1 M buffer, 25.5°C.
The value of *rho* is $+0.0512(\pm 0.0641)$.
k_3 refers to the third-order rate constant.
(Data of Table XXX Appendix D)

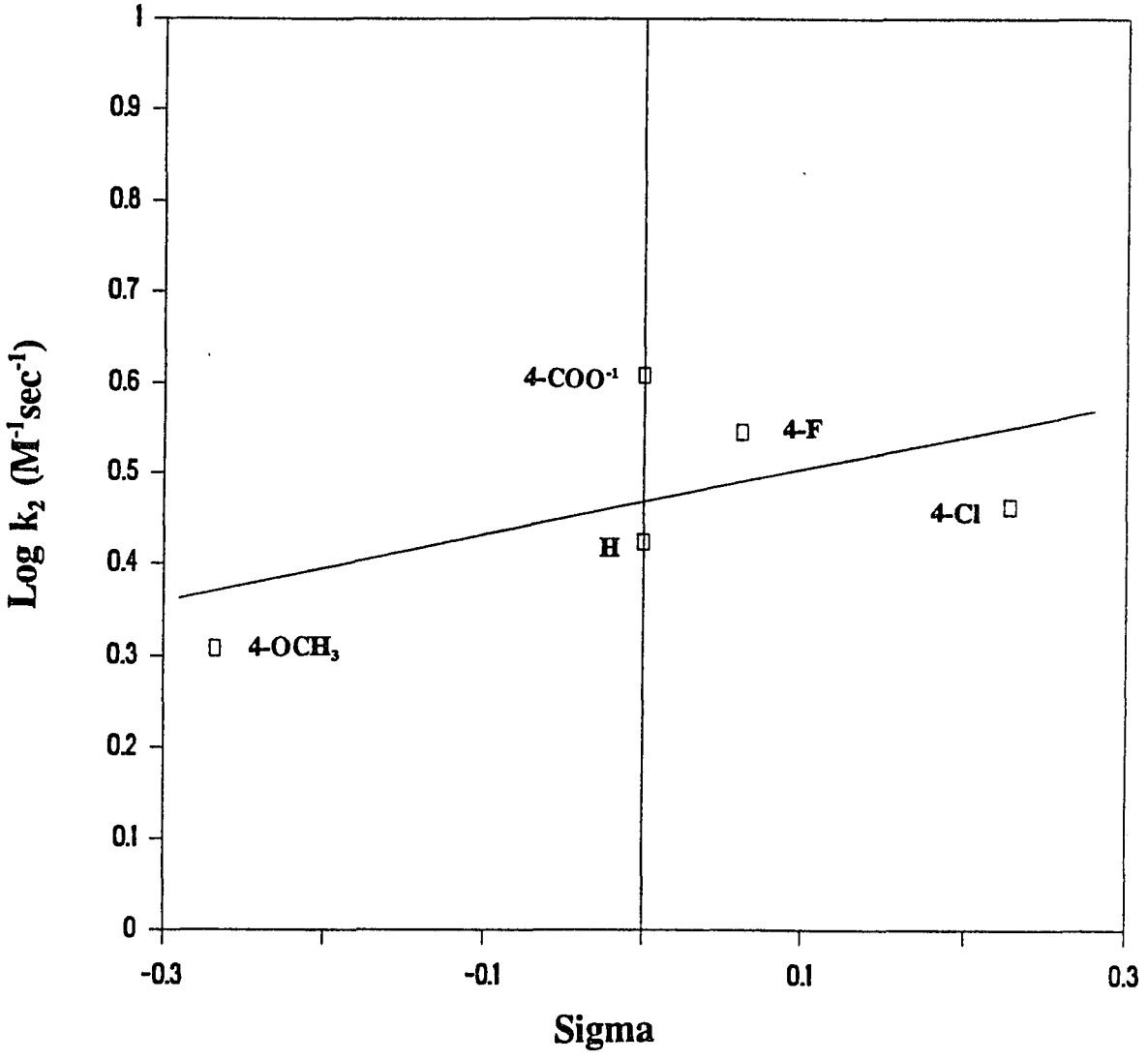

Fig.42 Hammett plot relating log k_2 and *sigma* for the spontaneous formation of salicylaldehyde phenylhydrazone with substituted phenylhydrazines in pH 6.0 0.1 M buffer, 25.5°C.
The value of *rho* is +0.363(±0.308).
k_2 refers to the second-order rate constant.
(Data of Table XXX Appendix D)

Unlike salicylaldehyde phenylhydrazone formation, the pseudo-first-order rate constants for the catalyzed and uncatalyzed *p*-hydroxybenzaldehyde phenylhydrazone formation reactions are nearly identical. This is also true for the *m*-hydroxybenzaldehyde phenylhydrazone formation (Table XI).

Since the boronic acid displayed no catalytic effect on the formation of *para* and *meta* hydroxybenzaldehyde phenylhydrazones, it is clear that the *ortho* phenolic hydroxyl group of salicylaldehyde is essential for the boronic acid catalysis.

Table XI

Comparison of Salicylaldehyde, *m*-Hydroxybenzaldehyde and *p*-Hydroxybenzaldehyde on the Phenylhydrazone Formation Reaction at 25.5°C, pH 6.0, Catalyzed by 3,5-Bis(trifluoromethyl)benzeneboronic acid

p-Hydroxy-benzaldehyde (μM)	Phenyl-hydrazine (mM)	Boronic acid (mM)	k_1* (sec^{-1})
33.74	13.14	0.000	0.01284 ($\pm 5.58 \times 10^{-6}$)
33.74	13.14	2.303	0.01236 ($\pm 6.73 \times 10^{-6}$)
m-Hydroxy-benzaldehyde (μM)	Phenyl-hydrazine (mM)	Boronic acid (mM)	k_1* (sec^{-1})
35.92	6.570	0.000	0.03108 ($\pm 6.81 \times 10^{-5}$)
35.92	6.570	2.303	0.03153 ($\pm 6.49 \times 10^{-5}$)
Salicyl-aldehyde (μM)	Phenyl-hydrazine (mM)	Boronic acid (mM)	k_1* (sec^{-1})
80.00	6.570	0.000	0.01583 ($\pm 4.18 \times 10^{-5}$)
80.00	6.570	1.151	0.1625 ($\pm 2.56 \times 10^{-4}$)

* k_1 refers to the pseudo-first-order rate constant.

CONCLUSIONS

Boron acids exhibit an efficient catalytic effect on the formation of salicylaldoxime. These reactions resemble enzymatic catalyses: the catalysts are active in buffered water solutions at room temperature; the catalysts show reversible binding to both substrate and product. The reaction system also displays substrate specificity: the *ortho* phenolic group in the structure of salicylaldehyde and the OH group of hydroxylamine are clearly important for the action of boron acids.

pH-dependent kinetics indicate that boric and boronic acids function in neutral trigonal configuration in their catalyses on salicylaldoxime formation. Diphenylborinic acid on the other hand is catalytically active in both ionized and unionized forms in this reaction system. Solvent deuterium isotope effect suggests the involvement of a proton transfer in the common rate determining step for all boron acids.

The Brønsted and Hammett relationships suggest that the catalytic effectiveness of boron acids is improved by electron-withdrawing substituents on the catalysts. The differences observed in the catalyses of salicylaldoxime formation by boric, boronic and borinic acids may be directly related to the different number of aryl groups attached to the boron atom.

The complexation of boron acids to salicylaldoxime is facilitated by electron-withdrawing groups on the boron acids. The stability of the oxime-boron acid complex increases as the hydroxyl groups of boric acid are replaced by benzene rings.

Boronic acids also accelerate the rate of salicylaldehyde phenylhydrazone formation. The catalytic behavior of boronic acids on the hydrazone formation is similar

to that observed in salicylaldoxime formation. In addition, substituents on the benzene ring of phenylhydrazine have no significant influence on the rate of catalyzed and uncatalyzed salicylaldehyde phenylhydrazone formation.

Based on the experimental data gathered in this study, the possible mechanisms for the boron acid catalyzed formation of salicylaldoxime and salicylaldehyde phenylhydrazone are proposed. They are all consistent with the reversibility of the catalyzed reactions.

Mechanism of boronic acid catalyzed salicylaldoxime formation. As presented in Scheme VII, two competing mechanisms may be involved in the catalysis. In path A (leading from **1** to **2**, **2a**, **4**, **5** and **6**), the first step is the formation of complex **2** from salicylaldehyde and unionized boronic acid. The boron atom in this complex acts as a Lewis acid and coordinates to the carbonyl oxygen. This makes the carbonyl carbon atom more electron deficient. In the next step, the intermolecular nucleophilic attack of the carbonyl carbon of complex **2** by neutral hydroxylamine generates the intermediate **2a** in which the hydroxyl group of hydroxylamine esterifies with the boron atom and forms complex **4**.

Path B (leading from NH_2-OH to **3**, **3a**, **4**, **5** and **6**) starts with the esterification of neutral trigonal boronic acid with the hydroxyl group of hydroxylamine. Complex **3** formed in the first step associates with salicylaldehyde and leads to **3a**. Within this structure, the boron atom coordinates with the carbonyl oxygen and facilitates the nucleophilic addition of the carbonyl group to generate complex **4** which is same to the one formed in path A.

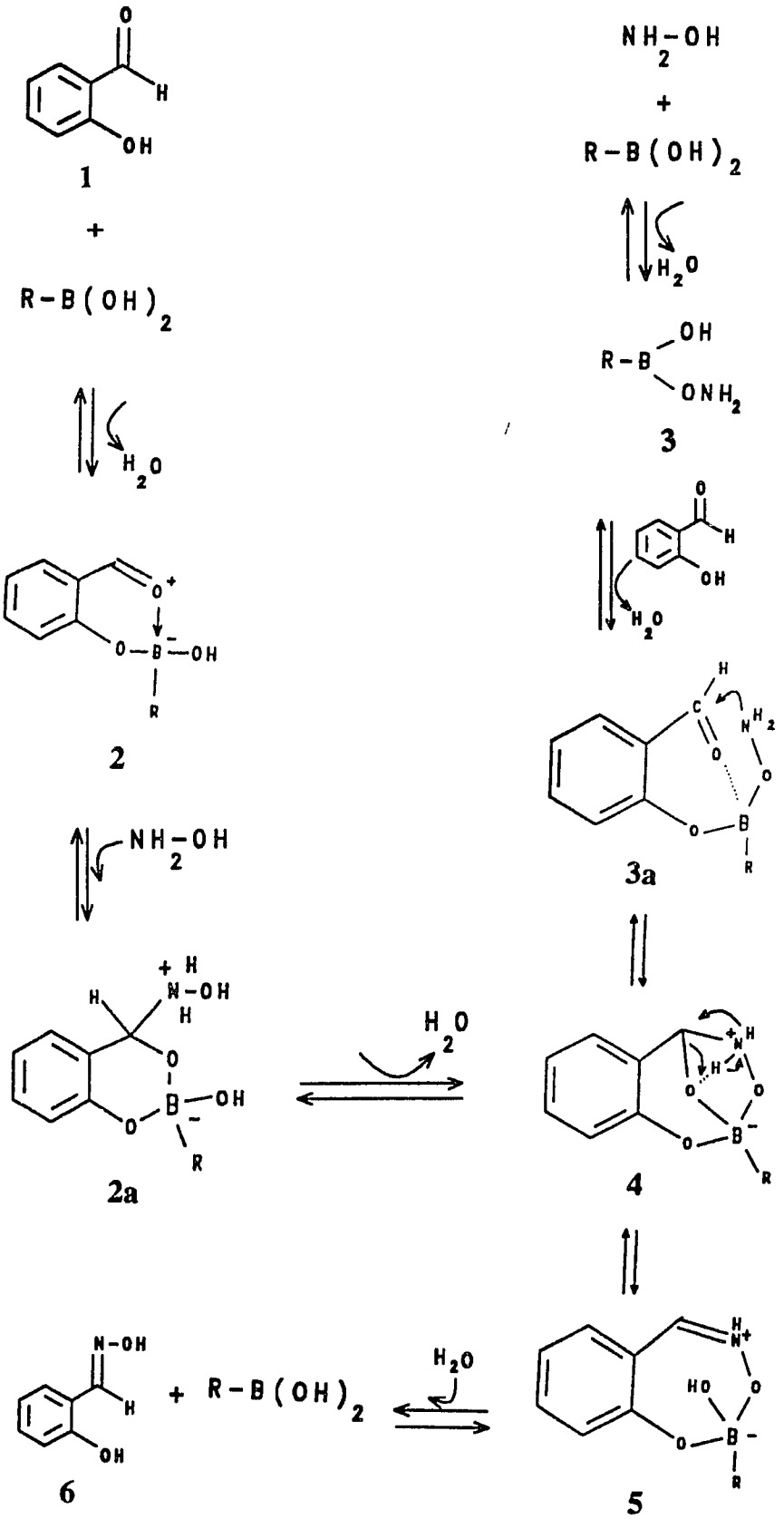

Scheme VII

The common rate determining step shared by the two reaction pathways must be the conversion of complex **4** to complex **5**. This step involves proton transfer which is consistent with the observed solvent deuterium isotope effect. As shown in complex **4**, the intramolecular proton transfer from the nitrogen to the oxygen atom results in the elimination of a hydroxyl group which is readily accepted by the boron atom and forms complex **5**. Within this complex, the reaction product salicylaldoxime is bound to the boronic acid. The hydrolysis of complex **5** releases free salicylaldoxime and regenerates the catalyst boronic acid.

Complex **4** is the structure closely related to the transition state on the common reaction pathway. The boron atom in this complex is anionic and tetrahedral, this configuration allows the boron atom to exist in the bicyclic structure. The electron-withdrawing substituents on the benzene ring of boronic acid are expected to stabilize the negative charge on the boron atom. This could explain the better catalysis observed in the cases of benzeneboronic acids containing electron-withdrawing groups compared to those containing electron-donating groups. Besides, the positive charge on the protonated amino group also makes important contribution to the stability of the structure.

Complex **5** is most likely to be the structure of the oxime-boronate complex. This is supported by the electronic effect observed in the complexation. The electron-withdrawing substituents on the boronic acid help to stabilize the anionic tetrahedral boron atom in such a complex.

Based on the structural differences between complex **4** and complex **5** presented here, boronic acids are expected to display higher binding affinity in complex **4** than in

complex **5**. This is consistent with the experimental data listed in Table VIII and Table X. The dissociation constant of complex **4** (Table VIII) is about 10-fold lower than that of complex **5** (Table X).

Mechanism of boric acid catalyzed salicylaldoxime formation. The steps involved in the boric acid catalysis shown in Scheme VIII are very similar to those proposed for boronic acid. There are two reaction pathways competing in the catalysis. Since the optimal catalysis was observed at pH 7.35 (Fig.13), trigonal boric acid must prefer the ionized phenol group of salicylaldehyde for binding in this reaction system.

Complex **4** can be generated in path A through **2** and **2a**, it also can be generated in path B through **3** and **3a**. In the rate-determining step, **4** undergoes dehydration and leads to **5**.

The oxime-borate complex may exist in two possible structures shown as **5** and **5a**. These complexes are in equilibrium. Their hydrolyses produce free salicylaldoxime and boric acid.

Mechanism of diphenylborinic acid catalyzed salicylaldoxime formation. Based on the pH-dependent kinetic data (Fig.14), diphenylborinic acid exhibits catalytic effects on oxime formation in both the ionized and unionized forms. When the pH of the reaction medium is above the pK of the borinic acid (pK = 6.2[45]), the tetrahedral species is prevalent. When the reaction pH is lower than the pK, the trigonal species is the major form.

As shown in Scheme IX, trigonal diphenylborinic acid esterifies to the hydroxyl

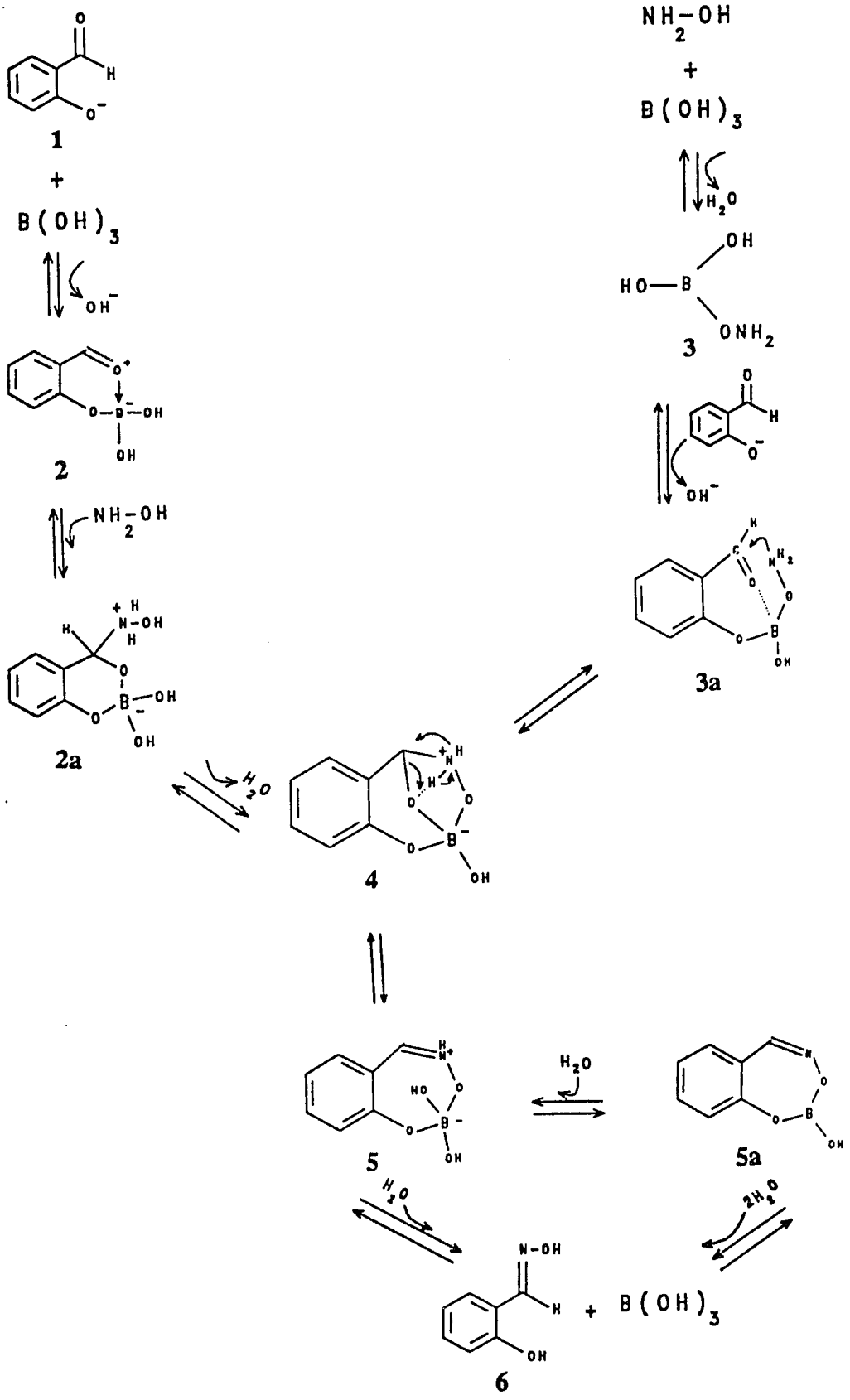
1
+
B(OH)3
OH-
2
NH2-OH
2a
NH2-OH
+
B(OH)3
H2O
3
3a
H2O
4
5
5a
H2O
2H2O
N-OH
+ B(OH)3
6

Scheme VIII

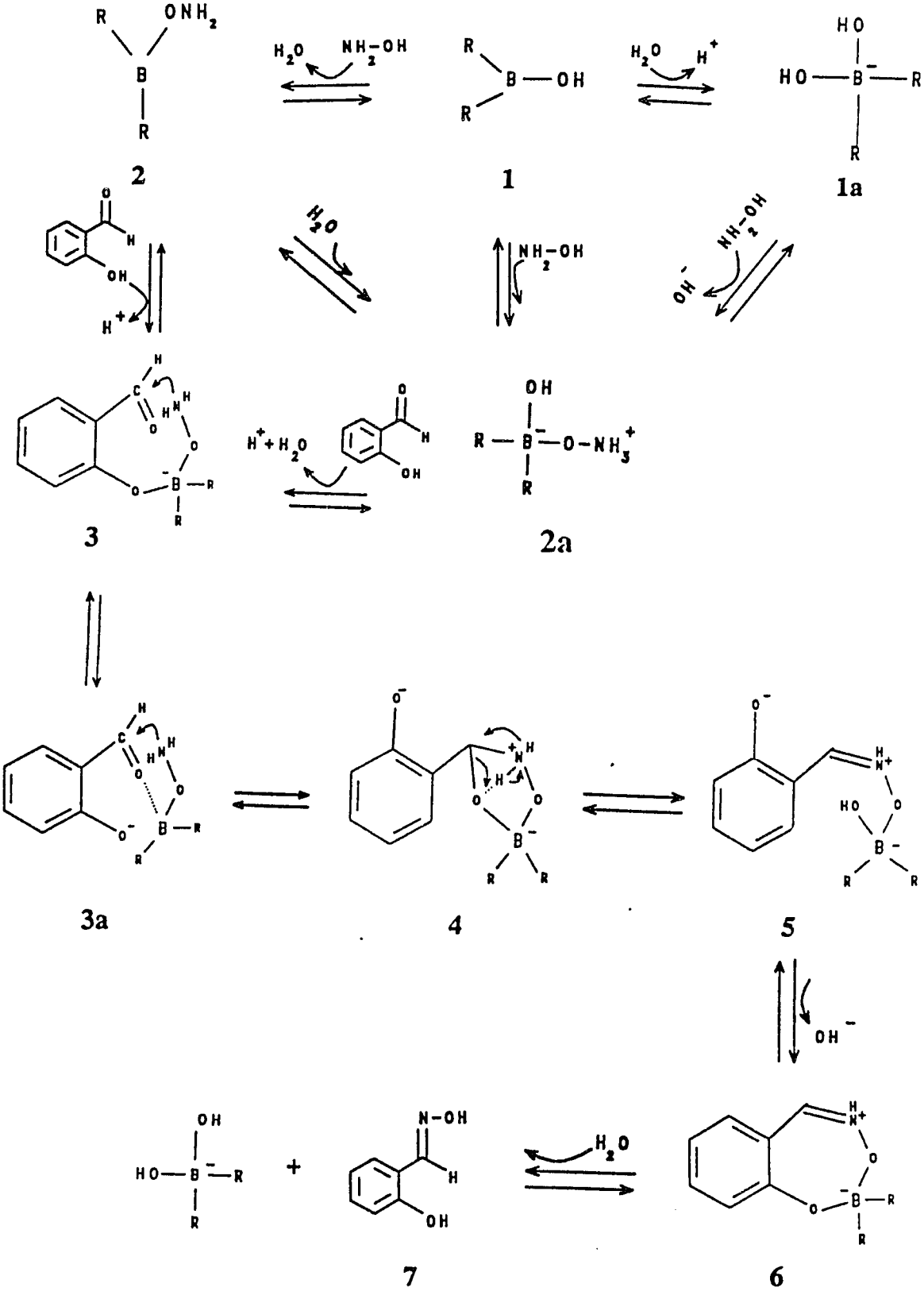

Scheme IX

group of hydroxylamine and forms either **2** or **2a**. The esterification of the anionic tetrahedral borinic acid with hydroxylamine produces **2a**. Complex **2** and complex **2a** are in equilibrium. Association of salicylaldehyde with either of these complexes leads to the formation of structure **3**. The boron atom in structure **3** can not directly assist the nucleophilic attack of the carbonyl carbon by the amino group, it contributes to binding not to catalysis. However, structure **3a** may exist in the equilibrium at low concentration. Within this structure, coordination of the boron atom with the carbonyl oxygen makes the carbonyl carbon more electron deficient and facilitates the nucleophilic addition of the carbonyl group.

In complex **4**, there is an intramolecular proton transfer which leads to the formation of C=N bond in structure **5**. In the next step, the intermediate **5** undergoes ring closure to give complex **6**. Hydrolysis of this complex produces free salicylaldoxime and diphenylborinic acid.

Unlike the case of boronic acid catalysis, the binding affinity of diphenylborinic acid in the transition state is similar to that exhibited in the oxime-borinic acid complex (Table VIII, X). The experimental data could be explained by the structural similarities between complex **4** and complex **6** proposed here.

Since the pK of hydroxylamine was not observed in the pH profile (Fig.14), it suggests that the binary complex **2a** may be prevalent in the catalysis. The negative tetrahedral boron atom clearly requires neutral phenol group of salicylaldehyde for binding. Besides, protonation of the amino group in the ternary complex (structure **4**) not only stabilizes the negative charges in the structure but also facilitates the intramolecular

proton transfer leading to the product. Therefore, the double-proton ionization reflected in the pH profile is presumably a composite of the ionizations of salicylaldehyde and the ternary complex.

Mechanism of boronic acid catalyzed formation of *p*-hydroxybenzaldehyde oxime and *m*-hydroxybenzaldehyde Oxime. Boronic and borinic acids accelerate the formation of oximes of *p*-hydroxybenzaldehyde and *m*-hydroxybenzaldehyde. The catalytic effectiveness of boron acid in these cases is much lower than that observed in salicylaldoxime formation. In Scheme X, *p*-hydroxybenzaldehyde is used to illustrate a possible catalytic mechanism involved in the formation of these oximes.

It is clear that the hydroxyl group of hydroxylamine plays an important role in the mechanism. The boron atom in complex 3 assists the nucleophilic addition of the carbonyl group by functioning as a Lewis acid. This leads to the formation of the five-membered ring intermediate (structure 4), in which the intramolecular proton transfer results in the generation of complex 5. Dissociation of this complex gives the product and regenerates boronic acid.

Mechanism of boronic acid catalyzed formation of salicylaldehyde phenylhydrazone. As presented in Scheme XI, the first step is the complexation of neutral boronic acid with salicylaldehyde to generate complex 2 which is the same as the one shown in the boronic acid catalyzed formation of salicylaldoxime (Scheme VII, structure 2). In the second step, phenylhydrazine attacks the electron deficient carbonyl carbon in complex 2 and forms complex 2a. The nitrogen atom of phenylhydrazine in 2a complexes with the boron atom leading to the formation of structure 3. The

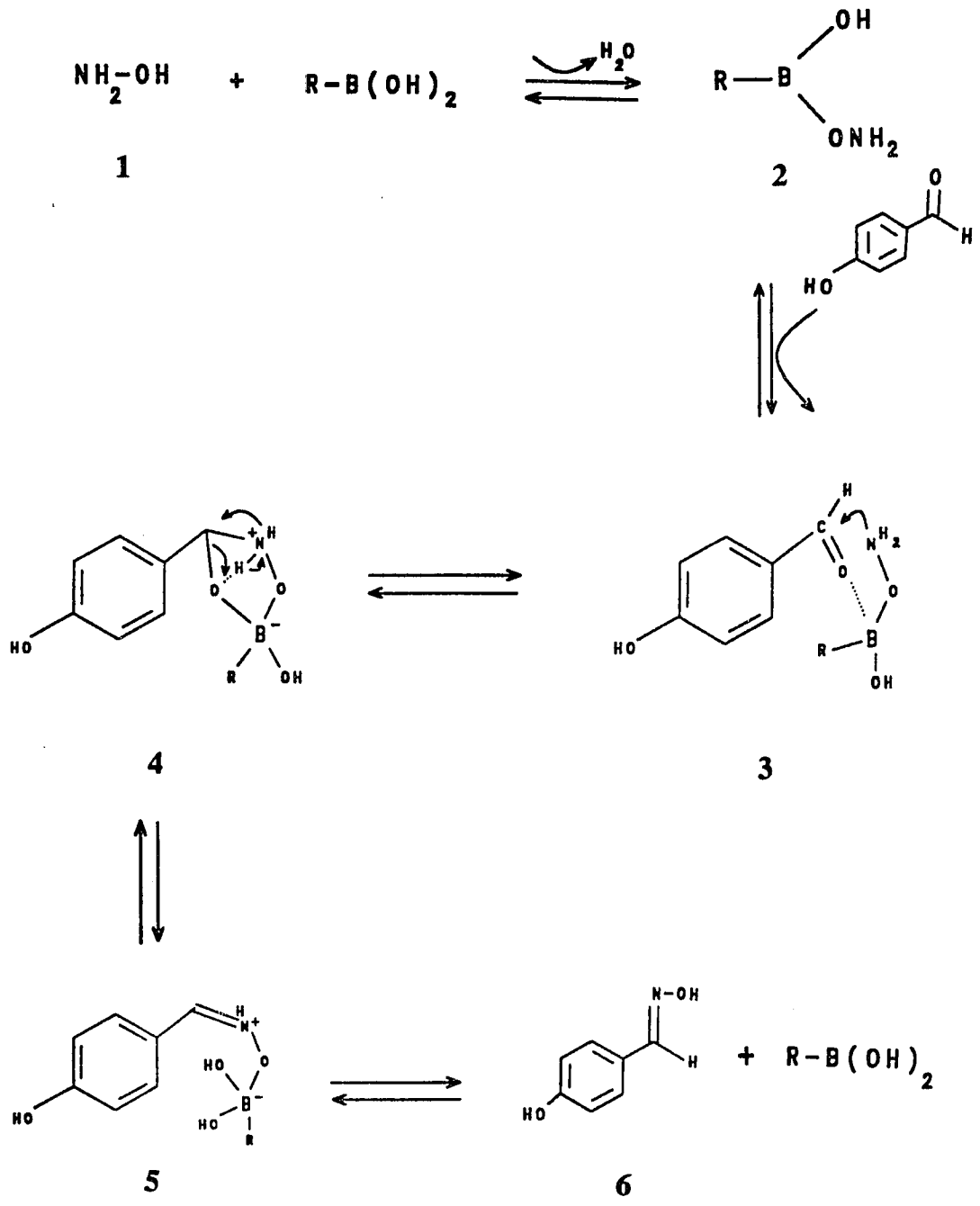

Scheme X

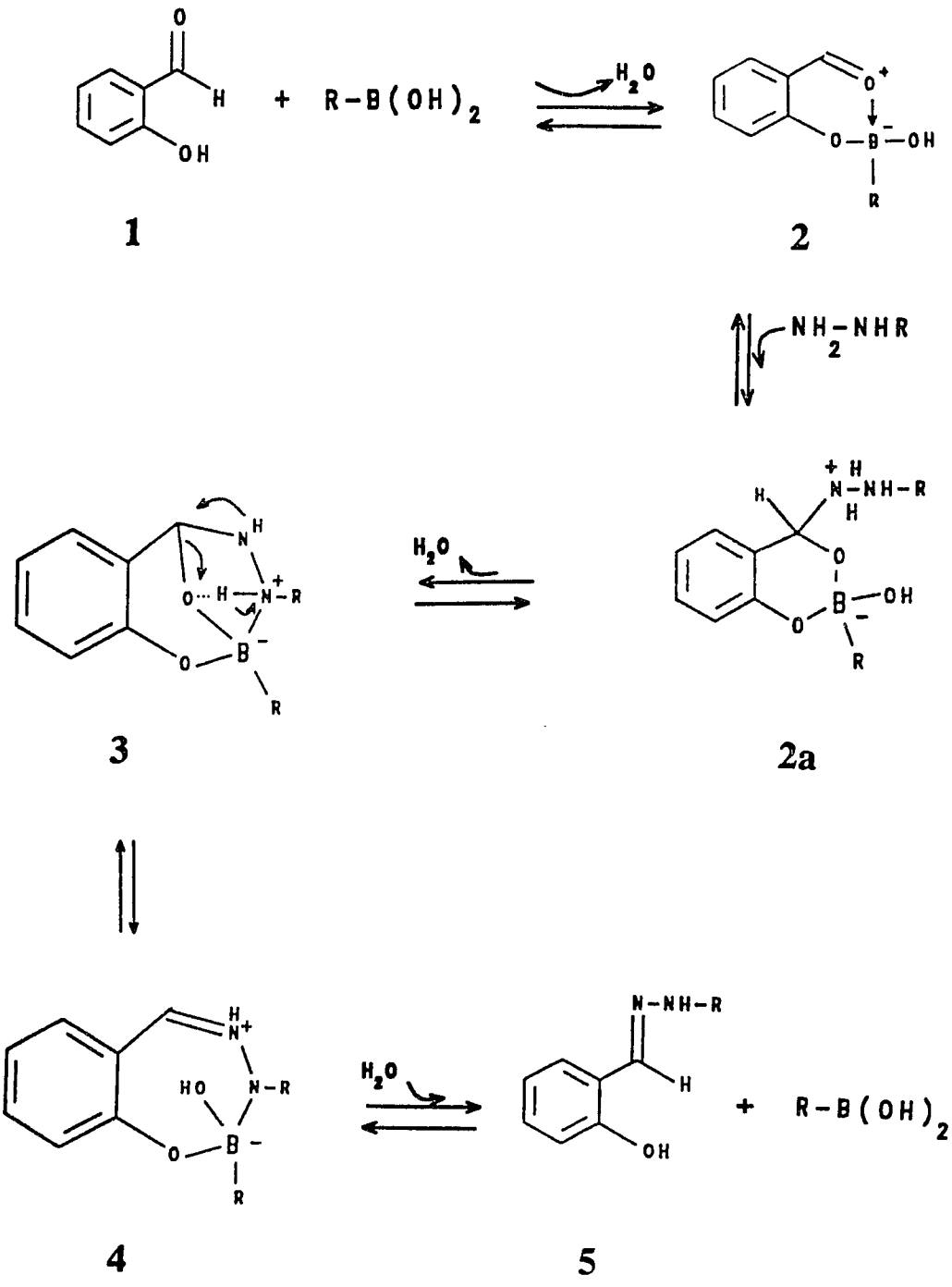

1 2 3 2a 4 5

Scheme XI

conversion of complex **3** to complex **4** must be the rate-determining step which involves the intramolecular proton transfer from the nitrogen to the oxygen in structure **3**. This agrees with the solvent deuterium isotope effect observed in the experiment. The boron atom in structure **3** facilitates the hydrazone formation by accepting the hydroxyl group. The positive charge on the nitrogen helps to stabilize the anionic tetrahedral boron atom in the bicyclic complex. The product, salicylaldehyde phenylhydrazone, is generated in the last step from the hydrolysis of complex **4**.

APPENDIX A

Tables of Data for Part I Fig.2 - Fig.39

(Error analysis results are shown on the corresponding figures)

Table I pH profile of k_{cat}/K_m for the bovine thrombin-catalyzed hydrolysis of N-t-Boc-Valyl-Prolyl-Arginine-7-AMC-HCl (Data of Fig.2 Part I)

pH	k_{cat}/K_m ($M^{-1}sec^{-1}$)
4.98	1.8700×10^{4}
5.36	7.2200×10^{4}
6.00	2.3600×10^{5}
6.40	5.5200×10^{5}
7.09	1.6300×10^{6}
7.55	2.8100×10^{6}
7.94	4.5000×10^{6}
8.82	4.4200×10^{6}
9.17	5.6200×10^{6}
9.63	3.9400×10^{6}
10.22	1.3900×10^{6}
10.75	2.1600×10^{5}

Table II pH profile of K_m for the bovine thrombin-catalyzed hydrolysis of N-t-Boc-Valyl-Prolyl-Arginine-7-AMC-HCl (Data of Fig.3 Part I)

pH	K_m (M)
5.00	2.64×10^{-5}
5.44	1.85×10^{-5}
6.09	9.60×10^{-6}
6.50	7.30×10^{-6}
7.09	8.31×10^{-6}
7.54	4.43×10^{-6}
7.81	4.40×10^{-6}
8.60	4.86×10^{-6}
9.00	3.92×10^{-6}
9.40	3.27×10^{-6}
1.00	3.43×10^{-6}

Table III Spectrofluorometric titration of 7-amino-4-methylcoumarin (Data of Fig.4 Part I)

pH	Fluorescence intensity
4.60	1.0810
5.00	1.1200
5.44	1.0580
6.16	1.2030
6.52	0.9430
7.08	0.9970
7.48	1.0960
7.85	1.1770
8.60	1.1380
9.05	0.9980
9.27	1.2420
9.80	1.0430
10.63	1.0370
11.11	1.0010

Table IV pH profile of K_m for the bovine thrombin-catalyzed hydrolysis of D-Phe-Pipecolyl-Arg-*p*NA (Data of Fig.5 Part I)

pH	K_m (M)
5.54	8.2510×10^{-5}
6.03	4.8850×10^{-5}
6.45	1.6370×10^{-5}
7.08	1.1110×10^{-5}
7.50	5.0480×10^{-6}
8.01	5.3690×10^{-6}
8.66	7.3760×10^{-6}
9.64	2.2470×10^{-5}
10.09	4.8710×10^{-5}
10.69	2.1300×10^{-4}

Table V pH profile of k_{cat} for the bovine thrombin-catalyzed hydrolysis of D-Phe-Pipecolyl-Arg-*p*NA (Data of Fig.6 Part I)

pH	k_{cat} (sec^{-1})
5.54	4.798
6.03	3.536
6.45	4.584
7.08	7.427
7.50	8.493
8.01	9.143
8.66	14.21
9.64	10.39
10.09	10.34
10.69	18.81

Table VI pH profile of k_{cat}/K_m for the bovine thrombin-catalyzed hydrolysis of D-Phe-Pipecolyl-Arg-*p*NA (Data of Fig.7 Part I)

pH	k_{cat}/K_m ($M^{-1}sec^{-1}$)
5.54	5.8151×10^4
6.03	7.2379×10^4
6.45	2.8001×10^5
7.08	6.6849×10^5
7.50	1.6824×10^6
8.01	1.7030×10^6
8.66	1.9267×10^6
9.64	4.6227×10^5
10.09	2.1219×10^5
10.69	8.8289×10^4

Table VII Initial inhibition of bovine thrombin by Ac-D-Phe-Pro-boroArg at pH 8.66 (Data of Fig.8 Part I)

[substrate] (M)	v_i (uninhi.) (OD sec^{-1})	v_i(inhi.) (OD sec^{-1})
1.881×10^{-5}	9.870×10^{-5}	5.133×10^{-5}
4.032×10^{-5}	1.175×10^{-4}	7.131×10^{-5}
5.376×10^{-5}	1.241×10^{-4}	8.433×10^{-5}
6.720×10^{-5}	1.257×10^{-4}	9.035×10^{-5}
9.408×10^{-5}	1.290×10^{-4}	9.894×10^{-5}
1.210×10^{-4}	1.307×10^{-4}	9.972×10^{-5}
1.478×10^{-4}	1.307×10^{-4}	1.067×10^{-4}
1.747×10^{-4}	1.298×10^{-4}	1.138×10^{-4}

Table VIII pH profile for the initial inhibition of bovine thrombin by Ac-D-Phe-Pro-boroArg (Data of Fig.10 Part I)

pH	K_i (M)
5.08	8.9681×10^{-9}
5.54	5.7589×10^{-9}
6.03	8.6982×10^{-9}
6.45	7.2020×10^{-9}
7.08	4.1739×10^{-9}
7.50	5.4806×10^{-9}
8.01	3.9702×10^{-9}
8.66	4.2010×10^{-9}
9.64	6.8251×10^{-9}
10.09	9.9390×10^{-9}
10.69	1.2777×10^{-7}

Table IX pH profile for the final inhibition of bovine thrombin by Ac-D-Phe-Pro-boroArg (Data of Fig.11 Part I)

pH	K_i (M)
6.03	1.3051×10^{-9}
6.45	5.7366×10^{-10}
7.08	1.2092×10^{-10}
7.50	6.9252×10^{-11}
8.01	7.3310×10^{-11}
8.66	4.3759×10^{-11}
9.10	7.8311×10^{-11}
9.64	2.3002×10^{-10}
10.09	5.5165×10^{-10}

Table X pH profile for the transition from initial inhibition to final inhibition of bovine thrombin by Ac-D-Phe-Pro-boroArg (Data of Fig.12 Part I)

pH	k_3 (sec^{-1})
5.54	2.2534×10^{-4}
6.03	1.3156×10^{-3}
6.45	1.9636×10^{-3}
7.08	4.8723×10^{-3}
7.50	5.6034×10^{-3}
8.01	5.8128×10^{-3}
8.66	5.6354×10^{-3}
9.10	5.2462×10^{-3}
9.64	4.0862×10^{-3}
10.09	1.0864×10^{-3}

Table XI pH profile for the transition from final inhibition to initial inhibition of bovine thrombin by Ac-D-Phe-Pro-boroArg (Data of Fig.13 Part I)

pH	k_4 (sec^{-1})
5.54	1.233×10^{-4}
6.03	1.846×10^{-4}
6.45	1.224×10^{-4}
7.08	1.238×10^{-4}
7.50	1.048×10^{-4}
8.01	9.103×10^{-5}
8.66	9.176×10^{-5}
9.10	1.026×10^{-4}
9.64	1.070×10^{-4}
10.09	3.375×10^{-5}

Table XII Complexation between pinanediol and Ac-D-Phe-Pro-boroArg at pH 6.45 (Data of Fig.16, 17 Part I)

[pinanediol] (M)	slope (sec^{-1})
6.250×10^{-4}	1.439×10^{-4}
1.250×10^{-3}	1.743×10^{-4}
2.500×10^{-3}	1.902×10^{-4}
5.000×10^{-3}	2.159×10^{-4}
1.000×10^{-2}	2.270×10^{-4}
2.000×10^{-2}	2.359×10^{-4}

Table XIII pH profile for the initial inhibition of bovine thrombin by Ac-D-Phe-Pro-Arg (Data of Fig.19 Part I)

pH	K_i (M)
5.010	1.1865×10^{-4}
5.410	7.3475×10^{-5}
6.030	5.3562×10^{-5}
6.410	4.3103×10^{-5}
7.010	2.0899×10^{-5}
7.400	1.5295×10^{-5}
7.800	3.0902×10^{-5}
8.600	4.9480×10^{-5}
9.020	1.1172×10^{-4}
10.040	2.4178×10^{-3}

Table XIV pH profile for the final inhibition of bovine thrombin by Ac-D-Phe-Pro-Arg (Data of Fig.20 Part I)

pH	K_i (M)
5.01	1.1518×10^{-4}
5.41	6.3532×10^{-5}
6.03	2.5820×10^{-5}
6.41	1.8129×10^{-5}
7.01	3.1124×10^{-6}
7.40	1.3187×10^{-6}
7.80	1.5487×10^{-6}
8.60	3.5075×10^{-6}
9.02	5.9952×10^{-6}
10.04	2.3170×10^{-4}

Table XV pH profile for the transition from initial inhibition to final inhibition of bovine thrombin by Ac-D-Phe-Pro-Arg (Data of Fig.21 Part I)

pH	k_3 (sec^{-1})
6.03	4.9726×10^{-4}
6.41	9.3817×10^{-4}
7.01	2.9388×10^{-3}
7.40	9.8873×10^{-3}
7.80	1.2689×10^{-2}
8.60	1.7394×10^{-2}
9.02	2.5262×10^{-2}
10.04	9.3023×10^{-3}

Table XVI pH profile for the transition from final inhibition to initial inhibition of bovine thrombin by Ac-D-Phe-Pro-Arg (Data of Fig.22 Part I)

pH	k_4 (sec^{-1})
6.03	6.515×10^{-4}
6.41	5.164×10^{-4}
7.01	5.076×10^{-4}
7.40	8.416×10^{-4}
7.80	7.392×10^{-4}
8.60	1.178×10^{-3}
9.02	1.871×10^{-3}
10.04	7.367×10^{-4}

Table XVII pH profile for the initial inhibition of bovine thrombin by Ac-D-Phe-Pro-Arg in D_2O (Data of Fig.23 Part I)

pH	K_i (M)
5.00	1.5304×10^{-4}
5.43	6.1966×10^{-5}
6.01	4.3430×10^{-5}
6.48	3.1834×10^{-5}
7.03	1.6027×10^{-5}
7.41	1.1489×10^{-5}
7.87	1.6135×10^{-5}
8.88	3.9726×10^{-5}
9.64	1.2151×10^{-4}
10.09	1.2808×10^{-3}

Table XVIII pH profile for the final inhibition of bovine thrombin by Ac-D-Phe-Pro-Arg in D_2O (Data of Fig.24 Part I)

pH	K_i (M)
5.00	1.5174×10^{-4}
5.43	5.3922×10^{-5}
6.01	2.8239×10^{-5}
6.48	1.4030×10^{-5}
7.03	5.6874×10^{-6}
7.41	1.5933×10^{-6}
7.87	1.2914×10^{-6}
8.88	7.6863×10^{-6}
9.64	1.4443×10^{-5}
10.09	4.5983×10^{-4}

Table XIX pH profile for the transition from initial inhibition to final inhibition of bovine thrombin by Ac-D-Phe-Pro-Arg in D_2O (Data of Fig.25 Part I)

pH	k_3 (sec^{-1})
6.01	2.0878×10^{-4}
6.48	1.0558×10^{-3}
7.03	2.7774×10^{-3}
7.41	8.8972×10^{-3}
7.87	9.7705×10^{-3}
8.88	7.0713×10^{-3}
9.64	4.3109×10^{-3}
10.09	3.4578×10^{-3}

Table XX pH profile for the transition from final inhibition to initial inhibition of bovine thrombin by Ac-D-Phe-Pro-Arg in D_2O (Data of Fig.26 Part I)

pH	k_4 (sec^{-1})
6.01	4.196×10^{-4}
6.48	7.148×10^{-4}
7.03	6.618×10^{-4}
7.41	1.273×10^{-3}
7.87	1.260×10^{-3}
8.88	2.423×10^{-3}
9.64	1.931×10^{-3}
10.09	1.620×10^{-3}

Table XXI Inhibition of bovine thrombin by Z-D-Phe-Pro-boroMPG at pH 7.4 (Data of Fig.27 Part I)

[substrate] (M)	v_i(uninhi.) (mOD min^{-1})	v_i(inhi.) (mOD min^{-1})
$6.72x10^{-5}$	1.75	1.60
$3.36x10^{-5}$	1.65	1.38
$1.68x10^{-5}$	1.51	1.20
$8.40x10^{-6}$	1.31	0.943
$4.20x10^{-6}$	0.976	0.609

Table XXII pH profile for inhibition of bovine thrombin by Z-D-Phe-Pro-boroMPG (Data of Fig.28 Part I)

pH	K_i (M)
5.03	$1.6255x10^{-6}$
5.45	$4.4777x10^{-7}$
6.05	$2.0268x10^{-7}$
6.44	$8.5833x10^{-8}$
7.01	$1.2808x10^{-8}$
7.42	$7.9186x10^{-9}$
7.91	$4.4864x10^{-9}$
8.54	$4.8977x10^{-9}$
9.07	$1.8404x10^{-8}$
9.46	$2.9539x10^{-8}$
10.06	$1.5393x10^{-6}$
10.55	$2.2604x10^{-5}$
10.75	$1.1680x10^{-4}$

Table XXIII Inhibition of bovine thrombin by N-(Z-D-Phe-Pro)-2-amino-5-methoxypentanoic acid at pH 7.1 (Data of Fig.29 Part I)

[substrate] (M)	v_i(uninhi.) (F sec^{-1})	v_i(inhi.) (F sec^{-1})
5.85×10^{-6}	4.20×10^{-2}	1.79×10^{-2}
5.20×10^{-6}	3.69×10^{-2}	1.63×10^{-2}
4.55×10^{-6}	3.20×10^{-2}	1.32×10^{-2}
3.90×10^{-6}	2.89×10^{-2}	1.15×10^{-2}
3.25×10^{-6}	2.60×10^{-2}	9.95×10^{-3}
2.60×10^{-6}	2.05×10^{-2}	8.35×10^{-3}

Table XXIV pH profile for inhibition of bovine thrombin by N-(Z-D-Phe-Pro)-2-amino-5-methoxypentanoic acid (Data of Fig.30 Part I)

pH	K_i (M)
4.98	5.3763×10^{-4}
5.36	3.7313×10^{-4}
6.00	4.4643×10^{-4}
6.40	3.7594×10^{-4}
7.09	4.5662×10^{-4}
7.55	3.1348×10^{-4}
7.94	2.0747×10^{-4}
8.82	1.9120×10^{-4}
9.17	2.1786×10^{-4}
9.63	3.7313×10^{-4}
10.22	1.9881×10^{-3}

Table XXV Inhibition of bovine thrombin by NAPAP at pH 7.8 (Data of Fig.32 Part I)

[substrate] (M)	v_i(uninhi.) (F sec^{-1})	v_i(inhi.) (F sec^{-1})
$6.50x10^{-7}$	$4.21x10^{-3}$	$1.67x10^{-3}$
$1.30x10^{-6}$	$6.99x10^{-3}$	$3.52x10^{-3}$
$1.95x10^{-6}$	$9.70x10^{-3}$	$4.37x10^{-3}$
$2.60x10^{-6}$	$1.29x10^{-2}$	$6.55x10^{-3}$
$3.25x10^{-6}$	$1.47x10^{-2}$	$7.70x10^{-3}$
$3.90x10^{-6}$	$1.64x10^{-2}$	$8.73x10^{-3}$
$4.55x10^{-6}$	$1.92x10^{-2}$	$7.27x10^{-3}$
$5.20x10^{-6}$	$1.89x10^{-2}$	$9.08x10^{-3}$

Table XXVI pH profile for inhibition of bovine thrombin by NAPAP (Data of Fig.33 Part I)

pH	K_i (M)
5.00	$4.0984x10^{-7}$
5.40	$1.7825x10^{-7}$
6.00	$4.6729x10^{-8}$
6.42	$1.8727x10^{-8}$
7.00	$5.9172x10^{-9}$
7.42	$5.3476x10^{-9}$
7.82	$2.9674x10^{-9}$
8.77	$3.8610x10^{-9}$
9.36	$4.5045x10^{-9}$
9.65	$1.9342x10^{-8}$
10.00	$6.9930x10^{-8}$

Table XXVII Spectrophotometric titration of NAPAP

(Data of Fig.34 Part I)

pH	AbpH-AbpH 6.16 (247nm)
6.16	0.0000
6.52	-2.0100
7.08	-8.0000
7.48	2.9000
7.85	-1.6600
8.46	0.0731
9.05	0.1204
9.27	0.1889
9.80	0.2977
10.63	0.4999
11.11	0.5146
12.03	0.4627
12.59	0.3381

Table XXVIII Inhibition of bovine thrombin by leupeptin at pH 7.8

(Data of Fig.35 Part I)

[substrate] (M)	v_i(uninhi.) (F sec^{-1})	v_i(inhi.) (F sec^{-1})
$1.95x10^{-6}$	$5.58x10^{-3}$	$2.67x10^{-3}$
$3.90x10^{-6}$	$8.09x10^{-3}$	$3.94x10^{-3}$
$5.85x10^{-6}$	$9.79x10^{-3}$	$4.68x10^{-3}$
$7.80x10^{-6}$	$9.89x10^{-3}$	$4.75x10^{-3}$
$9.75x10^{-6}$	$9.49x10^{-3}$	$5.29x10^{-3}$
$1.17x10^{-5}$	$9.54x10^{-3}$	$4.85x10^{-3}$

Table XXIX pH profile for inhibition of bovine thrombin by leupeptin (Data of Fig.36 Part I)

pH	K_i (M)
5.00	3.0841×10^{-4}
5.40	1.0427×10^{-4}
6.00	5.2876×10^{-5}
6.42	1.7106×10^{-5}
7.00	8.8612×10^{-6}
7.42	5.8831×10^{-6}
7.82	4.6460×10^{-6}
8.77	2.0860×10^{-6}
9.36	4.0647×10^{-6}
9.65	4.4492×10^{-6}
10.04	1.5252×10^{-5}
10.75	2.0243×10^{-4}

Table XXX Inhibition of bovine thrombin by phenylarsonic acid at pH 6.0 (Data of Fig.37 Part I)

[substrate] (M)	v_i(uninhi.) (F sec^{-1})	v_i(inhi.) (F sec^{-1})
1.30×10^{-6}	5.90×10^{-3}	2.98×10^{-3}
1.95×10^{-6}	8.98×10^{-3}	4.47×10^{-3}
2.60×10^{-6}	1.04×10^{-2}	5.44×10^{-3}
3.25×10^{-6}	1.30×10^{-2}	7.14×10^{-3}
3.90×10^{-6}	1.40×10^{-2}	8.76×10^{-3}
4.55×10^{-6}	1.68×10^{-2}	8.90×10^{-3}
5.20×10^{-6}	1.87×10^{-2}	9.92×10^{-3}

Table XXXI pH profile for inhibition of bovine thrombin by phenylarsonic acid (Data of Fig.38 Part I)

pH	K_i (M)
5.00	7.5188×10^{-3}
5.40	4.8077×10^{-3}
6.00	3.7879×10^{-3}
6.42	4.8544×10^{-3}
7.00	5.4645×10^{-3}
7.42	9.8039×10^{-3}
8.00	9.2593×10^{-3}
8.68	5.5866×10^{-2}

Table XXXII pH profile for inhibition of bovine thrombin by 2,7-bis-(4-amidinobenzylidene)-cycloheptan-1-one (Data of Fig.39 Part I)

pH	K_i (M)
5.03	2.1739×10^{-6}
5.43	1.4859×10^{-6}
6.08	2.2676×10^{-6}
6.45	1.7422×10^{-6}
7.08	5.6180×10^{-7}
7.43	3.9526×10^{-7}
7.87	1.2048×10^{-7}
8.56	2.4390×10^{-7}
9.06	1.4306×10^{-7}
9.49	3.1348×10^{-7}
10.11	7.1429×10^{-7}
10.70	4.9505×10^{-6}

APPENDIX B

Complexation between Pinanediol and Ac-D-Phe-Pro-boroArg

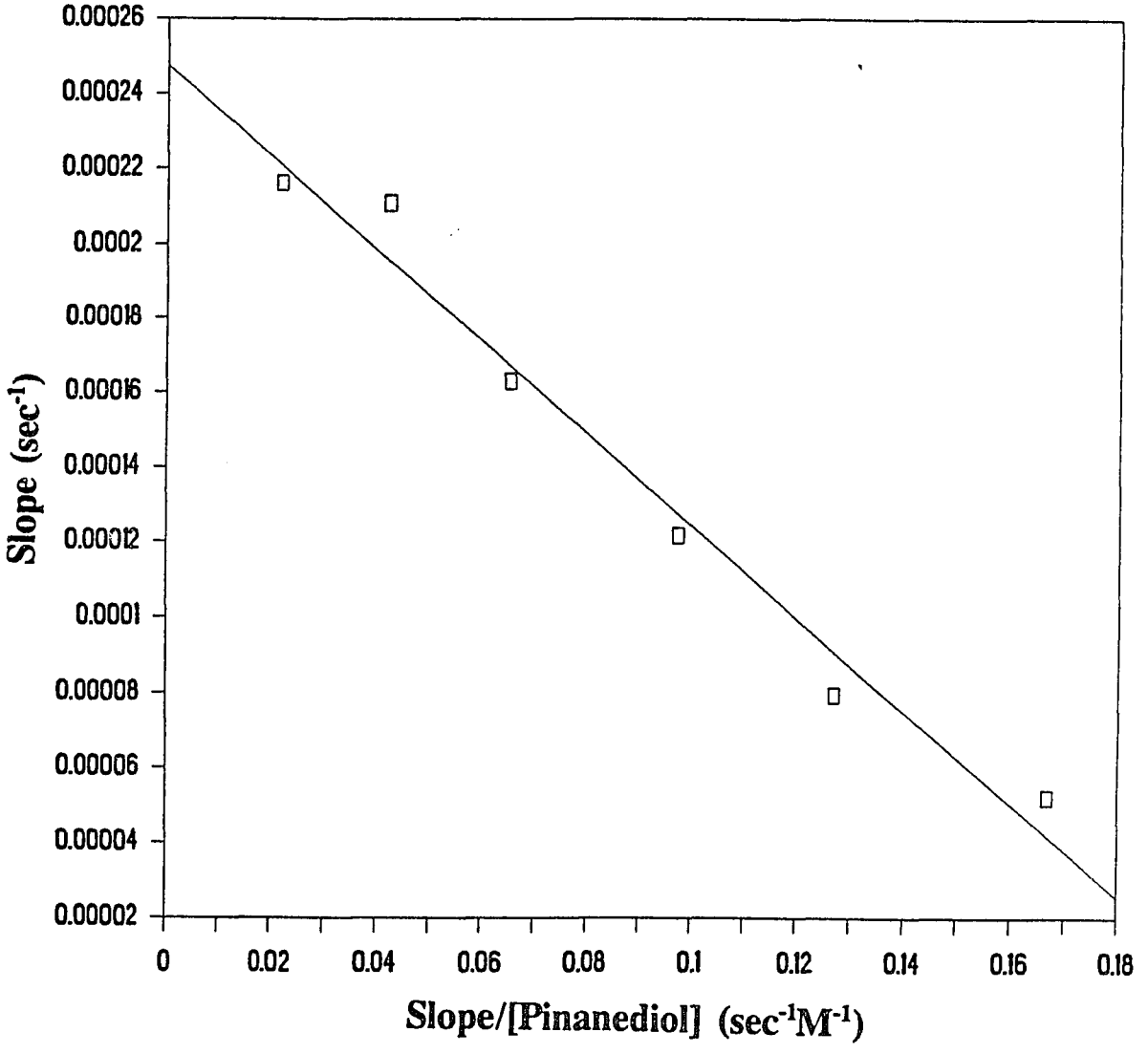

Fig.1 Complexation between pinanediol and Ac-D-Phe-Pro-boroArg at pH 7.50. The enzyme assay was run with 47 μM substrate, D-Phe-Pipecolyl-Arg-*p*NA, 13.3 nM inhibitor. K_{diss} = 1.23($\pm$0.0954) mM. Reaction conditions are given in the text.
(Data of Table I Appendix B)

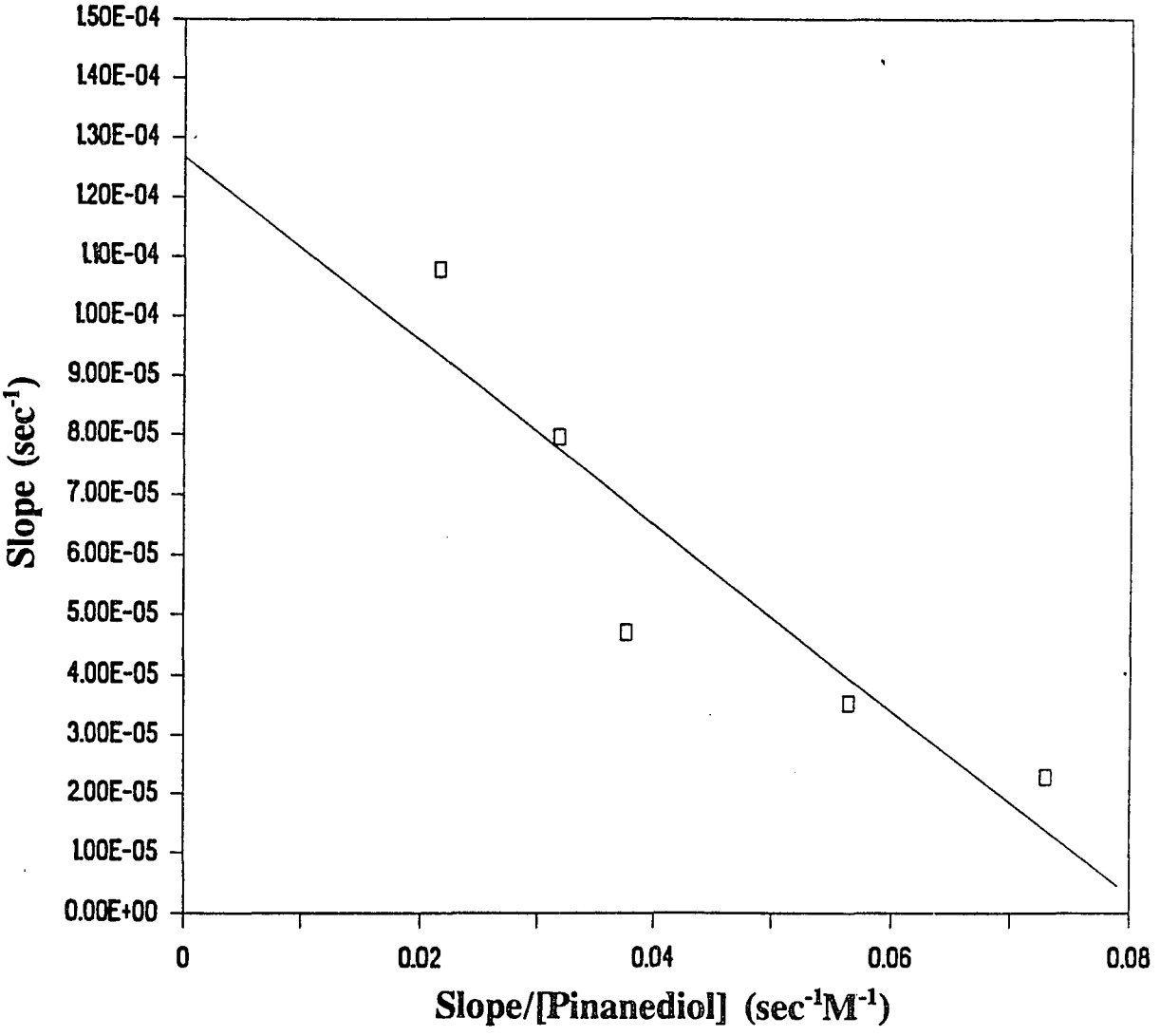

Fig.2 Complexation between pinanediol and Ac-D-Phe-Pro-boroArg at pH 9.18. The enzyme assay was run with 47 μM substrate, D-Phe-Pipecolyl-Arg-*p*NA, 13.3 nM inhibitor. K_{diss} = 1.55($\pm$0.39) mM. Reaction conditions are given in the text.
(Data of Table II Appendix B)

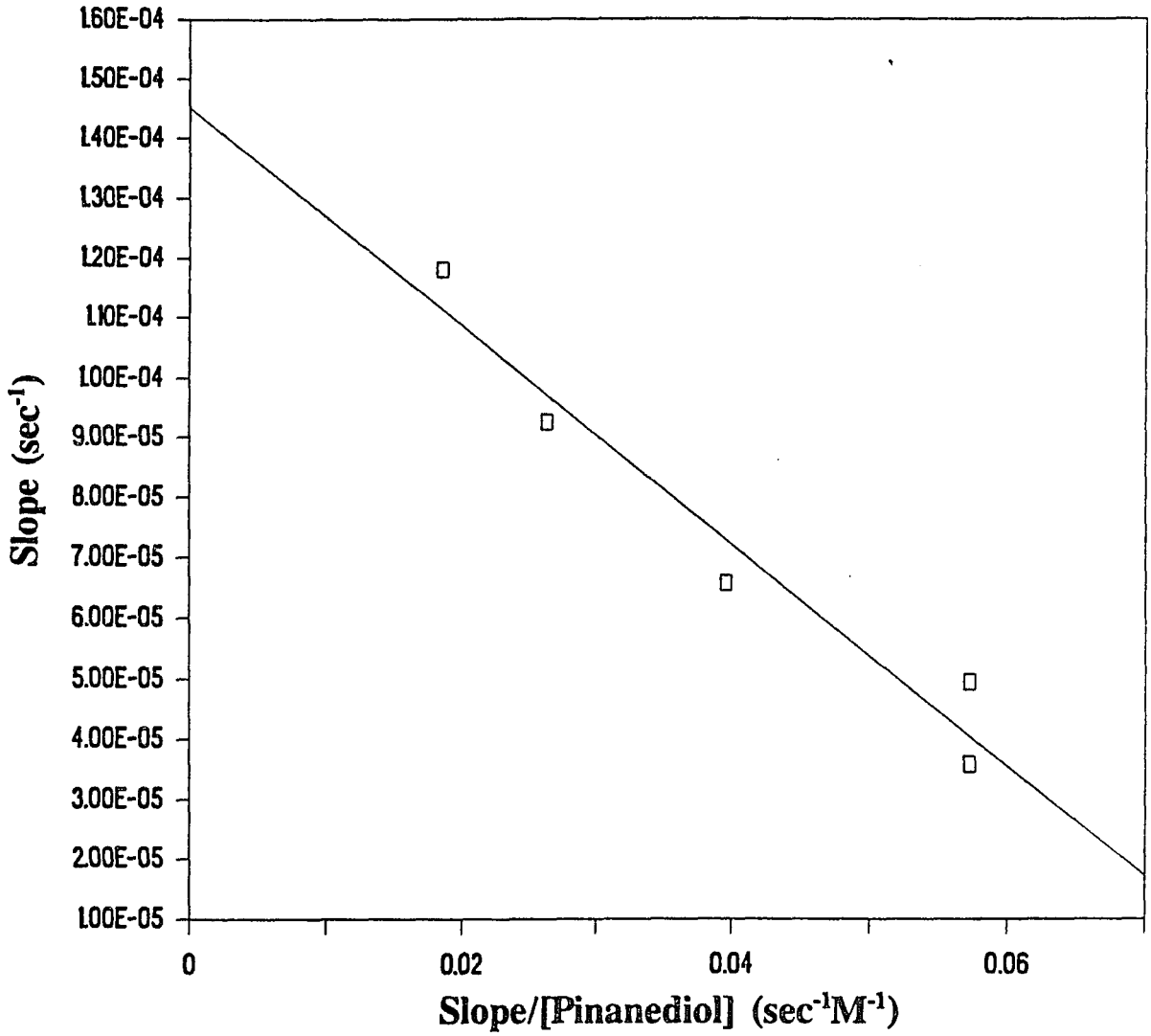

Fig.3 Complexation between pinanediol and Ac-D-Phe-Pro-boroArg at pH 9.64. The enzyme assay was run with 53.8 μM substrate, D-Phe-Pipecolyl-Arg-*p*NA, 13.3 nM inhibitor. K_{diss} = 1.83($\pm$0.24) mM. Reaction conditions are given in the text.
(Data of Table III Appendix B)

Table I Complexation between pinanediol and Ac-D-Phe-Pro-boroArg at pH 7.50 (Data of Fig.1 Appendix B)

[pinanediol] (M)	slope (sec^{-1})
$3.125x10^{-4}$	$5.211x10^{-5}$
$6.250x10^{-4}$	$7.943x10^{-5}$
$1.250x10^{-3}$	$1.218x10^{-4}$
$2.500x10^{-3}$	$1.630x10^{-4}$
$5.000x10^{-3}$	$2.109x10^{-4}$
$1.000x10^{-2}$	$2.162x10^{-4}$

Table II Complexation between pinanediol and Ac-D-Phe-Pro-boroArg at pH 9.18 (Data of Fig.2 Appendix B)

[pinanediol] (M)	slope (sec^{-1})
$3.125x10^{-4}$	$2.280x10^{-5}$
$6.250x10^{-4}$	$3.527x10^{-5}$
$1.250x10^{-3}$	$4.704x10^{-5}$
$2.500x10^{-3}$	$7.958x10^{-5}$
$5.000x10^{-3}$	$1.078x10^{-4}$

Table III Complexation between pinanediol and Ac-D-Phe-Pro-boroArg at pH 9.64 (Data of Fig.3 Appendix B)

[pinanediol] (M)	slope (sec^{-1})
$6.250x10^{-4}$	$3.582x10^{-5}$
$1.250x10^{-3}$	$4.943x10^{-5}$
$2.500x10^{-3}$	$6.579x10^{-5}$
$5.000x10^{-3}$	$9.258x10^{-5}$
$1.000x10^{-2}$	$1.180x10^{-4}$

APPENDIX C

Inhibition of Factor Xa, Kallikrein, Urokinase and Plasmin by Peptide Boronic Acids

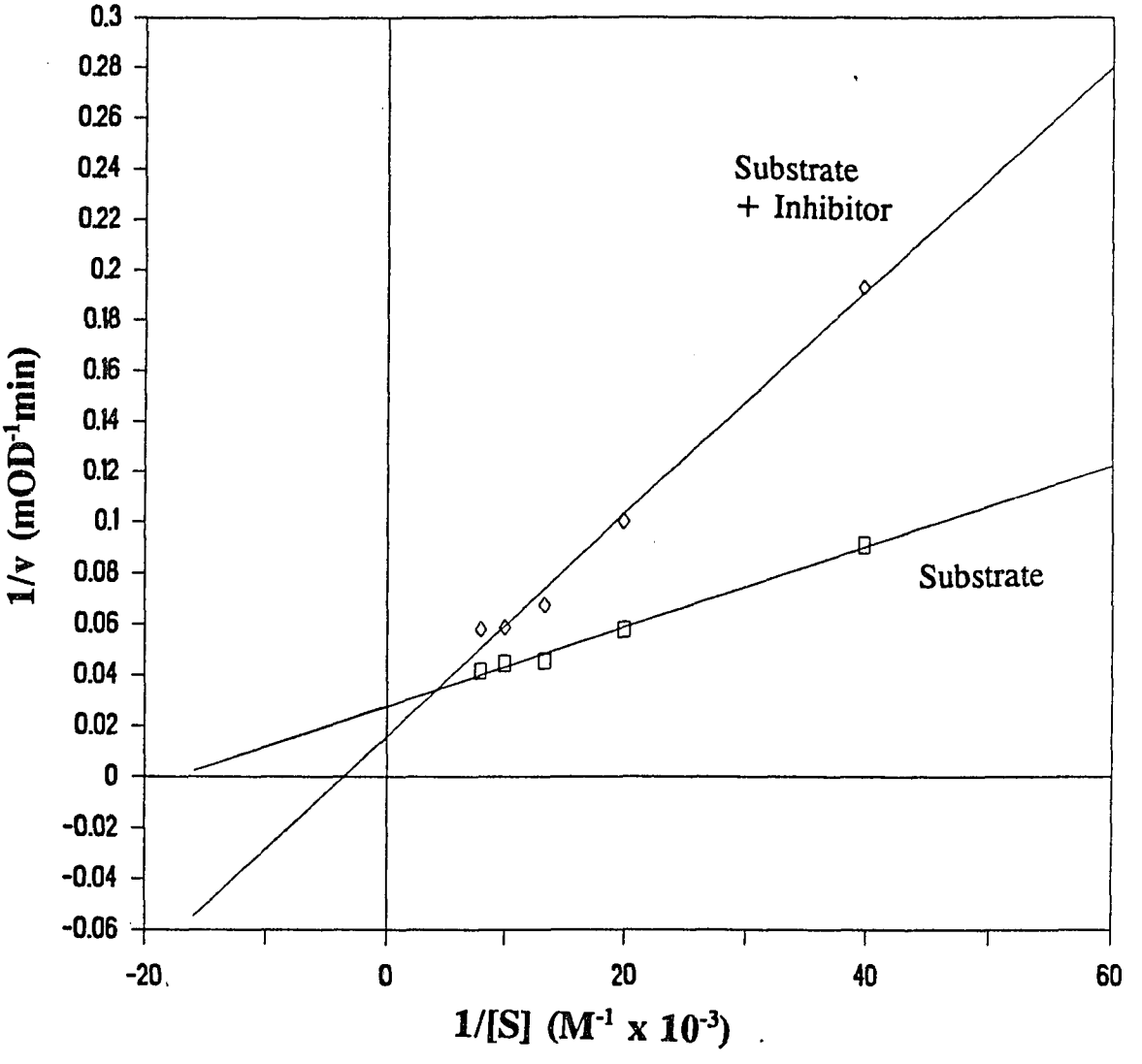

Fig.1 Inhibition of bovine factor Xa by Ac-D-Phe-Pro-boroArg at pH 7.4. [inhibitor] = 1.06×10^{-7} M, the substrate was Bz-Ile-Glu-Gly-Arg-*p*NA. K_i = 58.8($\pm$8.85) nM, K_m = 56.8$\pm$(8.32) μM.
Reaction conditions are given in the text.
(Data of Table I Appendix C)

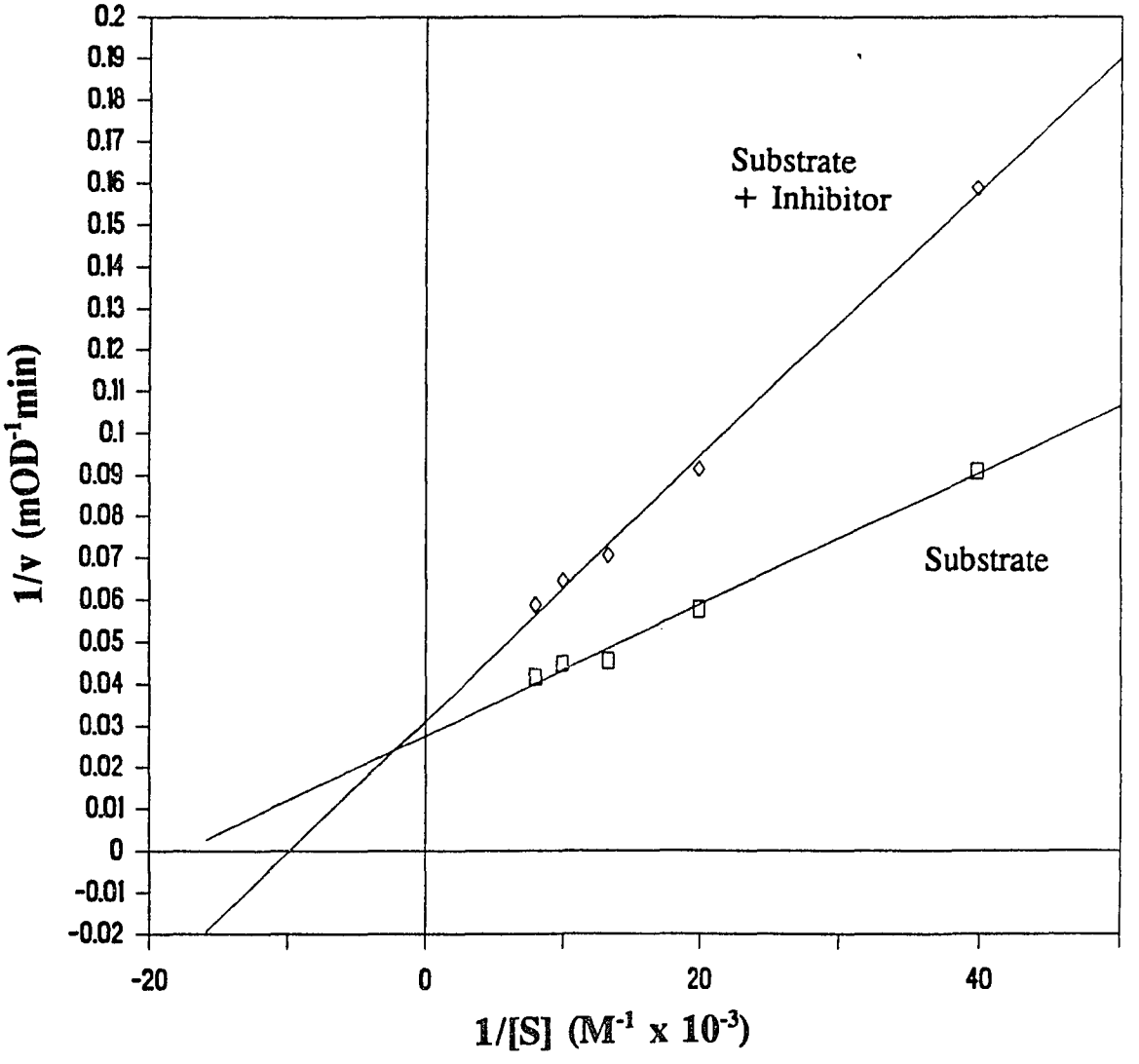

Fig.2 Inhibition of bovine factor Xa by Z-D-Phe-Pro-boroMPG at pH 7.4. [inhibitor] = 1.26×10^{-5} M, the substrate was Bz-Ile-Glu-Gly-Arg-*p*NA. K_i = 12.3($\pm$1.97) μM, K_m = 56.8($\pm$8.32) μM.
Reaction conditions are given in the text.
(Data of Table II Appendix C)

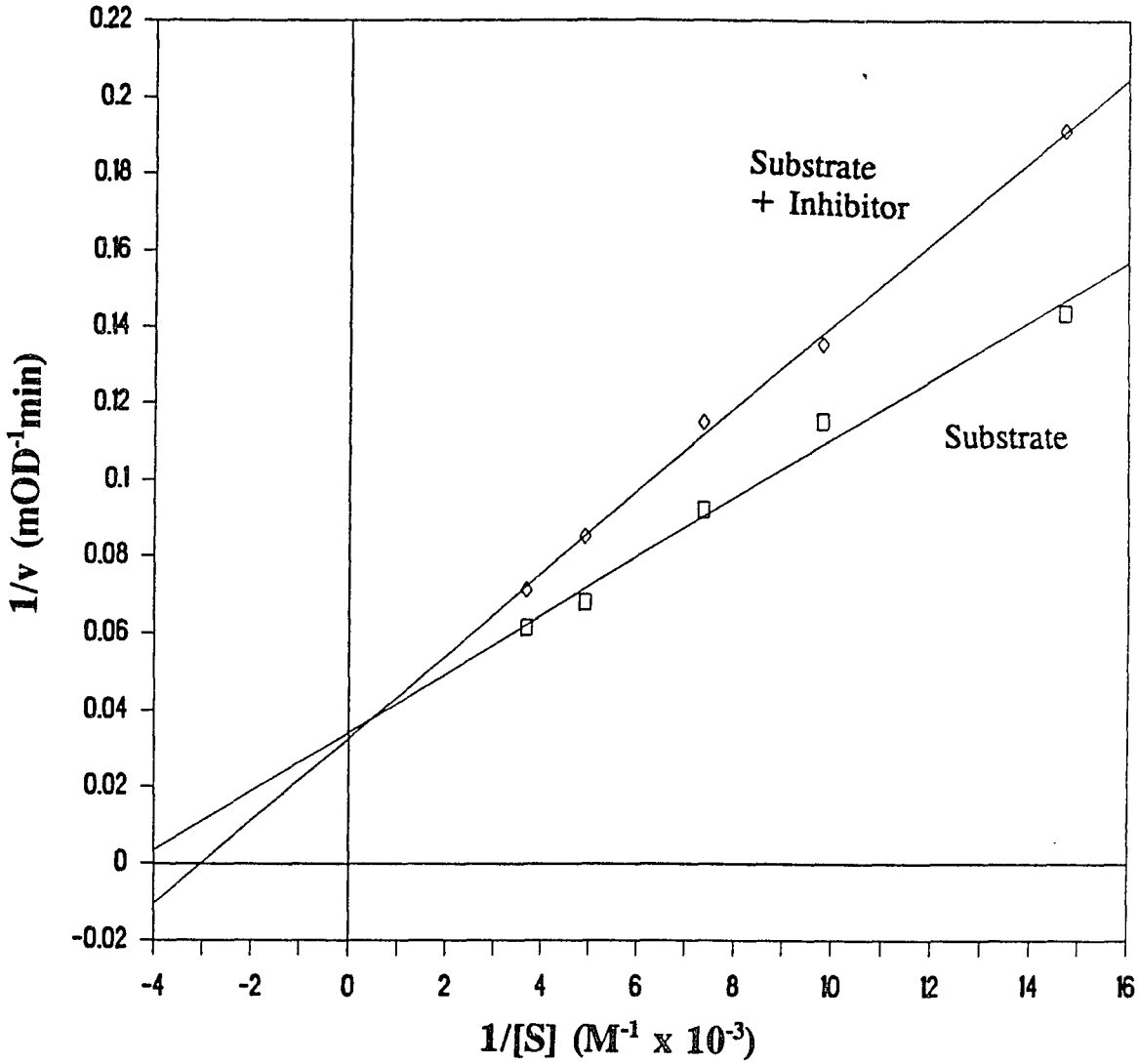

Fig.3 Inhibition of porcine pancreatic kallikrein by Z-D-Phe-Pro-boroMPG at pH 7.4. [inhibitor] = 3.15×10^{-5} M, the substrate was Bz-Pro-Phe-Arg-*p*NA. K_i = 77.3($\pm$20.0) μM, K_m = 2.25×10^{-4}($\pm 5.22 \times 10^{-5}$) M. Reaction conditions are given in the text.
(Data of Table III Appendix C)

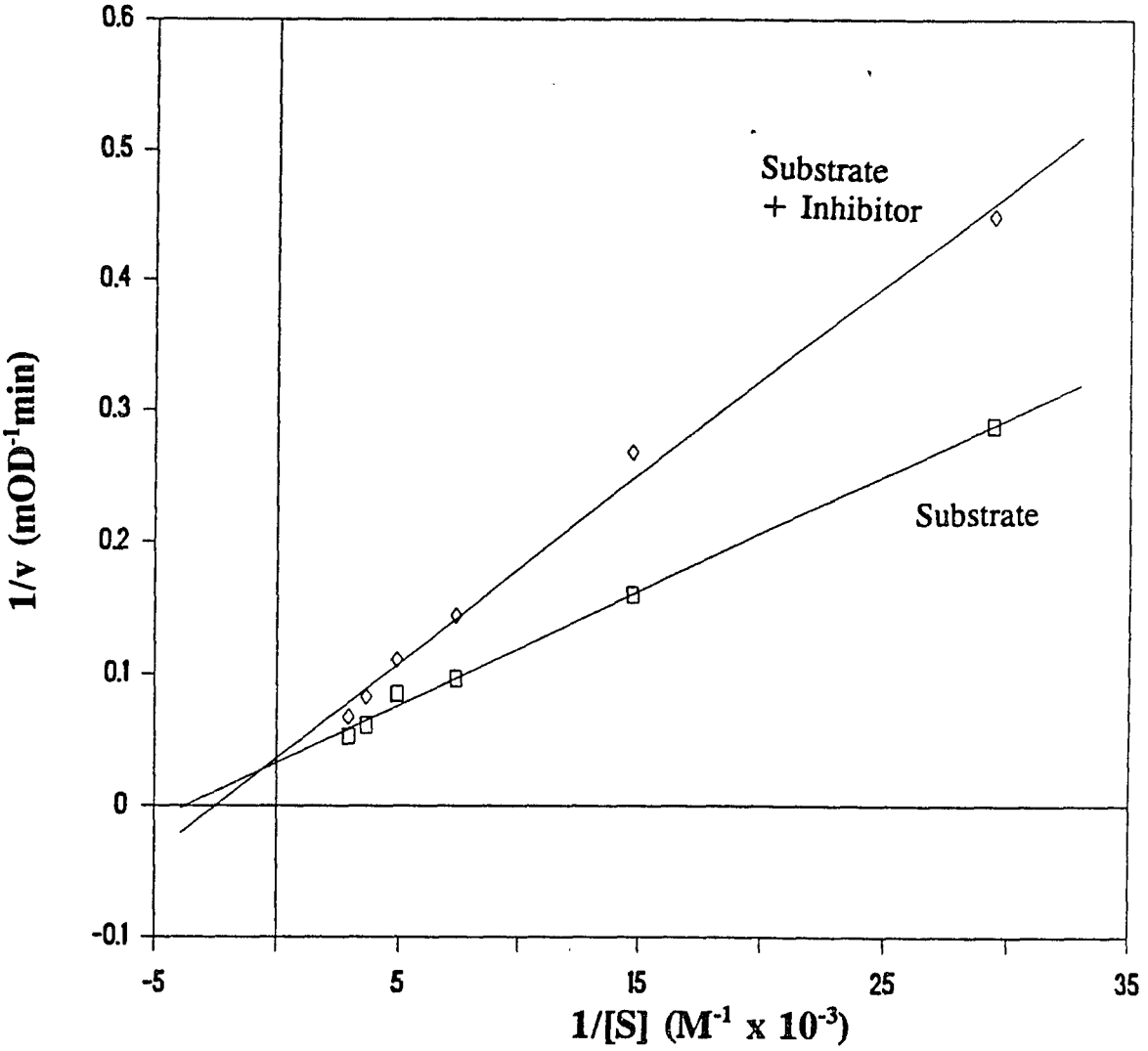

Fig.4 Inhibition of porcine pancreatic kallikrein by Ac-D-Phe-Pro-boroArg at pH 7.4. [inhibitor] = 5.31×10^{-7} M, the substrate was Bz-Pro-Phe-Arg-*p*NA. K_i = 0.811($\pm$0.125) μM, K_m = 2.65×10^{-4}($\pm 6.81 \times 10^{-5}$) M. Reaction conditions are given in the text.
(Data of Table IV Appendix C)

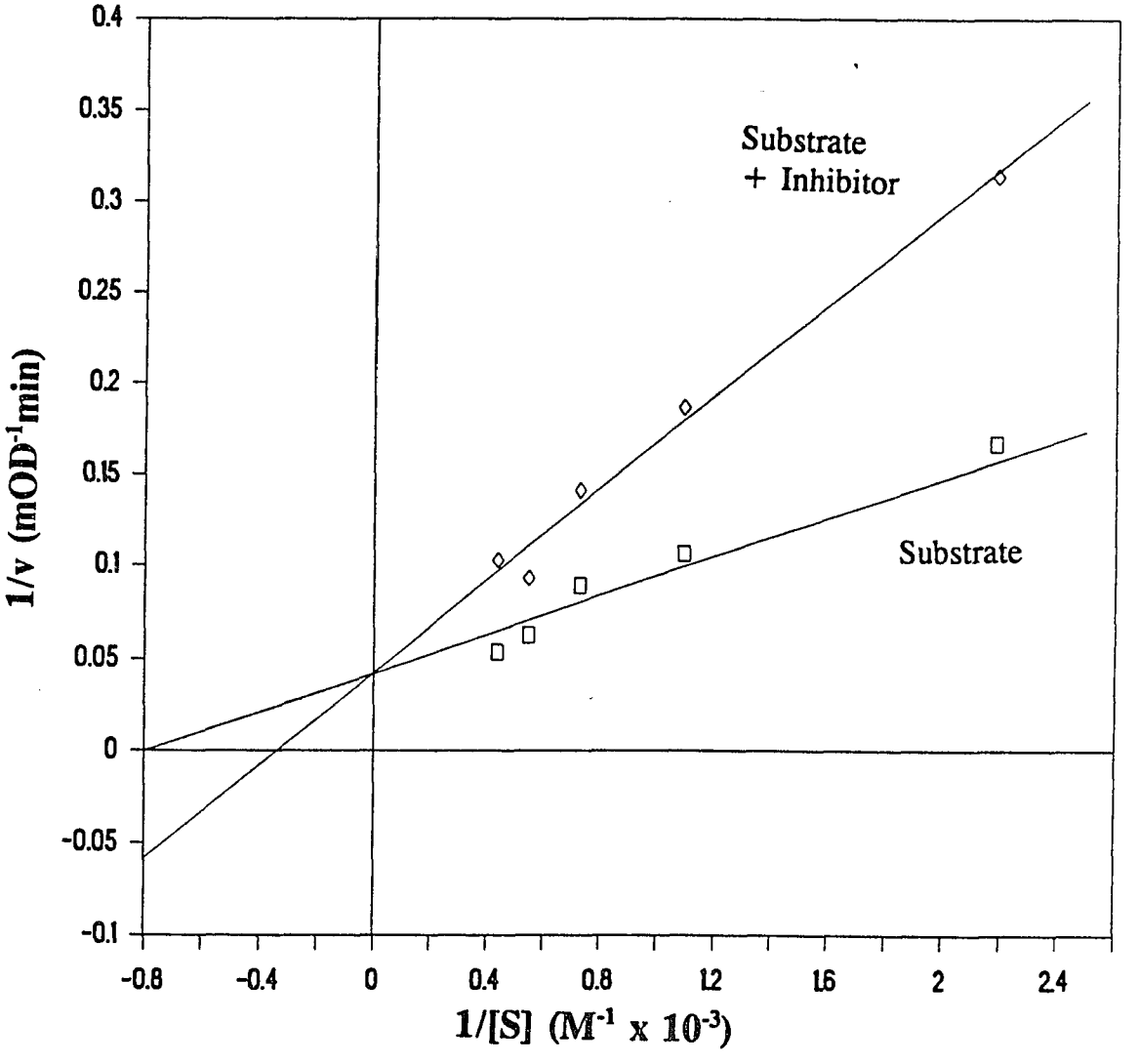

Fig.5 Inhibition of human kidney urokinase by Z-D-Phe-Pro-boroMPG at pH 7.4. [inhibitor] = 3.78×10^{-5} M, the substrate was Bz-Ile-Glu-Gly-Arg-*p*NA. K_i = 27.5(±5.30) μM, K_m = 1.26(±0.526) mM.
Reaction conditions are given in the text.
(Data of Table V Appendix C)

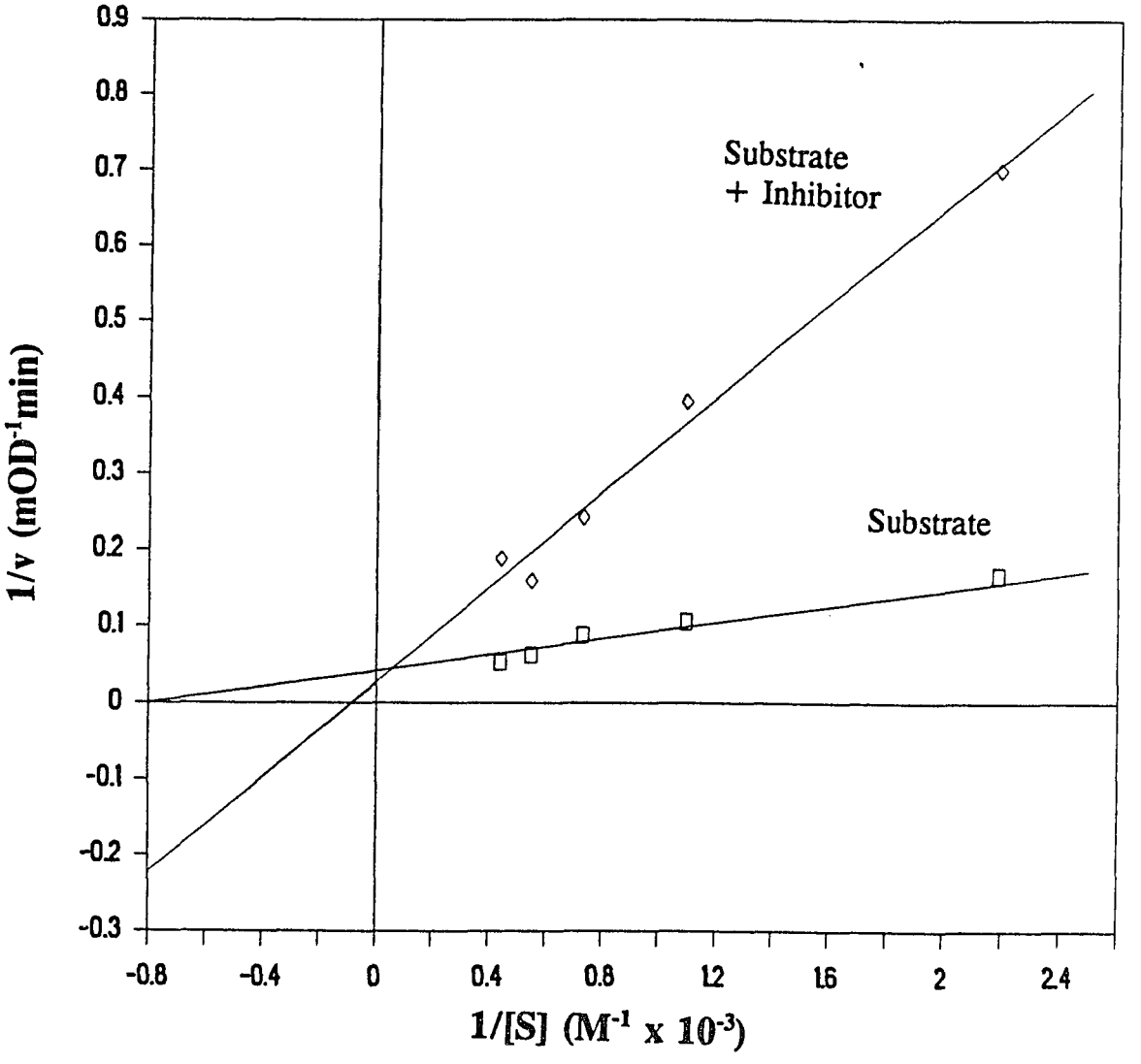

Fig.6 Inhibition of human kidney urokinase by Ac-D-Phe-Pro-boroArg at pH 7.4. [inhibitor] = 5.32×10^{-8} M, the substrate was Bz-Ile-Glu-Gly-Arg-*p*NA. K_i = 10.8(±1.56) nM, K_m = 1.26(±0.526) mM.
Reaction conditions are given in the text.
(Data of Table VI Appendix C)

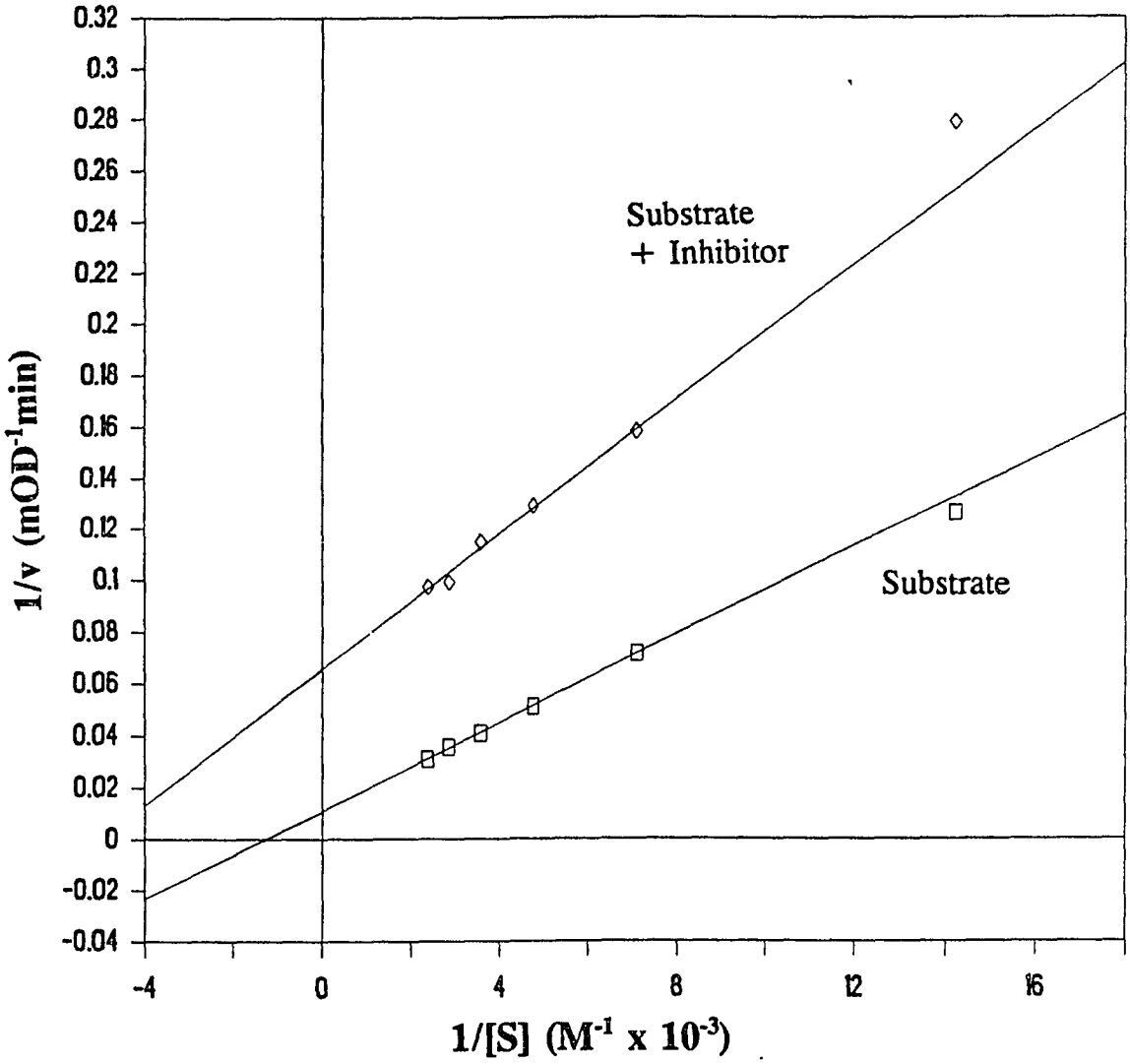

Fig.7 Inhibition of porcine serum plasmin by Z-D-Phe-Pro-boroMPG at pH 7.4. [inhibitor] = 1.26×10^{-5} M, the substrate was D-Val-Leu-Lys-*p*NA. K_i = 2.49($\pm$0.224) μM (1/v intercept), K_i = 23.7($\pm$3.90) μM (slope), K_m = 7.94×10^{-4}($\pm 4.19 \times 10^{-5}$) M. Reaction conditions are given in the text. (Data of Table VII Appendix C)

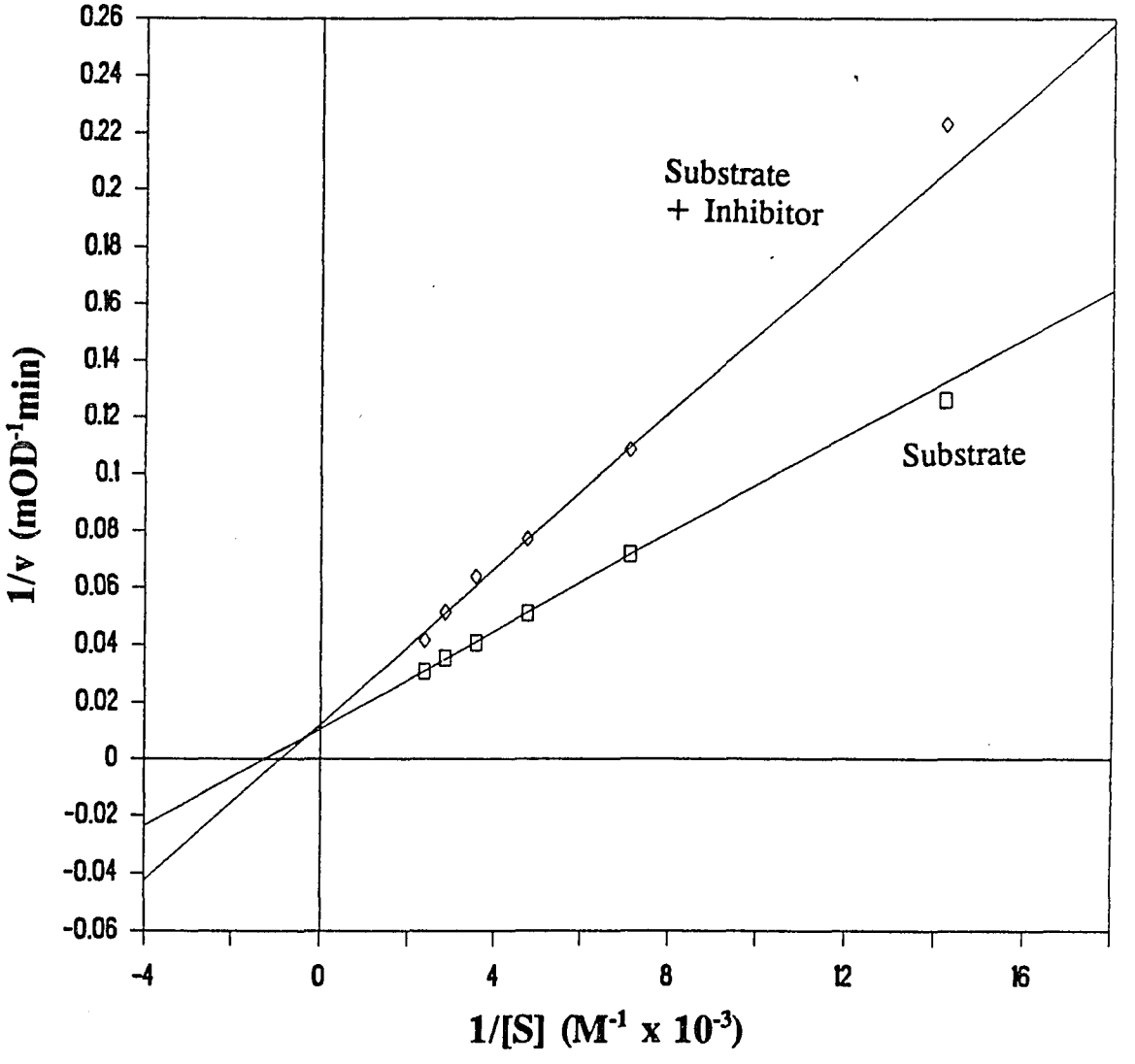

Fig.8 Inhibition of porcine serum plasmin by Ac-D-Phe-Pro-boroArg at pH 7.4. [inhibitor] = 1.33×10^{-8} M, the substrate was D-Val-Leu-Lys-*p*NA. K_i = 22.5($\pm$3.16) nM, K_m = 7.94×10^{-4}($\pm 4.19 \times 10^{-5}$) M.
Reaction conditions are given in the text.
(Data of Table VIII Appendix C)

Table I Inhibition of bovine factor Xa by Ac-D-Phe-Pro-boroArg at pH 7.4 (Data of Fig.1 Appendix C)

[substrate] (M)	v_i(uninhi.) (mOD min^{-1})	v_i(inhi.) (mOD min^{-1})
$2.52x10^{-5}$	11.0	5.18
$5.03x10^{-5}$	17.3	9.98
$7.55x10^{-5}$	21.9	14.8
$1.01x10^{-4}$	22.3	17.0
$1.26x10^{-4}$	23.9	17.2

Table II Inhibition of bovine factor Xa by Z-D-Phe-Pro-boroMPG at pH 7.4 (Data of Fig.2 Appendix C)

[substrate] (M)	v_i(uninhi.) (mOD min^{-1})	v_i(inhi.) (mOD min^{-1})
$2.52x10^{-5}$	11.0	6.29
$5.03x10^{-5}$	17.3	10.9
$7.55x10^{-5}$	21.9	14.1
$1.01x10^{-4}$	22.3	15.5
$1.26x10^{-4}$	23.9	17.0

Table III Inhibition of porcine pancreatic kallikrein by Z-D-Phe-Pro-boroMPG at pH 7.4 (Data of Fig.3 Appendix C)

[substrate] (M)	v_i(uninhi.) (mOD min^{-1})	v_i(inhi.) (mOD min^{-1})
$6.80x10^{-5}$	6.97	5.23
$1.02x10^{-4}$	8.68	7.39
$1.36x10^{-4}$	10.8	8.70
$2.04x10^{-4}$	14.7	11.7
$2.72x10^{-4}$	16.2	14.0

Table IV Inhibition of porcine pancreatic kallikrein by Ac-D-Phe-Pro-boroArg at pH 7.4 (Data of Fig.4 Appendix C)

[substrate] (M)	v_i(uninhi.) (mOD min^{-1})	v_i(inhi.) (mOD min^{-1})
$3.40x10^{-5}$	3.47	2.22
$6.80x10^{-5}$	6.24	3.73
$1.36x10^{-4}$	10.4	6.92
$2.04x10^{-4}$	11.7	9.00
$2.72x10^{-4}$	16.3	12.1
$3.40x10^{-4}$	18.9	14.8

Table V Inhibition of human kidney urokinase by Z-D-Phe-Pro-boroMPG at pH 7.4

(Data of Fig.5 Appendix C)

[substrate] (M)	v_i(uninhi.) (mOD min^{-1})	v_i(inhi.) (mOD min^{-1})
$4.57x10^{-4}$	5.99	3.19
$9.14x10^{-4}$	9.39	5.36
$1.37x10^{-3}$	11.2	7.08
$1.83x10^{-3}$	16.0	10.8
$2.29x10^{-3}$	18.7	9.71

Table VI Inhibition of human kidney urokinase by Ac-D-Phe-Pro-boroArg at pH 7.4

(Data of Fig.6 Appendix C)

[substrate] (M)	v_i(uninhi.) (mOD min^{-1})	v_i(inhi.) (mOD min^{-1})
$4.57x10^{-4}$	5.99	1.43
$9.14x10^{-4}$	9.39	2.53
$1.37x10^{-3}$	11.2	4.12
$1.83x10^{-3}$	16.0	6.26
$2.29x10^{-3}$	18.7	5.30

Table VII Inhibition of porcine serum plasmin by Z-D-Phe-Pro-boroMPG at pH 7.4

(Data of Fig.7 Appendix C)

[substrate] (M)	v_i(uninhi.) (mOD min^{-1})	v_i(inhi.) (mOD min^{-1})
$7.02x10^{-5}$	7.92	3.58
$1.40x10^{-4}$	13.9	6.32
$2.11x10^{-4}$	19.5	7.74
$2.81x10^{-4}$	24.5	8.71
$3.51x10^{-4}$	28.1	10.1
$4.21x10^{-4}$	32.3	10.3

Table VIII Inhibition of porcine serum plasmin by Ac-D-Phe-Pro-boroArg at pH 7.4

(Data of Fig.8 Appendix C)

[substrate] (M)	v_i(uninhi.) (mOD min^{-1})	v_i(inhi.) (mOD min^{-1})
$7.02x10^{-5}$	7.92	4.48
$1.40x10^{-4}$	13.9	9.22
$2.11x10^{-4}$	19.5	13.0
$2.81x10^{-4}$	24.5	15.7
$3.51x10^{-4}$	28.1	19.4
$4.21x10^{-4}$	32.3	23.9

APPENDIX D

Tables of Data for Part II Fig.1 - Fig.42

(Error analysis results are shown on the corresponding figures)

Table I Effect of hydroxylamine concentration on the rate of spontaneous salicylaldoxime formation at pH 6.0, 25.5°C (Data of Fig.1 Part II)

$[NH_2\text{-}OH]$ (M)	pseudo-k_1 (sec^{-1})
3.200×10^{-4}	2.156×10^{-4}
8.000×10^{-4}	4.082×10^{-4}
1.280×10^{-3}	7.563×10^{-4}
1.600×10^{-3}	9.765×10^{-4}
2.400×10^{-3}	1.438×10^{-3}
3.200×10^{-3}	1.985×10^{-3}
4.800×10^{-3}	2.985×10^{-3}
6.400×10^{-3}	3.599×10^{-3}
8.000×10^{-3}	4.662×10^{-3}
9.600×10^{-3}	5.739×10^{-3}
1.120×10^{-2}	6.559×10^{-3}

Table II Effect of salicylaldehyde concentration on the rate of spontaneous salicylaldoxime formation at pH 6.0, 25.5°C (Data of Fig.2 Part II)

[salicylaldehyde] (M)	initial rate (M/sec)
4.900×10^{-6}	4.486×10^{-8}
9.919×10^{-6}	9.080×10^{-8}
1.948×10^{-5}	1.784×10^{-7}
3.761×10^{-5}	3.443×10^{-7}
7.309×10^{-5}	6.691×10^{-7}
1.007×10^{-4}	9.220×10^{-7}
1.298×10^{-4}	1.188×10^{-6}
1.405×10^{-4}	1.286×10^{-6}

Table III Effect of 3,5-bis(trifluoromethyl)-benzeneboronic acid concentration on salicylaldoxime formation at pH 6.0, 25.5°C (Data of Fig.3 Part II)

[Boronic acid] (M)	pseudo-k_1 (sec^{-1})
$1.151x10^{-3}$	$3.869x10^{-3}$
$1.727x10^{-3}$	$5.389x10^{-3}$
$2.303x10^{-3}$	$7.391x10^{-3}$
$2.879x10^{-3}$	$9.155x10^{-3}$
$3.455x10^{-3}$	$1.021x10^{-2}$
$4.030x10^{-3}$	$1.263x10^{-2}$
$4.606x10^{-3}$	$1.411x10^{-2}$
$5.182x10^{-3}$	$1.497x10^{-2}$
$5.757x10^{-3}$	$1.554x10^{-2}$

Table IV Effect of hydroxylamine concentration on the rate of 3,5-bis(trifluoro-methyl)benzeneboronic acid catalyzed salicylaldoxime formation at pH 6.0, 25.5°C (Data of Fig.4 Part II)

[NH_2-OH] (M)	pseudo-k_1 (sec^{-1})
$1.600x10^{-4}$	$1.156x10^{-3}$
$3.200x10^{-4}$	$2.282x10^{-3}$
$8.000x10^{-4}$	$4.821x10^{-3}$
$1.280x10^{-3}$	$6.686x10^{-3}$
$1.600x10^{-3}$	$8.673x10^{-3}$
$2.400x10^{-3}$	$1.416x10^{-2}$
$3.200x10^{-3}$	$1.659x10^{-2}$
$4.800x10^{-3}$	$2.302x10^{-2}$
$6.400x10^{-3}$	$3.355x10^{-2}$

Table V Effect of salicylaldehyde concentration on the rate of 3,5-bis(trifluoro-methyl)benzeneboronic acid catalyzed salicylaldoxime formation at pH 6.0, 25.5°C (Data of Fig.5 Part II)

[salicylaldehyde] (M)	initial rate (M/sec)
5.651×10^{-6}	1.168×10^{-7}
1.630×10^{-5}	3.370×10^{-7}
2.171×10^{-5}	4.489×10^{-7}
4.633×10^{-5}	9.581×10^{-7}
5.436×10^{-5}	1.124×10^{-6}
7.417×10^{-5}	1.534×10^{-6}
9.612×10^{-5}	1.988×10^{-6}
1.251×10^{-4}	2.586×10^{-6}
1.367×10^{-4}	2.826×10^{-6}

Table VI Effect of diphenylborinic acid concentration on salicylaldoxime formation at pH 6.5, 25.5°C (Data of Fig.6, Fig.9 Part II)

[Borinic acid] (M)	pseudo-k_1 (sec^{-1})
7.092×10^{-4}	2.808×10^{-2}
1.064×10^{-3}	3.731×10^{-2}
1.418×10^{-3}	4.565×10^{-2}
1.773×10^{-3}	5.361×10^{-2}
2.128×10^{-3}	5.973×10^{-2}
2.482×10^{-3}	6.496×10^{-2}
2.837×10^{-3}	6.879×10^{-2}
3.191×10^{-3}	6.892×10^{-2}
3.546×10^{-3}	6.764×10^{-2}

Table VII Effect of hydroxylamine concentration on the rate of diphenylborinic acid catalyzed salicylaldoxime formation at pH 6.5 25.5°C (Data of Fig.7, Fig.10 Part II)

$[NH_2\text{-}OH]$ (M)	pseudo-k_1 (sec^{-1})
$6.844x10^{-4}$	$1.558x10^{-2}$
$1.027x10^{-3}$	$2.244x10^{-2}$
$1.369x10^{-3}$	$2.919x10^{-2}$
$1.711x10^{-3}$	$3.731x10^{-2}$
$2.053x10^{-3}$	$3.909x10^{-2}$
$2.395x10^{-3}$	$4.326x10^{-2}$
$2.738x10^{-3}$	$4.464x10^{-2}$
$3.080x10^{-3}$	$5.024x10^{-2}$
$3.422x10^{-3}$	$5.304x10^{-2}$
$4.278x10^{-3}$	$5.935x10^{-2}$
$5.133x10^{-3}$	$6.051x10^{-2}$
$5.989x10^{-3}$	$6.192x10^{-2}$
$6.844x10^{-3}$	$6.685x10^{-2}$

Table VIII Effect of salicylaldehyde concentration on the rate of diphenylborinic acid catalyzed salicylaldoxime formation at pH 6.5 25.5°C (Data of Fig.8 Part II)

[salicylaldehyde] (M)	initial rate (M/sec)
$4.565x10^{-6}$	$9.042x10^{-8}$
$1.024x10^{-5}$	$2.028x10^{-7}$
$2.266x10^{-5}$	$4.487x10^{-7}$
$5.239x10^{-5}$	$1.038x10^{-6}$
$6.251x10^{-5}$	$1.238x10^{-6}$
$7.343x10^{-5}$	$1.454x10^{-6}$
$8.691x10^{-5}$	$1.721x10^{-6}$
$1.111x10^{-4}$	$2.201x10^{-6}$
$1.433x10^{-4}$	$2.838x10^{-6}$

Table IX pH profile of spontaneous salicyl-aldoxime formation at 25.5°C in buffers (Data of Fig.11 Part II)

pH	k_2 ($M^{-1}sec^{-1}$)
3.75	0.7774
4.52	0.7897
4.53	0.8381
5.06	0.7856
5.41	0.7305
5.78	0.5691
6.12	0.4655
6.52	0.3197
6.60	0.2951
6.65	0.2602
6.80	0.2367
7.41	0.1117
7.66	0.08181
9.01	0.04785
9.29	0.03545
9.66	0.0352
10.00	0.03792

Table X pH profile of 3,5-bis(trifluoromethyl)-benzeneboronic acid catalyzed salicylaldoxime formation in 0.1 M buffers at 25.5°C (Data of Fig.12 Part II)

pH	k_3 ($M^{-2}sec^{-1}$)
4.73	$5.256x10^2$
5.05	$1.164x10^3$
5.41	$2.660x10^3$
5.98	$4.552x10^3$
6.36	$5.621x10^3$
6.96	$4.459x10^3$
7.43	$2.215x10^3$
7.53	$2.038x10^3$
8.10	$4.239x10^2$
8.91	$4.689x10^1$

Table XI pH profile of boric acid catalyzed salicylaldoxime formation in 0.1 M buffers at 25.5°C

(Data of Fig.13 Part II)

pH	k_3 ($M^{-2}sec^{-1}$)
4.59	3.0703
5.10	6.9631
5.47	13.661
6.03	29.399
6.38	46.489
6.93	64.202
7.37	68.425
8.61	36.255
8.94	24.458
9.10	20.860

Table XII pH profile of diphenylborinic acid catalyzed salicylaldoxime formation in 0.1 M buffers at 25.5°C

(Data of Fig.14 Part II)

pH	k_3 ($M^{-2}sec^{-1}$)
4.61	8.0531×10^3
5.10	1.4441×10^4
5.48	2.2143×10^4
6.13	2.9941×10^4
6.50	2.7289×10^4
7.07	1.9636×10^4
7.35	1.4911×10^4
7.47	9.1607×10^3
8.34	4.3470×10^2
8.81	6.8093×10^1
9.04	2.1040×10^1

Table XIII Formation of salicylaldoxime catalyzed by substituted benzeneboronic acids at 25.5°C, 0.1 M buffer

(Data of Fig.15 Part II)

boron acid	sigma*	k_3 (Lim.) ($M^{-2}sec^{-1}$)	pH (optimum)
benzeneboronic acid	0.00	$5.546x10^{2}$	6.65
2,4-dichloro-benzeneboronic acid	$4.27x10^{-1}$	$3.083x10^{3}$	6.40
3,5-dichloro-benzeneboronic acid	$7.46x10^{-1}$	$7.681x10^{3}$	6.45
3-chloro-4-fluoro-benzeneboronic acid	$4.35x10^{-1}$	$3.225x10^{3}$	6.45
4-bromobenzene-boronic acid	$2.32x10^{-1}$	$1.602x10^{3}$	6.50
4-chlorobenzene-boronic acid	$2.27x10^{-1}$	$1.463x10^{3}$	6.60
4-fluorobenzene-boronic acid	$6.20x10^{-2}$	$7.027x10^{2}$	6.60
3,5-bis(trifluoro-methyl)benzene-boronic acid	$8.60x10^{-1}$	$1.149x10^{4}$	6.40
4-methoxybenzene-boronic acid	$-2.68x10^{-1}$	$2.422x10^{2}$	6.65

* sigma values are taken from ref.48

Table XIV pH profile of boric acid catalyzed formation of salicyaldehyde O-methyloxime at 25.5°C in 0.1 M buffers (Data of Fig.16 Part II)

pH	k_3 ($M^{-2}sec^{-1}$)
5.93	11.855
6.62	11.136
7.02	11.245
8.15	8.9934
8.55	5.1113
8.71	3.9584

Table XV pH profile of 4-bromobenzeneboronic acid catalyzed formation of salicyaldehyde O-methyloxime at 25.5°C in 0.1 M buffers (Data of Fig.17 Part II)

pH	k_3 ($M^{-2}sec^{-1}$)
5.03	140.96
5.32	166.95
5.50	233.86
6.09	211.95
6.74	211.73
7.18	192.77
7.20	178.94
8.01	75.386
8.35	70.705
8.51	56.481

Table XVI pH profile of diphenylborinic acid catalyzed formation of salicyaldehyde O-methyloxime at 25.5°C in 0.1 M buffers (Data of Fig.18 Part II)

pH	k_3 ($M^{-2}sec^{-1}$)
4.68	27820
5.04	34864
5.40	30634
5.93	27260
6.34	23426
6.96	8504.5
7.47	2889.4
7.58	2230.4
8.21	1118.9
8.92	56.748
9.34	6.4808

Table XVII Spectrophotometric titration for salicylaldoxime at 25.5°C (Data of Fig.20 Part II)

pH	OD_{350nm}/OD_{304nm}
4.67	0.0168
5.15	0.00975
5.54	0.00908
6.10	0.01906
6.58	0.02641
7.24	0.05403
7.66	0.07318
7.99	0.1375
9.06	0.9414
9.30	1.365
9.56	1.518
9.94	1.878
10.00	1.703
11.86	2.100
12.63	2.199

Table XVIII Spectrophotometric titration for the complex of salicylaldoxime and diphenylborinic acid at 25.5°C
(Data of Fig.24 Part II)

pH	OD_{310nm}/OD_{340nm}
4.67	0.4476
5.15	0.4535
5.54	0.4676
6.25	0.5041
6.58	0.5321
7.24	0.5192
7.66	0.5202
7.99	0.5228
9.06	0.4862

Table XIX Effect of diphenylborinic acid concentration on the complexation between salicylaldoxime and diphenylborinic acid at pH 6.58, 25.5°C
(Data of Fig.25, Fig.26 Part II)

[borinic acid] (M)	absorbance increase (340 nm)
$3.432x10^{-5}$	0.1388
$6.864x10^{-5}$	0.2387
$1.030x10^{-4}$	0.3161
$1.373x10^{-4}$	0.3721
$1.716x10^{-4}$	0.4136
$2.574x10^{-4}$	0.4691
$3.432x10^{-4}$	0.4976
$5.148x10^{-4}$	0.5239
$6.864x10^{-4}$	0.5355
$8.580x10^{-4}$	0.5394
$1.030x10^{-3}$	0.5411
$1.201x10^{-3}$	0.5470
$1.373x10^{-3}$	0.5506

Table XX pH profile of diphenylborinic acid complexation with salicylaldoxime at 25.5°C (Data of Fig.27 Part II)

pH	k_{diss} (M)
4.67	2.7430×10^{-4}
5.15	2.0810×10^{-4}
5.54	1.5650×10^{-4}
6.25	9.9340×10^{-5}
6.58	6.4560×10^{-5}
7.24	5.9020×10^{-5}
7.66	7.5940×10^{-5}
8.00	6.8540×10^{-5}
9.06	5.5350×10^{-4}

Table XXI pH profile of Benzeneboronic acid complexation with salicylaldoxime at 25.5°C (Data of Fig.30 Part II)

pH	k_{diss} (M)
6.60	5.1810×10^{-2}
7.12	2.5160×10^{-2}
7.65	6.4180×10^{-3}
7.82	4.8410×10^{-3}
8.96	1.4820×10^{-3}
9.30	2.3090×10^{-3}
9.56	3.0370×10^{-3}
9.94	1.8160×10^{-2}

Table XXII Complexation of salicylaldoxime with substituted benzeneboronic acids at 25.5°C, pH 6.6.

(Data of Fig.31 Part II)

boron acid	sigma*	K_{diss} (M)
benzeneboronic acid	0.00	5.510×10^{-2}
2,4-dichloro-benzeneboronic acid	4.27×10^{-1}	4.560×10^{-3}
3,5-dichloro-benzeneboronic acid	7.46×10^{-1}	4.789×10^{-3}
3-chloro-4-fluoro-benzeneboronic acid	4.35×10^{-1}	7.802×10^{-3}
4-bromobenzene-boronic acid	2.32×10^{-1}	1.564×10^{-2}
4-chlorobenzene-boronic acid	2.27×10^{-1}	1.238×10^{-2}
4-fluorobenzene-boronic acid	6.20×10^{-2}	1.832×10^{-2}
3,5-bis(trifluoro-methyl)benzene-boronic acid	8.60×10^{-1}	2.843×10^{-3}

* sigma values are taken from ref.48

Table XXIII

Brønsted plots for the formation of salicylaldoxime and salicylaldehyde O-methyloxime catalyzed by boron acids at 25.5°C (Data of Fig.34 Part II)

boron acid	pK*	k_3(Lim.) (M^{-2} sec^{-1}) (oxime)	k_3(Lim.) (M^{-2} sec^{-1}) (O-methyloxime)
boric acid	8.98	75.50	11.54
benzeneboronic acid	8.80	5.546×10^2	76.98
4-bromobenzene-boronic acid	8.06	1.602×10^3	2.28×10^2
3,5-bis(trifluoro-methyl)benzene-boronic acid	6.96	1.149×10^4	2.266×10^3
2,4-dichloro-benzeneboronic acid	7.81	3.083×10^3	
3,5-dichloro-benzeneboronic acid	7.18	7.681×10^3	
3-chloro-4-fluoro-benzeneboronic acid	7.80	3.225×10^3	
4-chlorobenzene-boronic acid	8.21	1.463×10^3	
4-flourobenzene-boronic acid	8.53	7.027×10^2	
4-methoxybenzene-boronic acid	9.185	2.422×10^2	
diphenyl-borinic acid	6.20	2.497×10^4	3.731×10^4

* pK values are taken from Table I Appendix E

Table XXIV

Brønsted plot for the complexation of salicylaldoxime with boron acids at 25.5°C, pH 6.6 (Data of Fig.35 Part II)

Boron acid	K_{diss} (M)	pK [a]
Boric acid	0.4288 [b]	8.98
benzeneboronic acid	5.510×10^{-2}	8.80
4-bromobenzene-boronic acid	1.564×10^{-2}	8.06
3,5-bis(trifluoro-methyl)benzene-boronic acid	2.843×10^{-3}	6.96
2,4-dichloro-benzeneboronic acid	4.56×10^{-3}	7.81
3,5-dichloro-benzeneboronic acid	4.79×10^{-3}	7.18
3-chloro-4-fluoro-benzeneboronic acid	7.802×10^{-3}	7.80
4-chlorobenzene-boronic acid	1.238×10^{-2}	8.21
4-flourobenzene-boronic acid	1.832×10^{-2}	8.53
diphenyl-borinic acid	6.456×10^{-5}	6.2

[a] pK values are taken from Table I Appendix E

[b] K_{diss} was determined at pH 6.8

Table XXV pH profile of spontaneous formation of salicylaldehyde phenylhydrazone at 25.5°C in water buffers (Data of Fig.36 Part II)

pH	k_2 ($M^{-1}sec^{-1}$)
4.61	8.227
5.08	5.729
5.44	4.464
6.00	2.651
6.41	1.714
7.00	0.7420
7.66	0.4648
8.05	0.3360

Table XXVI pH profile of 3,5-bis(trifluoromethyl)-benzeneboronic acid catalyzed formation of salicylaldehyde phenylhydrazone at 25.5°C in water buffers (Data of Fig.37 Part II)

pH	k_3 ($M^{-2}sec^{-1}$)
4.61	3.5450×10^3
5.11	7.6310×10^3
5.48	1.2280×10^4
6.00	1.9020×10^4
6.51	1.6450×10^4
7.07	1.1020×10^4
7.47	6.3680×10^3
7.69	3.3200×10^3

Table XXVII pH profile of benzeneboronic acid catalyzed formation of salicylaldehyde phenylhydrazone at 25.5°C in water buffers (Data of Fig.38 Part II)

pH	k_3 ($M^{-2}sec^{-1}$)
4.67	$4.394x10^2$
5.03	$8.425x10^2$
5.40	$1.091x10^3$
5.96	$1.519x10^3$
6.33	$1.503x10^3$
6.40	$1.605x10^3$
7.00	$1.546x10^3$
7.47	$1.347x10^3$
7.61	$1.275x10^3$
8.70	$1.271x10^2$
8.83	$7.979x10^1$

Table XXVIII pH profile of spontaneous formation of salicylaldehyde phenylhydrazone in deuterium oxide buffers at 25.5°C (Data of Fig.39 Part II)

pH	k_2 ($M^{-1}sec^{-1}$)
4.97	4.900
5.37	3.341
5.82	1.758
6.34	0.9212
6.90	0.4898
7.20	0.3560

Table XXIX pH profile of 3,5-bis(trifluoromethyl)-benzeneboronic acid catalyzed formation of salicylaldehyde phenylhydrazone at 25.5°C in deuterium oxide buffers (Data of Fig.40 Part II)

pH	k_3 ($M^{-2}sec^{-1}$)
4.99	$3.5310x10^3$
5.41	$6.7220x10^3$
5.92	$8.8480x10^3$
6.44	$9.1940x10^3$
6.99	$7.9590x10^3$
7.30	$4.5280x10^3$

Table XXX Spontaneous and 3,5-bis(trifluoromethyl)benzeneboronic acid catalyzed formation of salicylaldehyde phenylhydrazones with substituted phenylhydrazines at pH 6.0, 25.5°C

(Data of Fig.41, Fig.42 Part II)

Hydrazine	sigma*	k_2 ($M^{-1}sec^{-1}$)	k_3 ($M^{-2}sec^{-1}$)
phenylhydrazine	0.00	2.651	$1.877x10^4$
4-chlorophenylhydrazine	0.227	2.898	$2.056x10^4$
4-fluorophenylhydrazine	0.062	3.513	$2.014x10^4$
4-carboxyphenylhydrazine	0.00	4.054	$2.135x10^4$
4-methoxyphenylhydrazine	-0.268	2.035	$1.939x10^4$

*sigma values from ref.48

APPENDIX E

Hammett Plot of Boronic Acid pK Values and pH Profiles for Boronic Acid Catalyzed Formation of Salicylaldoxime: Figures and Data Tables

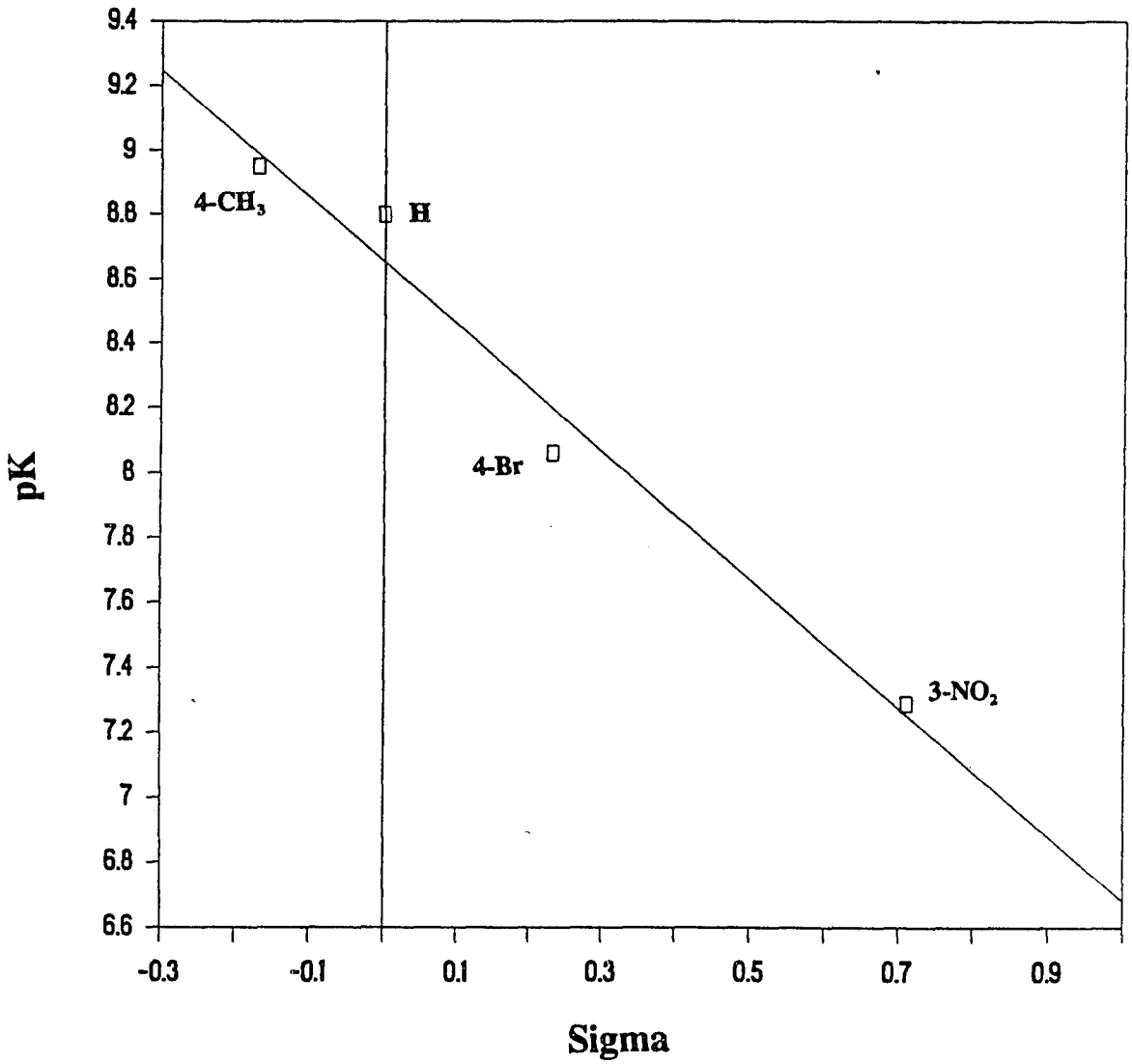

Fig.1 Hammett plot relating pK values of substituted benzeneboronic acids and *sigma*. The value of *rho* is -1.97($\pm$0.221).
(Data of Table I Appendix E)

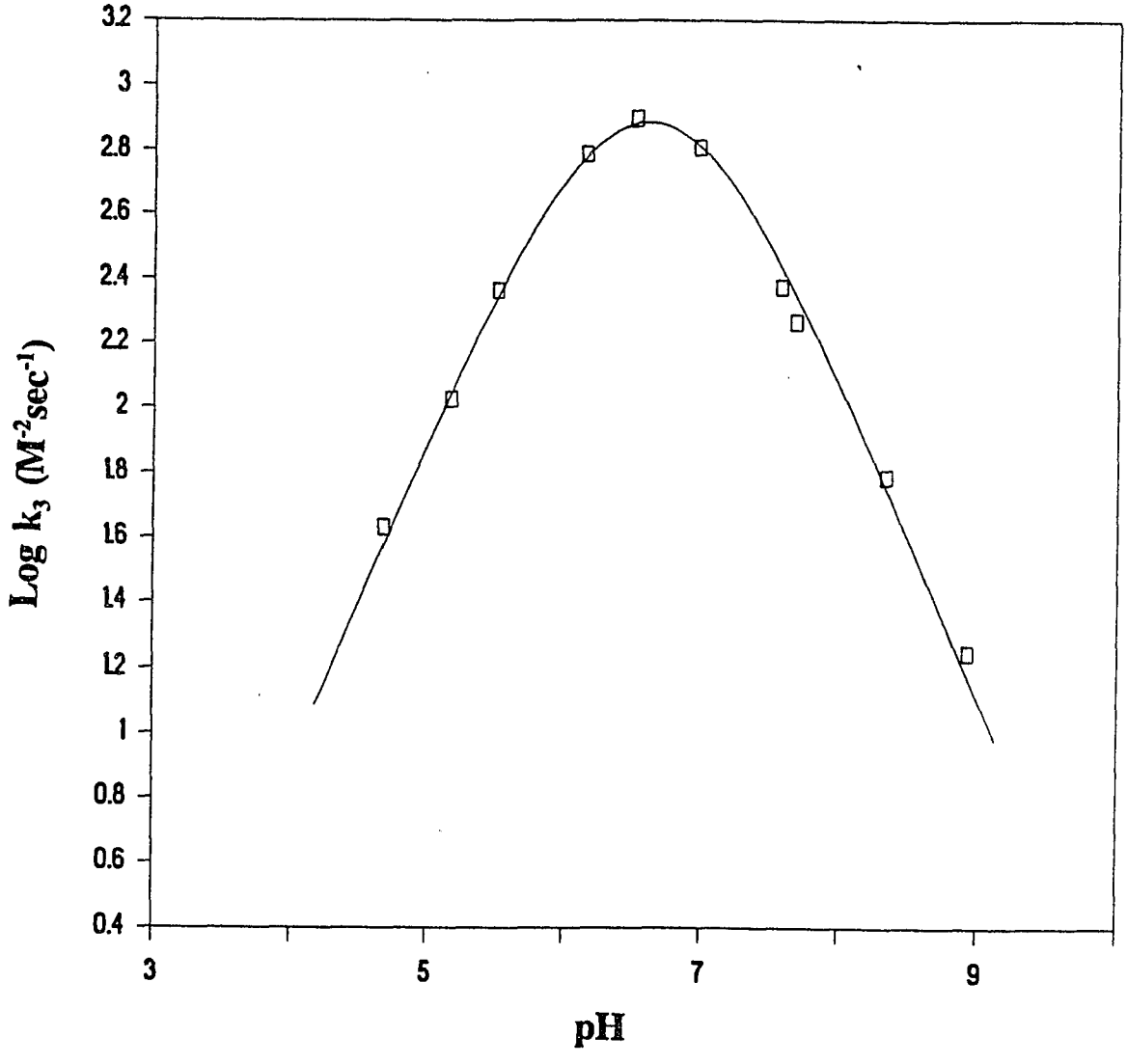

Fig.2 pH profile of 4-chlorobenzeneboronic acid catalyzed formation of salicylaldoxime in 0.1 M buffers, 25.5°C.
pK_1 = 6.26(±0.05), pK_2 = 6.95(±0.10), optimum pH = 6.60(±0.07),
k_3 (Lim) = $1.46x10^3(\pm 1.926x10^2)$ M^{-2} sec^{-1}.
k_3 refers to the third-order rate constant.
(Data of Table II Appendix E)

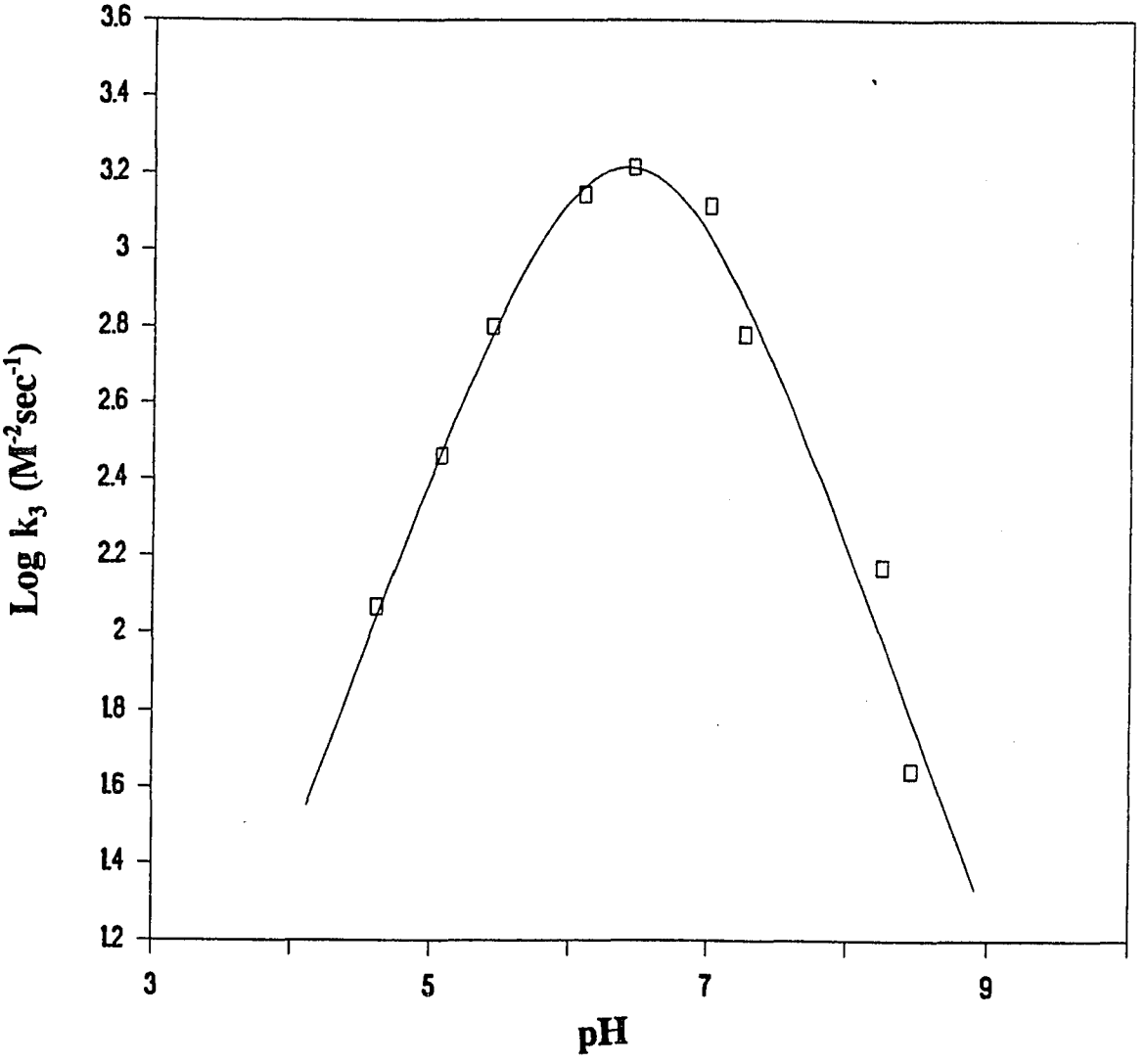

Fig.3 pH profile of 2,4-dichlorobenzeneboronic acid catalyzed formation of salicylaldoxime in 0.1 M buffers, 25.5°C. pK_1 = 6.04($\pm$0.05), pK_2 = 6.76($\pm$0.15), optimum pH = 6.40($\pm$0.10), k_3 (Lim) = 3.08×10^3($\pm 5.515 \times 10^2$) M^{-2} sec^{-1}.
k_3 refers to the third-order rate constant.
(Data of Table III Appendix E)

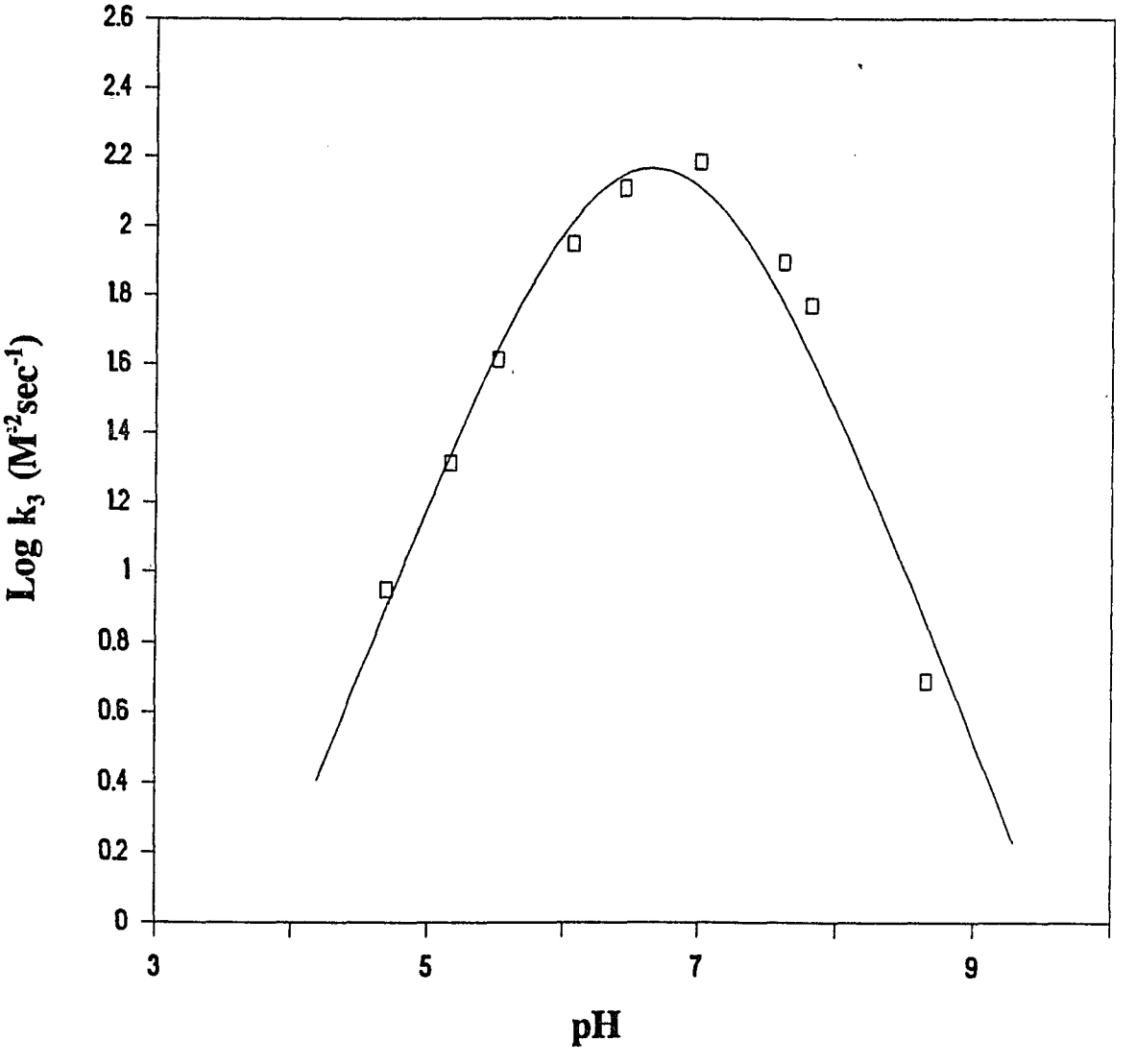

Fig.4 pH profile of 4-methoxybenzeneboronic acid catalyzed formation of salicylaldoxime in 0.1 M buffers, 25.5°C.
pK_1 = 6.16(±0.05), pK_2 = 7.14(±0.17), optimum pH = 6.65(±0.11), k_3 (Lim) = $2.42x10^2$(±71.17) M^{-2} sec^{-1}.
k_3 refers to the third-order rate constant.
(Data of Table IV Appendix E)

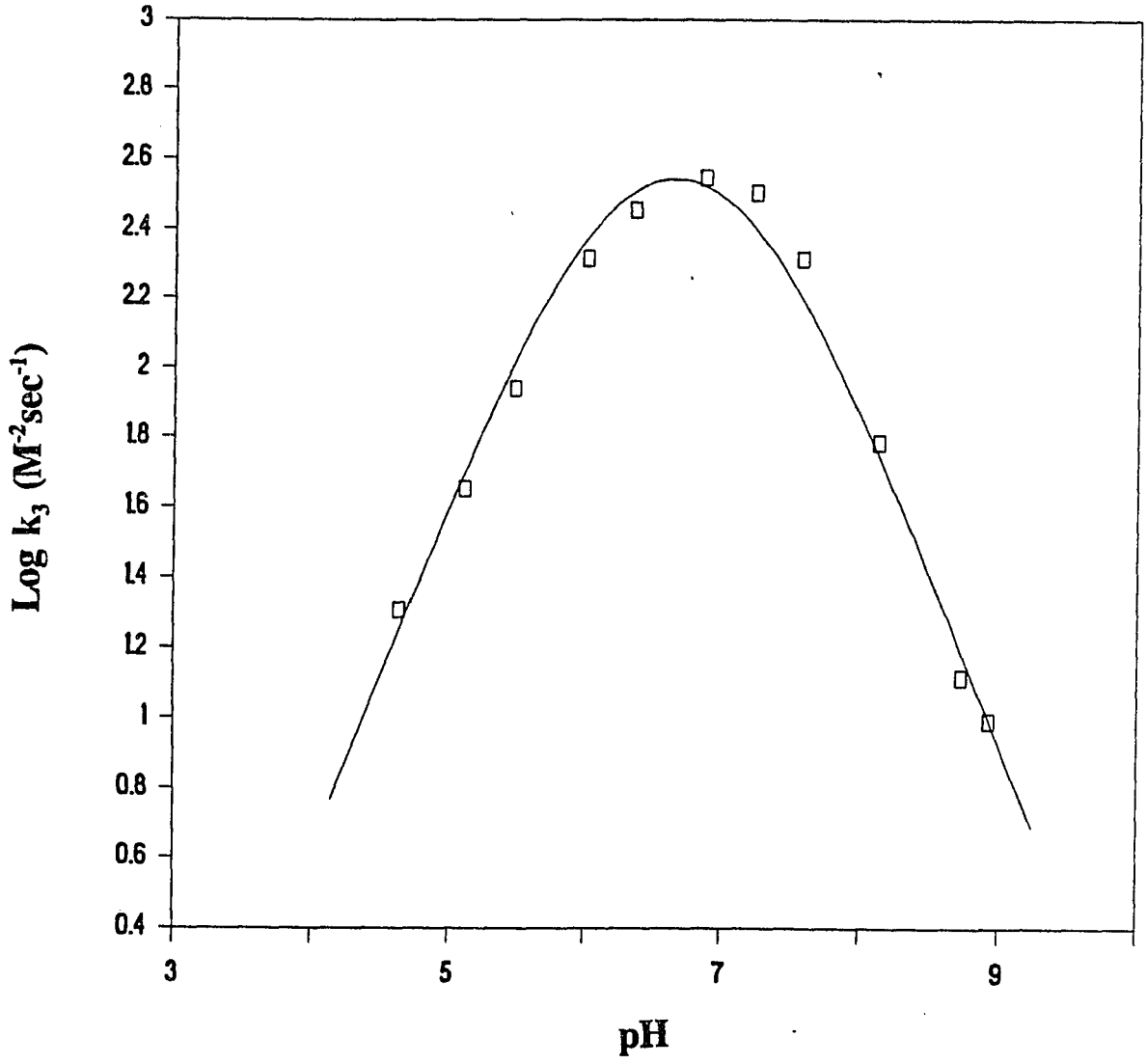

Fig.5 pH profile of benzeneboronic acid catalyzed formation of salicylaldoxime in 0.1 M buffers, 25.5°C.
pK_1 = 6.12(±0.05), pK_2 = 7.19(±0.10), optimum pH = 6.65(±0.07),
k_3 (Lim) = $5.55x10^2$(±93.4) M^{-2} sec^{-1}.
k_3 refers to the third-order rate constant.
(Data of Table V Appendix E)

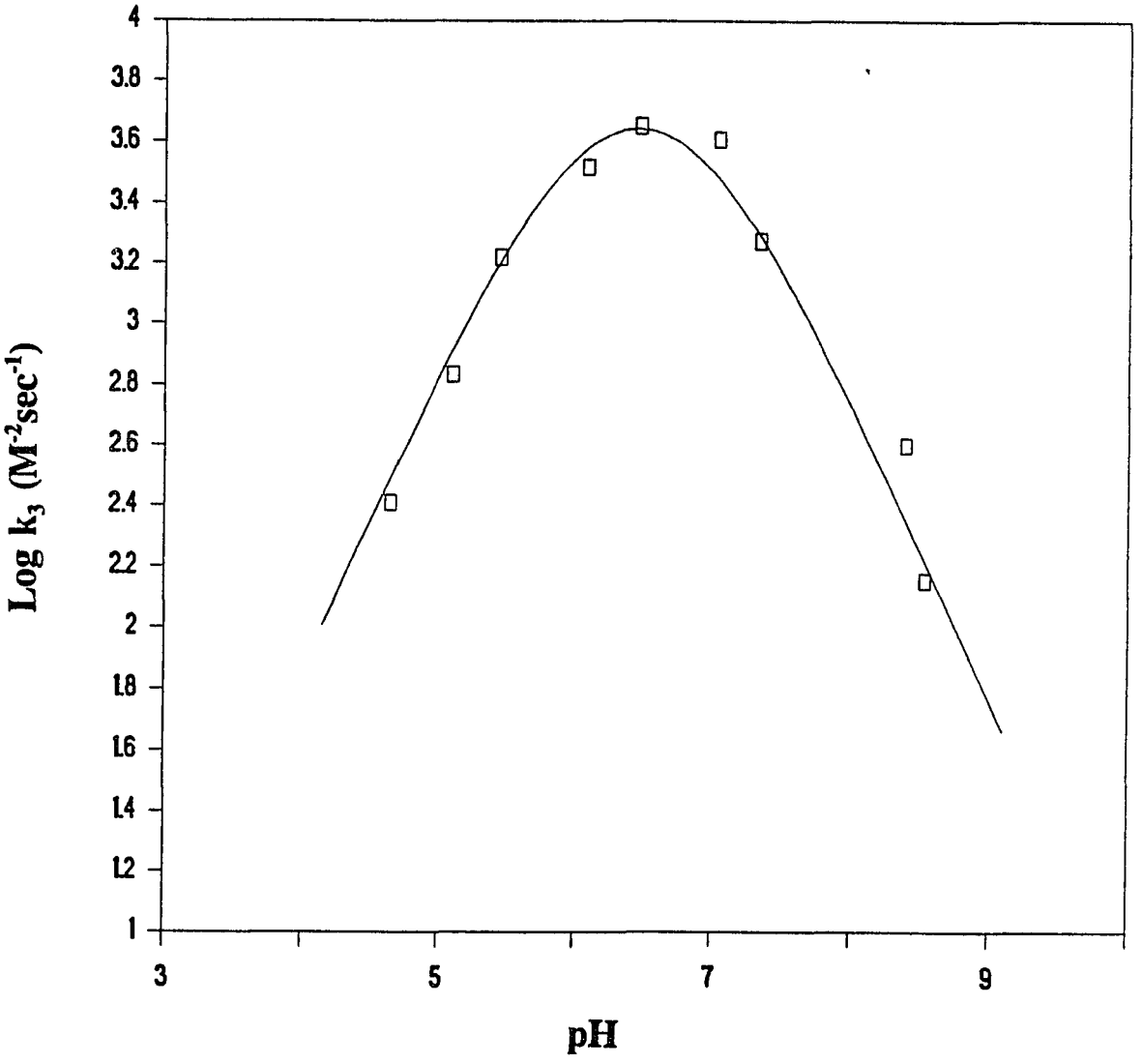

Fig.6 pH profile of 3,5-dichlorobenzeneboronic acid catalyzed formation of salicylaldoxime in 0.1 M buffers, 25.5°C.
pK_1 = 6.02(±0.08), pK_2 = 6.88(±0.15), optimum pH = 6.45(±0.11),
k_3 (Lim) = $7.68x10^3(\pm 2.17x10^3)$ M^{-2} sec^{-1}.
k_3 refers to the third-order rate constant.
(Data of Table VI Appendix E)

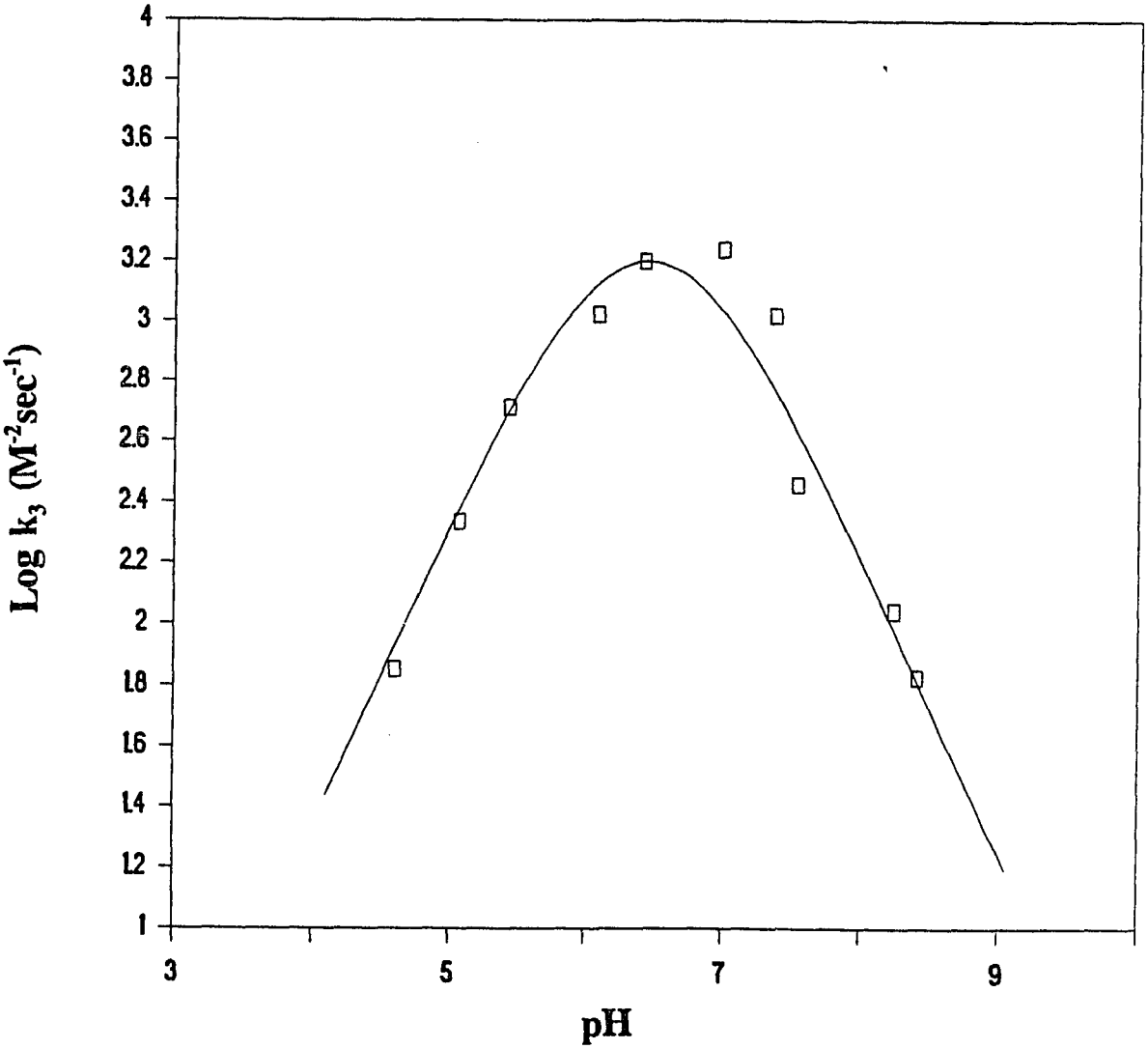

Fig.7 pH profile of 3-chloro-4-fluorobenzeneboronic acid catalyzed formation of salicylaldoxime in 0.1 M buffers, 25.5°C.
pK_1 = 6.17(±0.10), pK_2 = 6.73(±0.20), optimum pH = 6.45(±0.15),
k_3 (Lim) = $3.23x10^3(\pm 9.13x10^2)$ M^{-2} sec^{-1}.
k_3 refers to the third-order rate constant.
(Data of Table VII Appendix E)

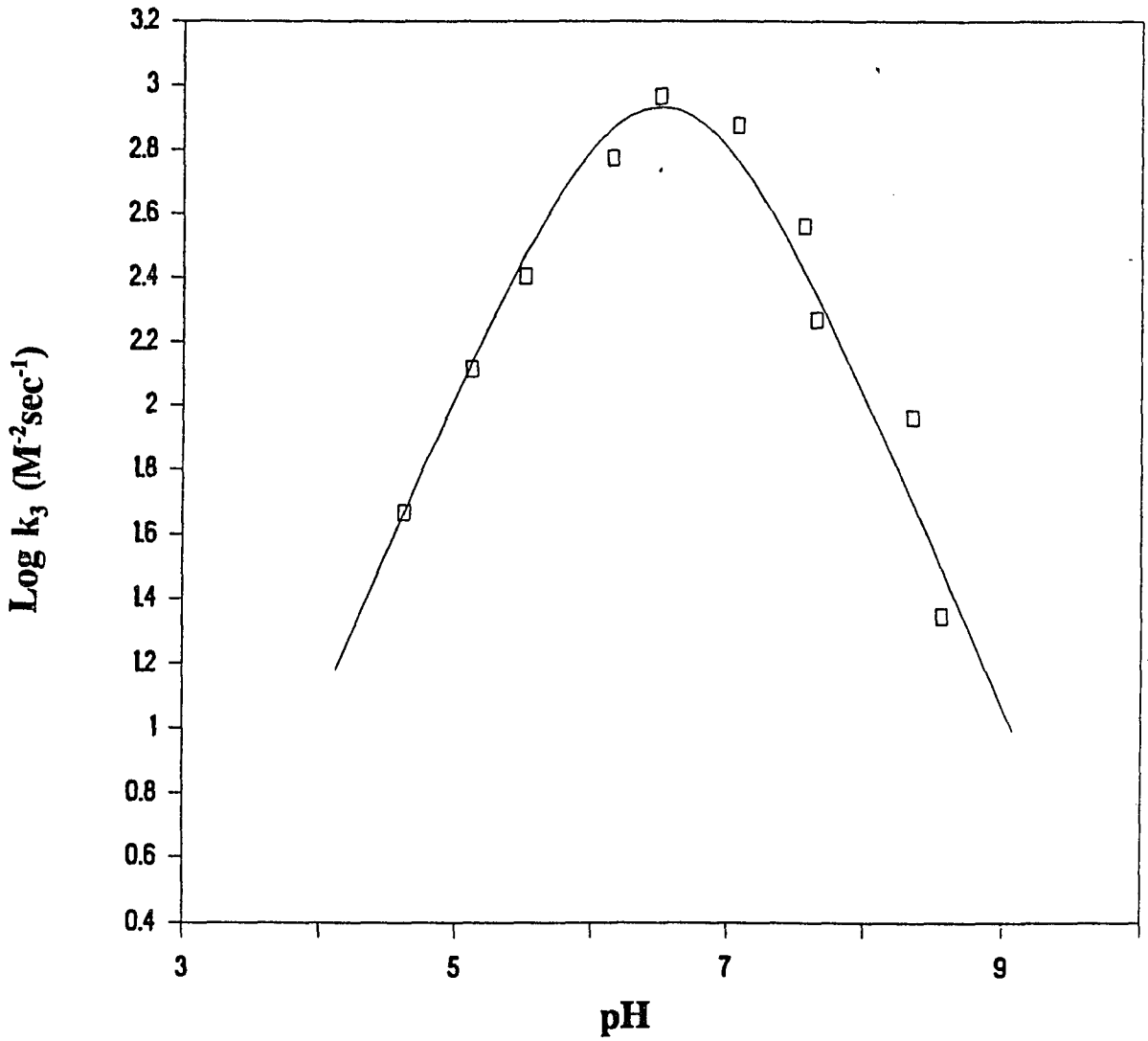

Fig.8 pH profile of 4-bromobenzeneboronic acid catalyzed formation of salicylaldoxime in 0.1 M buffers, 25.5°C.
$pK_1 = 6.14(\pm 0.05)$, $pK_2 = 6.86(\pm 0.15)$, optimum pH = $6.50(\pm 0.10)$,
k_3 (Lim) = $1.60 \times 10^3(\pm 3.61 \times 10^2)$ M^{-2} sec^{-1}.
k_3 refers to the third-order rate constant.
(Data of Table VIII Appendix E)

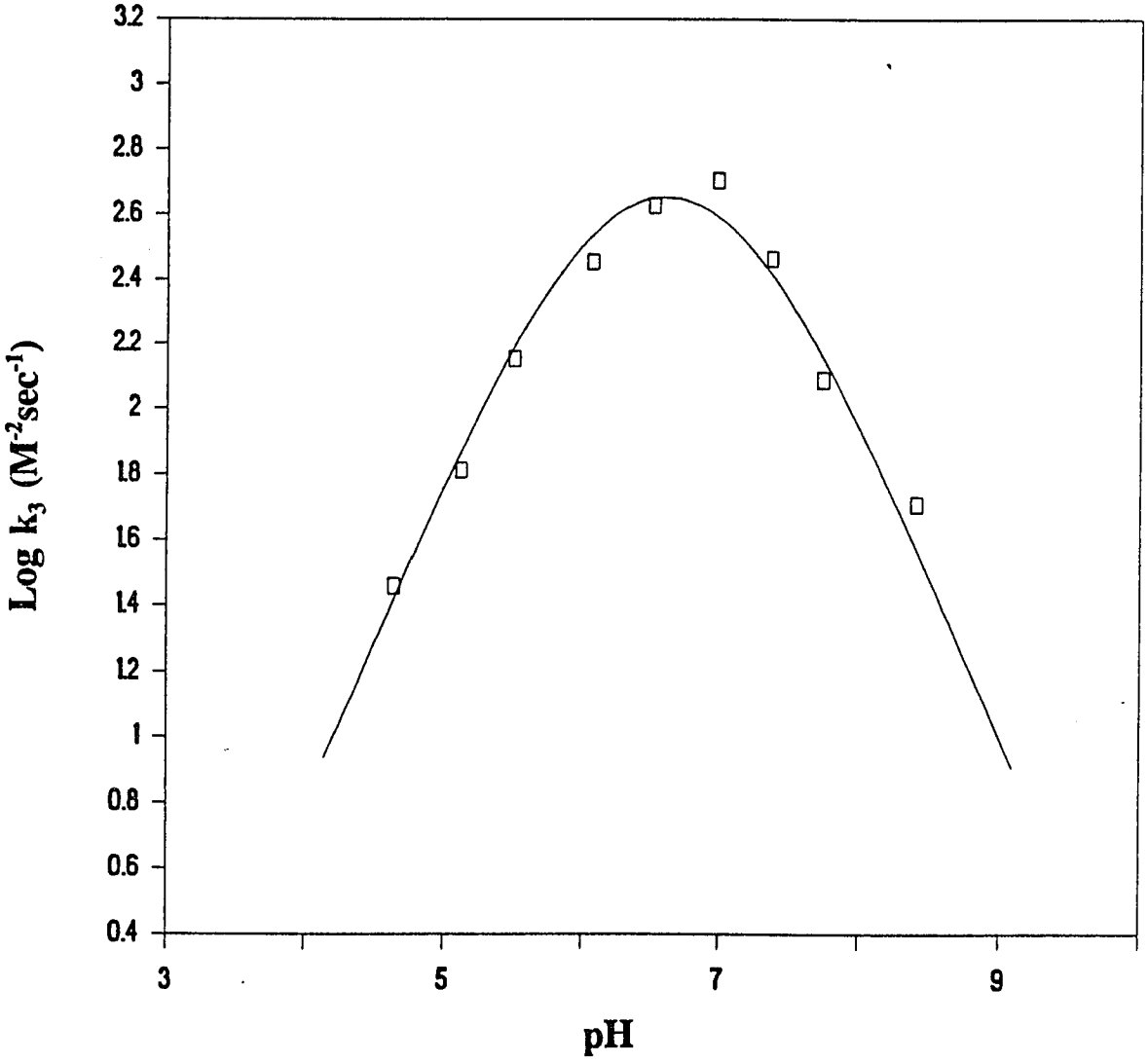

Fig.9 pH profile of 4-fluorobenzeneboronic acid catalyzed formation of salicylaldoxime in 0.1 M buffers, 25.5°C.
pK_1 = 6.05(±0.05), pK_2 = 7.15(±0.10), optimum pH = 6.60(±0.07),
k_3 (Lim) = $7.03 \times 10^2(\pm 1.54 \times 10^2)$ M^{-2} sec^{-1}.
k_3 refers to the third-order rate constant.
(Data of Table IX Appendix E)

Table I pK values of boron acids

(Data of Fig.1 Appendix E)

boron acid	sigma [a]	pK (ref.)
benzeneboronic acid	0.00	8.80 (ref.50)
2,4-dichloro-benzeneboronic acid	0.427	7.81 [b]
3,5-dichloro-benzeneboronic acid	0.746	7.18 [b]
3-chloro-4-fluoro-benzeneboronic acid	0.435	7.80 [b]
4-bromobenzene-boronic acid	0.232	8.06 (ref.50)
4-chlorobenzene-boronic acid	0.227	8.21 [b]
4-fluorobenzene-boronic acid	0.062	8.53 [b]
3,5-bis(trifluoro-methyl)benzene-boronic acid	0.860	6.96 [b]
3-nitrobenzene-boronic acid	0.710	7.29 (ref.50)
4-tolueneboronic acid	-0.170	8.95 (ref.51)
4-methoxybenzene-boronic acid	-0.268	9.185 [b]
boric acid		8.98 (ref.8)
diphenylborinic acid		6.20 (ref.45)

[a] sigma values are taken from ref.48

[b] pK values were determined from the Hammett plot constructed using the boronic acid pK values reported in the references.

Table II pH profile of 4-chlorobenzeneboronic acid catalyzed salicylaldoxime formation at 25.5°C (Data of Fig.2 Appendix E)

pH	k_3 ($M^{-2}sec^{-1}$)
4.68	$4.2750x10^{1}$
5.17	$1.0591x10^{2}$
5.51	$2.3098x10^{2}$
6.15	$6.1043x10^{2}$
6.51	$7.8656x10^{2}$
6.97	$6.4081x10^{2}$
7.58	$2.3787x10^{2}$
7.69	$1.8503x10^{2}$
8.34	$6.1620x10^{1}$
8.93	$1.7673x10^{1}$

Table III pH profile of 2,4-dichlorobenzeneboronic acid catalyzed salicylaldoxime formatiom at 25.5°C (Data of Fig.3 Appendix E)

pH	k_3 ($M^{-2}sec^{-1}$)
4.61	$1.1657x10^{2}$
5.07	$2.8874x10^{2}$
5.43	$6.3434x10^{2}$
6.09	$1.3926x10^{3}$
6.45	$1.6409x10^{3}$
7.00	$1.3003x10^{3}$
7.25	$6.0558x10^{2}$
8.25	$1.4873x10^{2}$
8.46	$4.4037x10^{1}$

Table IV pH profile of 4-methoxybenzeneboronic acid catalyzed salicylaldoxime formatiom at 25.5°C (Data of Fig.4 Appendix E)

pH	k_3 ($M^{-2}sec^{-1}$)
4.69	8.8863
5.16	20.629
5.51	40.940
6.06	88.732
6.45	128.07
7.00	152.90
7.62	78.741
7.82	58.918
8.65	4.9116

Table V pH profile of benzeneboronic acid catalyzed salicylaldoxime formatiom at 25.5°C (Data of Fig.5 Appendix E)

pH	k_3 ($M^{-2}sec^{-1}$)
4.64	20.338
5.11	44.922
5.48	87.264
6.01	207.26
6.36	285.96
6.87	353.99
7.24	320.67
7.58	206.76
8.14	61.186
8.73	13.115
8.93	9.8179

Table VI pH profile of 3,5-dichlorobenzeneboronic acid catalyzed salicylaldoxime formatiom at 25.5°C (Data of Fig.6 Appendix E)

pH	k_3 ($M^{-2}sec^{-1}$)
4.65	$2.5605x10^2$
5.10	$6.7855x10^2$
5.45	$1.6587x10^3$
6.09	$3.2990x10^3$
6.47	$4.4753x10^3$
7.04	$4.0429x10^3$
7.34	$1.8762x10^3$
8.40	$3.9958x10^2$
8.54	$1.4280x10^2$

Table VII pH profile of 3-chloro-4-fluoro-benzeneboronic acid catalyzed salicylaldoxime formatiom at 25.5°C (Data of Fig.7 Appendix E)

pH	k_3 ($M^{-2}sec^{-1}$)
4.60	$7.1179x10^1$
5.07	$2.1709x10^2$
5.44	$5.1460x10^2$
6.09	$1.0522x10^3$
6.43	$1.5818x10^3$
7.00	$1.7338x10^3$
7.38	$1.0454x10^3$
7.55	$2.8824x10^2$
8.25	$1.1073x10^2$
8.42	$6.7389x10^1$

Table VIII pH profile of 4-bromobenzeneboronic acid catalyzed salicylaldoxime formatiom at 25.5°C (Data of Fig.8 Appendix E)

pH	k_3 ($M^{-2}sec^{-1}$)
4.62	$4.6575x10^{1}$
5.11	$1.3124x10^{2}$
5.50	$2.5495x10^{2}$
6.15	$5.9437x10^{2}$
6.50	$9.2542x10^{2}$
7.07	$7.5070x10^{2}$
7.56	$3.6680x10^{2}$
7.65	$1.8612x10^{2}$
8.35	$9.2194x10^{1}$
8.56	$2.2340x10^{1}$

Table IX pH profile of 4-fluorobenzeneboronic acid catalyzed salicylaldoxime formatiom at 25.5°C (Data of Fig.9 Appendix E)

pH	k_3 ($M^{-2}sec^{-1}$)
4.64	$2.8891x10^{1}$
5.12	$6.4867x10^{1}$
5.50	$1.4186x10^{2}$
6.07	$2.8549x10^{2}$
6.52	$4.2517x10^{2}$
6.98	$5.0901x10^{2}$
7.37	$2.9299x10^{2}$
7.74	$1.2294x10^{2}$
8.41	$5.1014x10^{1}$

APPENDIX F

Solvent Deuterium Isotope Effect on the Formation of Salicylaldoxime: pH Profiles and Data Tables

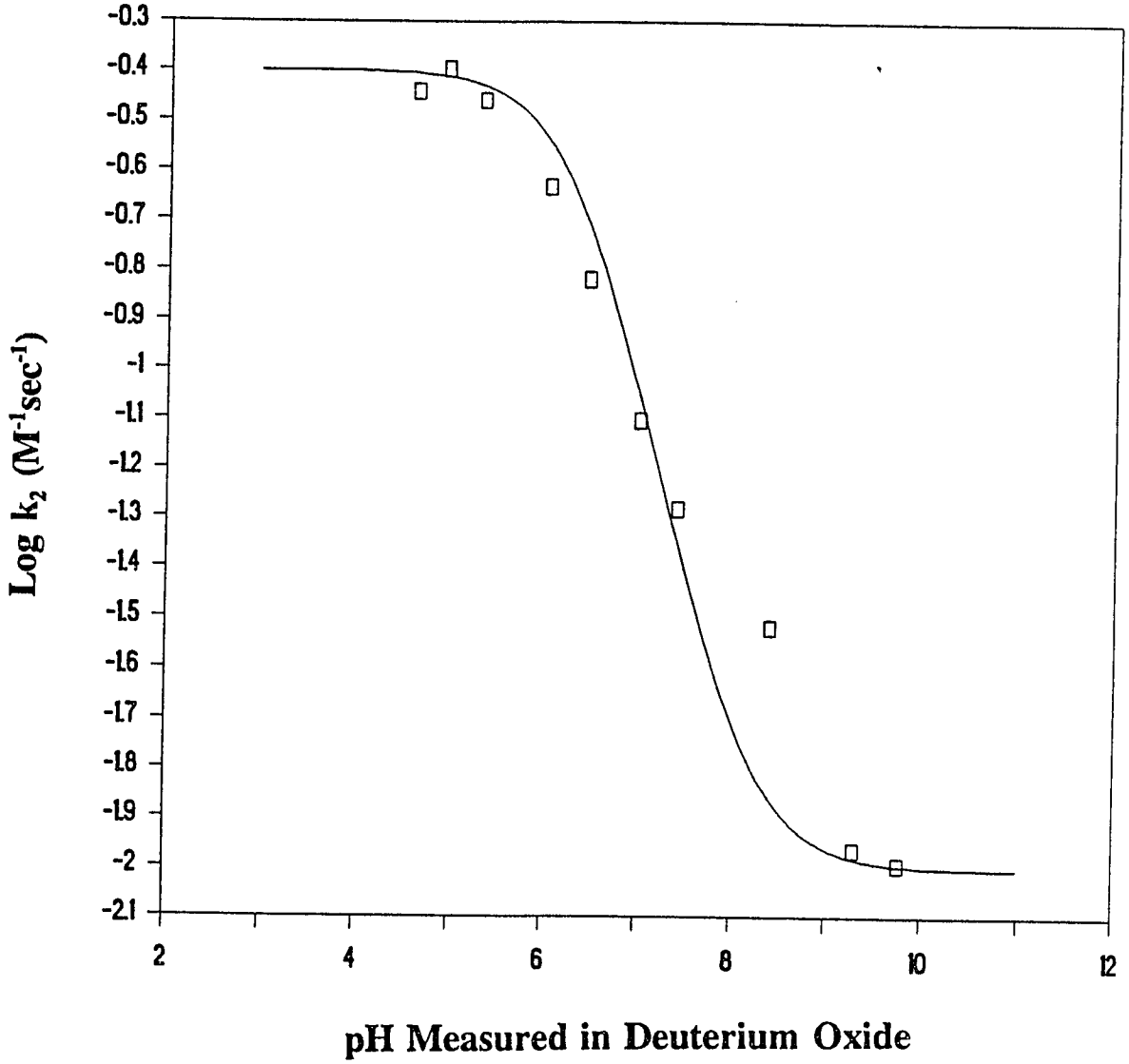

Fig.1 pH profile of spontaneous formation of salicylaldoxime in 0.1 M deuterium oxide buffers, 25.5°C. pK = 5.90($\pm$0.15),
In acidic region, k_2 (Lim) = 0.400($\pm$0.030) M^{-1} sec^{-1}.
In alkali, k_2 (Lim) = 9.90×10^{-3}($\pm 1.0 \times 10^{-4}$) M^{-1} sec^{-1}.
k_2 refers to the second-order rate constant.
(Data of Table I Appendix F)

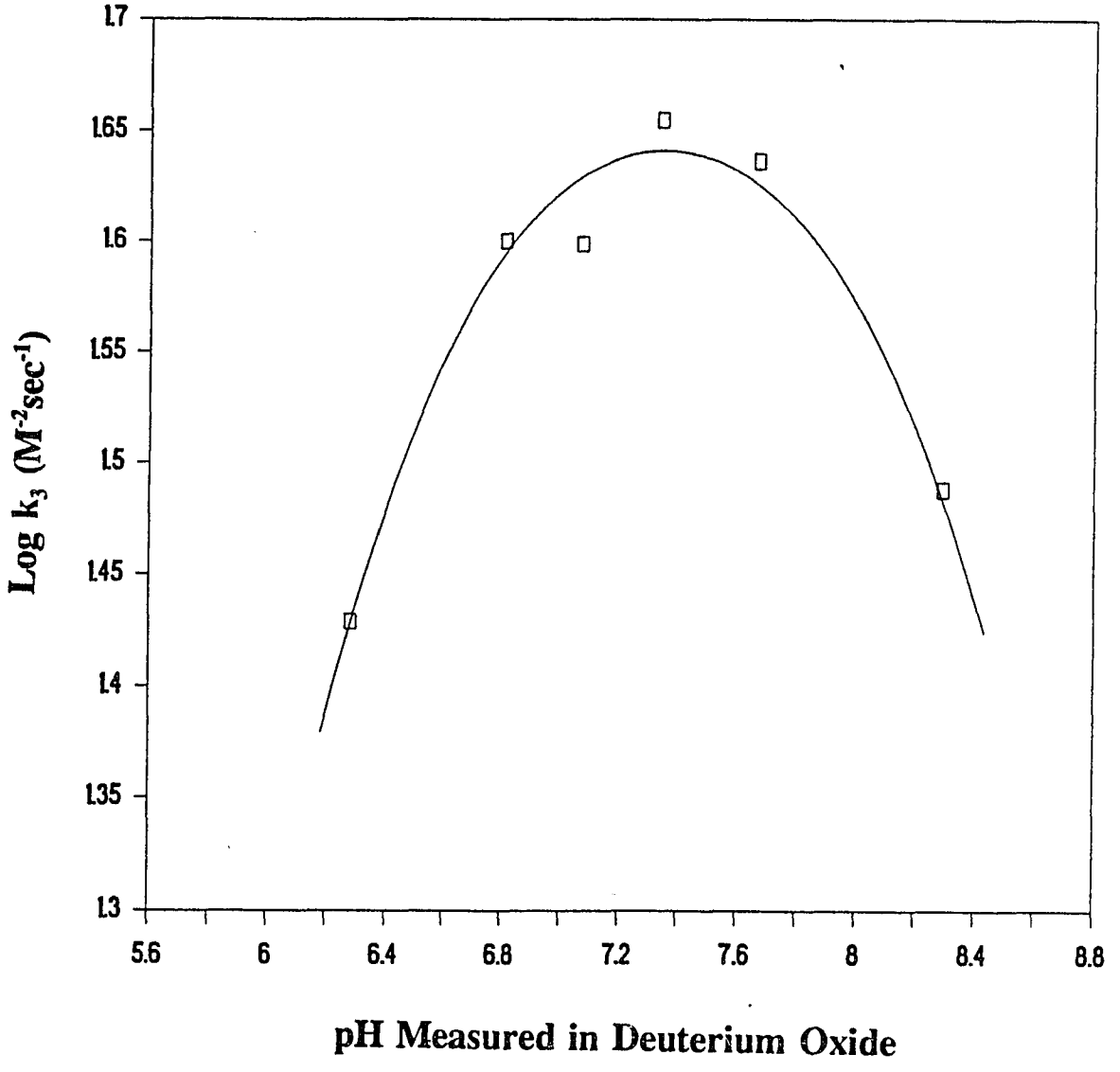

Fig.2 pH profile of boric acid catalyzed formation of salicylaldoxime in 0.1 M deuterium oxide buffers, 25.5°C.
$pK_1 = 6.22(\pm 0.05)$, $pK_2 = 8.48(\pm 0.05)$, optimum pH = $7.35(\pm 0.05)$,
k_3 (Lim) = $50.2(\pm 2.62)$ M^{-2} sec^{-1}.
k_3 refers to the third-order rate constant.
(Data of Table II Appendix F)

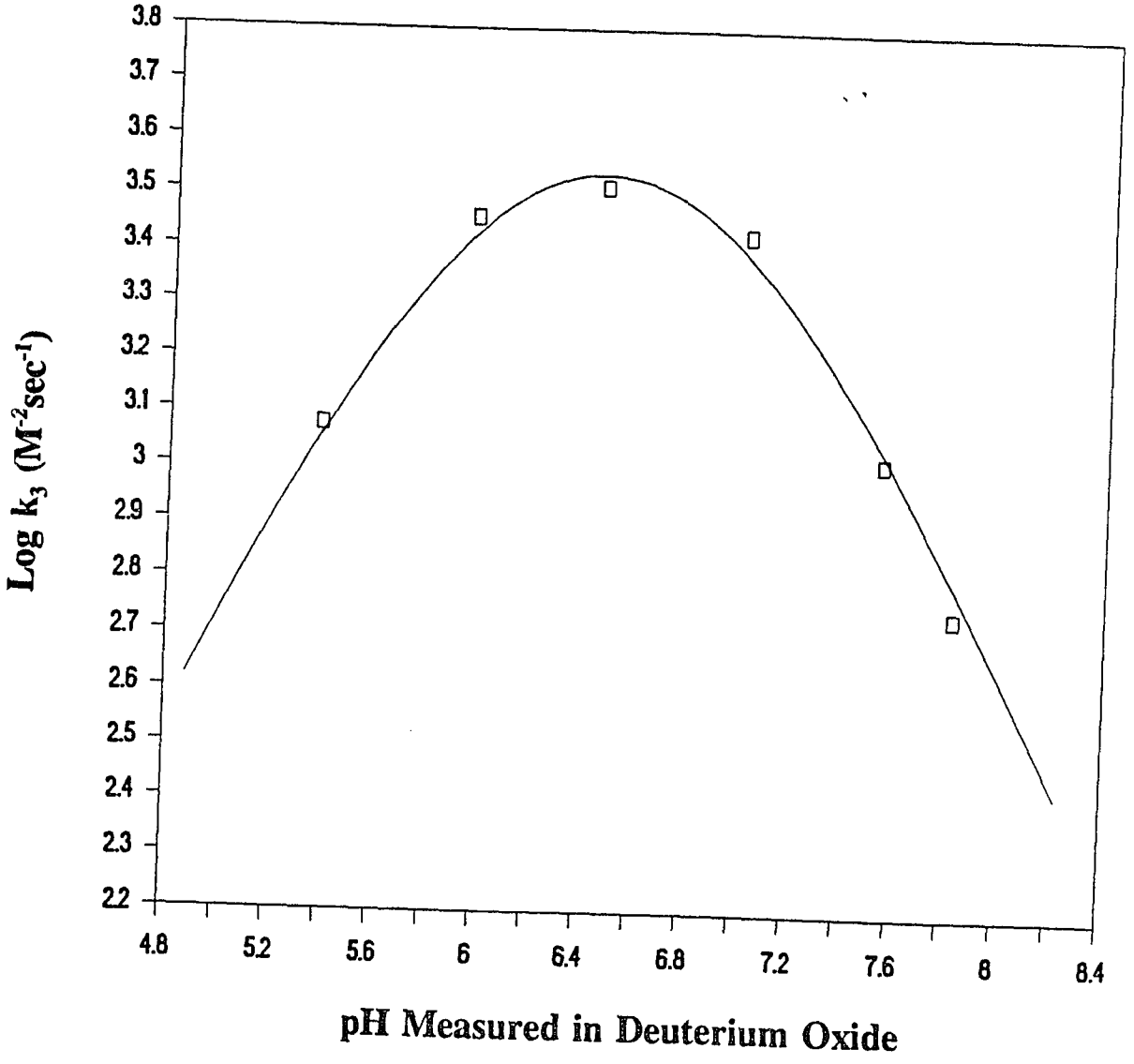

Fig.3 pH profile of 3,5-bis(trifluoromethyl)benzeneboronic acid catalyzed formation of salicylaldoxime in 0.1 M deuterium oxide buffers, 25.5°C. $pK_1 = 5.99(\pm 0.05)$, $pK_2 = 6.91(\pm 0.05)$, optimum pH = $6.45(\pm 0.05)$, k_3 (Lim) = $5.837 \times 10^3(\pm 6.59 \times 10^2)$ M^{-2}
k_3 refers to the third-order rate constant.
(Data of Table III Appendix F)

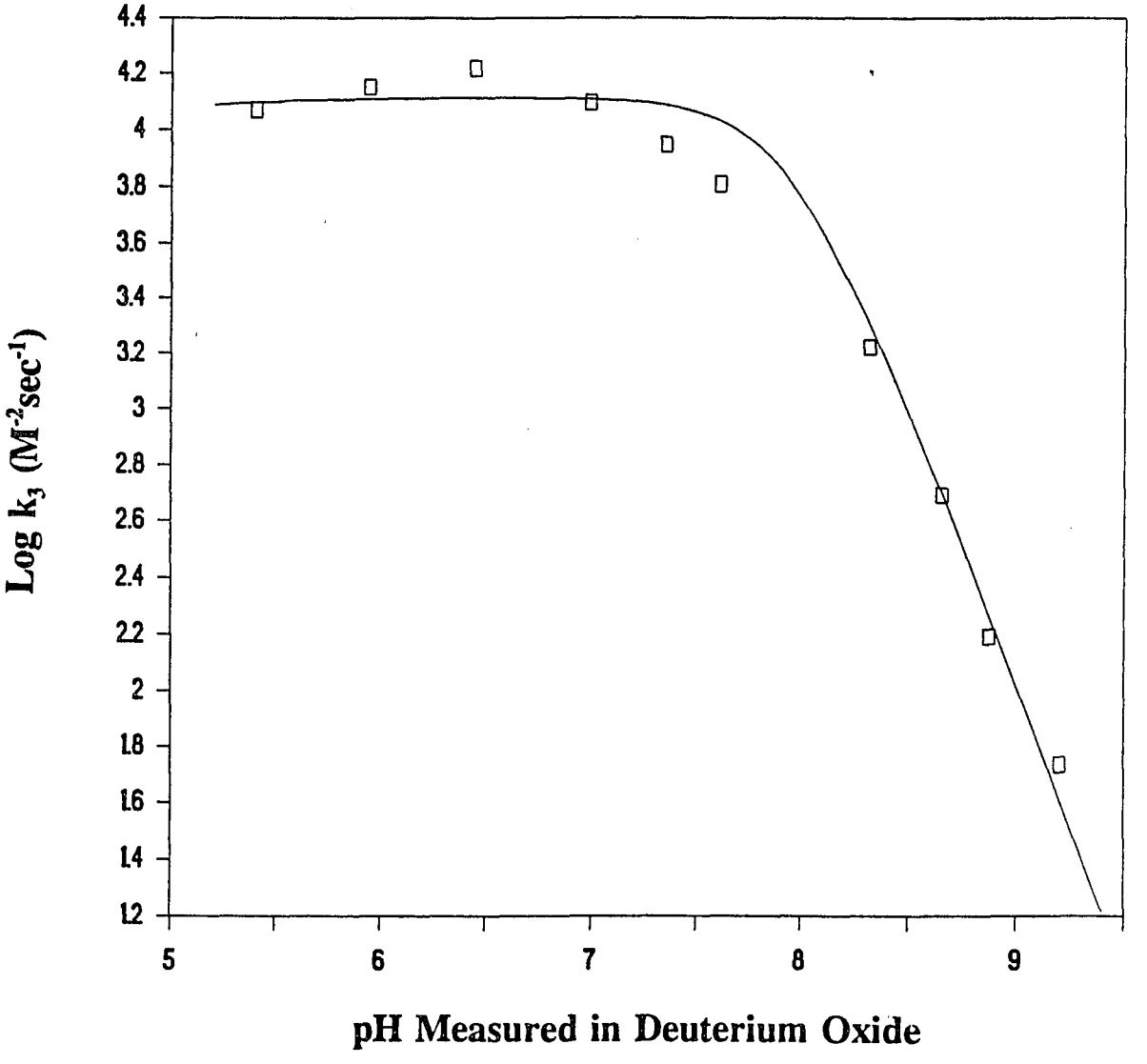

Fig.4 pH profile of diphenylborinic acid catalyzed formation of salicylaldoxime in 0.1 M deuterium oxide buffers, 25.5°C.
Double-ionization pK (average) = 7.95($\pm$0.05),
k_3 (Lim) = $1.30 \times 10^4 (\pm 2.0 \times 10^3)$ M^{-2} sec^{-1}.
k_3 refers to the third-order rate constant.
(Data of Table IV Appendix F)

Table I pH profile of spontaneous salicylaldoxime formation at 25.5°C in deuterium oxide buffers (Data of Fig.1 Appendix F)

pH	k_2 ($M^{-1}sec^{-1}$)
4.61	0.36158
4.93	0.40218
5.32	0.34772
6.03	0.23307
6.46	0.15194
7.01	0.078795
7.42	0.052309
8.40	0.030290
9.30	0.010817
9.77	0.010094

Table II pH profile of boric acid catalyzed salicylaldoxime formation at 25.5°C in deuterium oxide buffers (Data of Fig.2 Appendix F)

pH	k_3 ($M^{-2}sec^{-1}$)
6.28	26.846
6.81	39.833
7.07	39.694
7.34	45.160
7.67	43.301
8.29	30.770

Table III pH profile of 3,5-bis(trifluoromethyl)-benzeneboronic acid catalyzed salicylaldoxime formation at 25.5°C in deuterium oxide buffers (Data of Fig.3 Appendix F)

pH	k_3 ($M^{-2}sec^{-1}$)
5.38	$1.1891x10^3$
5.96	$2.8539x10^3$
6.46	$3.2540x10^3$
7.02	$2.6793x10^3$
7.55	$1.0350x10^3$
7.83	$5.5294x10^2$

Table IV pH profile of diphenylborinic acid catalyzed salicylaldoxime formation at 25.5°C in deuterium oxide buffers (Data of Fig.4 Appendix F)

pH	k_3 ($M^{-2}sec^{-1}$)
5.40	$1.1797x10^4$
5.94	$1.4208x10^4$
6.44	$1.6576x10^4$
6.99	$1.2501x10^4$
7.35	$8.8795x10^3$
7.61	$6.4530x10^3$
8.32	$1.6724x10^3$
8.65	$4.9230x10^2$
8.87	$1.5599x10^2$
9.20	$5.4412x10^1$

APPENDIX G

pH Profiles for Spontaneous, Benzeneboronic Acid and 3,5-Bis(trifluoromethyl)benzeneboronic Acid Catalyzed Formation of Salicylaldehyde O-Methyloxime: Figures and Data Tables

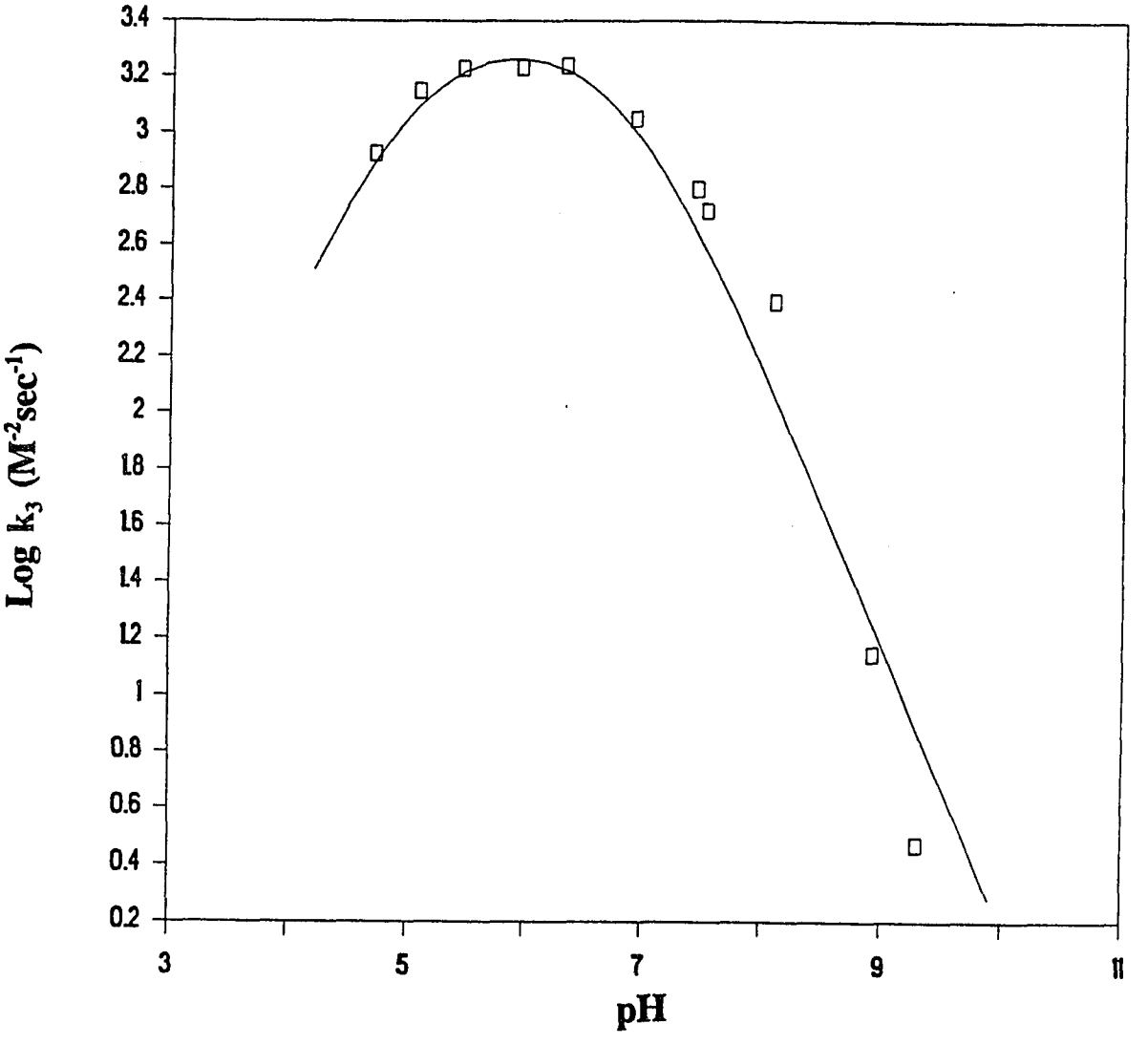

Fig.1 pH profile of 3,5-bis(trifluoromethyl)benzeneboronic acid catalyzed formation of salicylaldehyde O-methyloxime in 0.1 M buffers, 25.5°C.
pK_1 = 4.98(±0.05), pK_2 = 6.82(±0.20), optimum pH = 5.90(±0.12),
k_3 (Lim) = $2.266 \times 10^3 (\pm 3.56 \times 10^2)$ M^{-2} sec^{-1}.
k_3 refers to the third-order rate constant.
(Data of Table I Appendix G)

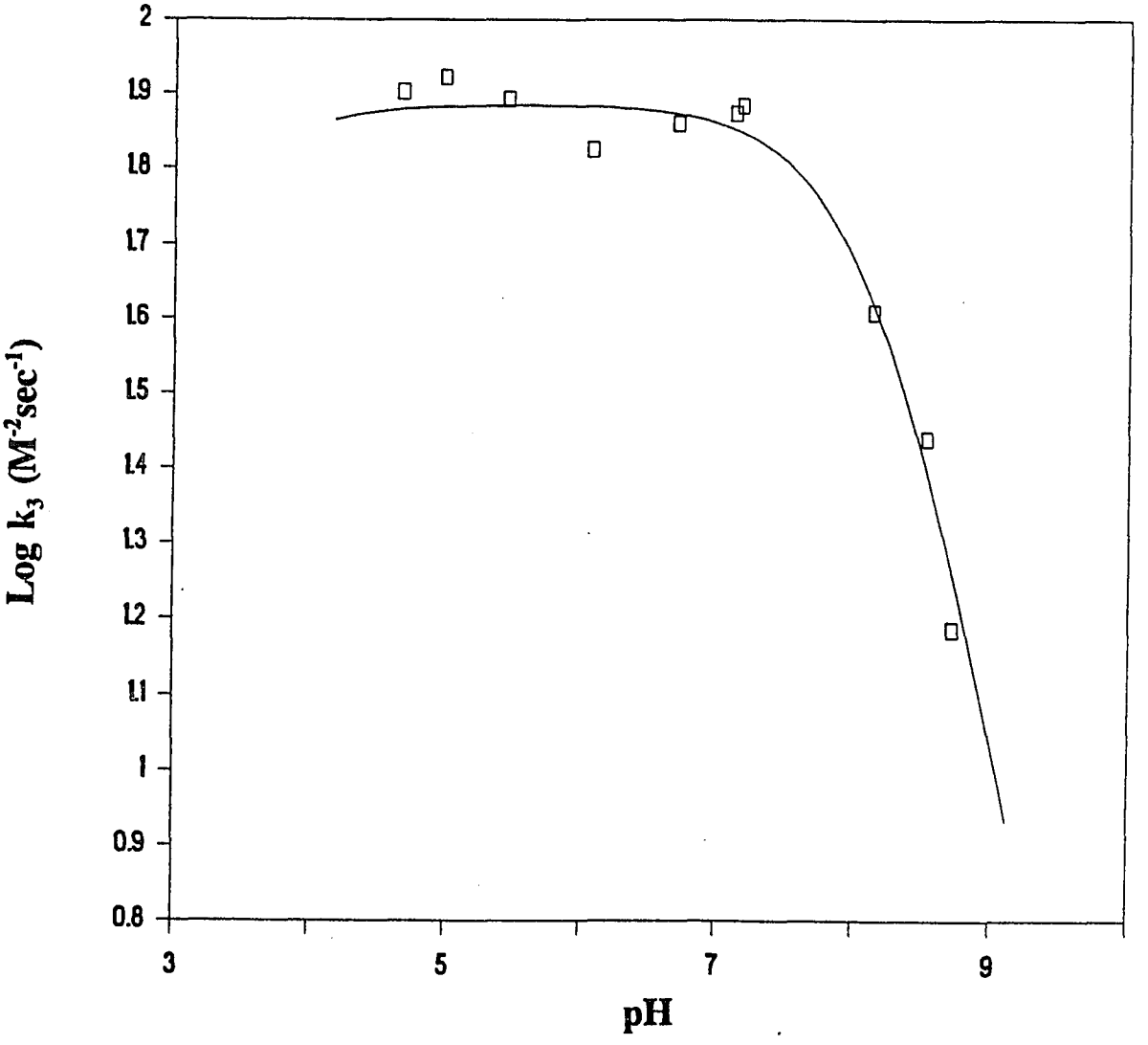

Fig.2 pH profile of benzeneboronic acid catalyzed formation of salicylaldehyde O-methyloxime in 0.1 M buffers, 25.5°C.
pK = 8.22($\pm$0.05), k_3 (Lim) = 76.98($\pm$2.70) M^{-2} sec^{-1}.
k_3 refers to the third-order rate constant.
(Data of Table II Appendix G)

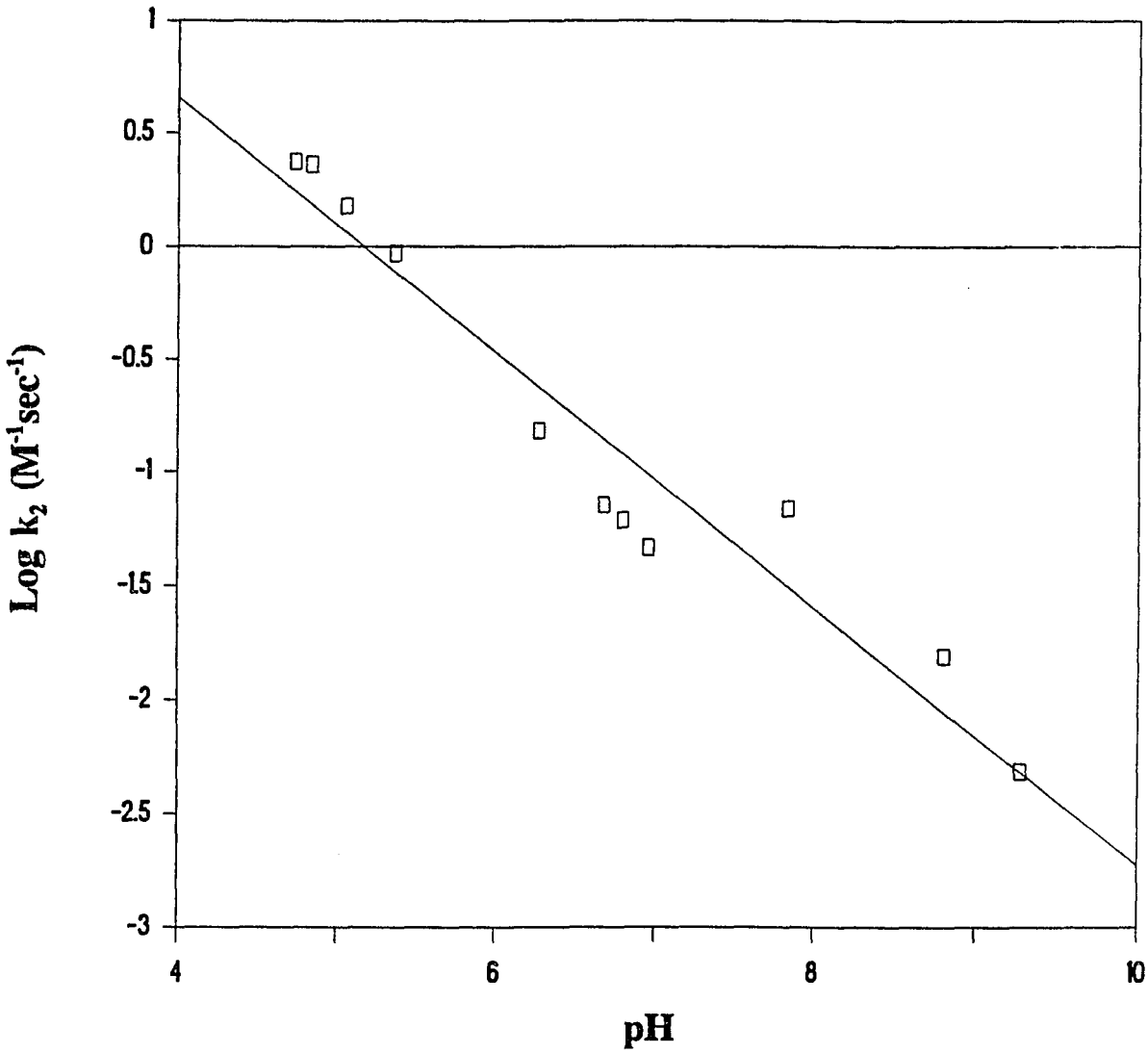

Fig.3 pH profile of spontaneous formation of salicylaldehyde O-methyloxime in 0.1 M buffers, 25.5°C.
Slope is -0.563(±0.050).
k_2 refers to the second-order rate constant.
(Data of Table III Appendix G)

Table I pH profile of 3,5-bis(trifluoromethyl)-benzeneboronic acid catalyzed salicylaldehyde O-methyloxime formation at 25.5°C (Data of Fig.1 Appendix G)

pH	k_3 ($M^{-2}sec^{-1}$)
4.70	846.96
5.07	1415.7
5.44	1699.8
5.94	1712.4
6.32	1729.9
6.92	1118.3
7.44	633.12
7.52	529.69
8.10	249.67
8.93	14.085
9.30	2.9710

Table II pH profile of benzeneboronic acid catalyzed salicylaldehyde O-methyloxime formation at 25.5°C (Data of Fig.2 Appendix G)

pH	k_3 ($M^{-2}sec^{-1}$)
4.67	79.975
4.98	83.704
5.45	78.111
6.07	66.918
6.71	72.451
7.13	74.783
7.18	76.531
8.15	40.667
8.54	27.561
8.73	15.372

Table III pH profile of spontaneous formation of salicylaldehyde O-methyloxime at 25.5°C (Data of Fig.3 Appendix G)

pH	k_2 ($M^{-1}sec^{-1}$)
4.73	2.363
4.83	2.295
5.05	1.502
5.36	0.9326
6.27	0.1521
6.68	0.0716
6.80	0.0613
6.96	0.04656
7.83	0.06856
8.81	0.01551
9.27	0.00486

APPENDIX H

Eadie-Hofstee Plots for the Complexation between Boronic Acids and Salicylaldoxime: Figures and Data Tables

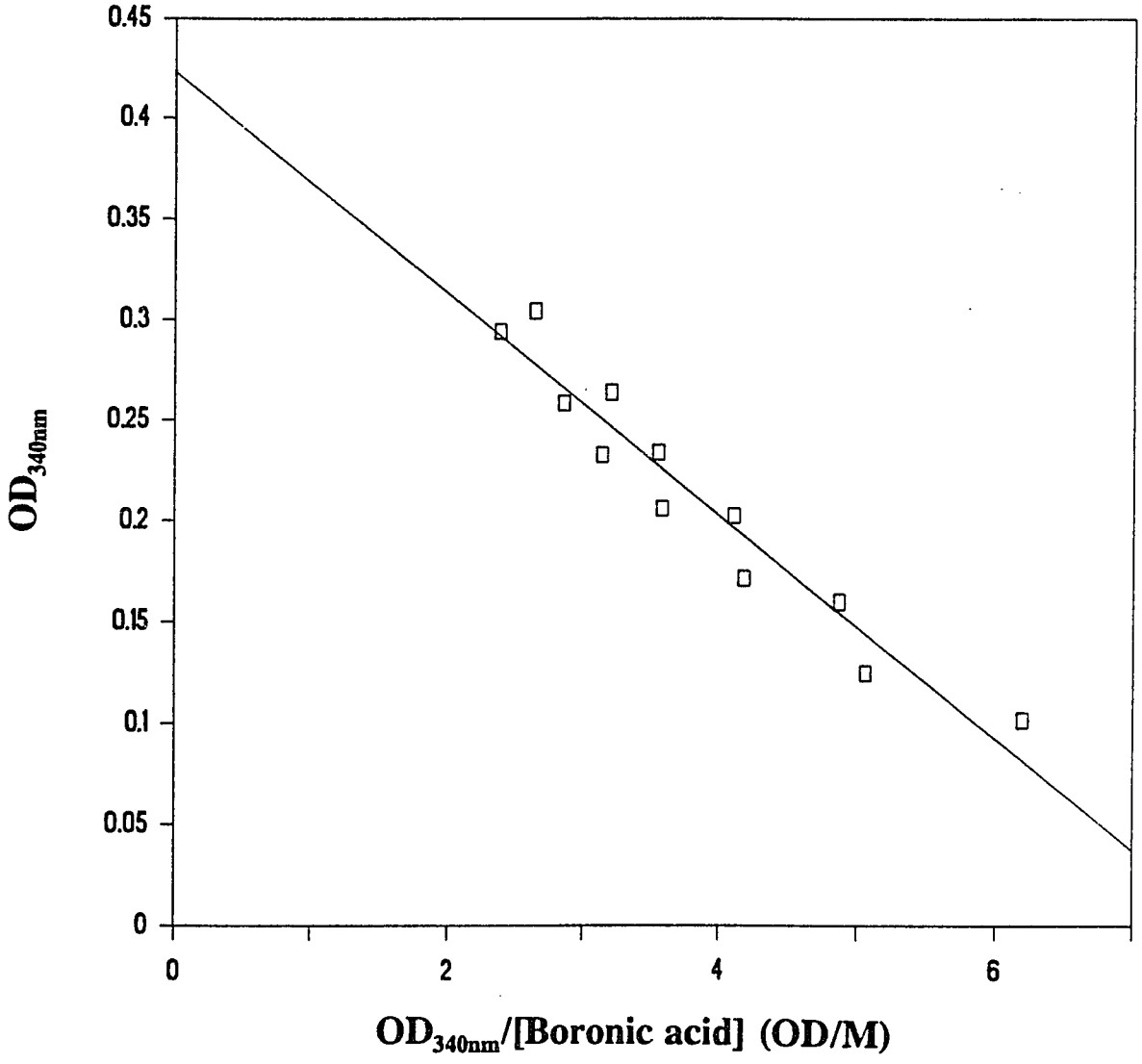

Fig.1 Eadie-Hofstee plot for the complexation between benzeneboronic acid and salicylaldoxime (0.1097 mM) in pH 6.6 0.1 M buffer, 25.5°C. K_{diss} = 55.1(±4.73) mM.
(Data of Table I Appendix H)

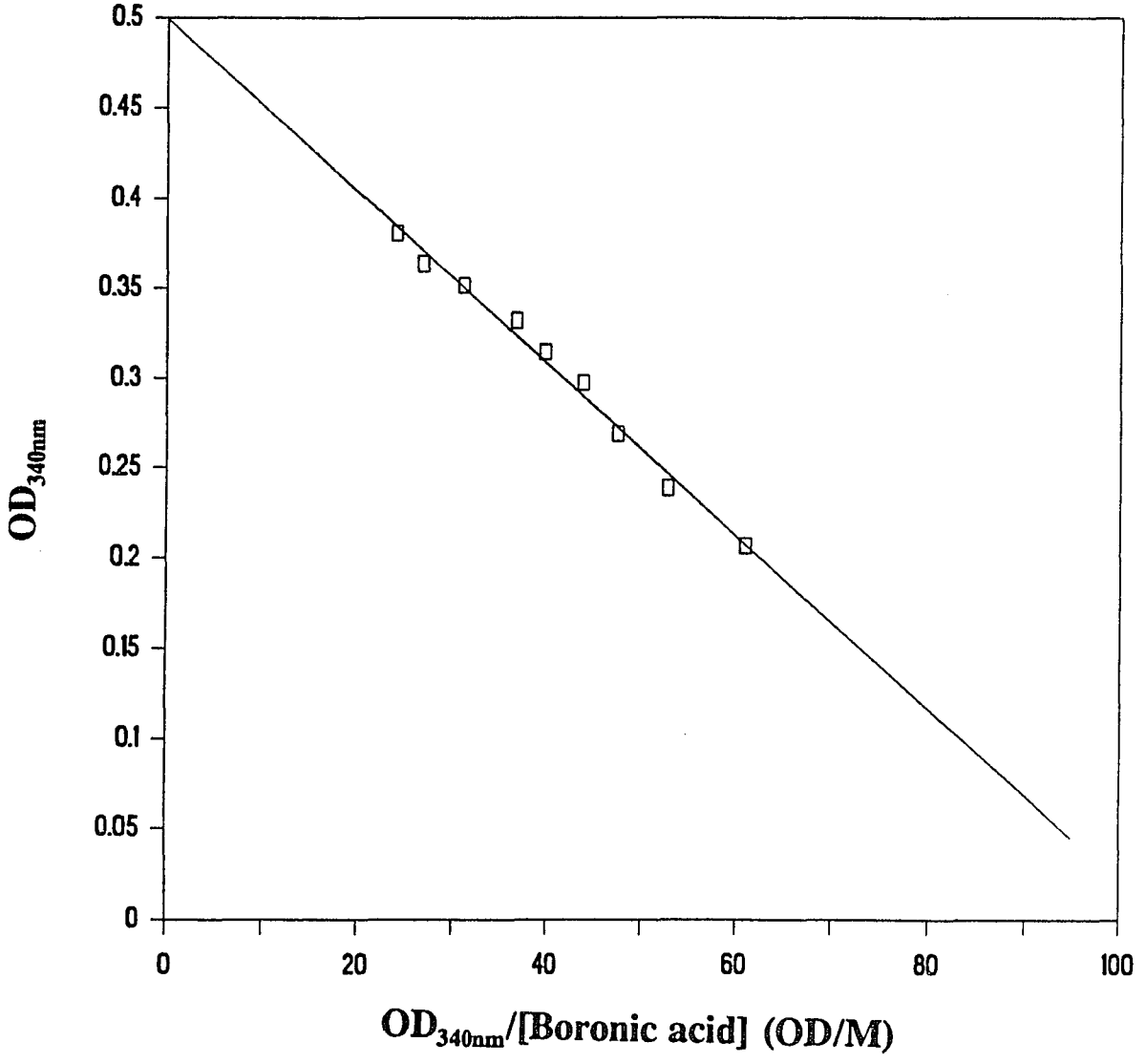

Fig.2 Eadie-Hofstee plot for the complexation between 3,5-dichlorobenzeneboronic acid and salicylaldoxime (0.1097 mM) in pH 6.6 0.1 M buffer, 25.5°C. K_{diss} = 4.79($\pm$0.189) mM.
(Data of Table II Appendix H)

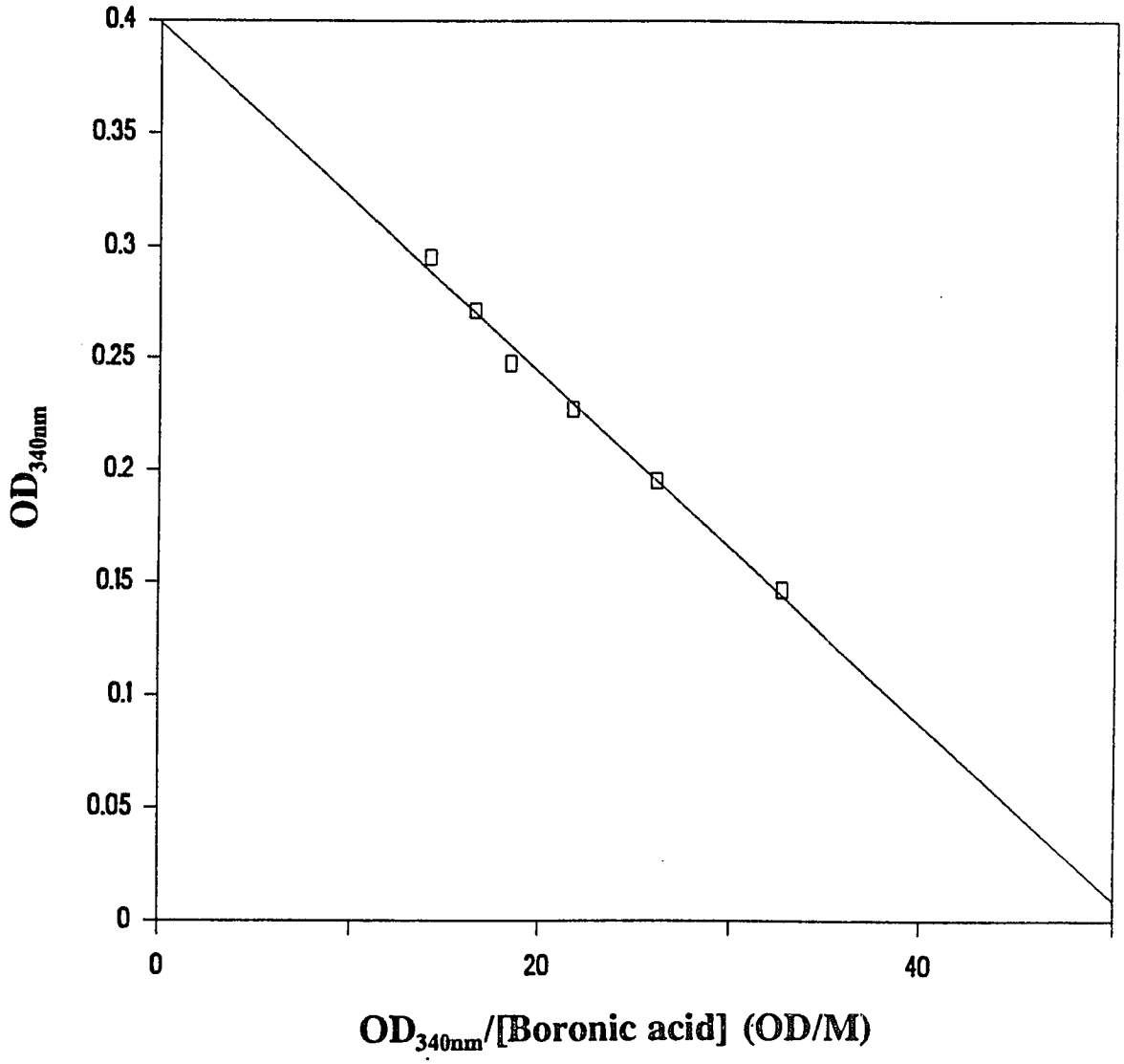

Fig.3 Eadie-Hofstee plot for the complexation between 3-chloro-4-fluorobenzeneboronic acid and salicylaldoxime (0.1097 mM) in pH 6.6 0.1 M buffer, 25.5°C. K_{diss} = 7.80($\pm$0.355) mM.
(Data of Table III Appendix H)

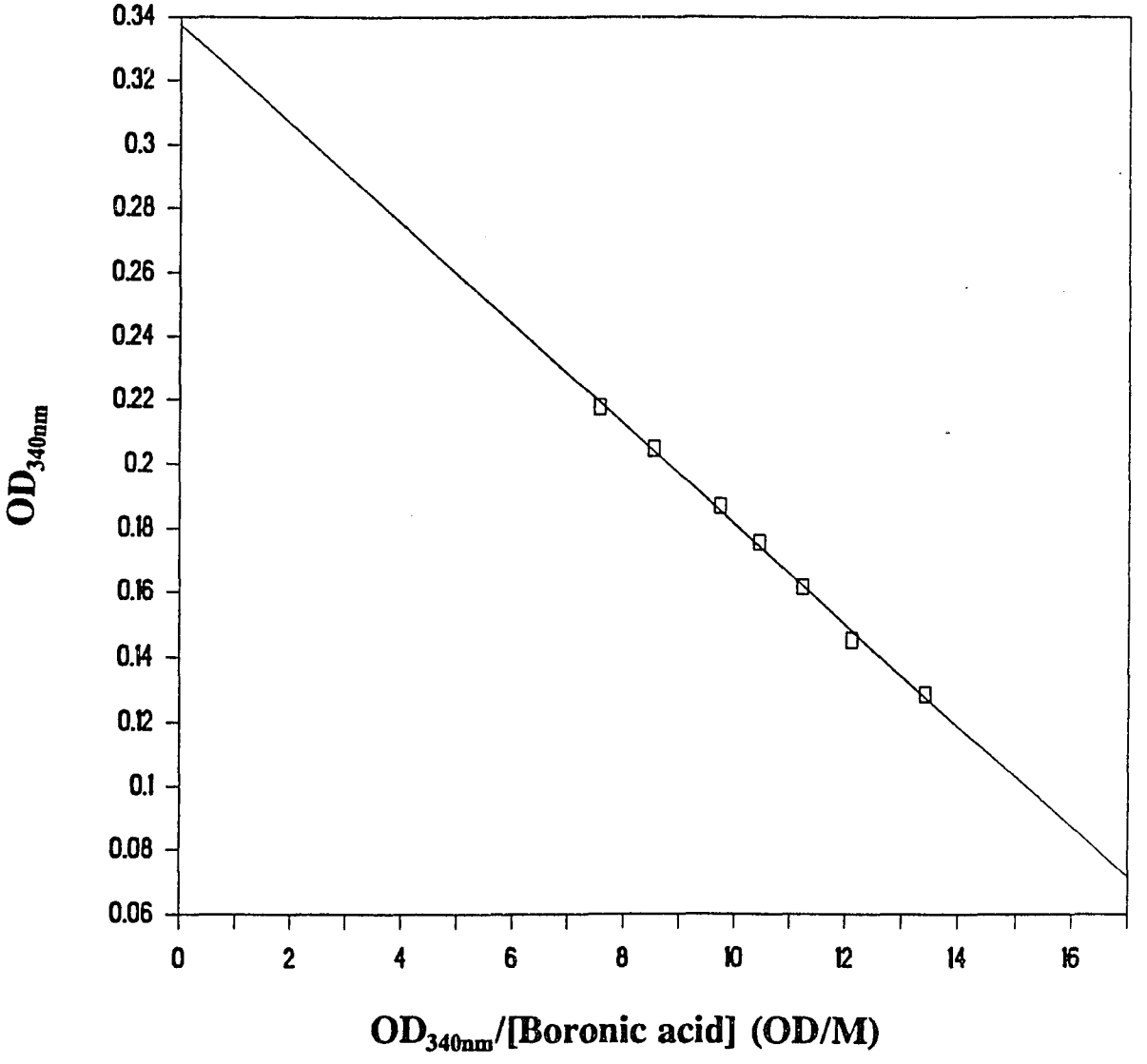

Fig.4 Eadie-Hofstee plot for the complexation between 4-bromobenzeneboronic acid and salicylaldoxime (0.1097 mM) in pH 6.6 0.1 M buffer, 25.5°C. K_{diss} = 15.6(±0.376) mM.
(Data of Table IV Appendix H)

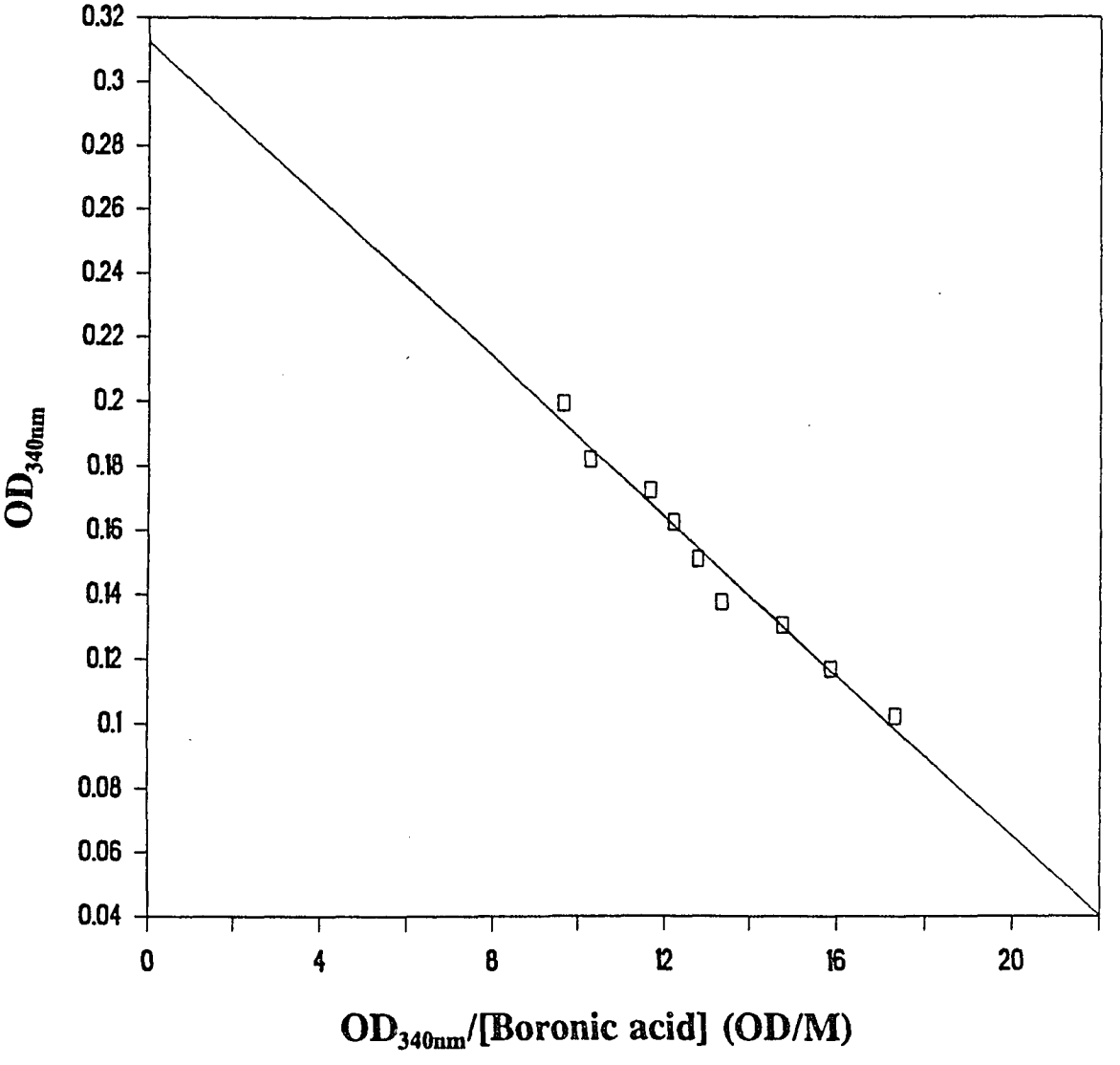

Fig.5 Eadie-Hofstee plot for the complexation between 4-chlorobenzeneboronic acid and salicylaldoxime (0.1097 mM) in pH 6.6 0.1 M buffer, 25.5°C. K_{diss} = 12.4(±0.730) mM.
(Data of Table V Appendix H)

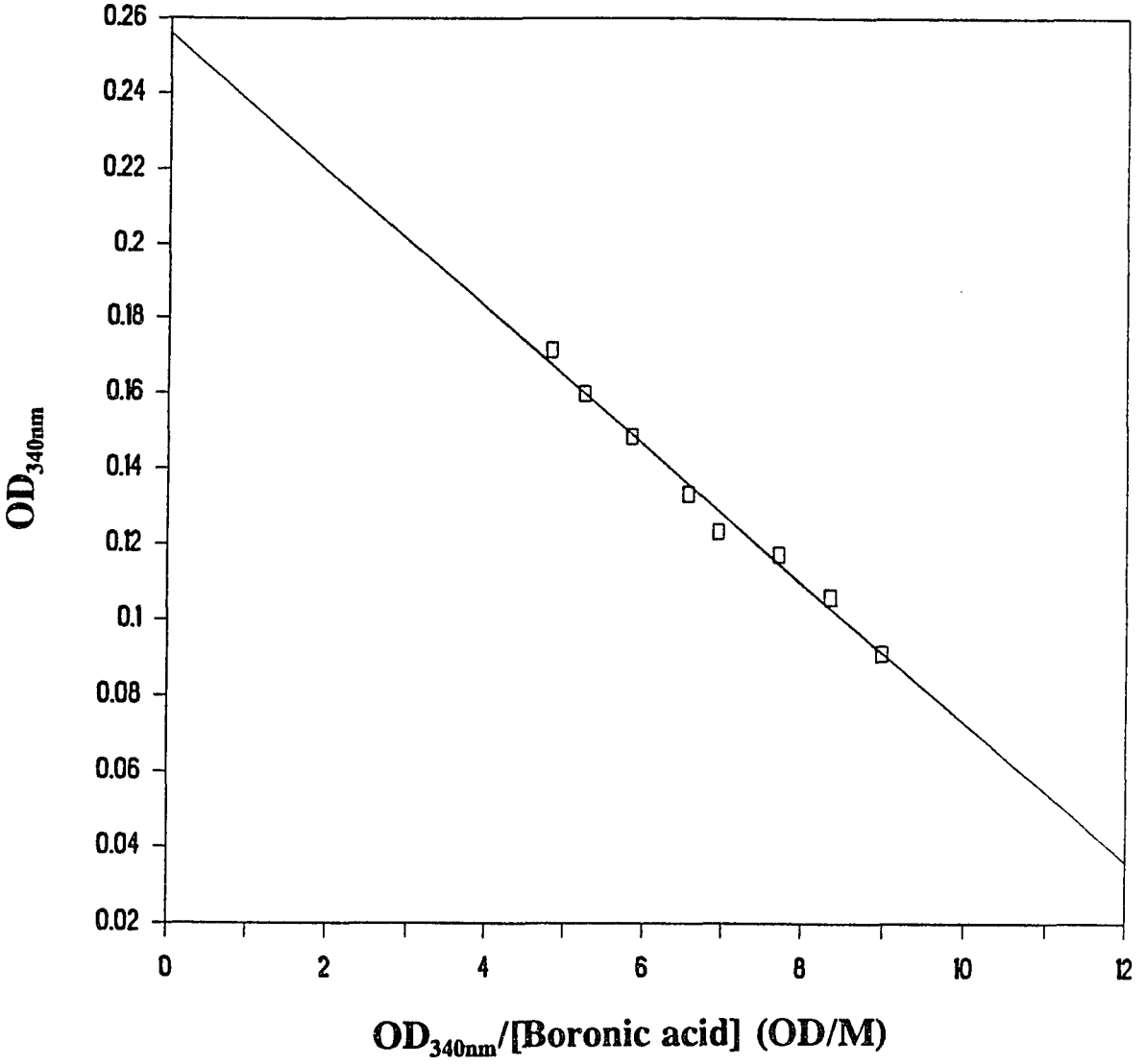

Fig.6 Eadie-Hofstee plot for the complexation between 4-fluorobenzeneboronic acid and salicylaldoxime (0.1097 mM) in pH 6.6 0.1 M buffer, 25.5°C. K_{diss} = 18.3($\pm$0.852) mM.
(Data of Table VI Appendix H)

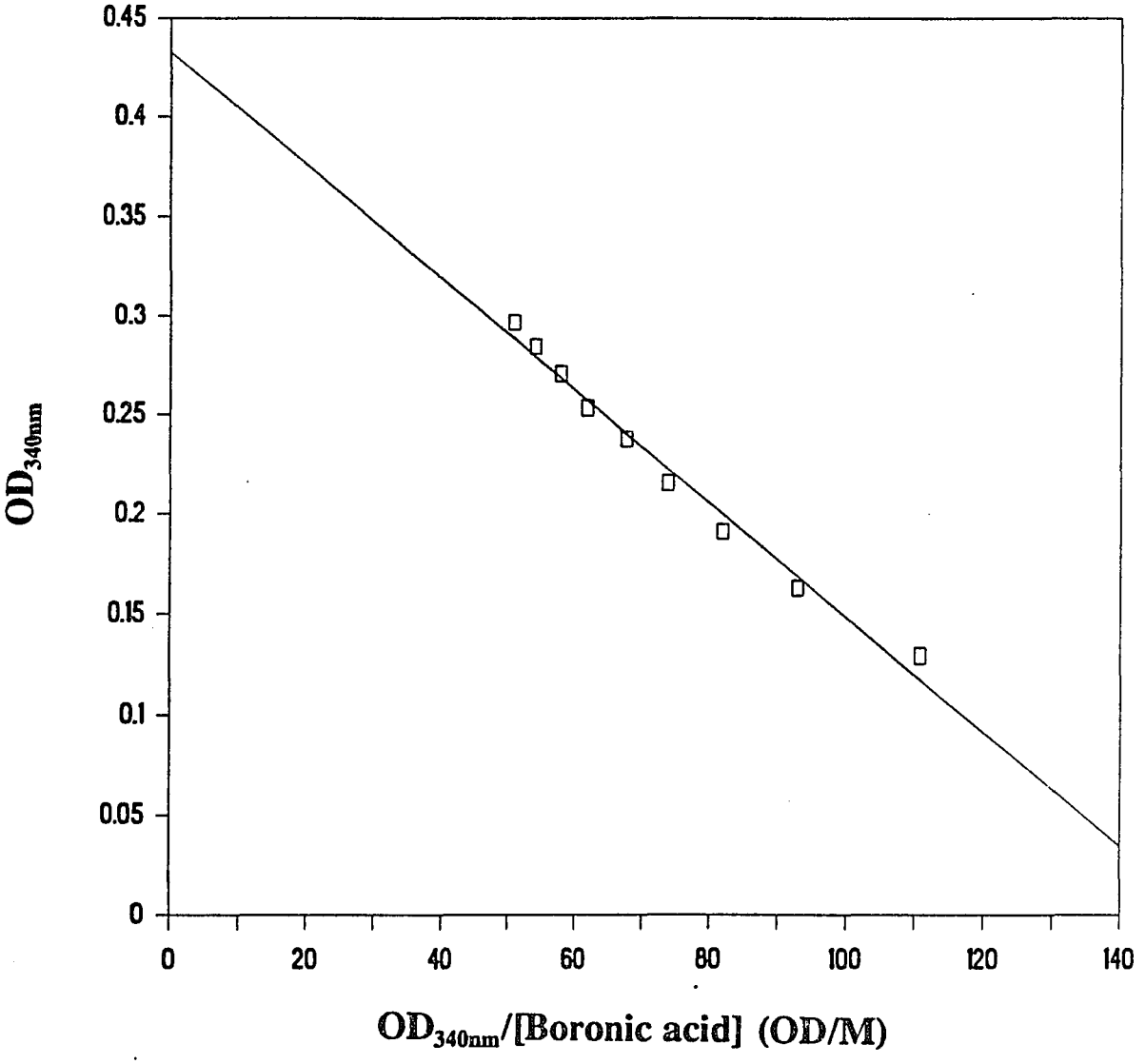

Fig.7 Eadie-Hofstee plot for the complexation between 3,5-bis(trifluoromethyl)benzeneboronic acid and salicylaldoxime (0.1097 mM) in pH 6.6 0.1 M buffer, 25.5°C. K_{diss} = 2.84(±0.138) mM. (Data of Table VII Appendix H)

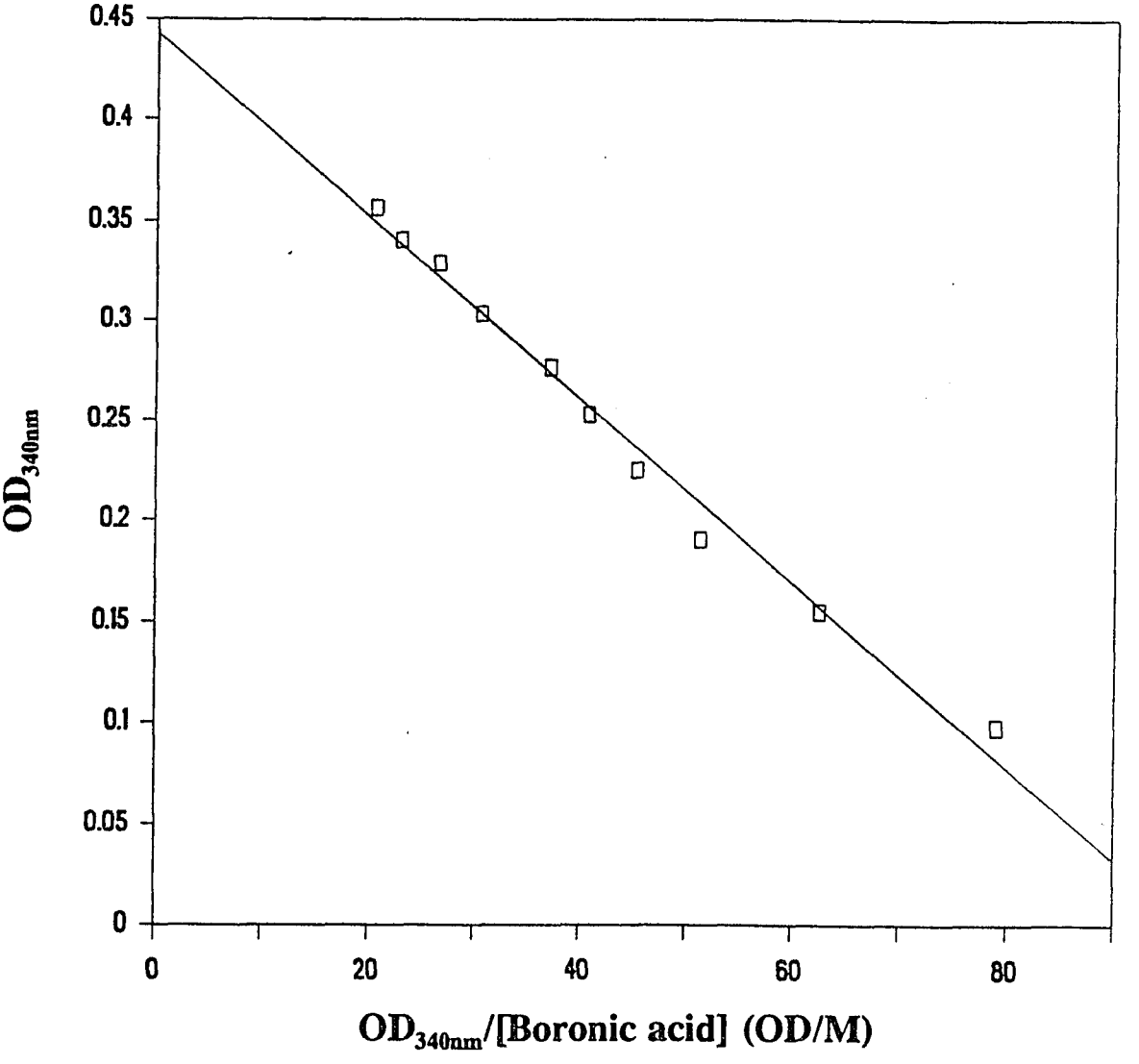

Fig.8 Eadie-Hofstee plot for the complexation between 2,4-dichlorobenzeneboronic acid and salicylaldoxime (0.1097 mM) in pH 6.60 0.1 M buffer, 25.5°C. K_{diss} = 4.56($\pm$0.182) mM.
(Data of Table VIII Appendix H)

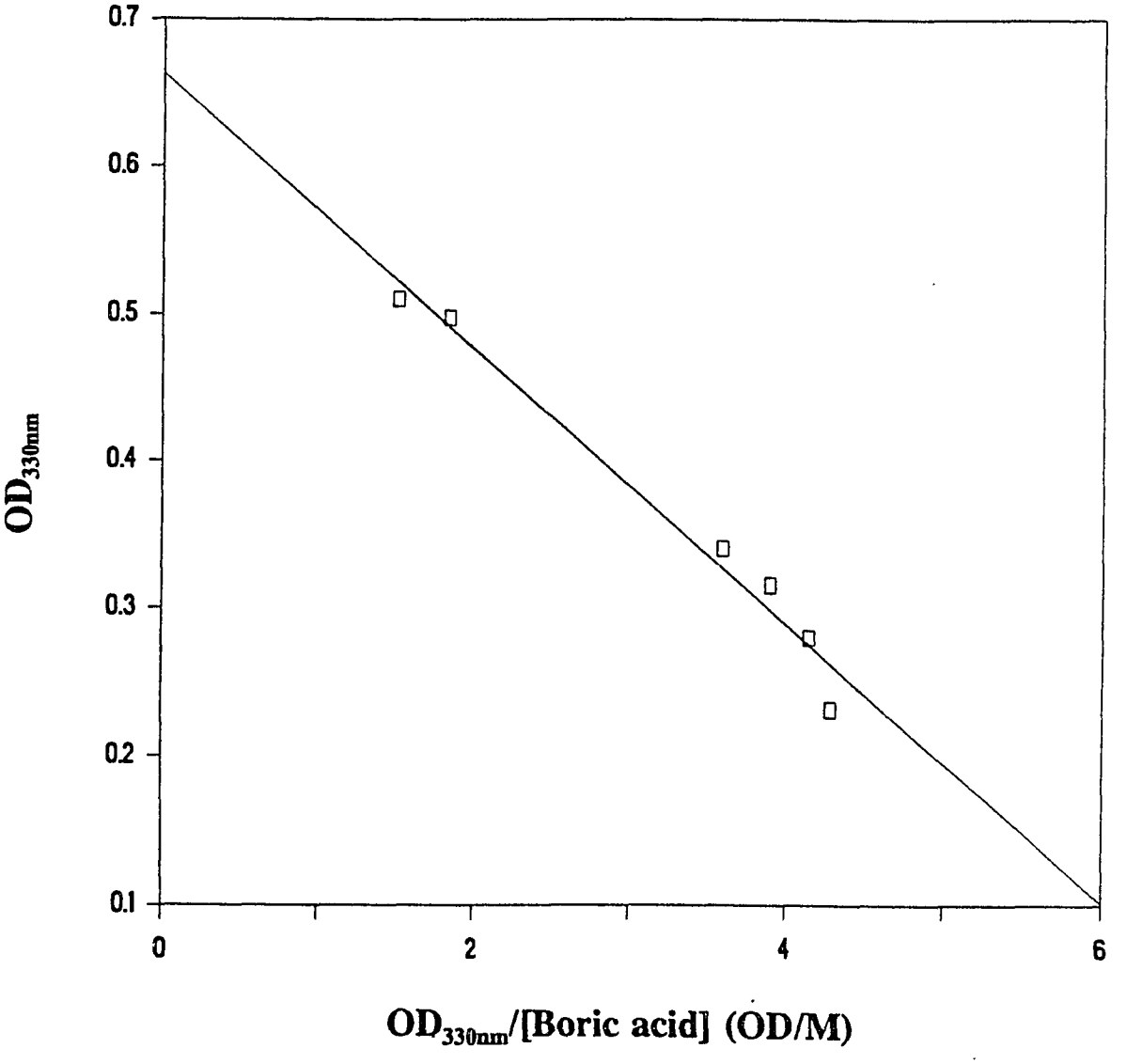

Fig.9 Eadie-Hofstee plot for the complexation between boric acid and salicylaldoxime (0.1097 mM) in pH 7.8 0.1 M buffer, 25.5°C.
K_{diss} = 93.6($\pm$7.33) mM.
(Data of Table IX Appendix H)

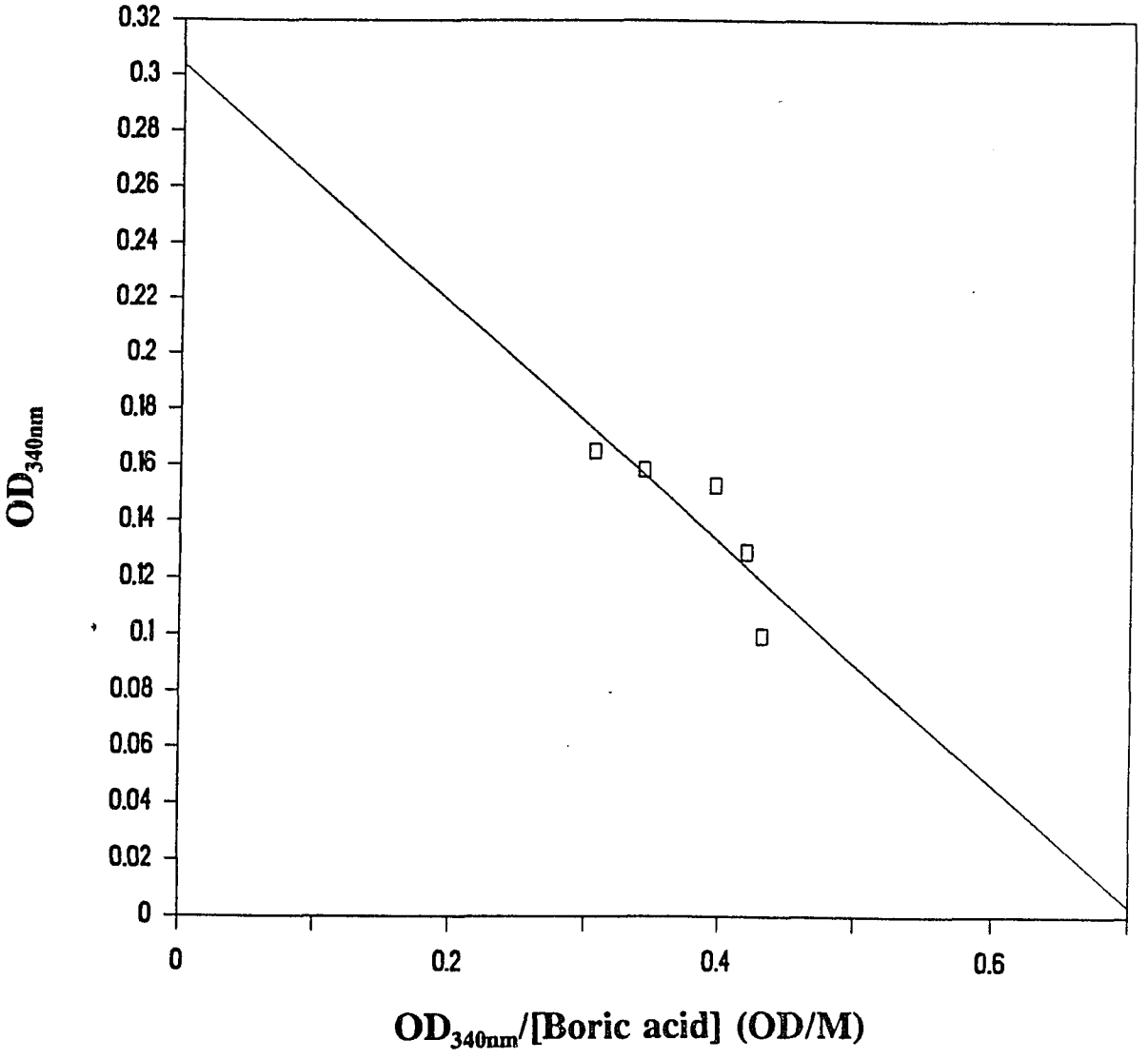

Fig.10 Eadie-Hofstee plot for the complexation between boric acid and salicylaldoxime (0.1097 mM) in pH 6.8 0.1 M buffer, 25.5°C.
K_{diss} = 0.429($\pm$0.154) M.
(Data of Table X Appendix H)

Table I Complexation of salicylaldoxime with benzeneboronic acid at pH 6.6, 25.5°C (Data of Fig.1 Appendix H)

[boronic acid] (M)	absorbance increase (340 nm)
1.646×10^{-2}	0.1019
2.469×10^{-2}	0.1249
3.292×10^{-2}	0.1603
4.115×10^{-2}	0.1719
4.938×10^{-2}	0.2028
5.761×10^{-2}	0.2063
6.584×10^{-2}	0.2339
7.407×10^{-2}	0.2325
8.230×10^{-2}	0.2638
9.053×10^{-2}	0.2584
1.152×10^{-1}	0.3043
1.234×10^{-1}	0.2940

Table II Complexation of salicylaldoxime with 3,5-dichlorobenzeneboronic acid at pH 6.6, 25.5°C (Data of Fig.2 Appendix H)

[boronic acid] (M)	absorbance increase (340 nm)
3.388×10^{-3}	0.2067
4.518×10^{-3}	0.2387
5.647×10^{-3}	0.2685
6.777×10^{-3}	0.2971
7.906×10^{-3}	0.3146
9.036×10^{-3}	0.3320
1.129×10^{-2}	0.3516
1.355×10^{-2}	0.363
1.581×10^{-2}	0.3806

Table III Complexation of salicylaldoxime with 3-chloro-4-fluorobenzeneboronic acid at pH 6.6, 25.5°C (Data of Fig.3 Appendix H)

[boronic acid] (M)	absorbance increase (340 nm)
4.482×10^{-3}	0.1465
7.470×10^{-3}	0.1951
1.046×10^{-2}	0.2270
1.345×10^{-2}	0.2474
1.643×10^{-2}	0.2713
2.092×10^{-2}	0.2952

Table IV Complexation of salicylaldoxime with 4-bromobenzeneboronic acid at pH 6.6, 25.5°C (Data of Fig.4 Appendix H)

[boronic acid] (M)	absorbance increase (340 nm)
9.610×10^{-3}	0.1289
1.201×10^{-2}	0.1454
1.442×10^{-2}	0.1616
1.682×10^{-2}	0.1756
1.922×10^{-2}	0.1870
2.403×10^{-2}	0.2050
2.883×10^{-2}	0.2178

Table V Complexation of salicylaldoxime with 4-chlorobenzeneboronic acid at pH 6.6, 25.5°C (Data of Fig.5 Appendix H)

[boronic acid] (M)	absorbance increase (340 nm)
5.908×10^{-3}	0.1023
7.385×10^{-3}	0.1170
8.862×10^{-3}	0.1306
1.034×10^{-2}	0.1378
1.182×10^{-2}	0.1510
1.329×10^{-2}	0.1624
1.477×10^{-2}	0.1723
1.772×10^{-2}	0.1821
2.068×10^{-2}	0.1993

Table VI Complexation of salicylaldoxime with 4-fluorobenzeneboronic acid at pH 6.6, 25.5°C (Data of Fig.6 Appendix H)

[boronic acid] (M)	absorbance increase (340 nm)
1.018×10^{-2}	0.0913
1.272×10^{-2}	0.1061
1.526×10^{-2}	0.1174
1.781×10^{-2}	0.1234
2.035×10^{-2}	0.1333
2.544×10^{-2}	0.1483
3.053×10^{-2}	0.1598
3.562×10^{-2}	0.1714

Table VII Complexation of salicylaldoxime with 3,5-bis(trifluoromethyl)-benzeneboronic acid at pH 6.6, 25.5°C (Data of Fig.7 Appendix H)

[boronic acid] (M)	absorbance increase (340 nm)
1.170×10^{-3}	0.1297
1.754×10^{-3}	0.1630
2.339×10^{-3}	0.1915
2.924×10^{-3}	0.2159
3.509×10^{-3}	0.2379
4.094×10^{-3}	0.2534
4.678×10^{-3}	0.2705
5.263×10^{-3}	0.2844
5.848×10^{-3}	0.2968

Table VIII Complexation of salicylaldoxime with 2,4-dichlorobenzeneboronic acid at pH 6.6, 25.5°C (Data of Fig.8 Appendix H)

[boronic acid] (M)	absorbance increase (340 nm)
1.240×10^{-3}	0.0979
2.479×10^{-3}	0.1551
3.719×10^{-3}	0.1907
4.958×10^{-3}	0.2248
6.198×10^{-3}	0.2529
7.437×10^{-3}	0.2762
9.916×10^{-3}	0.3031
1.240×10^{-2}	0.3288
1.487×10^{-2}	0.3405
1.735×10^{-2}	0.3564

Table IX Complexation of salicylaldoxime with boric acid at pH 7.8, 25.5°C (Data of Fig.9 Appendix H)

[boric acid] (M)	absorbance increase (330 nm)
5.408×10^{-2}	0.2316
6.760×10^{-2}	0.2802
8.112×10^{-2}	0.3155
9.464×10^{-2}	0.3401
2.704×10^{-1}	0.4973
3.380×10^{-1}	0.5098

Table X Complexation of salicylaldoxime with boric acid at pH 6.8, 25.5°C (Data of Fig.10 Appendix H)

[boric acid] (M)	absorbance increase (340 nm)
2.314×10^{-1}	0.0998
3.085×10^{-1}	0.1293
3.857×10^{-1}	0.1528
4.628×10^{-1}	0.1586
5.399×10^{-1}	0.1653

APPENDIX I

Eadie-Hofstee Plots for the Complexation of Diphenylborinic Acid with Salicylic Acid and Salicylaldehyde Derivatives: Figures and Data Tables

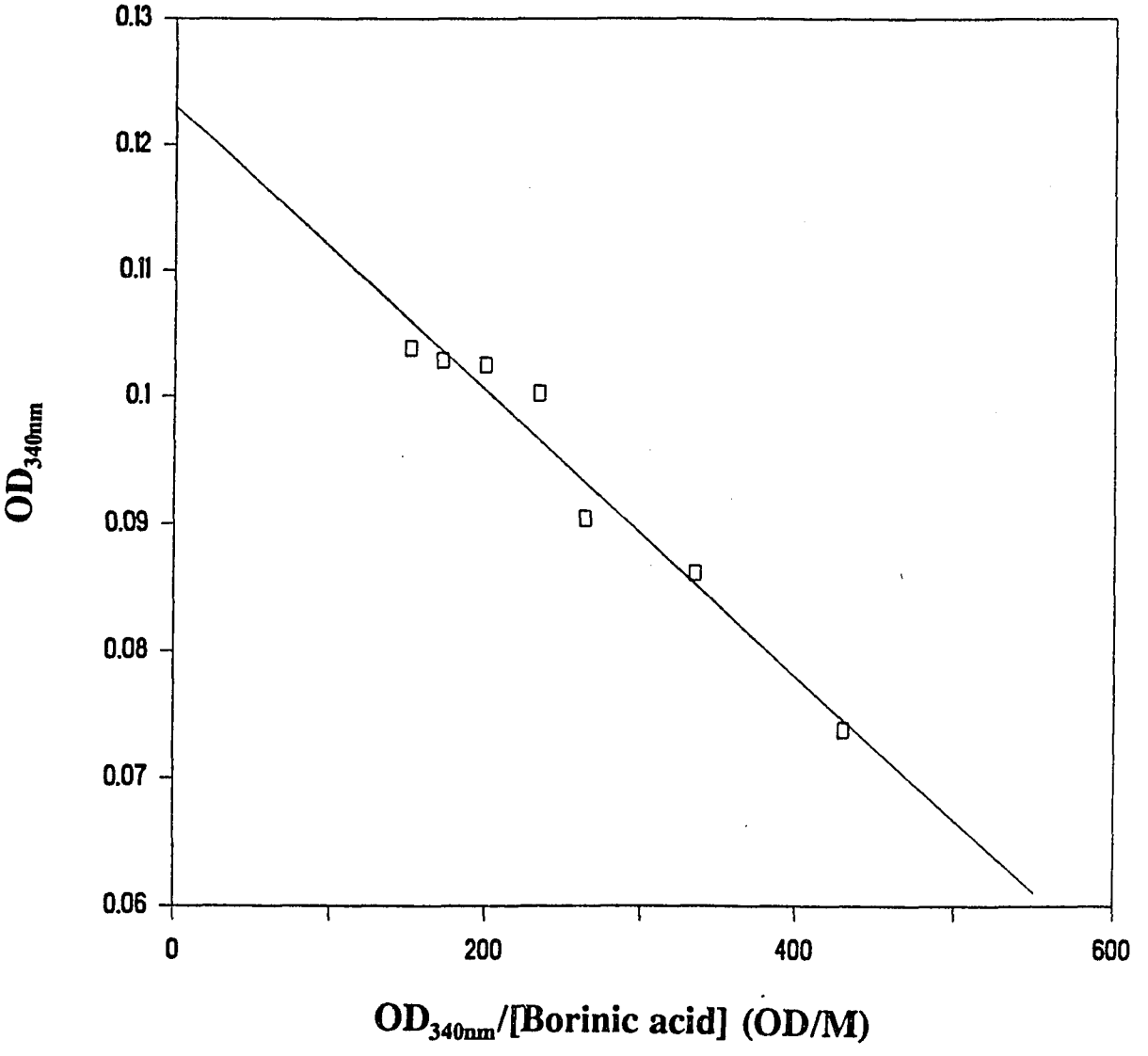

Fig.1 Eadie-Hofstee plot for the complexation between diphenylborinic acid and salicyloylhydrazide (87.4 μM) in pH 6.6 0.1 M buffer, 25.5°C. K_{diss} = 0.113($\pm$0.0104) mM.
(Data of Table I Appendix I)

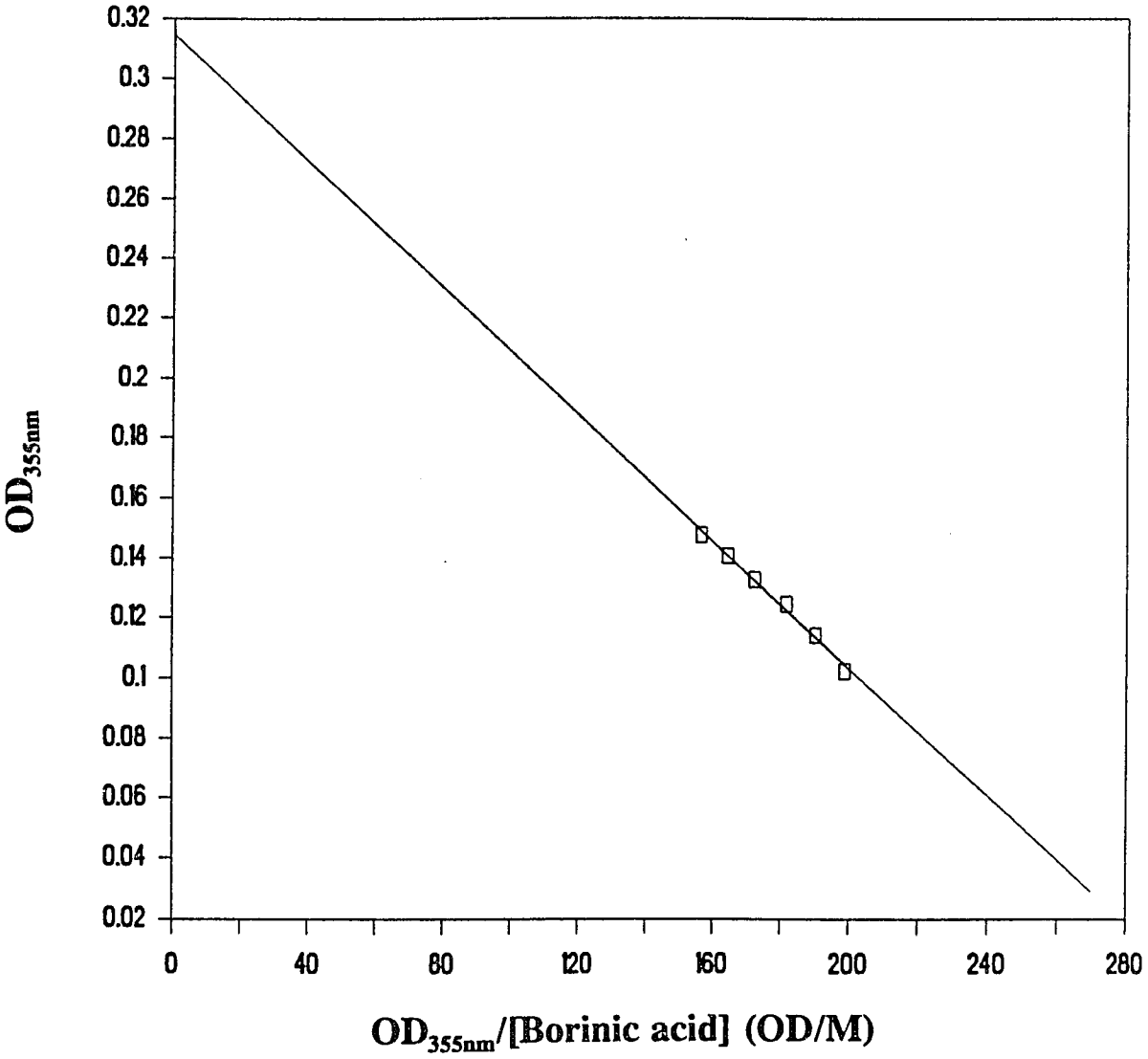

Fig.2 Eadie-Hofstee plot for the complexation between diphenylborinic acid and salicylhydroxamic acid (86.4 μM) in pH 6.6 0.1 M buffer, 25.5°C. K_{diss} = 1.06($\pm$0.0491) mM.
(Data of Table II Appendix I)

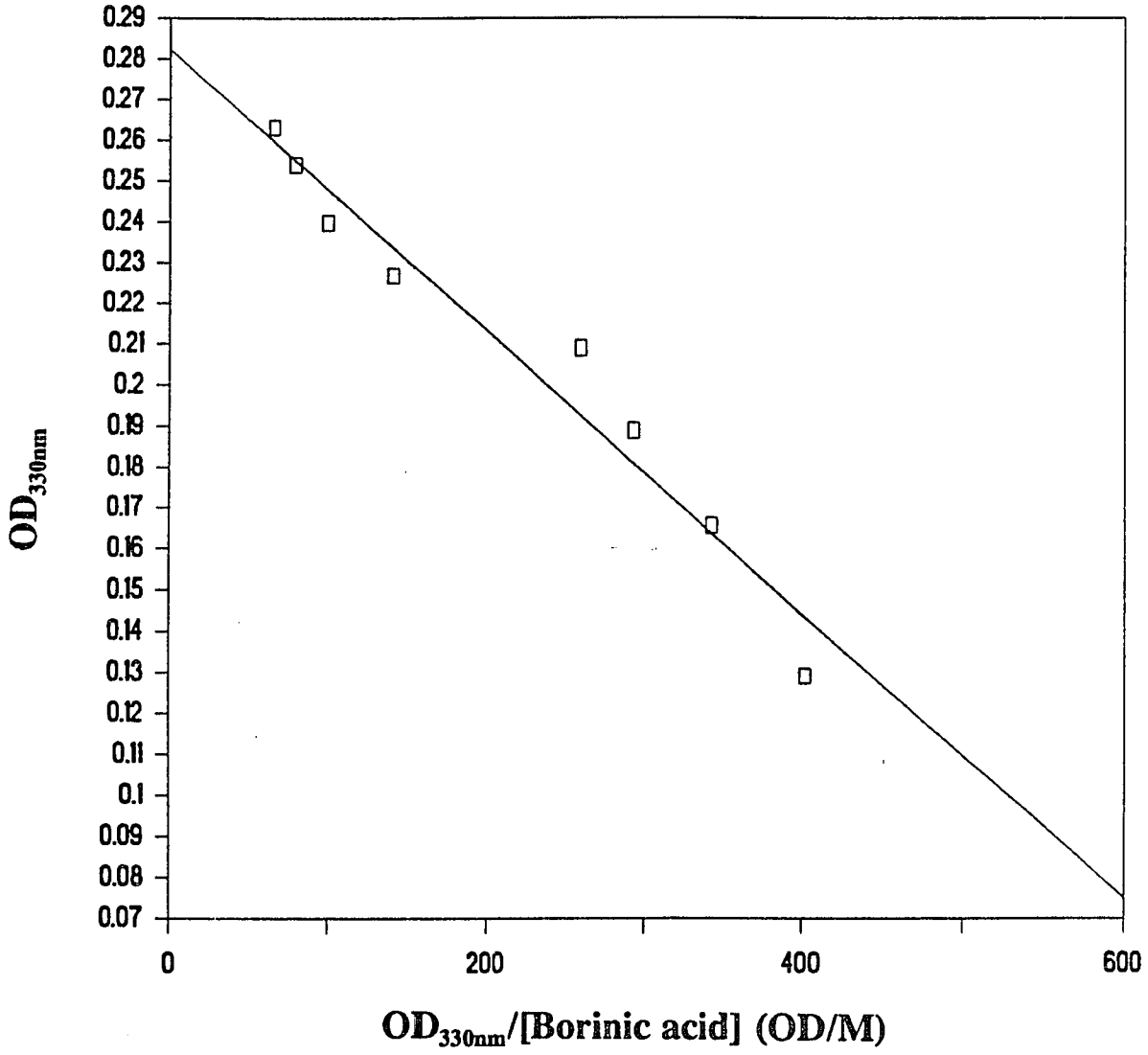

Fig.3 Eadie-Hofstee plot for the complexation between diphenylborinic acid and salicylamide (0.185 mM) in pH 6.6 0.1 M buffer, 25.5°C.
K_{diss} = 0.346(±0.0305) mM.
(Data of Table III Appendix I)

Table I Complexation of salicyloylhydrazide with diphenylborinic acid at pH 6.6, 25.5°C (Data of Fig.1 Appendix I)

[boriric acid] (M)	absorbance incease (340 nm)
1.716×10^{-4}	0.07379
2.574×10^{-4}	0.08613
3.432×10^{-4}	0.09045
4.290×10^{-4}	0.1003
5.148×10^{-4}	0.1025
6.006×10^{-4}	0.1029
6.864×10^{-4}	0.1039

Table II Complexation of salicylhydroxamic acid with diphenylborinic acid at pH 6.6, 25.5°C (Data of Fig.2 Appendix I)

[borinic acid] (M)	absorbance increase (355 nm)
5.148×10^{-4}	0.1023
6.006×10^{-4}	0.1142
6.864×10^{-4}	0.1247
7.722×10^{-4}	0.1330
8.580×10^{-4}	0.1409
9.438×10^{-4}	0.1477

Table III Complexation of salicylamide with diphenylborinic acid at pH 6.6, 25.5°C (Data of Fig.3 Appendix I)

[borinic acid] (M)	absorbance increase (330 nm)
3.217×10^{-4}	0.1292
4.826×10^{-4}	0.1657
6.435×10^{-4}	0.1889
8.044×10^{-4}	0.2089
1.609×10^{-3}	0.2269
2.413×10^{-3}	0.2399
3.217×10^{-3}	0.2541
4.022×10^{-3}	0.2632

REFERENCES OF PART I

1. Fenton II, J. W. *Ann. N.Y. Acad. Sci.* **485**, 5 (1986).

2. Fenton II, J. W. *Ann. N.Y. Acad. Sci.* **370**, 468 (1981).

3. Fenton II, J. W.; Bing, D. H. *Semin. Thromb. Hemostasis* **12**, 200 (1986).

4. Fenton II, J. W. *Semin. Thromb. Hemostasis* **14**, 234 (1988).

5. Henschen, A.; Lottspeich, F.; Kehl, M.; Southan C. *Ann. N.Y. Acad. Sci.* **408**, 28 (1983).

6. Scheraga, H. A. *Ann. N.Y. Acad. Sci.* **408**, 330 (1983).

7. Scheraga, H. A. *Ann. N.Y. Acad. Sci.* **485**, 124 (1986).

8. Shuman, M. A. *Ann. N.Y. Acad. Sci.* **485**, 228 (1986).

9. Bode, W.; Mayr, I.; Baumann, U.; Huber, R.; Stone, S. R.; Hofsteenge, J. *EMBO Journal* **8**, 3467 (1989).

10. Rydel, T. J.; Ravichandran, K. G.; Tulinsky, A.; Bode, W.; Huber, R.; Roitsch, C.; Fenton II, J. W. *Scinece* **249**, 277 (1990).

11. Grütter, M. G.; Priestle, J. P.; Rahuel, J.; Grossenbacher, H.; Bode, W.; Hofsteenge, J.; Stone, S. R. *EMBO Journal* **9**, 2361 (1990).

12. Damus, P. S.; Rosenberg, R. D. *Methods in Enzymol.* **45**, 653 (1976).

13. Kurachi, K; Fujikawa, K.; Schmer, G.; Davie, E. W. *Biochem.* **15**, 373 (1976).

14. Schechter, I.; Berger, A. *Biochem. Biophys. Res. Commun.* **27**, 157 (1967).

15. Markwardt, F. *Folia Haematol., Leipzig* **109**, 1, 7 (1982).

16. Markwardt, F. *Ann. N.Y. Acad. Sci.* **485**, 204 (1986).

17. Walsmann, P.; Markwardt F. *Pharmazie* **36**, 653 (1981).

18. Petersen, T. E.; Roberts, H. R.; Sottrup-Jensen, L.; Magnusson, S. *Protides. Biol. Fluids Proc. Colloq.* **23**, 145 (1976).

19. Dodt, J.; Machleidt, W.; Seemüller, V.; Maschler, R.; Fritz, H. *Biol. Chem. Hoppe-Seyler* **367**, 803 (1986).

20. Stone, S. R.; Hofsteenge, J. *Biochem.* **25**, 4622 (1986).

21. Rydel, T. J.; Ravichandran, K. G.; Tulinsky, A.; Bode, W.; Huber, R.; Roitsch, C.; Fenton II, J. W. *Scinece* **249**, 277 (1990).

22. Fenton II, J. W.; Ofosu, F. A.; Moon, D. G.; Maraganore, J. W. *Blood Coag. Fibrinolysis* **2**, 69 (1991).

23. Ashley, G. W.; Bartlett, P. A. *Biochem. Biophys. Res. Comm.* **108**, 1467 (1982).

24. Dafforn, A.; Neenan, J. P.; Ash, C. E.; Betts, L.; Finke, J. M.; Garman, J. A.; Rao, M.; Walsh, K.; Williams, R. R. *Biochem. Biophys. Res. Comm.* **104**, 597 (1982).

25. Brodbeck, U.; Schweikert, K.; Gentinetta,R.; Rottenberg, M. *Biochem. Biophys. Acta* **567**, 357 (1979).

26. Komiyama, T.; Suda, H.; Aoyagi, T.; Takeuchi, T.; Umezawa, H.; Fujimoto, K.; Umezawa, S. *Arch. Biochem. Biophys.* **171**, 727 (1975).

27. Matteson, D. S.; Sadhu, K. M.; Lienhard, G. E. *J. Am. Chem. Soc.* **103**, 5241 (1981).

28. Glasstone, S.; Laidler, K. J.; Eyring, H. *Theory of Rate Processes* McGraw-Hill: New York; (1941).

29. Zerner, B.; Bender, M. L. *Org. Biol. Chem.* **86**, 3669 (1964).

30. Bone, R.; Shenvi, A. B.; Kettner C. A.; Agard, D. A. *Biochem.* **26**, 7609 (1987).

31. Hauptmann, J.; Markwardt, F. *Beiträge zur Wirkstofforschung* **26**, 1 (1986).

32. Blombäck, B.; Hessel, R.; Hogg, D.; Claeson, G. in: *Chemistry and Biology of Thrombin* (eds. Lundblad; Fenton II, J. W.; Mann, K. G.). Ann Arbor Science pp 275-290 (1977).

33. Ni, F.; Konishi, Y.; Frazier, R. D.; Scheraga, H. A. *Biochem.* **28**, 3082 (1989).

34. Rae, I. D.; Scheraga, H. A. *Int. J. Peptide and Protein Research* **13**, 304 (1979).

35. Claeson, G.; Aurell, L. *Ann. N.Y. Acad. Sci.* **370**, 798 (1981).

36. Bajusz, S.; Barabás, É.; Tolnay, P.; Széll, E.; Bagdy, D. *Int. J. Peptide and Protein research* **12**, 217 (1978).

37. Kettner, C.; Shaw, E. *Thromb. Res.* **14**, 969 (1979).

38. Umezawa, K. *Methods in Enzymol.* **45**, 678 (1976).

39. Chen, R.; Gorenstein, D. G.; Kennedy, W. P.; Lowe, G.; Nurse, D.; Schultz, R. M. *Biochem.* **18**, 921 (1979).

40. Markwardt, F.; Wagner, G.; Stürzebecher, J.; Walsmann, P. *Thromb. Res.* **17**, 425 (1980).

41. Stürzebecher, J.; Markwardt, F.; Voigt, B.; Wagner, G.; Walsmann, P. *Thromb. Res.* **29**, 635 (1983).

42. Stürzebecher, J.; Markwardt, F.; Wagner, G.; Walsmann, P. *Acta Biol. Med. Ger.* **35**, 1665 (1976).

43. Bode, W.; Turk, D.; Stürzebecher, J. *Eur. J. Biochem.* **193**, 175 (1990).

44. Antonov, V. K.; Ivaniva, T. V.; Berezin, I. V.; Martinek, K. *FEBS Lett.* **7**, 23 (1971).

45. Philipp, M.; Bender, M. L. *Proc. Nat. Acad. Sci. USA* **68**, 478 (1971).

46. Koehler, K. A.; Lienhard, G. E. *Biochem.* **10**, 2477 (1971).

47. Kettner, C. A.; Shenvi, A. B. *J. Biol. Chem.* **259**, 15106 (1984).

48. Koehler, K. A.; Jackson, R. C.; Lienhard, G. E. *J. Org. Chem.* **37**, 2232 (1972).

49. Nakatani, H.; Uehara, Y.; Hiromi, K. J. *Biochem.* **78**, 611 (1975).

50. Kettner, C. A.; Bone, R.; Agard, D. A.; Bachovchin, W. W. *Biochem.* **27**, 7682 (1988).

51. Adebodun, F.; Jordan, F. *J. Cell. Biochem.* **40**, 249 (1989).

52. Robillard, G.; Schulman, R. G. *J. Mol. Biol.* **86**, 541 (1974).

53. Bachovchin W.; Wong, W. Y. L.; Farr-Jones, S.; Shenvi, A. B.; Kettner, C. A. *Biochem.* **27**, 7689 (1988).

54. Baldwin, J. E.; Claridge, T. D. W.; Derome, A. E.; Schofield, C.J.; Smith, B. D. *Bioorg. Med. Chem. Lett.* **1**, 9 (1991).

55. Tulinsky, A; Blevins, R. A. *J. Biol. Chem.* **262**, 7737 (1987).

56. Matthews, D. A.; Alden, R. A.; Birktoft, J. J.; Freer, S. T.; Kraut, J. *J. Biol. Chem.* **250**, 7120 (1975).

57. Takahashi, L. H.; Radhakrishnan, R.; Rosenfeld, Jr., R. E.; Meyer, Jr., E. F. *Biochem.* **28**, 7610 (1989).

58. Bone, R.; Frank, D.; Kettner, C. A.; Agard, D. A. *Biochem.* **28**, 7600 (1989).

59. Long, C. *Biochemists' Handbook;* Van Norstrand Reinhold Co.: New York, pp 30-42 (1961).

60. Chase, Jr., T.; Shaw, E. *Methods. in Enzymol.* **XIX**, 20 (1970).

61. Cha, S. *Biochem. Pharmacol.* **24**, 2177 (1975).

62. Williams, J. W.; Morrison, J. F. *Methods. in Enzymol.* **63**, 437 (1979).

63. Glasoe, P. K.; Long, F. L. *J. Phys. Chem.* **64**, 188 (1960).

64. Pentz, L.; Thornton, E. R. *J. Am. Chem. Soc.* **89**, 6931 (1967).

65. Ascenzi, P.; Menegatti, E.; Guarneri, M.; Bortolotti, F.; Antonini, E. *Biochem.* **21**, 2483 (1982).

66. Kettner, C. A.; Mersinger, L.; Knabb, R. *J. Biol. Chem.* **265**, 18289 (1990).

67. Philipp, M.; Bender, M. L. *Molec. and Cell. Biochem.* **51**, 5 (1983).

68. Di Cera, E.; De Cristofaro, R.; Albright, D. J.; Fenton II, J. W. *Biochem.* **30**, 7913 (1991).

69. De Soyza, T. V. *Doctoral Thesis* City University of New York (1990).

70. Hirohara, H.; Philipp, M.; Bender, M. L. *Biochem.* **16**, 1573 (1977).

71. Kézdy, F. J.; Thompson, A.; Bender, M. L. *J. Am. Chem. Soc.* **89**, 1004 (1967).

72. Kennedy, W. P.; Schultz, R. M. *Biochem.* **18**, 349 (1979).

73. Martin, C. J.; Marini, M. A. *J. Biol. Chem.* **242,** 5736 (1967).

74. Glazer, A. N. *J. Biol. Chem.* **243,** 3693 (1968).

75. Stürzebecher, J.; Markwardt, F; Walsmann, P. *Thromb. Res.* **17,** 545 (1980).

76. Banner, D. W.; Hadváry, P. *J. Biol. Chem.* **266,** 20085 (1991).

77. Pauling, L. *The Nature of the Chemical Bond* Cornell University Press, pp 221-264 (1960).

78. Gorenstein, D. G.; Shah, D. O. *Biochem.* **21,** 4679 (1982).

79. Walsmann, P.; Horn, H.; Markwardt, F.; Richter, P.; Stürzebecher, J.; Vieweg, H.; Wagner, G. *Acta biol. med. germ.* **35,** K_1 - K_8 (1976).

80. Bone, R.; Fujishige, A.; Kettner, C. A.; Agard, D. A. *Biochem.* **30,** 10388 (1991).

REFERENCES OF PART II

1. Lorand, J. P.; Edwards, J. O. *J. Org. Chem.* **24**, 769 (1959).

2. Steinberg, H.; Hunter, D.L. *Ind. Eng. Chem.* **49**, 174 (1957).

3. Kustin, K.; Pizer, R. *J. Am. Chem. Soc.* **91**, 317 (1969).

4. Friedman, S.; Pace, B.; Pizer, R. *J. Am. Chem. Soc.* **96**, 5381 (1974).

5. Lorber, G.; Pizer, R. *Inorg. Chem.* **15**, 978 (1976).

6. Friedman, S.; Pizer, R. *J. Am. Chem. Soc.* **97**, 6059 (1975).

7. Pizer, R.; Babcock, L. *Inorg. Chem.* **16**, 1677 (1977).

8. Babcock, L.; Pizer, R. *Inorg. Chem.* **19**, 56 (1980).

9. Philipp, M.; Bender, M. L.; Valenzuela, P. V. U.S. Patent No. 3,912,595, October 14, (1975).

10. Maestas, R. R.; Prieto, J. R.; Kuehn, G. D.; Hageman, J. H. *J. Chromatogr.* **189**, 225 (1980).

11. Bouriotis, V.; Galpin, I. J.; Dean, P. D. G. *J. Chromatogr.* **210**, 267 (1981).

12. Weith, H. L.; Wiebers, J. L.; Gilham, P. T. *Biochem.* **9**, 4396 (1970).

13. Seliger, H.; Rössner, E.; Aumann, G.; Genrich, V.; Holupirek, M.; Knäble, T.; Philipp, M. *Makromol. Chem.* **176**, 2915 (1975).

14. Seliger, H.; Haas, B.; Holupirek, M.; Knäble, T.; Tödling, G.; Philipp, M. *Nucl. Acids Res.* **7**, 191 (1980).

15. Peer, H. G. *Recl. Trav. Chim. Pays-Bas* **79**, 825 (1960).

16. Jencks, W. P. *Catalysis in Chemistry and Enzymology;* McGraw-Hill: New York, pp 30-32 (1969).

17. Letsinger, R. L.; Dandegaonker, S.; Vullo, W. J.; Morrison, J. D. *J. Am. Chem. Soc.* **85**, 2223 (1963).

18. Letsinger, R. L.; Morrison, J. D. *J. Am. Chem. Soc.* **85**, 2227 (1963).

19. Letsinger, R. L.; MacLean, D. B. *J. Am. Chem. Soc.* **85,** 2230 (1963).

20. Capon, B.; Ghosh, B. C. *J. Chem. Soc. B* 472 (1966).

21. Okuyama, T.; Nagamatsu, H.; Fueno, T. *J. Org. Chem.* **46,** 1336 (1981).

22. Matsuda, H.; Nagamatsu, H.; Okuyama, T.; Fueno, T. *Bull. Chem. Soc. Jpn.* **57,** 500 (1984).

23. Hoffman, J.; Sterba, V. *Collect. Czech. Chem. Commun.* **37,** 2043 (1972).

24. Nagamatsu, H.; Okuyama, T.; Fueno, T. *Bull. Chem. Soc. Jpn.* **57,** 2502 (1984).

25. Nagamatsu, H.; Okuyama, T.; Fueno, T. *Bull. Chem. Soc. Jpn.* **57,** 2508 (1984).

26. Rao, G.; Philipp, M. *J. Org. Chem.* **56,** 1505 (1991).

27. Rao, G.; Philipp, M. *The Bioorganic Chemistry of Enzymatic Catalysis,* D'Souza, V. and Feder, J., eds.; CRC Press, pp 129-142 (1992).

28. Werber, M. M. *Adv. Clin. Chem.* **5,** 123-130 (1987).

29. Overberger, C. G.; Salamone, J. C. *Acc. Chem. Res.* **2,** 217 (1969).

30. Kiefer, H. C.; Congdon, W. I.; Scarpa, I. S.; Klotz, I. M. *Proc. Nat. Acad. Sci. U.S.A.* **69,** 2155 (1972).

31. Moss, R. A.; Lee, Y. S.; Lukas, T. J. *J. Am. Chem. Soc.* **101,** 2499 (1979).

32. Komiyama, M.; Bender, M. L. in: *The Chemistry of Enzyme Action;* Page, M. I., eds.; Elsevier: Amsterdam, pp 505-527 (1984).

33. Chao, Y.; Cram, D. J. *J. Am. Chem. Soc.* **98,** 1015 (1976).

34. Lehn, J. M.; Sirlin, C. *J. Chem. Soc., Chem. Commun.* 949 (1978).

35. Shimidzu, T.; Letsinger, R. L. *Bull. Chem. Soc. Jpn.* **46,** 3270 (1973).

36. Tramontano, A.; Janda, K. D.; Lerner, R. A. *Science* **234,** 1566 (1986).

37. Pollack, S. J.; Jacobs, J. W.; Schultz, P. G. *Science* 1986, **234,** 1570.

38. Rao, G.; Philipp, M. *Federation Proceedings* **46,** 2206 (1987).

39. Wechsberg, M.; Schönbeck, R. *Alpha-Hydroxycarboxylic Acid Amides,* Austrian Patent No. 358,552, (1978); *Chem. Abstr.* **94,** 120904k (1981).

40. Long, C. *Biochemists' Handbook;* Van Norstrand Reinhold Co.: New York, pp 30-42 (1961).

41. Glasoe, P. K.; Long, F. L. *J. Phys. Chem.* **64,** 188 (1960).

42. Pentz, L.; Thornton, E. R. *J. Am. Chem. Soc.* **89,** 6931 (1967).

43. Windholz, M. *The Merk Index;* Merck & Co., Inc. pp 4746 **(1983).**

44. Fasman, G. D. *Handbook of Biochemistry and Molecular Biology* Volume I; CRC Press, Inc. pp 314 (1976).

45. Chremos, G. N.; Zimmermann, H. K. *Chim. Chronika* **28,** 103 (1963).

46. Wolfenden, R. *Annual Rev. Biophys. Bioengin.* **Vol. V,** 271 (1976).

47. Windholz, M. *The Merk Index;* Merck & Co., Inc. pp 7176 (1983).

48. Hine, J. *Physical Organic Chemistry;* McGraw-Hill: New York, pp 87 (1962).

49. Fasman, G. D. *Handbook of Biochemistry and Molecular Biology* Volume I; CRC Press, Inc. pp 323 (1976).

50. Juillard, J.; Geugue, N. *C. R. Acad. Paris C* **264,** 259 (1967).

51. Brisson, C.; Pasdeloup, M. *Bull. Soc. Chim. Fr.* I-11-13 (1979).

52. Lumme, P.; Nieminen, K. *Suom. Kemistilehti B* **45(7-8),** 214 (1972).

53. Bhaskare, C. K.; Hankare, P. P.; Rampure, R. S. *J. Indian Chem. Soc.* **65(2),** 120 (1988).

54. Kliegel, W.; Nanninga, D. *Monatshefte für Chemie* **114(4),** 465 (1983).

55. Stepniak-Biniakiewicz, D. *Polish J. of Chem.* **60,** 725 (1986).

56. Kezdy, F. J.; Bender, M. L. *Biochem.* **1,** 1097 (1962).

VITA

Linghao Niu was born in Beijing, Peoples' Republic of China on January 25, 1962. After completing her B.S. degree in Pharmaceutical Chemistry at Beijing Medical University in 1985, she worked as a research assistant at the Institute of Clinic Pharmacology of Beijing Medical University until 1987. She joined the Ph.D. program in Biochemistry at The Graduate School of the City University of New York in Fall 1988.

Publications during her study in the Biochemistry program include "pH-Dependent Binding Constants for the Inhibition of Thrombin by Transition State Analogs" by M. Philipp, L.-H. Niu, T. DeSoyza, G. Claeson, R. Metternich, *Advances in Experimental Biology and Medicine,* in Press, 1993, and " Z-D-Phe-Pro-methoxypropyl-boroglycine - a Novel Inhibitor of Thrombin with High Selectivity Containing a Neutral Side Chain at the P_1 Position" by G. Claeson, M. Philipp, E. Agner, M.F. Skully, V.V. Kakkar, T. DeSoyza, & L.-H. Niu, *Biochemical Journal,* in press, 1993.